BIOMOLECULAR STRATEGIES FOR CELL SURFACE

ENGINEERING

A Dissertation
Presented to
The Academic Faculty

by

John Tanner Wilson

In Partial Fulfillment
of the Requirements for the Degree
Doctor of Philosophy in Bioengineering

Georgia Institute of Technology
May 2009

BIOMOLECULAR STRATEGIES FOR CELL SURFACE ENGINEERING

Approved by:

Dr. Elliot L. Chaikof, Advisor
The Wallace H. Coulter Department of
Biomedical Engineering
Georgia Institute of Technology
Department of Surgery
Emory University School of Medicine

Dr. Julia E. Babensee
The Wallace H. Coulter Department of
Biomedical Engineering
Georgia Institute of Technology

Dr. Clifford L. Henderson
School of Chemical and Biomolecular
Engineering
Georgia Institute of Technology

Dr. Larry V. McIntire
The Wallace H. Coulter Department of
Biomedical Engineering
Georgia Institute of Technology

Dr. Athanassios Sambanis
School of Chemical and Biomolecular
Engineering
Georgia Institute of Technology

Date Approved: December 5, 2008

ACKNOWLEDGEMENTS

I would first and foremost like to thank my research advisor, Dr. Elliot Chaikof, for his support and inspiration during my time as a graduate student in his lab. Dr. Chaikof has has taught me to think beyond the obvious or incremental and to persevere when saboteurs abound, and for this I am greatful. I would also like to thank the members of the thesis reading committee, Dr. Babensee, Dr. Henderson, Dr. McIntire, and Dr. Sambanis for their guidance and insightful comments that have helped shape the face of this dissertation. I also thank members of the Chaikof lab, both past and present, for their advice, assistance, effort, and camaraderie. In particular, I would like to thank Dr. Wanxing Cui who, without, the research in this dissertation would not be possible. Moreover, I would like to acknowledge Dr. Carolyn Haller for always being willing to open her office or put down her pipet to serve as a sounding board for my thoughts.

I am forever grateful for the love and support of my family, in particular my parents, John and Debbie, sister, Nessa, and grandparents Mary, Marge, and Tanner who always believed in my endeavors, but never asked for anything more than my happiness. I also thank the teachers and mentors who have initiated and propagated my enthusiasm for science and research: Nannette Weinhold, Joel Kuper, Mary Omberg, Joe McGuire, and Michelle Bothwell. I would also like to thank the many friends I have made along this journey; it is a great blessing that there are too many people to acknowledge individually, but I thank you all for your friendship and for the memories. In particular, I would like to thank Mary Millner for her continued and unwavering love and support throughout graduate school.

I would also like to acknowledge the Whitaker Foundation and the Medtronic Foundation for financial support received through graduate fellowships.

TABLE OF CONTENTS

LIST OF TABLES

LIST OF FIGURES

xi

by-layer manner (C) demonstrate little or no fluorescence, indicating that alginate deposition is polycation-dependent. After assembly of eight bilayers, alginate incorporated into PEM films is localized predominantly on the extracellular surface of islets (D). By contrast, fabrication of a single PLL/alginate bilayer results in intercellular internalization of alginate by peripheral cells (E,F). Cell nuclei were identified via Hoechst staining (scale bar: A,B,C,E = 50 μm; D,E = 10 μm).

Figure 3.7. Polyelectrolyte multilayer (PEM) films assembled using PLL$_M$-g[x$_c$]-PEG$_n$ copolymers and alginate demonstrate unique growth profiles on planar substrates. Solid-state UV-vis spectroscopy was used to monitor film growth on quartz substrates. (A) Example of absorbance spectra recorded after the second PLL$_M$-g[x$_c$]-PEG$_n$ (e.g., P12P24[4]) incubation and every other incubation thereafter through twelve depositions. (B) Absorbance values at 495 nm, corrected to account for differences in degree of labeling, as a function of layer number (mean ± SD). Use of P12P4[2.5] (●), P12P12[3.3] (○), and P12P24[4] (▼) as polycations resulted in layer-by-layer film growth with a non-linear, exponential-like growth pattern. By contrast, film growth using P45P4[1.7] (△) stagnated after six bilayers. After incubation of all films in 5 M NaCl for 20 minutes absorbance at 495 nm was essentially absent, indicating complete film decomposition and, hence, assembly through electrostatic interactions.

Figure 3.8. Film thickness increases with layer number and may be tailored through PLL$_{12kD}$-g[x$_c$]-PEG$_n$ properties. Ellipsometric film thickness measurements (mean ± SD) after assembly of 4, 6, and 8 bilayers using P12P24[4] (●), P12P12[3.3] (○), and P12P4[2.5] (▼) as polycations and alginate as the polyanion. Measured thicknesses and statistical analysis are provided in Table 3.4.

Figure 4.1. Cytocompatible PLL$_{12kD}$-g[x]-PEG$_n$(R) copolymers bearing biotin, hydrazide, and azido functional groups may be generated through proper control of grafting ratio and PEG chain length. (A) Islet viability after 40 m incubation with functionalized copolymers synthesized with PEG$_4$ and a grafting ratio, x, between 2.0 and 2.5. Copolymers containing hydrazide and biotin PEG head groups, R, had no discernable effect on islet viability relative to untreated controls or copolymers bearing methyl R groups (p>0.05). An azido-functionalized variant, however, induced a significant reduction (p<0.01) in islet viability (A,C). Increasing the length of PEG spacer from 4 to 12 repeat units significantly (p<0.05) increased islet viability to levels statistically similar to controls as well as other functionalized polymers (B, D). Bars labeled with the letter a are statistically different (p<0.01) from all other bars as well as untreated controls. Scale bars in C,D are 50 μm.

Scheme 4.1. Cell surface engineering using functionalized PLL-g-PEG copolymers. Adsorption of PLL-g-PEG copolymers functionalized with biotin, azide, and hydrazide moieties facilitates selective capture of

SUMMARY

Islet transplantation has emerged as a promising cell-based therapy for the treatment of diabetes, but its clinical efficacy remains limited by deleterious host responses that underlie islet destruction. In this dissertation, we describe the assembly of ultrathin conformal coatings that confer molecular-level control over the composition and biophysicochemical properties of the islet surface with implications for improving islet engraftment. Significantly, this work provides novel biomolecular strategies for cell surface engineering with broad biomedical and biotechnological applications in cell-based therapeutics and beyond.

Encapsulation of cells and tissue offers a rational approach for attenuating deleterious host responses towards transplanted cells, but a need exists to develop cell encapsulation strategies that minimize transplant volume. Towards this end, we endeavored to generate nanothin films of diverse architecture with tunable properties on the extracellular surface of individual pancreatic islets through a process of layer-by-layer (LbL) self assembly. We first describe the formation of poly(ethylene glycol) (PEG)-rich conformal coatings on islets via LbL self assembly of poly(L-lysine)-*g*-PEG(biotin) and streptavidin. Multilayer thin films conformed to the geometrically and chemically heterogeneous islet surface, and could be assembled without loss of islet viability or function. Significantly, coated islets performed comparably to untreated controls in a murine model of allogenic intraportal islet transplantation, and, to our knowledge, this is the first study to report in vivo survival and function of nanoencapsulated cells or cell aggregates.

Based on these findings, we next postulated that structurally similar PLL-*g*-PEG copolymers comprised of shorter PEG grafts might be used to initiate and propagate the

assembly of polyelectrolyte multilayer (PEM) films on pancreatic islets, while simultaneously preserving islet viability. Through control of PLL backbone molecular weight, PEG chain length, and grafting ratio, PLL-*g*-PEG copolymers were rendered cytocompatible and used to initiate and propagate the growth of cell surface-supported PEM films. Planar characterization of this novel class of PEM films indicated that film thickness and composition may be tailored through appropriate control of layer number and copolymer properties. Furthermore, these investigations have helped establish a conceptual framework for the rational design of cell surface-supported thin films, with the objective of translating the diverse biomedical and biotechnological applications of PEM films to cellular interfaces.

Important to the development of effective conformal islet coatings is an inherent strategy through which to incorporate bioactive molecules for directing desired biochemical or cellular responses. Towards this end, PLL-*g*-PEG copolymers functionalized with biotin, azide, and hydrazide moieties were synthesized and used, either alone or in combination, to capture streptavidin-, triphenylphosphine-, and aldehyde-labeled probes, respectively, on the islet surface. Additionally, PEM films assembled using alginate chemically modified to contain aldehyde groups could be used to introduce hydrazide-functionalized molecules to the islet surface. Hence, modified film constituents may be used as modular elements for controlling the chemical composition cell and tissue surfaces.

Finally, we report a strategy for tethering thrombomodulin (TM) to the islet surface. Through site-specific, C-terminal biotinylation of TM and optimization of cell surface biotinylation, TM could be integrated with the islet surface. Re-engineering of islet surfaces with TM resulted in an increased catalytic capacity of islets to generate the powerful anti-inflammatory agent, activated protein C (APC), thereby providing a facile strategy for increasing the local concentration of APC at the site of transplantation.

CHAPTER 1

Introduction

1.1. CENTRAL HYPOTHESIS AND OBJECTIVES

Clinical islet transplantation remains limited, in part, by early islet destruction and primary non-function, processes largely facilitated by pernicious inflammatory responses triggered by islet-derived procoagulant and proinflammatory mediators. Under normal physiological conditions, endothelial cells lining the extensive microvasculature of pancreatic islets provide a natural barrier to thrombosis and inflammation [1]. During islet isolation and culture, however, this barrier is disrupted [1, 2], exposing procoagulant and inflammatory mediators while simultaneously stripping away endothelial cell-derived regulators of inflammation. In this regard, we have postulated that the native endothelium offers a paradigm for re-engineering the islet surface. The ***central hypothesis*** of this work is that conformal coatings assembled on the surface of individual islets may be designed to provide barriers to thrombosis and inflammation. Specifically, we have postulated that layer-by-layer (LbL) polymer self assembly can be used to generate ultrathin ***physical barriers***, and that incorporation of thrombomodulin will provide a ***biochemical barrier*** through its capacity generate activated protein C, a potent inhibitor of thrombosis and inflammation. The ***objectives*** of the work described in this dissertation were to ***i)*** design cytocompatible conformal islet coatings of diverse architecture and properties through a process of LbL polymer self assembly, ***ii)*** devise general strategies for immobilizing or otherwise integrating anti-coagulant and anti-inflammtory molecules into LbL thin films, and ***iii)*** develop a strategy to tether thromobomodulin to the surface of islets. Resultant to fulfillment of these objectives is the development of novel biomolecular strategies for cell surface engineering.

1

1.2. BACKGROUND[†]

The design characteristics of conformal coatings for intraportal islet transplantation are dictated by an intent to limit the deleterious effects of thrombosis and inflammation, and must therefore be governed by an understanding of the pathophysiologic mechanisms underlying these processes as well as a recognition of the challenges inherent to islet encapsulation and conformal coating. Accordingly, background information relevant to the design of anti-inflammatory conformal barriers is presented in three key areas. First, the pathophysiology of thrombotic and inflammatory responses that facilitate early islet destruction during intraportal islet transplantation is discussed. Next, limitations of existing approaches to islet encapsulation and conformal coating are reviewed. Finally, emerging approaches to improve islet engraftment through attenuation of thrombotic and inflammatory responses are highlighted.

1.2.1. Pathophysiology of Thrombosis and Inflammation in Intraportal Islet Transplantation

Insulin dependent diabetes mellitus (IDDM) afflicts nearly 4 million people in North America and Europe [3], including over 120,000 people under the age of 19 in the United States, making IDDM one of the most frequent chronic childhood diseases in the US [4]. Islet transplantation has long been conceived as a promising treatment for type 1 diabetes [5-9]. Despite advantages over whole pancreas transplantation [10-16], between 1990 and 1998 more than half of islet allografts failed within two months and

---

[†] Reproduced in part from Wilson JT and Chaikof EL. *Thrombosis and Inflammation in Intraportal Islet Transplantation: A Review of Pathophysiology and Emerging Therapeutics.* Journal of Diabetes Science and Technology 2008;2:746-759., and Wilson JT and Chaikof EL. *Challenges and Emerging Technologies in the Immunoisolation of Cells and Tissues.* Advanced Drug Delivery Reviews 2008;60:125-145.

only 8% of patients remained insulin independent beyond one year [17]. In 2000 Shapiro and colleagues introduced the Edmonton Protocol, which combined transplantation of freshly isolated islets with a steroid-free immunosuppressive regimen [18]. During this procedure islets are infused percutaneously into the hepatic portal vein (intraportally) where they travel to and ultimately lodge within the liver sinusoids. In their seminal report, 7 of 7 patients remained insulin independent one year post-transplantation [18]. This success has reinvigorated widespread interest in islet allotransplantation, and since 2000 more than 500 patients worldwide have received islet transplantation using the Edmonton Protocol and slight modifications thereof [17]. Importantly, at the three leading islet transplant centers, 90% of patients receiving islet transplants remain insulin independent by one year [19] and Shapiro and colleagues have reported 60% insulin independence at three years [17], rates comparable, albeit lower, to those observed in whole pancreas transplantation [16].

Islet transplantation is compromised by early islet destruction. Despite such marked improvements, islet transplantation remains limited, in part, by the need to transplant islets from 2-4 donor organs, often in separate infusions, to reverse diabetes in a single patient [12, 18, 20-23], further burdening a limited donor islet source [24], increasing health care costs [16], and the incidence of procedural complications. Though single-donor islet transplantation has been reported [25], in a recent international trial of the Edmonton Protocol, 44% of patients required three islet infusions, less than half of which remained insulin independent at one year [26]. It has been estimated that a normal human pancreas contains approximately 500,000 islet equivalents (IEQ) [23], only 10-20% of which appear to be necessary to maintain euglycemia [27]. Currently, patients receive ~10,000-12,000 IEQ/kg (~700-850 thousand IEQ for a 70 kg person), nearly twice the number in a normal pancreas and substantially more than should be

3

required to maintain insulin independence [18, 23, 27]. This discrepancy suggests that transplanted islets are functionally impaired and/or fail to engraft. Indeed, metabolic challenges after transplantation indicate that the functional capacity of transplanted islets is only 20-40% of that of a non-diabetic person even in insulin independent islet recipients [28], and it has been estimated that as few as 10-20% of infused islets survive clinical islet transplantation [23]. This is supported by animal models, whereby 50-70% of transplanted islets are lost in the immediate post-transplant period [29-31]. Importantly, rates of insulin independence drop to ~10% five years post-transplant [32], and it has been suggested that early islet destruction results in engraftment of a limited islet mass that becomes exhausted with long term metabolic demands [16, 31, 32].

Early islet destruction and primary non-function are mediated by innate inflammatory responses. Despite being transplanted across identical auto- and allo-immune barriers, the extent of graft destruction is significantly greater in islet transplantation than in whole pancreas transplantation. This is perhaps most clearly illustrated in experimental models of *syngeneic* islet transplantation into *non-autoimmune* diabetic mice [31, 33, 34]. Even under such ideal transplantation conditions, islet insulin content and function are significantly compromised [34, 35], and an estimated 60% of transplanted islet tissue is lost within 3 days post transplantation [31] by both necrotic and apoptotic mechanisms [31, 33], demonstrating that *early* islet destruction is not allo- or autoantigen-specific. By contrast, in the absence of immunosupression, allografted islets that survive such initial inflammatory insults are destroyed by *specific* immune responses ~7-22 days later (i.e., allorejection) [36-40]. While a number of factors likely contribute to early islet destruction in the immediate post-transplant period, including delayed and insufficient revascularization of the graft [41], ischemia-reperfusion injury [42], glucose and lipotoxicity [43, 44], compelling

4

evidence has emerged that early islet destruction is largely mediated by innate inflammatory responses. Animal models of islet transplantation have demonstrated significant inflammation at the graft site characterized by activation of portal vein endothelial cells (ECs) [45], intense infiltration of leukocytes into and around islets [37, 45-47], and elevated levels of proinflammatory mediators [45, 47-50] that adversely effect β-cell viability and function [49, 51, 52]. Unlike conventional implantable materials, which are largely passive bystanders of inflammatory responses and subsequent device failure [53], islets directly contribute to their own destruction via expression and secretion of bioactive mediators that initiate and propagate inflammatory and procoagulant pathways. This is perhaps best illustrated by Bottino et al. who demonstrated that intraportal infusion of islets, but not equivalently sized glass microspheres, triggered increased cytokine production in the immediate post transplant period [48].

Islets initiate activation of coagulation cascades. Recent evidence indicates that deleterious inflammatory responses may be generated, in large part, by an instantaneous blood-mediated inflammatory reaction triggered by islets in direct contact with blood [3, 54-56] (Figure 1.1). Korsgren and colleagues have demonstrated that tissue factor (TF), the primary physiological initiator of the coagulation system [57], is expressed by and released from β and α cells of isolated islets [55]. TF initiates the extrinsic arm of the coagulation pathway by interacting with factor VIIa, catalyzing the conversion of factor X to its active form, fXa, resulting in conversion of prothrombin to thrombin. Indeed, islets incubated in non-anticoagulated blood in vitro induced a significant thrombotic response, as evidenced by fibrin clots surrounding islets and increased levels of thrombin-antithrombin complex (TAT), prothrombin fragments 1 and 2, and fXIa-antithrombin complex [54, 55]. Platelets were also activated, as evidenced by reduced platelet counts and release of β-thromboglobulin from alpha granules [55],

5

further amplifying thrombin generation and promoting aggregation of platelets on the islet surface, presumably through interactions between platelet adhesion molecules and islet-derived extracellular matrix proteins [58]. Interestingly, in a porcine allograft model, Lamblin et al. observed elevated TAT upon islet transplantation, but found no such effect when a similar volume of polystyrene beads was infused, demonstrating the cell-specific nature of the thrombotic response [59]. Perhaps more compelling, in nine patients undergoing clinical islet transplantation, serum levels of prothrombotic markers (TAT, fVIIa-antithrombin, and D-dimer) were significantly elevated 15 minutes to 24 hours post-transplantation [56], and patient serum levels of cross-linked fibrin degradation product have been shown to correlate with pre-transplant levels of TF expression by islets [60].

Islet-initiated coagulation contributes to inflammatory responses. Though perhaps better known for its role in coagulation, thrombin also acts as a conductor of cellular responses during inflammation [61]. Thrombin can trigger expression of endothelial cell (EC) adhesion molecules [61-63], and stimulate EC production of the proinflammatory cytokines IL-6 and IL-8 as well as platelet activating factor, a potent neutrophil activator [62]. Furthermore, thrombin acts as a chemoattractant [64] and directly triggers platelet activation, resulting in the release of alpha-granule chemokines and expression of P-selectin, thereby attracting neutrophils and monocytes to the portal bed and promoting their arrest and activation [62, 65, 66].

In accord with the known effector functions of thrombin, EC activation (ICAM-1, E-selectin, P-selectin expression), neutrophil infiltration, and increased production of cytokines and inflammatory mediators (IL-1β, TNF-α, IL-6, IFN-γ, NO) are observed 6-12 hours after islet transplantation in syngeneic animal models, resulting in significant islet apoptosis within 24 hours [45, 46, 67]. Though monocytes, Kupffer cells, portal vein ECs, and hepatocytes likely participate in generation of this cytoxic inflammatory milieu

6

[52], evidence is emerging that neutrophilic granulocytes act as the principle effector cell in early islet destruction [46, 68]. Yasunami et al. have recently demonstrated that IFN-γ produced by neutrophils plays a crucial role in early islet destruction and that injection of antibodies against neutrophil surface markers Gr-1 and CD11b dramatically attenuates this effect [46]. Interestingly, despite use of a simplified in vitro model of islet-blood contact, Moberg et al. have demonstrated that neutrophils begin to infiltrate islets within 15 minutes, and are the predominant the cellular infiltrate [68]. Significantly, addition of Melagatran, a low molecular weight thrombin inhibitor, has been shown to reduce neutrophil infiltration while preserving islet morphology [69]. Hence, islet-initiated thrombin generation appears to contribute significantly to the initiation and/or elaboration of inflammatory responses implicated in islet destruction and primary non-function.

Islet-derived inflammatory mediators contribute to thrombotic and inflammatory responses. While blood-mediated responses play a critical role in islet destruction, evidence of inflammation and islet death in syngeneic animal models of islet transplantation into the kidney capsule suggest that direct islet-blood contact is not a prerequisite for initiation of inflammatory responses [31, 33, 47, 49, 69]. As a result of metabolic and mechanical stress associated with isolation and culture, isolated islets have been shown to express and/or release an array of inflammatory mediators [1, 36, 52, 70-81] which may trigger or exacerbate thrombotic and inflammatory response post-transplantation (Figure 1.1). Indeed, an inverse correlation between pre-transplant expression levels of inflammatory mediators and islet engraftment has been observed in both animal models [74, 78] as well as in clinical islet transplantation [60, 79]. Significantly, Piemonti et al. have demonstrated increased rates of insulin independence and significant reduction in insulin requirements in patients who received islet grafts expressing low levels of monocyte chemoattract protein-1 (MCP-1) [79]; similar results

have been reported in syngeneic murine models [78]. Soluble factors released from islets have been shown to activate portal vein ECs [45, 82] and Kupffer cells [52, 83], further contributing to elaboration of inflammatory responses. Indeed, in an animal model of islet transplantation, transient inhibition of Kupffer cells has been found to reduce levels of proinflammatory mediators (TNF-α, IL-β, NO) 3-6 hours post transplantation, resulting in improved islet engraftment [48]. While the contribution of islet-derived inflammatory mediators in early islet destruction has yet to be fully elucidated, particularly in intraportal islet transplantation where coagulation-mediated inflammatory events are presumed to dominate, their role in potentiating the inflammatory response must be considered.
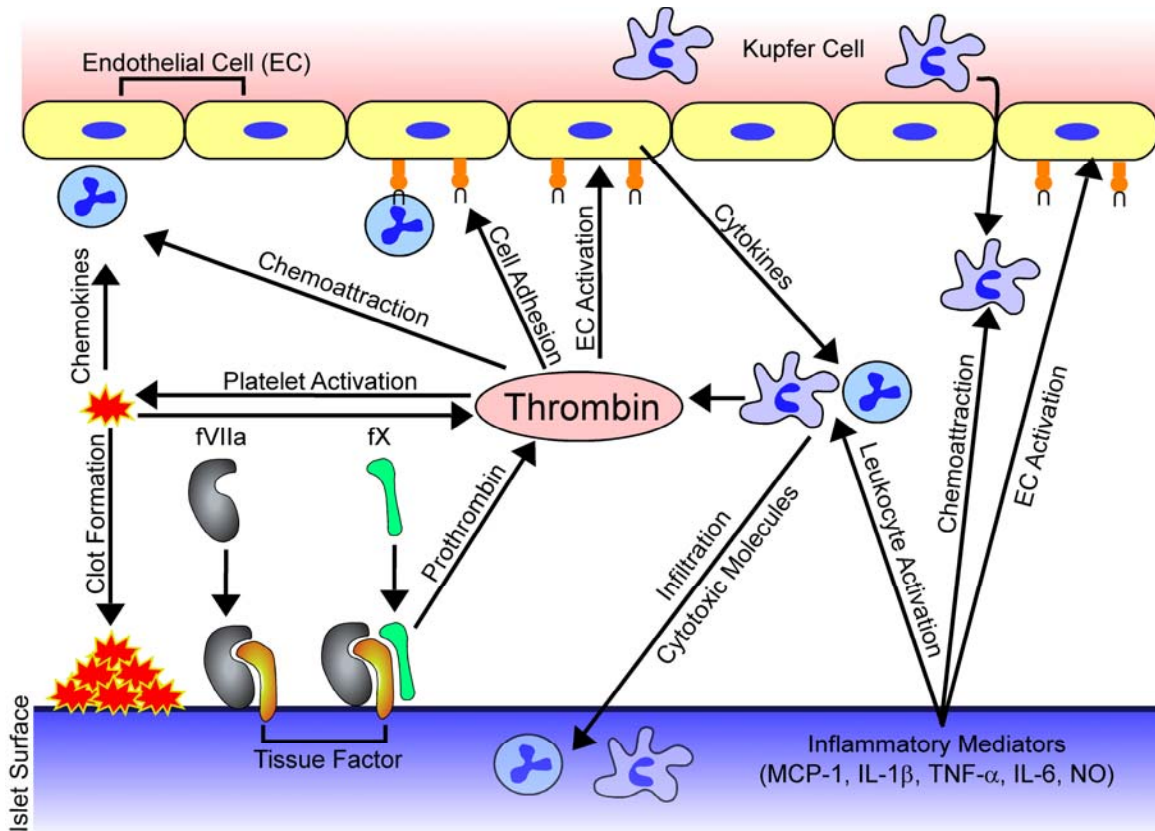
Figure 1.1. Mechanisms of thrombosis and inflammation in intraportal islet transplantation. Tissue factor expressed on islets interacts with factor VIIa (fVIIa), activating factor X (fX) which converts prothrombin to thrombin, a key mediator of thrombotic and inflammatory events. Local thrombin generation triggers platelet activation and adhesion, further amplying coagulation cascades, and ultimately entrapping islets within fibrin clots. Furthermore, thrombin acts as a chemoattractant and can trigger expression of endothelial cell adhesion molecules, promoting migration of neutrophils, monocytes, and Kupfer cells to the portal bed. Additionally, islets release a number of inflammatory mediators including MCP-1, IL-1β, TNF-α, IL-6, and nitric oxide, which may trigger or exacerbate thrombotic and inflammatory responses post-transplantation through activation of endothelial cells and attraction and activation of leukocytes.

1.2.2. Current Challenges in Islet Encapsulation and Conformal Coating

Since the pioneering work by Chick et al. in the development of a bioartificial pancreas [84] and Lim and Sun's introduction of alginate-encapsulated islets [85], decades of extensive research has focused on the design and application of immunoisolation devices capable of protecting transplanted allo- and xenogenic cells from the host, while facilitating adequate transport of oxygen, nutrients, and secreted therapeutic molecules. While a variety of polymeric and inorganic matrices and membranes have been utilized to produce immunoisolation devices of diverse physiochemical properties and geometries [86], which include vascular perfusion devices, avascular diffusion chambers, and macrocapsules [87, 88], to date, most strategies have employed microcapsules consisting of cells or cell clusters entrapped within a spherical semi-permeable membrane, an inherently more favorable geometry for diffusive nutrient transport that can be implanted with minor surgery [87, 88]. While the principle objective of the work presented in this dissertation is not to generate *immuno*protective barriers per se, the lessons afforded by earlier efforts directed towards islet microencapsulation will prove to be highly valuable in the design of conformal coatings for intraportal islet transplantation.

Mass transport limitations in microencapsulation. Although the high surface-to-volume ratio provided by microencapsulation considerably improves mass transport relative to macrocapsules or extravascular diffusion chambers [14, 87], the relatively large size of conventional microcapsules, typically 400-800 μm in diameter, continues to impose transport limitations that, if not accounted for, may adversely effect cell survival and function. Experimental evidence and mathematical models demonstrate that oxygen concentration decreases radially within cylindrical or spherical devices due to the consumption of oxygen by the encapsulated cells [89-92]. Therefore, if oxygen levels

10

are insufficient at the site of transplantation, cell density must be reduced as device diameter increases to minimize hypoxia of centrally located cells. Even sublethal levels of hypoxia can have deleterious effects on ATP-dependent cell functions, such as insulin secretion [93] and may also induce expression of inflammatory mediators [1]. Consequently, the number of cells that may be transplanted within a given microcapsule is limited both by device size and the related metabolic profile of the donor cells, often leading to an increase in cell transplant volume and an associated increased incidence of device defects [94] and surgical risk [95].

Effective cell-based therapy often relies on the ability of transplanted cells to respond to physiological stimuli in a concentration- and time-dependent manner [96]. The characteristic time for diffusion through a sphere of radius, R, scales as R^2/D, where D is the diffusivity of the solute through the encapsulation matrix and/or permselective membrane [97]. Therefore, cells in the center of the device will experience a given solute concentration at a later time than those on the periphery, leading to a lag in response time [92]. Moreover, depending on the pore size and other physiochemical properties of the immunoisolation membrane and cell immobilization matrix, the diffusivity of important solutes such as glucose, insulin, and oxygen may be substantially less than their diffusivity in water [92, 98-101], further delaying responses as compared to those observed for non-encapsulated tissue. This is perhaps most clearly illustrated by microencapsulated islets, where the distance between the capsule surface and outer cell layer of the islet may be on the order of 100-400 μm, creating a void space which glucose and insulin must cross prior to transport in or out of the device. Indeed, delayed in vitro insulin secretion in responses to step changes in glucose have been observed for a variety of different capsule formulations [85, 102-105]. Decreasing capsule size has been shown to minimize this delay [106-108].

11

Arguably more detrimental than diffusion limitations inherent to conventional microcapsules are constraints imposed by the transplant sites necessary to accommodate the volume of microencapsulated cells. For example, current clinical islet transplantation protocols require ~600-700 thousand islets, a volume of roughly 5-10 ml [18]. In contrast, a current clinical trial using islets entrapped in 500 μm microcapsules requires a transplant volume of 50 ml [109], representing approximately a 5-10 fold increase in transplant volume. Consequently, most microencapsulated cells have been transplanted into sites that have a relatively limited vascular supply, such as the omentum [110, 111] or peritoneal cavity [109, 112-114]. The anatomy of the peritoneal cavity does not facilitate instantaneous transport of insulin or glucose to and from the systemic circulation, as insulin must be absorbed by the peritoneum and extracted by the liver [115, 116]. As such, insulin production within the peritoneal cavity results in a delayed systemic response relative to intraportal administration [117, 118], with impaired metabolic control. In response to a meal challenge, Tatarkiewicz et al. observed blunted C-peptide concentrations in animals transplanted with *non-encapsulated, syngeneic islets* in the peritoneal cavity, indicating that transplantation site is critical to proper maintenance of metabolic processes [103]. Though successful reversal of diabetes has been achieved despite impaired insulin and C-peptide responses [103, 104, 119], it is unclear whether metabolic control will be sufficiently robust to minimize the chronic complications of diabetes [120-122].

Viability and function of microencapsulated cells transplanted into relatively avascular sites may be further exacerbated by partial pressures of oxygen which are 40% of that found in arterial circulation [89]. Microencapsulated islet *autografts* retrieved from the peritoneum upon graft failure often have necrotic cores [123], a hallmark of hypoxia [1]. Interestingly, core necrosis may be observed even in the absence of

encapsulation [123], corroborating previous findings that the peritoneal cavity provides a sub-optimal environment for islet transplantation [124-126].

Transplantation of microencapsulated islets into the portal bed. Though several clinical trials and large animal studies have demonstrated the potential efficacy of intraperitoneally transplanted encapsulated islets [109, 112-114, 127], the International Islet Registry reports that, compared to other sites, transplantation of islets into the portal vein is associated with the highest success rate one year after transplantation [128]. Thus, the portal bed remains the clinically preferred site for islet transplantation [10, 18, 19]. While, as discussed previously, direct islet-blood contact has been shown to mediate thrombosis [54-56], the portal vein offers a oxygen and nutrient rich environment and provides physiologically normal drainage of insulin, minimizing delayed insulin secretion in response to glucose. However, most conventional microcapsules are not suitable for transplantation into microvascular beds due to their large diameter [129-131]. Intraportal infusion of 420 µm microparticles has been shown to result in dangerous elevations of intraportal pressure and, in some instances, increased mortality in animal models [130]. Bottino et al. have observed impaired hyaluronic acid clearance after intraportal infusion of both islets and an equivalent volume of microparticles, indicating that portal vein endothelial cells are injured in response to particle infusion in a non-specific manner [48]. Schnedier et al. have recently demonstrated *impaired* engraftment of islets encapsulated in 350 µm alginate/Ba^{2+} micrcapsules transplanted into the portal vein compared to non-encapsulated controls, apparently due to occlusion of small and medium sized portal venules and subsequent islet hypoxia [131]. Clearly, encapsulation strategies for transplantation of cells into microvascular beds must minimize transplant volume.

13

An obvious but non-trivial approach to improving transport properties of microcapsules is to produce smaller capsules by optimizing the process parameters used in traditional microcapsule fabrications. Several groups have addressed the feasibility of intraportal transplantation of microcapsules slightly smaller than conventional microcapsules. Hallé and colleagues have generated 300-350 μm microcapsules using a high voltage electrostatic pulse system [130, 132, 133]. Injection of 10,000 315 μm diameter microcapsules into the portal vein of rats resulted in only modest and transient increases in portal pressure [130]. Similarly, Toso et al. intraportally injected 10,000 400 μm alginate/poly(methylene-co-guanidine) hydrocholoride microcapsules per kilogram body weight. While portal pressures were elevated immediately post-implant, the increase was comparable to that observed during clinical islet transplantation and returned to normal after three months [134]. However, these [134] and other intraportally infused microcapsules [135] elicited a significant foreign body reaction. The dose of microcapsules used in both of these studies is comparable to the islet dose used in clinical islet transplantation [18], demonstrating the potential to infuse 300-400 μm capsules in vascularized sites. However, decreasing the size of alginate microcapsules from 800 to 500 μm is associated with a ~4 fold increase in the percentage of incompletely encapsulated islets [136]. Host response to even 2-10% of encapsulated islets has been shown to result in destruction of 40% of the graft [123, 137].

Conformal coatings via fluidic entrainment and interfacial precipitation. To circumvent limitations associated with random entrapment of cell aggregates within microparticles, several investigators have deposited coatings of defined thickness that conform to surface of the cell or tissue. Transplant volume is, therefore, defined only by the size of the object being coated and the thickness of the coating, significantly

14

reducing void volume while retaining the presence of a polymer barrier to provide protection.

Fluidic entrainment of polymer solution around cell aggregates followed by interfacial precipitation of the polymer has been most commonly utilized to generate conformal coatings on cell aggregates. In light of the promise and widespread use of alginate-based microcapsules, Zekorn et al. [138], and subsequently Park et al. [139], have fabricated conformal alginate hydrogel coatings on the surface of individual pancreatic islets. To accomplish this, they utilized a discontinuous density centrifugation gradient composed of a top layer of islets suspended in sodium alginate, followed by denser spacer layers composed of dextran or Ficoll, one of which contained a divalent cation ($CaCl_2$ or $BaCl_2$). During centrifugation, islets approach and deform the alginate-dextran (Ficoll) interface, entraining a film of alginate around the islet, provided the drainage between the islet and interface is sufficiently slow. When the islet and entrained alginate cross into the layer containing the divalent cation, the alginate is crosslinked, resulting in a 5-10 μm film of alginate that largely conforms to shape of the islet. Islets coated in this manner demonstrated normal biphasic insulin secretion in a dynamic perfusion assay, indicating that islet function and viability are preserved and that the thin coating prevents the lag in insulin secretion often observed with larger alginate microcapsules [138]. In a similar manner, Sefton and colleagues have used density centrifugation to coat islets [140] and HegG2 cell aggregates [141] with water insoluble poly(hydroxyethyl methacrylate-co-methyl methacrylate) (HEMA-MMA) co-polymers by interfacial precipitation, generating polymer films as thin as 1.5 μm. The non-aqueous nature of HEMA-MMA is anticipated to improve stability relative to aqueous hydrogels, which are susceptible to hydrolytic degradation. However, conformal coating of cells with HEMA-MMA results in a significant degree of cell death, owing to the need to expose cells to an organic solvent (polyethylene glycol, MW 200

15

Da) [142]. Recently, improved cell viability has been observed by decreasing coating times and pre-encapsulating cells in agarose beads prior to HEMA-MMA conformal coating to minimize exposure to non-aqueous solvents [142].

Emulsification has also been used to generate a conformal coating on islets and cell aggregates [143, 144]. Calafiore and colleagues placed islets into an alginate/polyethylene glycol (PEG)/Ficoll emulsion, whereby alginate-containing Ficoll droplets suspended in a continuous PEG phase, coalesced on the islet surface, engulfing individual islets in a layer of alginate, which was subsequently crosslinked with calcium chloride and coated with a poly(L-ornithine)/alginate bilayer [143]. This conformal barrier prevented direct cell-islet and antibody-islet contact, and did not impair insulin in response to glucose stimulation [129]. Leung et al. have recently optimized this emulsion process to minimize the incidence of incomplete and non-uniform coating, and have coated cell clusters with 20-25 µm thin films of alginate [144]. Importantly, conformally coated canine islets transplanted intraportally into a porcine model were viable and free of inflammatory reaction 15 days post transplant; however, a dense inflammatory infiltrate was observed 15 days later [145]. Nonetheless, these studies demonstrate the feasibility using conformal barriers in intravascular cell transplantation.

Selective withdrawal of one fluid through a second immiscible fluid has recently been used to encapsulate pancreatic islets [146]. Islets suspended in PEG-diacrylate were layered onto a more dense immiscible oil phase, and fluid was withdrawn through a tube placed immediately below the interface. At an appropriate flow rate, the PEG-diacrylate solution, containing islets, was entrained in a thin spout within the oil phase. When the diameter of an islet is greater than that of the spout, surface tension causes the spout to break at both ends, leaving a thin layer of polymer solution around the islet. PEG-diacrylate is subsequently photocrosslinked, resulting in ~10 µm thick coatings independent of the size of the encapsulated islet. The investigators found it necessary to

repeat this process in order to prevent coating defects, ultimately generating ~20 µm thick coatings. In principle, sequential coating may allow for the generation of composite coatings with each layer having independent properties designed to elicit a preferred biological response. For example, the authors cite examples in which the outer layer may contain anti-inflammatory or pro-angiogenic molecules, while the inner layer may contain molecules to improve islet function. The authors found that two-layer conformal coatings inhibited the transport of a 140 kD macromolecule and enabled normal dynamic insulin secretion in response to glucose stimulation. Despite these promising results, ~75% of islets were lost during the coating process, a problem that must be remedied in light of donor shortage for human islet transplantation. Moreover, scalability of the technique to allow for encapsulation of a clinically relevant number of islets in a timely manner must be addressed.

Conformal coating via interfacial polymerization. Conformal coating strategies have also utilized the islet surface as a template upon which coatings may be grown or chemically deposited. Hubbell and colleagues have generated ~35-50 µm thick PEG-diacrylate coatings on both porcine [147-149] and human [150] islets through a process of interfacial polymerization. In this polymerization scheme, Eosin Y, a photoinitiator, is non-specifically adsorbed to the islet surface, and islets are placed in a solution containing PEG-diacrylate and triethanolamine. Upon illumination with light, eosin Y is excited and donates an electron to triethanolamine, which initiates the free-radical polymerization of PEG diacrylate at the islet-macromer interface [148]. Through parametric optimization of key process variables, greater than 90% islet viability and encapsulation efficiency was reported [148], and conformally coated islets were shown to behave comparably to non-coated islets in a dynamic glucose perfusion experiment and intraperitoneal glucose tolerance test, respectively [147]. Preclinical trials in diabetic

17

cynomolgus moneys and baboons demonstrated function of subcutaneously transplanted conformally coated islets for up to 20 months, despite discontinuation of low dose immunosupression (cyclosporine) one month post transplant [150]. This technology is currently the basis for phase I/II clinical trials by Novocell for encapsulated human islet allografts, which began in 2005 [151]. Although patients are currently receiving transplants in a subcuateous site, the low-void volume of the graft and the high blood compatibility of PEG may also facilitate transplantation into the portal bed.

Molecular camouflage. While conformal coatings on cell aggregates offer a significant decrease in void volume relative to conventional microcapsules, cell encapsulation may, in principle, be accomplished using coatings or membranes of submicron, or nanoscale, thickness. A common approach to generating such barriers has been through immobilization of PEG chains to the cell or tissue surface, creating a molecular barrier of PEG to prevent molecular recognition between cell surface receptors and soluble ligands [13, 152-157]. This has generally been accomplished through covalent coupling of PEG to amines of cell surface proteins or carbohydrates, or by direct insertion of PEG-lipid conjugates into the cell membrane [157]. PEG is a hydrated, flexible polymer chain due to repeating, highly mobile, ether units, which allows the polymer chain to act as a steric barrier on the cell surface [158]. Through proper control of polymer chain length and surface grafting density, cell surface PEGylation has been shown to camouflage antigenic sites, alter surface charge, and attenuate cell-cell and receptor-ligand interactions [159]. In an effort to create a universal red blood cell (RBC) donor, PEGylation of RBCs has been shown to mask major and minor blood group antigens from host antibodies [154, 160, 161]. Evidence has recently emerged that conjugation of PEG to human peripheral blood mononuclear cells [153] and isolated murine splenocytes [152] can interrupt a number of receptor-

18

ligand interactions important in allorecognition, including weakening CD28-B7 costimulation, resulting in T-cell apoptosis. Furthermore, transplantation of PEGylated C57BL/6 splenocytes into lethally irradiated Balb/c mice significantly abrogated donor T-cell proliferation and improved survival rates in a model of graft versus host disease relative to non-PEGylated controls [152].

Based on such promising findings, several groups have demonstrated that PEG can be grafted to islets without compromising viability or function [155, 156, 162] and have began to explore whether or not PEG grafting provides a mechanism of preventing, or at least attenuating, host response to both allo- [163-168] and xenografts [13, 162]. Byun and colleagues have recently reported some efficacy of this strategy in a rat allograft model of islet transplantation into the kidney capsule [165-168]. In their most recent experience, islets were serially PEGylated three times in an effort to increase PEG surface density and improve uniformity [165]. In contrast to non-PEGylated controls, which all mice rejected within one week, 3 of 7 recipients transplanted with PEGylated islets provided maintenance of normoglycemia for more than 100 days without any immunosuppression. Histological evaluation demonstrated that PEGylation prevented graft infiltration by host immune cells, a protective mechanism that may be operative in intraportal transplantation as well. Similarly, Contreras et al. have used islet-surface PEGylation in a xenogenic model of intraportal islet transplantation [13]. While the authors did not monitor engraftment beyond two weeks, animals that received islets treated with PEG presented significantly better control of glucose than animals receiving non-modifed islets. PEG with a molecular weight of 5 kD performed slightly better than 2 kD PEG, and capping of surface grafted PEG with albumin proved most efficacious. Though this effect was attributed to shielding of islets from complement and xenoreactive antibodies [13, 162], it is conceivable that TF expressed on the islet

19

surface was also masked. Indeed, Scott and Hering have reported similar results in an allograft model [158].

Despite these encouraging results, it is unclear whether or not surface grafted PEG will remain stable enough to provide protection for the anticipated lifetime of the transplant. Covalently modified cell surfaces are likely to be turned over and remodeled with time due to endocytosis and/or shedding of PEG-conjugated cell surface macromolecules. Moreover, PEG on the surface of cells with a finite lifecycle is likely to be lost and replaced with fresh tissue, thereby restoring immunogenicity [158]. Lee et al. have demonstrated via avidin staining of biotinylated PEG, that PEG is present for at least one month [168], but further time points were not explored. The efficacy of PEGylation may also be limited, in part, by the lack of a defined pore structure and dependence on a steric exclusion effect to provide an immunoprotective barrier. However, the nanoscale thickness of such coatings does offer an important potential advantage relative to traditional encapsulation or conformal coating approaches. Stuhlmeir and Yin demonstrated that PEGylation of endothelial cells inhibited binding of immunoglobulins and TNF-α, and reasoned that perfusion of hearts with reactive PEG might attenuate hyperacute xenograft rejection [169]. Though in vivo results were discouraging, this study exemplifies the potential utility of nanoassembled coatings to immunoprotect individual cells within whole organs.

Early inflammatory events in the transplantation of encapsulated islets.
While conventional microencapsulation strategies and conformal coatings might be used shield islet-derived tissue factor from contact with blood, some level of inflammation is likely to persist. As discussed previously, islets produce low molecular weight inflammatory mediators capable of diffusing across most cell encapsulation membranes, potentially triggering inflammatory cell recruitment and activation [102, 119, 170-173].

20

Indeed, co-culture of isolated peritoneal macrophages and *syngeneic* islets encapsulated in alginate/PLL/alginate (APA) microcapsules mediated islet-specific macrophage activation accompanied by TNF-α and IL-1β release, suggesting that factors other than alloantigens are capable of diffusing across the capsular membrane to activate macrophages [174]. Significantly, co-culture of conformally coated islets and macrophages resulted in the production of several inflammatory mediators, including MIP-2, IL-1, TNF-α, and IL-6 [175].

Moreover, encapsulation devices also subject to the foreign body response to implanted biomaterials, a dynamic biochemical process initiated by non-specific adsorption of proteins to the material surface, followed by recruitment of neutrophils and macrophages to the implant site, and the subsequent attachment and overgrowth of the device by macrophages, foreign body giant cells, and fibroblasts [53, 176-179]. While the severity of foreign body responses to cell encapsulation devices is dependent on transplantation site and material properties, such as surface charge, porosity, roughness, surface chemistry and free energy, and implant size [176], this generalized response has been observed on a variety of microcapsules [177], including the commonly employed APA microcapsule [180, 181]. For many years, the inherent biocompatibility of materials used in encapsulation devices was implicated as the principle cause for capsular overgrowth and subsequent graft failure [182]; accordingly, many groups focused their efforts on improving the biocompatibility of immunoisolation membranes and encapsulation devices. Surface PEGylation has been used to improve the biocompatibility of synthetic immunoisolation membranes [183, 184], as well as APA microcapsules [185]. Use of highly purified alginate of appropriate composition has improved the biocompatibility of alginate-based microencapsulation devices [186]. The use of polycations, in particular PLL, in membrane forming processes has been shown

21

to mediate adhesion of fibroblasts and macrophages [187] and induce cytokine production [188], and, consequently, many groups have recently abandoned use of polycations in microcapsule formulations [119, 189-191]. However, several polycation-containing microcapsules have been optimized such that fibrotic overgrowth of empty capsules is minimized [105, 192-194]. Most notably, poly(L-ornithine) (PLO) and PLL containing alginate capsules are currently being utilized in clinical trials of encapsulated islets [109, 195].

While early inflammatory responses clearly play a critical role in the destruction of *non-encapsulated* islets, elegant studies by de Vos and colleagues suggest that comparable mechanisms may be active in the failure of encapsulated islet grafts as well [123, 137, 174]. Examination of encapsulated islet allografts retrieved from the peritoneum revealed that only ~10% of capsules were overgrown with fibrotic tissue [123, 137, 192, 196]; however, this was accompanied by a 40% loss of viable cells within the first 4 weeks of transplantation [123]. Notably, encapsulated islet autografts performed comparably, suggesting that graft failure was mediated by non-specific mechanisms [192, 196]. Histological evaluation indicated that activated macrophages were the predominant cell type attached to overgrown capsules, and co-culture of macrophages and encapsulated islets resulted in macrophage activation, cytokine production, and impaired islet function [123, 174]. Similarly, de Groot et al. co-cultured encapsulated islets overgrown with host cells retrieved from the peritoneum with freshly encapsulated islets at a 1:9 ratio (i.e. 10% overgrowth) [197]. Impaired insulin secretion in response to glucose, decreased beta cell replication, and increased cell necrosis occurred after 48 hours of coculture. IL-1β, TNF-α, and nitrite, a marker for nitric oxide (NO), were elevated in the culture media and analysis of mRNA expression profiles of encapsulated islets suggested that NO mediated islet damage [197]. While some immunoisolation membranes have been reported to protect cells from IL-1β and/or TNF-

22

α [102, 172], blockade of free radical diffusion is not likely. Indeed, Wiegand et al. and Chae et al. have demonstrated that, despite its short half-life, NO can destroy encapsulated islets [198, 199]. This has recently been supported by a mathematical model of free radical diffusion through a spherical matrix containing pancreatic islets [200]. Not surprisingly, depletion of macrophages improves engraftment of both encapsulated and non-encapsulated cells [48, 201]. Hence, non-immune, inflammatory responses are at least partially responsible for limited survival and function of encapsulated islets.

1.2.3. Emerging Strategies to Inhibit Thrombotic and Inflammatory Responses

Pre-transplant manipulation of islet inflammatory pathways. Through appropriate culture conditions and additives, cell signaling processes may be manipulated to downregulate expression of islet-derived prothrombotic and inflammatory mediators [75, 77, 202-205]. Use of specially formulated culture media [203] or supplementation with the vitamin nicotinamide [202] has been shown to downregulate TF and MPC-1 production by islets. Matsuda et al. have recently demonstrated that incubation of islets with the p38 pathway inhibitor, SB203580, for one hour prior to transplantation suppressed IL-1β, TNF-α, and iNOS expression by islets, markedly increasing the diabetes reversal rate after transplantation of a marginal islet mass [75]. Additionally, signaling pathways may be modulated to reduce islet susceptibility to cytokine or nitric oxide mediated damage [36, 206-209]. Pre-transplant overnight culture with the anti-inflammatory agent Lisofylline has been shown to reduce proinflammatory cytokine-induced islet apoptosis, thereby allowing insulin independence to be achieved using 30% fewer islets [208]. As islet culture and shipping are being used more

23

frequently in clinical islet transplantation [12, 21, 25, 210], supplementation of media with modulators of inflammatory pathways should provide a facile approach for abrogating islet-initiated thrombosis and inflammation.

Systemic administration of anticoagulant and anti-inflammatory agents.
While the immunosuppressive agents administered under the Edmonton Protocol are effective T- and B-cell inhibitors [18, 211], they appear to have minimal impact on *innate* inflammatory responses against islets mediated principally by neutrophils and macrophages. Therefore, adjunctive administration of anticoagulant and/or anti-inflammatory agents presents a rational strategy for improving islet engraftment. Table 1.1 summarizes notable systemic anticoagulant and anti-inflammatory therapies which have improved early outcomes in animal models of islet transplantation. Renal subcapsule transplantations have also been included as the efficacy of such therapies may translate to intraportal transplantation despite potential differences in the pathophysiology of early graft destruction. For example, pravastatin [212, 213] and 15-deoxyspergualin [214, 215] have proven effective in both kidney and intraportal transplant models. Nonetheless, a need exists to evaluate the efficacy of anti-inflammatory agents in the proper clinical context.

While anticoagulants such as melagatran [69], heparin [54], and N-acetyl-L-cysteine [216] have demonstrated efficacy in vitro, few investigations have adequately explored the efficacy of systemic anticoagulant therapies in vivo [45, 217, 218]. Contreras et al. have recently demonstrated that intravenous administration of activated protein C (APC) dramatically inhibited interhepatic fibrin deposition, portal vein endothelial cell activation, cytokine production, and leukocyte infiltration, consequently reducing the incidence of islet apoptosis and increasing the rate of conversion to euglycemia after transplantation of a marginal islet mass [45]. Interestingly, single-dose

24

administration of APC an hour prior to transplantation dramatically attenuated inflammatory events 6-12 hours later. This is particularly compelling given the relatively short half-life of APC (10-20 minutes) [219], suggesting that the portal bed may be "primed" to receive islets. Yasunami et al. have demonstrated this phenomenon through repeated administration of the glycolipid α-galactosylceramide *prior* to transplantation, a process that dramatically reduces early islet loss through inhibition of Vα14 NKT cell-dependent IFN-γ production by neutrophils [46].

In contrast to immunosuppression [211], effective inhibition of deleterious early inflammatory responses may be achieved with short-course therapy. In a murine model of intraportal islet transplantation, Satoh et al. have recently shown that islet dose may be reduced four-fold through simultaneous blockade of IL-1β, TNF-α, and IFN-γ in the four days post-transplant [50]. Similarly, short-course oral administration of Pravacol, an FDA approved cholesterol lowering drug, has been shown to reduce the number of islets required to reverse diabetes in a canine autograft model [220]. While single dose or short term therapy holds considerable promise for improving the outcome of islet transplantation, challenges remain to find therapeutics and treatment regimens that minimize adverse complications.

Localized protection through re-engineering the islet-host interface. As adverse side effects of systemic anticoagulant and anti-inflammatory therapy may limit their potential therapeutic impact, recent efforts have focused on developing strategies to *locally* attenuate thrombosis and inflammation through both passive and active mechanisms. A promising passive approach has been to block tissue factor (TF) expressed on the islet through pre-incubation of islets with site inactivated fVIIa [55] or anti-TF antibody [55, 221]. Consistent with its role as a critical initiator of inflammation in islet transplantation, TF blockade has been shown to inhibit thrombotic responses and

25

improve islet survival both in vitro [55] and in vivo [221]. As microencapsulation devices and conformal coatings may be designed prevent cell-cell contact and dramatically impede diffusion of antibodies and other macromolecules to their respective targets on the islet surface [85, 87, 88, 222], these studies lend credence to the concept of generating polymeric barriers that shield islet-associated TF.

Perhaps more importantly, several investigators have begun to explore generation of bioactive barriers to thrombosis and inflammation. Heparin, an endothelial cell surface glycosaminoglycan, provides one such biochemical barrier through its ability to enhance the capacity of cofactor II and antithrombin to inactivate thrombin. Moreover, heparin can inhibit the formation of nitric oxide through its capacity to bind superoxide disumtase [223] and has been shown to limit complement activity [224-226]. Korsgren and colleagues have recently employed biotin/avidin interactions to immobilize macromolecular heparin complexes to the surface of islets [227]. Significantly, surface heparinization of intraportal islet grafts reduced TAT production and early islet damage in an allogenic porcine model. In light of the significant thrombotic response observed after clinical islet transplantation [55, 56, 60], where heparin is delivered *systemically* during islet infusion [18, 25], these findings potentially illustrate the increased therapeutic efficacy achieved through local delivery of anticoagulants to the portal bed. Direct comparison between delivery of islet-grafted and systemic heparin will be necessary to unequivocally demonstrate this concept.

While thrombin plays a key role in directing inflammatory responses, local release of adenine nucleotides, including ATP and ADP, from activated endothelium and platelets further potentiate proinflammatory and prothrombotic events. CD39, a transmembrane protein expressed on endothelial cells, regulates these events through its capacity to catalyze the degradation of ATP and ADP to AMP [228, 229]. Dwyer et al. have recently generated transgenic mice which express human CD39 on pancreatic

islets. These islets were found to have increased ATPase activity compared to wild-type controls and a consequent capacity to inhibit islet-mediated coagulation [230]. Similarly, genetic engineering approaches have been used to induce expression of the potent anticoagulant hirudin [231] as well as the anti-inflammatory IL-1ra [232, 233], an inhibitor of IL-1β action that has improved islet engraftment when administered systemically [234]. Both genetic engineering [235] and cell surface chemistry approaches [236] have been used to display Fas ligand (FasL) on the islet surface, a strategy which could improve early outcomes of islet transplantation by local induction of neutrophil and macrophage apoptosis via the Fas-FasL pathway [237, 238].

Recent efforts have also focused on integrating anti-inflammatory capabilities into cell encapsulation devices. Loading of microcapsules with anti-inflammatory molecules, for example dexamethasone [239], offers a simple approach, but may be limited by undesirable release kinetics and/or cytotoxic intracapsular concentrations. Co-encapsulation of cells and drug delivery vehicles offers a rational alternative for controlled delivery of anti-inflammatory agents. Luca et al. co-encapsulated cellulose acetate microspheres (30-70 µm) containing the antioxidant vitamin D3 with rat islets in alginate/PLO microcapsules [240]. Similarly, Ricci et al. found that microcapsules charged with 5 µm polyester microspheres releasing the non-steroidal anti-inflammatory drug ketoprofen reduced the foreign body response to polycation coated microcapsules [241].

Encapsulated cells may be further protected through immobilization of cells or molecules that scavenge, inhibit, or metabolize cytotoxic molecules that diffuse across the barrier. Wiegand et al. have demonstrated that coencapsulation of islets with autologous erthyrocytes within alginate capsules provided nearly complete protection from macrophage-mediated cell lysis due to the capacity of erthyrocytes to scavenge NO and/or convert it to nitrate [199]. Recently, Chae et al. have extended this concept,

replacing erthyrocytes with hemoglobin crosslinked with PEG. APA capsules containing crosslinked hemoglobin protected rat islets and RINm5F insulinoma cells from nitric oxide mediated cellular damage [198]. Significantly, after transplantation of a suboptimal mass of encapsulated islet xenografts these microcapsules were found to prolong normoglyemia and improve glucose clearance relative to capsules formulated without crosslinked hemoglobin [242]. While this effect may have also been mediated by improved oxygen tension in the capsule [242, 243], this study exemplifies the potential efficacy of actively anti-inflammatory cell encapsulation devices.

Table 1.1. Anti-inflammatory and anticoagulant agents for improving islet engraftment in vivo

Therapeutic Agent	Animal Model	Tx Site	Treatment Regimen	Proposed Mechanism(s)	Ref.
anti-IFN-γ mAb	Mouse iso & allo	Liver	IP (d 0,2,4)	IFN-γ blockade	[50]
anti-IL-1β mAb	Mouse iso & allo	Liver	IP (d 0,2,4)	IL-1β blockade	[50]
anti-TNF-α mAb	Mouse iso & allo	Liver	IP (d 0,2,4)	TNF-α blockade	[50]
acetylsalicylic acid	Rat to mouse	Kidney	Oral (daily)	Inhibition of COX-2 and NF-κB, $\uparrow$ anti-inflammatory cytokine production	[160]
IL-1ra (Anakinra)	Rat to mouse	Kidney	IP (d -1, 0, 4h)	Inhibition of IL-1 action	[45]
activated protein C	Mouse iso	Liver	IV (-1 h)	Inactivation of tVa and tVIIIa, fibrinolysis, anti-apoptotic, NF-κB inhibition	[220]
pravastatin (Pravacol)	Canine auto	Liver	Oral (d -2 to 13)	Inhibition of Ras production, suppression of macrophages, neutrophils, NK cells	[213]
pravastatin (Pravacol)	Mouse iso	Kidney	Oral (d 0-14)	Inhibition of Ras production, suppression of macrophages, neutrophils, NK cells	[217]
low MW dextran sulfate	Porcine to mouse*	Liver	IV (-10 m, d 1-6)	Inhibition of complement and coagulation	[36]
α1-antitrypsin	Mouse allo	Kidney	IP (d -1, 1x/3 d)	Serine protease inhibition, inhibition of neutrophil elastase, inhibition of cytokines	[244]
S-methyl-isothiourea	Porcine to rat*	Liver	SC (7 d continuous)	Inhibition of iNOS, hepatic NO generation	[244]
S-(2-aminoethyl)-isourea	Porcine to rat	Liver	SC (7 d continuous)	Inhibition of iNOS, hepatic NO generation	[244]
4-phenylbutyrate	Mouse iso	Kidney	Oral (d -2 to 7, 2x/d)	Inhibition of IL-1β production	[245]
α-galactosylceramide	Mouse iso	Liver	IP (d -15, -11, -7)	Inhibition of IFN-γ by NKT cells	[46]
anti-tissue factor mAb	Primate allo	Liver	IV (- 10 to 20 m)	Tissue factor blockade	117]
Nicotinamide	Rat iso	Liver	IP (daily)	Inhibition of NO-mediated toxicity	[246]
15-deoxyspergualin	Mouse iso	Kidney	IP (d 0-4)	Inhibition of macrophage function, inhibition of NF-κB dependent cytokine production	[214]
15-deoxyspergualin	Primate allo	Liver	IV (-4 h to d 14)	Inhibition of macrophage function, inhibition of NF-κB dependent cytokine production	[215]

IP: intraperitoneal. IV: intravenous. SC: subcutaneous. iso: isograft. allo: allograft. auto: autograft. *athymic animals

CHAPTER 2

Layer-by-Layer Assembly of a Conformal Nanothin Poly(ethylene glycol) Coating for Intraportal Islet Transplantation[‡]

2.1. INTRODUCTION

Islet transplantation has emerged as a promising treatment for diabetes [26]. However, widespread clinical application of islet transplantation remains limited, in part, by the deleterious side effects of immunosuppressive therapy necessary to prevent host rejection of transplanted cells [247]. Decades of extensive research have led to the development of semipermeable microcapsules capable of protecting donor cells from the host immune system while allowing transport of glucose, insulin, and other essential nutrients [85, 87, 248]. To date, most microencapsulation approaches have employed 400-800 μm diameter microcapsules of diverse composition, formed via various drop generating processes, to randomly entrap 50-250 μm diameter islets [87, 182, 222]. Unfortunately, the relatively large size of conventional microcapsules imposes consequential mass transport limitations, and produces transplant volumes not suitable for infusion into the portal vein of the liver [129-131], the clinically preferred and currently most successful site for islet transplantation [26, 128]. Consequently, most microencapsulated islets are transplanted into sites with a limited vascular supply, such as the omentum [111] or peritoneal cavity [109, 113, 114], which ultimately contributes to

---

[‡]Reproduced with permission from Wilson JT, Cui W, Chaikof EL. *Layer-by-layer assembly of a conformal nanothin PEG coating for intraportal islet transplantation.* Nano Letters 2008;8:1940-1948. Copyright 2008 American Chemical Society.

cell hypoxia and subsequent graft failure [137]. Therefore, encapsulation strategies for intraportal islet transplantation must minimize capsule void volume.

To reduce capsule size, several investigators have developed approaches to deposit coatings of defined thickness that conform to the surface of individual islets [141, 145, 146, 148]. Transplant volume is, therefore, defined only by the size of the islet and the thickness of the coating, significantly reducing void volume while retaining the presence of a protective polymer barrier. Such conformal coatings have been fabricated using a number of processes including emulsification [145], discontinuous gradient density centrifugation [141], selective withdrawal [146], and interfacial polymerization [148] to generate 5-50 μm thick polymeric coatings. Attempts to further reduce coating thickness often lead to incomplete encapsulation or coating defects. Additionally, islet loss [146] and limited process scalability [141] are obstacles that must be addressed to coat a clinically relevant number of islets.

Layer-by-layer (LbL) polymer self assembly has emerged as an attractive alternative to traditional thin film fabrication techniques due to its ability to generate films of nanometer thickness on chemically and geometrically diverse substrates [249-251]. Of particular relevance to cell encapsulation, film properties may be tailored to inhibit molecular recognition between complementary molecules on opposite sides of films. For example, Caruso et al. assembled multilayer films of poly(sodium styrenesulfonate) and poly(allylamine hydrochloride) on the surface of catalyase crystals to protect the encapsulated enzyme from protease degradation [252]. Similarly, Hubbell and co-workers have assembled alginate/poly(L-lysine) films on gelatin to limit cell adhesion to the proteinaceous surface [253], while Thierry et al. have coated deendothelialized blood vessels with chitosan/hyaluronic acid films to inhibit platelet deposition [254]. Moreover, through proper control of film constituents, multilayer films may also be used to elicit specific biochemical responses. Enzymes and other proteins [255, 256], DNA [257], lipid

31

vesicles [258], drug-containing nanoparticles [259], and polymers covalently functionalized with bioactive motifs [260, 261] have been used as film components to control the local biochemical milieu. Such capabilities hold considerable promise for generating biologically active cell and tissue coatings with the potential to abrogate deleterious inflammatory and immune responses to encapsulated islet grafts [222]. All told, LbL polymer self assembly represents a rational approach for coating cells and cell aggregates with nanothin films of tailored surface chemistry, permeability, and bioactivity. In this report, we describe a nanothin, PEG-rich conformal coating that can be assembled on individual pancreatic islets via a process of layer-by-layer polymer self assembly. This research establishes an important step towards the design nanoassembled structures for cell encapsulation and surface modification, and importantly, to our knowledge, is the first study to report in vivo survival and function of nanoencapsulated cells or cell aggregates.

2.2. MATERIALS AND METHODS

Film components. Poly(L-lysine hydrobromide) (PLL, MW 15-30 kD), FITC-labeled PLL (FITC-PLL, MW 15-30 kD), poly(allylamine hydrochloride) (PAH, MW 15 kD), poly(diallyldimethylammonium choloride) (PDDA, MW 200-350 kD), protamine chloride, poly(sodium 4-styrenesulfonate) (PSS, MW 70 kD), streptavidin (SA), Cy3-labeled SA (Cy3-SA), and FITC-labeled SA (FITC-SA) were purchased from Sigma-Aldrich (St. Louis, MO). Sodium alginate (UP LVM) was purchased from NovaMatrix (Norway).

Poly(L-lysine)-*g*-poly(ethylene glycol)biotin (PPB) was synthesized as described elsewhere [262] with minor modifications. PLL was dissolved at 40 mg/ml in 50 mM sodium tetraborate buffer (pH 8.5). Biotin-PEG$_{3.4kD}$-NHS (Nektar Therapeutics, Huntsville, AL) was then slowly added under vigorous stirring, and allowed to react for 6

32

hours. The solution was transferred to dialysis tubing (Spectra/Por MWCO 12-14 kD, Spectrum Laboratories, Rancho Dominguez, CA) and dialyzed first against phosphate buffered saline (pH 7.4, 2 x 24 hours) and, subsequently against distilled deionized water (2 x 24 hours). The product was then lyophilized until completely dry.

Biotin-PEG$_{3.4kD}$-NHS was added at appropriate stoichiometric amounts to generate PPB with a grafting ratio, x, of 2.5 and 5, where grafting ratio is defined as 1 grafted PEG-biotin chain every x repeat units. Grafting ratio of PPB was determined using ^{1}H NMR [262] (INOVA 600) by taking the ratio of chemical shifts assigned to biotin-PEG linked to lysine (3.05 ppm, m, -C$\underline{H}_2$NHC(O)OCH$_2$-) and the lysine backbone (4.25 ppm, m, -NHC(O)C$\underline{H}$-). To facilitate identification of PPB on islets with confocal microscopy, a fraction of PPB was labeled with FITC (Pierce Biotechnology, Rockford, IL) according to manufacturer's instructions. FITC was added at an appropriate stoichiometric ratio to ensure labeling of less than 1% of backbone amines. Non-reacted FITC was removed via dialysis (Slide-A-Lyzer Dialysis Cassette, 3.5 kD MWCO, Pierce Biotechnology, Rockford, IL).

Animals. Male C57BL/6J (B6), and B10.BR-H2k H2-T18a/SgSnJ (B10) mice (8 weeks old, Jackson Laboratory Bar Harbor, ME) were used as islet recipients and donors, respectively. All animal studies followed local Institutional Animal Care and Use Committee guidelines at Emory University. The B6 mice were made chemically diabetic by intraperitoneal injection of 200 mg/kg streptozotocin in citrate buffer saline and screened for the development of diabetes. Mice whose non-fasting blood glucose was over 250 mg/dl on two consecutive measurements were considered diabetic [263].

Islet isolation. *Murine islets.* Pancreatic islet isolations were performed, as previously described [264]. B10 mouse pancreata were removed after distension with collagenase P (1 mg/ml, Roche, Indianapolis, IN) through the common bile duct.

33

Following digestion, islets were purified by a Ficoll-Histopaque discontinuous gradient (Ficoll: 1.108, 1.096, and 1.037; Mediatech Inc., Manassas, VA). Isolated islets were cultured for 48 hours in RPMI 1640 supplemented by 10% FCS, L-glutamine (2 mM), and penicillin (100 U/ml), streptomycin (100 μg/ml) and amphotericin B (0.25 μg/ml) (Mediatech Inc.), and media was changed daily. *Human islets.* Human islets were provided by the Cell and Tissue Processing Laboratory in the Emory University Transplantation Center and by the University of Illinois at Chicago Islet Cell Resource Center, and cultured 24-120 hours in Miami Medium #1A (Mediatech Inc.) prior to use.

Islet coating. Islets (<1000) were placed into 12 mm cell culture inserts with 12 μm pores (Millicell-PCF; Millipore, Billercia, MA). Prior to introduction of coating solution, islets were washed by adding 700 μl serum free RPMI 1640 to the insert, followed by gentle repeated tapping of the insert on a polystyrene surface to facilitate drainage of the wash solution through pores while retaining islets. The insert was placed into a well of a 24 well plate (Corning Inc., Corning, NY) and 700 μl of coating solution was added to the cell culture insert. After incubation in coating solution, the insert was removed from the well, solution was drained through the insert, and islets were washed four times as described above to ensure adequate removal of non-adsorbed polymer. To fabricate multilayer thin films, the process of polymer incubation and washing was repeated using appropriate polymer solutions and incubation times. To assemble PPB/SA multilayer films, islets were incubated in PPB for 15 minutes, washed four times with RPMI 1640, incubated in SA for 30 minutes, and washed again. This process was repeated, reducing the PPB and SA incubation times to 10 minutes after the formation of the first bilayer.

Assessment of islet viability and function. Islet viability was assessed as previously described [148] with some modifications. Briefly, islets were incubated in

DPBS (Mediatech Inc., Manassas, VA) containing 4 μM calcein AM and 8 μM ethidium homodimer-1 (Molecular Probes, Eugene, OR) for one hour, and a representative number of individual islets (35-65) were imaged with two-channel confocal microscopy (Zeiss LSM 510 META; Carl Zeiss, Inc., Thornwood, NY). Confocal micrographs were analyzed using LSM5 Image Examiner software (Carl Zeiss, Inc.) to quantify the number of pixels corresponding to fluorescent emission from live (green) and dead (red) cells. Viability is expressed as the percentage of fluorescent pixels associated with emission from live cells. Human islet viability was further measured by a water soluble tetrazolium compound of MTS (3-[4,5, dimethylthiazol-2-yl]-5-[3-carboxymethoxyphenyl]-2-[4-sulfophenyl]-2H-tetrazolium, inner salt) in the presence of phenazine ethosulfate (PES), as an intermediate electron acceptor (CellTiter 96® AQ$_{ueous}$ One Solution Cell Proliferation Assay, Promega, Madison, WI) as previously described [198] with minor modifications. Three hours after coating, groups of 150-200 islets were placed into wells of a 96 well polystyrene plate, washed with cell culture media, and finally suspended in 150 μl media and 30 μl assay solution. After 2.5 hour incubation at 37°C, 100 μl of solution was removed and the absorbance at 492 nm was measured by a microplate reader. A standard curve relating islet number to absorbance at 492 nm was generated and used to determine the number of viable islets in a treatment or control group. Viability is reported as the percentage of viable islets within the group. In some instances, lactose dehydrogenase (LDH) release was measured as a marker of cytotoxicity (CytoTox 96® Non-Radioactive Cytotoxicity Assay, Promega). To monitor LDH release during exposure to PAH, groups of 75 islets were placed into microcentrifuge tubes, pelleted by low-speed centrifugation, and the medium exchanged with 60 μl PAH solution. As described previously [265], islets were resuspended in PAH, incubated for 5 minutes, and pelletted by low-speed centrifugation for 5 minutes; 50 μl of

35

supernatant was subsequently removed and LDH content determined according to manufacturer's instructions. To monitor LDH release after coating, groups of 150 coated or uncoated islets were placed into wells of a 96 well polystyrene plate, washed with cell culture media, and finally suspended in 100 μl Miami 1A culture media for 3 hours at 37°C. After incubation, 50 μl of solution was removed and LDH content determined according to manufacturer's instructions. LDH release is reported as microunits (μU) released/islet, where 1 U reduces 1 μmole pyruvate to L-lactate per minute.

Islet function was evaluated by glucose-stimulated insulin secretion under static incubation. Ten islets were hand selected, placed in a cell culture insert in a 24 well plate, and pre-incubated in 1 ml of HEPES buffered RPMI 1640 (25 mM HEPES, 0.2% BSA) supplemented with glucose at 60 mg/dl glucose for one hour at 37°C. Following pre-incubation, islets were rinsed and incubated in 1 ml for 1 hour, followed by another rinse and incubation in HEPES buffered RPMI 1640 containing 300 mg/dl glucose for an additional hour at 37°C. Samples were collected at the end of each incubation period, and insulin levels were determined using a mouse insulin ELISA kit (Mercodia, Inc., Winston Salem, NC).

Film assembly and characterization on planar substrates. Quartz slides (0.5 x 1 in.; Chemglass, Vineland, NJ) were cleaned by immersion in a H_2SO_4/H_2O_2 (7:3) bath for 1 hour and subsequently in a $H_2O/H_2O_2/NH_3$ (5:1:1) bath at 60°C for 30 minutes. The surface was rinsed thoroughly in distilled water, incubated in 1% (w/v in water) PDDA (MW 100-200 kD, Sigma-Aldrich, St. Louis, MO) for 30 minutes, rinsed, and incubated in 0.15% (w/v in phosphate buffered saline) sodium alginate (UP LVM; NovaMatrix, Norway) for 20 minutes to generate a negatively charged, carbohydrate-rich surface. PPB and Cy-3 labeled streptavidin were dissolved at 1 mg/ml and 0.1 mg/ml, respectively, in RPMI 1640 culture media. Planar surfaces were incubated in PPB for 15

minutes, rinsed 3x with 15 ml RPMI 1640, and then incubated in Cy3-SA for 30 minutes. Samples were again rinsed, and absorption spectra were recorded using a UV-vis spectrophotometer (Cary 50; Varian Inc., Palo Alto, CA). After the formation of the first bilayer, PPB and Cy3-SA incubation times were reduced to 10 minutes, and absorbance spectra were recorded after each Cy3-SA deposition.

Intraportal islet transplantation. Recipients were anesthetized via intramuscular injection of ketamine (87 mg/kg) and xylazine (13/mg/kg). Prior to transplantation, a fraction of islets were removed and viability was assessed to ensure >90% viability. Two hundred and fifty (250) B10 islets were infused in a total volume of 200 µl into the recipient liver through the portal vein using a 27 Ga insulin syringe, as previously described [266]. Mice undergoing islet transplantation were monitored by measuring nonfasting blood glucose daily for two weeks with using an ACCU-CHECK glucose monitor. Euglycemia was defined as a nonfasting blood glucose less than 200 mg/dl on two or more consecutive days. B6 diabetic mice were randomly assigned into two groups that received either islets alone or islets coated with a (PPB/SA)$_8$/PPB multilayer film.

Statistics. Tests for statistical significance between the means of two groups were conducted with the Student's t-test (two-tailed, homoscedastic). Tests between three or more groups were conducted with the one-way ANOVA followed by the Tukey HSD test.

2.3. RESULTS AND DISCUSSION

Polycation cytotoxicity limits PEM film assembly on islets. Polyelectrolyte multilayer (PEM) films, in particular poly(L-lysine) (PLL)/alginate PEM films, have been widely employed to confer permselectivity to conventional microcapsules [109, 186, 192]. Therefore, it was hypothesized that such films could be assembled directly on the surface of pancreatic islets in an analogous manner, using the negatively charged cell surface as a substrate for film assembly. Islets were first incubated with PLL (MW 15-30 kD, 1 mg/ml in RPMI 1640) for 5 minutes, rinsed 3x with RPMI 1640, and subsequently incubated with alginate (2 mg/ml in RPMI 1640) for 5 minutes to form a single PLL/alginate bilayer. Maintenance of cell viability is critical to effective islet transplantation and, accordingly, islet viability was assessed shortly after film formation using confocal microscopy to image a representative population of islets stained with calcein AM (live) and ethidum homodimer (dead). Formation of even a single PLL/alginate bilayer exerted significant toxicity. The toxicity of PLL, as well as many other polycations, towards a variety of cell types has been well documented [165, 267-269]. In accord with these reports, incubation of islets with 1 mg/ml PLL for 15 minutes resulted in a ~60% decrease in islet viability relative to untreated controls (Figure 2.1). Hence, direct contact between PLL and islets significantly decreases viability and precludes the use of PLL to initiate film growth on the islet surface. The toxicity of several other commonly employed polycations, including poly(allylamine hydrochloride) (PAH), poly(diallyldimethylammonium chloride) (PDDA), and protamine was also assessed and all were found to exert significant toxicity after 15 minutes at 1 mg/ml; similar findings have been recently reported by Lee et al. [165]. To the contrary, Krol et al. maintain that a PAH/poly(sodium 4-styrenesulfonate)/PAH (PAH/PSS/PAH) film may be assembled on the surface of human islets without significantly influencing islet viability or function [265]. To explore this apparent inconsistency, human islets were

38

coated with a PAH/PSS/PAH multilayer using identical polyion properties (PAH: 15 kD, PSS: 70 kD), concentrations (2 mg/ml), incubation times (5 minutes), and solvent (RPMI 1640, dissolved one day in advance) as previously reported. Islet viability was assessed after film formation via calcein AM and ethidium homodimer-1 (Live/Dead) staining and imaging with confocal microscopy (Figure 2.2A-E). The majority of cells within islets coated with a PAH/PSS/PAH film were found to be non-viable (Figure 2.2B), as indicated by a significant decrease in intercellular esterase activity (live, green) and an increase in ethidium homodimer (EthD-1) staining (red, dead). Consistent with the binding of EthD-1 to nucleic acids, punctate staining was distributed within cell nuclei (Figure 2.2D). Indeed, image analysis of confocal micrographs revealed a significant difference in viability between untreated and PAH/PSS/PAH coated islets (Figure 2.2E). Comparable results were obtained when film assembly was performed on murine islets (data not shown). The toxicity of PAH/PSS/PAH films was further confirmed through an MTS assay, which demonstrated that the viability of PAH/PSS/PAH coated islets was significantly less than that of untreated controls (30.7 ± 0.8% vs. 103.7 ± 8%, $p < 0.01$, Figure 2.2E). These data were consistent with those obtained using an independent islet isolation (PAH/PSS/PAH: 29.9 ± 2.5%; control: 100.7 ± 11.0%). As an additional confirmation of toxicity, the cytosolic enzyme, lactose dehydrogenase (LDH), could be detected in coating and wash solutions. Specifically, islets were found to release significantly more LDH during the initial PAH coating step relative to those exposed solely to cell culture media, but otherwise treated in a similar manner (296 ± 21 vs. 4.7 ± 4.2 μU/islet, $p < 0.01$, Figure 2.2F). Additionally, LDH continued to leak from islets during a 3-hour period immediately after PAH/PSS/PAH coating, whereas significantly less was released from controls (76.8 ± 5.9 vs. 5.5 ± 0.6 μU/islet, $p < 0.01$, Figure 2.2F). Human islet isolations are highly variable by nature, and, consequently, the susceptibility of islets to toxic agents, including polycations, may depend on the unique characteristics

of an islet preparation or islet subpopulation, including size, viability, metabolic capacity, purity, and integrity of the peri-insular extracellular matrix. Nonetheless, results obtained using three viability assays (calcein AM/EthD-1, MTS, and LDH) and three independent islet isolations obtained from separate transplant centers with extensive islet isolation experience, indicate that PAH/PSS/PAH multilayer films cannot be assembled on islets without significant adverse effects on islet viability.
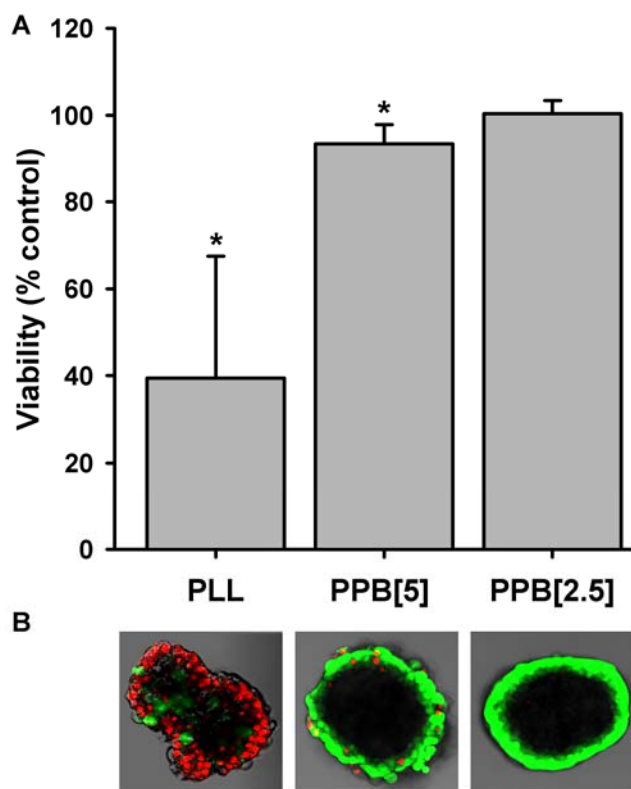
Figure 2.1. (A) Islets were incubated with PLL, PPB[5], and PPB[2.5] at 1 mg/ml, and viability was assessed after various incubation times (mean ± SD, *$p<0.05$ compared to untreated controls). PLL exerted significant toxicity after only 15 minutes, while incubation with PPB[5] decreased islet viability slightly, but significantly, after 4 hours. PPB[2.5] did not reduce islet viability even after a 12 hour incubation ($p>0.05$). (B) Representative confocal micrographs of islets stained with calcein AM (green, viable) and ethidum homodimer (red, non-viable) overlaid on bright field micrographs demonstrate changes in islet morphology associated with polycation-mediated cell death (from left to right: PLL, PPB[5], PPB[2.5]).

40
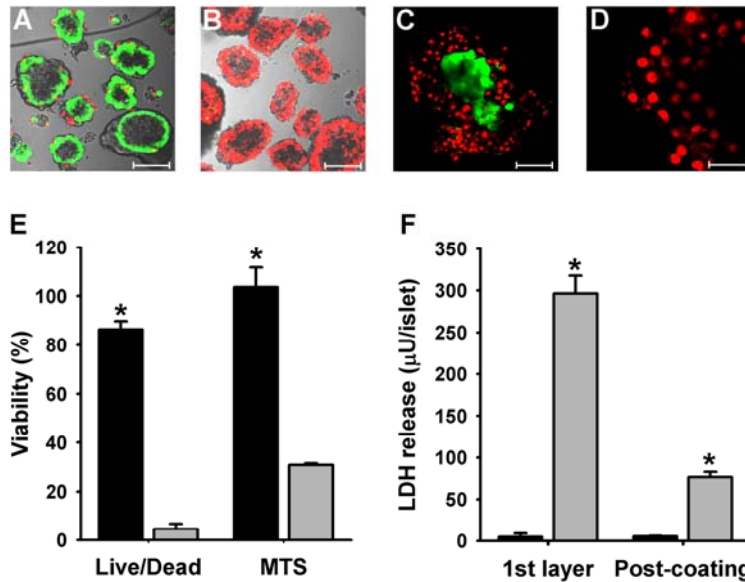
Figure 2.2. PAH/PSS/PAH film assembly is toxic to human pancreatic islets. Representative confocal micrographs of (A) untreated and (B) PAH/PSS/PAH coated human islets stained with calcein AM (green, viable) and ethidum homodimer-1 (red, non-viable) overlaid on bright field micrographs (scale bar = 50 μm). (C) In a subpopulation of islets, coating with a PAH/PSS/PAH film resulted in considerable peripheral cell death, but a viable islet core (scale bar = 50 μm).   (D) Fluorescent emission associated with ethidium homodimer-1 staining demonstrates a punctate distribution consistent with binding to nucleic acids within islet cell nuclei (scale bar = 20 μm). (E) Image analysis of confocal micrographs (Live/Dead) as well as viability assessment by MTS assay revealed a significant difference (*$p<0.01$) in viability between untreated (black bar) and PAH/PSS/PAH coated (grey bar) islets. (F) Lactose dehydrogenase (LDH) release from islets during deposition of the initial PAH layer (1st layer), as well as after formation of a PAH/PSS/PAH film (grey bars) was significantly greater (*$p<0.01$) than untreated controls (black bars), indicating that islet cell membranes are compromised as a result of PAH/PSS/PAH coating.

www.manaraa.com

Design of cytocompatible poly(L-lysine)-*g*-poly(ethylene glycol)biotin copolymers. Poly(L-lysine)-*graft*-poly(ethylene glycol) copolymers have been used to modify the surface of synthetic and natural implantable materials [270-274] and, importantly, have been reported to exert minimal toxicity towards fibroblasts in culture [270]. Therefore, to reduce the toxicity of PLL, NHS-PEG$_{3.4kD}$(biotin) was grafted to primary amines on the PLL backbone to generate PLL-*g*[x]-PEG$_{3.4kD}$(biotin) (PPB) graft copolymers [262, 275] with grafting ratios, x, of 5 and 2.5 (PPB[5] and PPB[2.5], respectively), where x is the average number of modified and unmodified lysine residues per grafted side chain. Islets were incubated with PPB[5] and PPB[2.5] at 1 mg/ml for 15 minutes, 1 hour, 4 hours, and 12 hours and islet viability was assessed until significant decreases in islet viability were observed relative to untreated controls. Incubation of islets with PPB[5] resulted in a statistically significant ($p<0.01$) 6.5% decrease in viability after 4 hours which was largely due to death of cells on the islet periphery (Figure 2.1). While such small changes in viability may not have a significant impact on overall islet function or engraftment, death of peripheral cells and concomitant changes in islet morphology (Figure 2.1B) will likely compromise film assembly and properties. By contrast, islets could be incubated in PPB[2.5] for at least 12 hours without adversely influencing islet viability or morphology (Figure 2.1). Therefore, cytotoxicity tends to decrease (PPB[2.5]<PPB[5]<PLL) with decreasing polycation charge density (PPB[2.5]<PPB[5]<PLL), a phenomenon in accord with previous findings [269]. The dramatic reduction in toxicity achieved with increased PEG grafting might be explained by differences in the three-dimensional arrangement of cationic monomers on the cell membrane. Ryser suggested that the membrane permeabilization potential of polyamines decreased as the space between amino groups increased [276]. Interestingly, it was speculated that a three-point attachment mechanism was necessary to invoke membrane pore formation, and, therefore, it is perhaps not coincidental that

the toxicity of PLL is abrogated as the grafting ratio decreases below 3 (i.e. charge neutralization of one in every three lysine residues). Alternatively, Hartmann et al. suggested that PLL transitions from a random coil in solution to an alpha helical conformation at the cell surface in order to maximize interfacial contact [277], a phenomenon that may be sterically interrupted by grafted PEG chains.

PLL-*g*-PEG(biotin) copolymers adsorb to surfaces through coulombic interactions between positively charged backbone lysine monomers and negatively charged surfaces, causing PEG chains terminated with biotin to extend into solution [262, 275]. To demonstrate adsorption of PPB[2.5] on islets, Cy3-labeled SA (Cy3-SA, 0.1 mg/ml, 30 min) was used to identify accessible biotin groups. Incubation with PPB[2.5] (1 mg/ml, 15 minutes) facilitated the specific binding of Cy3-SA to the islet surface (Figure 2.3A), as islets incubated with only Cy3-SA demonstrated no fluorescent emission (Figure 2.3B). Islets incubated with non-modifed PLL (1 mg/ml, 15 minutes) prior to Cy3-SA demonstrated sporadic and concentrated domains of fluorescent emission (Figure 2.3C), likely a result of membrane permeabilization by PLL and subsequent diffusion of Cy3-SA into the cytoplasm [267]. Therefore, unlike PLL, PPB provides a foundation for initiating growth of multilayer thin films on the surface of viable pancreatic islets.
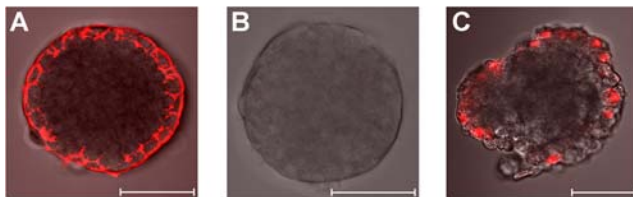
Figure 2.3. PPB facilitates specific binding of streptavidin to the surface of pancreatic islets. (A) Islets incubated with PPB for 15 minutes and subsequently with Cy3-labeled streptavidin (Cy3-SA) demonstrated fluorescent emission around the islet periphery. Islets incubated in only Cy3-SA demonstrated no fluorescent signal (B), and treatment of islets with non-modified PLL prior to Cy3-SA resulted in discontinuous, concentrated domains of fluorescent emission (C) (scale bar = 50 μm).

Assembly of nanothin films through layer-by-layer deposition of PPB and streptavidin. As an alternative to PEM film formation, receptor-ligand interactions have been used to fabricate multilayer architectures [278, 279]. A ligand-derivatized polymer adsorbed to a surface creates a ligand-rich interface capable of binding soluble receptors. Provided each receptor has multiple binding sites for the ligand, a fraction of binding sites may remain unoccupied, facilitating binding of the ligand-derivatized polymer and regeneration of a ligand-rich interface. Such films have commonly been assembled through alternating deposition of biotin derivatized polycations and (strept)avidin [279-281]. Many of these films, however, have utilized polycations of high charge density [280-282], and, therefore, are likely unsuitable for assembly on living cells or tissues. Moreover, PEG-rich multilayer films have not been constructed in this manner. To determine if multilayer thin films could be fabricated through layer-by-layer deposition of PPB[2.5] and SA (Scheme 2.1), solid state spectroscopy was used to monitor the absorbance of Cy3-SA as a function of layer number. Figure 2.4 shows a series of representative absorption spectra, with each successive curve corresponding to a different bilayer. Plotting absorbance at 554 nm (Figure 2.4, inset), which corresponds to the amount of surface-bound Cy3-SA, as a function of layer number demonstrates that film growth occurs in a linear manner. This behavior is in accord with previously published spectroscopic measurements of biotin-PEI/avidin multilayer films [280]. From the approximate molecular dimensions of streptavidin (5.4 x 5.8 x 4.8 nm) [279], the molar extinction coefficient of Cy3 (1.3×10^5 M^{-1} cm^{-1}), and the fluorophore:protein ratio of the Cy3-SA conjugate (7.0), the absorbance of a monolayer of Cy3-SA is estimated to be 5.7×10^{-3}. The absorbance change per PPB/Cy3-SA layer was found to be 5.4×10^{-3}, indicating that just under a monolayer of streptavidin is bound after each deposition.

Islet coated with (PPB/SA)_n
multilayer thin film
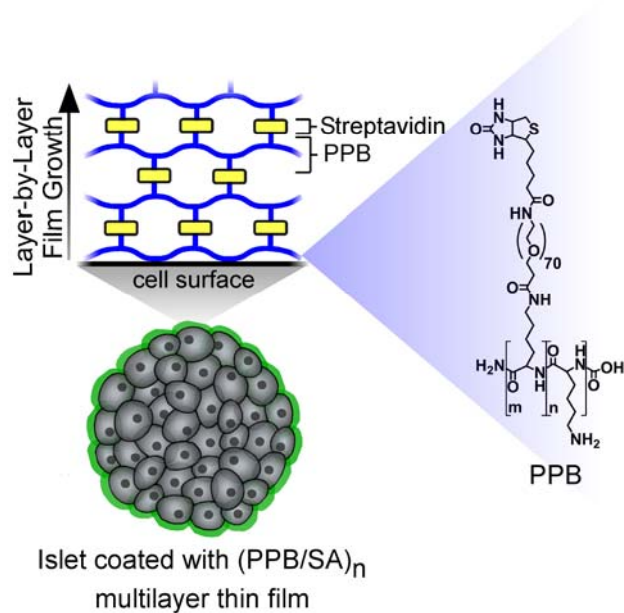
Scheme 2.1. Assembly of PEG-rich, nanothin conformal islet coatings via layer-by-layer deposition of poly(L-lysine)-*g*-poly(ethylene glycol) (PPB) and streptavidin (SA). PPB interacts electrostatically with negatively charged cell surfaces, facilitating the binding of SA. Unoccupied biotin binding sites of immobilized SA allow a second layer of PPB to be added, thereby enabling incorporation of a second SA layer. This process may be repeated to generate thin films assembled via alternating deposition of PPB and SA.
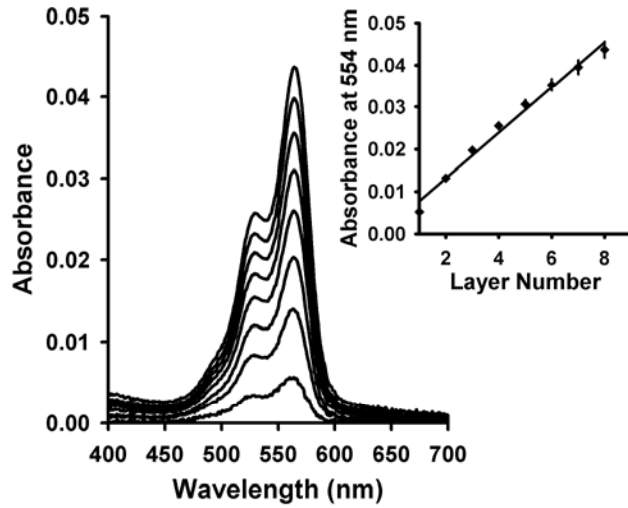
Figure 2.4. PPB/SA multilayer thin films can be assembled on planar substrates. Solid-state UV-vis spectroscopy was used to monitor film growth on quartz slides. Absorbance spectra recorded after each PPB/Cy3-SA bilayer deposition demonstrates a regular layer-by-layer growth pattern. Inset: absorbance at 554 nm (Cy3; mean ± SD) increases linearly with layer number through at least eight bilayers.

46

Conformal coating of islets with PPB/SA multilayer thin films. Confocal microscopy was next used to demonstrate multilayer film growth on the surface of individual pancreatic islets (Figure 2.5). Islets were incubated in PPB[2.5] for 15 minutes, rinsed three times with culture media, and incubated in Cy3-SA for 30 minutes. After formation of a single PPB[2.5]/Cy3-SA bilayer, islets were divided into two groups: one group was incubated in PPB[2.5] for an additional 15 minutes (Figure 2.5A) while the other was placed in RPMI 1640 (Figure 2.5B). Both groups were then incubated in FITC-labeled SA (FITC-SA) for 5 minutes, and imaged with two-channel confocal microscopy. Receptor-ligand binding kinetics predicts that the initial rate of streptavidin binding increases with increased surface density of free biotin. Therefore, islets incubated with a second layer of PPB would be expected to bind more FITC-SA than islets that were not, due to regeneration of accessible biotin groups in the former. Indeed, fluorescent emission from FITC-SA was observed around the periphery of islets that were incubated with a second layer of PPB, while the signal was essentially absent for islets that were not. These observations indicate that multilayer architectures can be assembled on the surface of islets via alternating deposition of PPB[2.5] and streptavidin.

Live cell confocal microscopy was also used to assess the localization, distribution, and gross uniformity of PPB/SA multilayer films assembled on islets. Three dimensional reconstructions of serial optical sections of islets coated with a (PPB[2.5]/Cy3-SA)$_4$ film (Figure 2.6) demonstrate that the film conforms to undulations on the islet surface, and is grossly uniform at the resolution used here. Using Hoechst nuclear stain to identify individual cells within islets, FITC-labeled PPB (FITC-PPB), and Cy3-SA, confocal microscopy demonstrated that the film is localized both on the periphery of the islet (Figure 2.7A) as well as within the interstitial space between individual cells within the core of the islet (Figure 2.7B). Hence, all surfaces which are accessible to film constituents may be coated, reflecting the truly conformal nature of

47

such nano-assembled films, and demonstrating the potential to encapsulate and/or modify individual cells within a multicellular tissue such as islets. Importantly, film constituents were concentrated predominately on the surface of cells (i.e. in the extracellular space), as fluorescent emission from both Cy3-SA and FITC-PPB did not colocalize with cell nuclei, was not distributed throughout the cytoplasm of cells, and existed in discrete domains consistent with the extracellular architecture of isolated pancreatic islets. In contrast, FITC-labeled PLL (1 mg/ml, 15 minutes) was found colocalized with cell nuclei and distributed throughout the cytoplasm of individual cells (Figure 2.7C), which adopted an extended morphology, likely due to cell necrosis [269]. PLL, and many other polycations, have been shown to induce pore formation in the plasma membrane, a phenomenon which often mediates cell death and enables transport of molecules, including the polycation itself, across the cell membrane [267, 269, 276, 283]. The extracellular localization of PPB/SA films, in particular the PPB component, suggests that conjugation of $PEG_{3.4kD}$(biotin) to the PLL backbone inhibits or reduces its capacity to form pores in the cell membrane and/or diffuse into the cytoplasm, consistent with the observed reduction in toxicity. Interestingly, Krol et al. also observed polycation (PAH) penetration into the cytoplasm of cells within islets [265], consistent with the cytotoxic effects exerted by PAH reported herein.

48
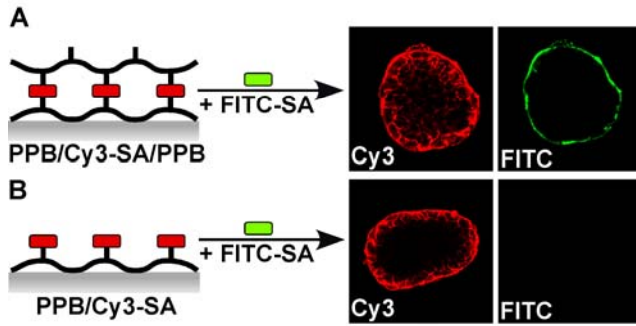
Figure 2.5. PPB/SA multilayer films can be assembled on individual pancreatic islets. After formation of a PPB/Cy3-SA bilayer, islets were either incubated with a second layer of PPB (A) or placed into cell culture media (B). Both groups were then incubated with FITC-labeled streptavidin (FITC-SA) for 5 minutes. Only islets incubated with a second layer of PPB (A) demonstrated fluorescence emission from FITC-SA due to regeneration of accessible biotin groups on the islet surface.
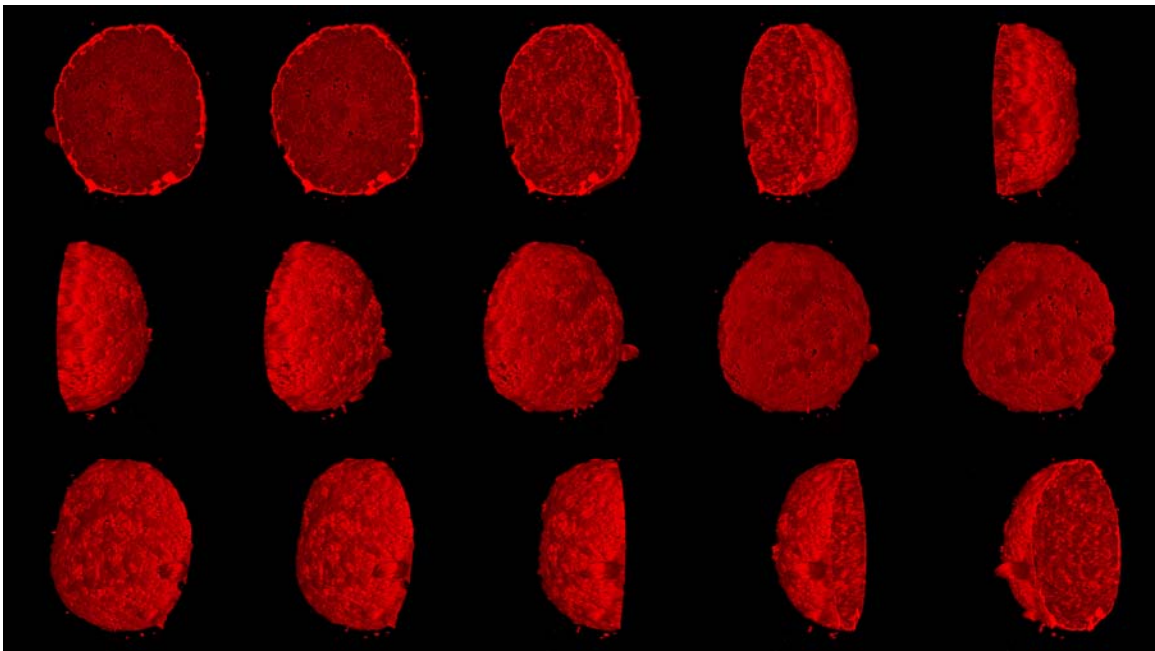
Figure 2.6. Three dimensional reconstruction of optical confocal microscope sections (0.5 μm) of the lower half of an islet coated with a (PPB/Cy3-SA)$_4$ multilayer film. Each image is rotated ~24° from the previous (left to right, top to bottom). The film is grossly uniform and conforms to protrusions and indentations of the islet surface.
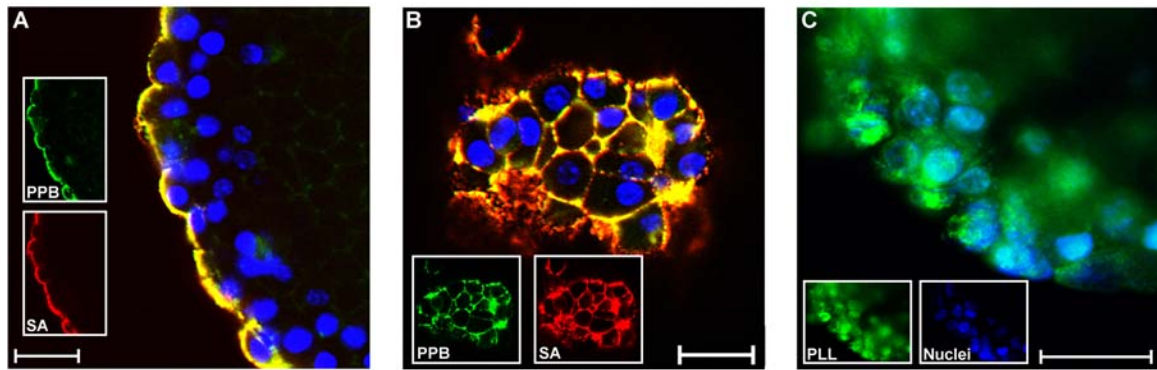
Figure 2.7. PPB/SA multilayer films assemble extracellularly. Islet cell nuclei were stained with Hoechst (blue) to identify individual cells within islets. Islets were coated with a (FITC-PPB/Cy3-SA)$_4$ multilayer film, and confocal microscopy was used to identify film components. PPB and SA were colocalized on the surface of cells on the islet periphery (A) as well as in the interstitial space between individual cells within the core of the islet (B). Conversely, FITC-PLL was observed throughout the cytoplasm of cells and often colocalized with cell nuclei (C).

Islet viability and function are not compromised by PPB/SA film assembly.

As a consequence of cell encapsulation, diffusive transport of essential nutrients may be hampered, potentially resulting in decreased cell viability and/or improper temporal response to physiological stimuli [89]. Furthermore, fabrication of PPB[2.5]/SA multilayer films is anticipated to concentrate PPB on the cell surface, potentially generating locally toxic concentrations. Therefore, islet viability and function were assessed after fabrication of a (PPB/SA)$_8$ multilayer film. Coating islets did not affect islet viability (Figure 2.8A) indicating that neither the polymers employed nor the coating process caused damage to islets. Of clinical significance, human islets could also be coated with a (PPB[2.5]/SA)$_8$ multilayer film without compromising islet viability (Figure 2.8A); this was further confirmed using an MTS assay whereby the viability of coated and untreated islets was indistinguishable (p>>0.1). Additionally, the coating process did not result in islet loss. Islet function was assessed in vitro by measuring insulin secretion in response to a step change in glucose concentration. As shown in Figure 2.8B, islets coated with a (PPB[2.5]/SA)$_8$ multilayer film function comparably to non-treated islets in response to glucose stimulation. Impaired in vitro insulin secretion has been observed for a variety of conventional microcapsule formulations [85, 104, 105] due to significant void space which glucose and insulin must cross prior to transport across the membrane. Due to the nanothin and conformal nature of PPB/SA coatings this behavior was not observed. While no attempts were made to fabricate more than eight bilayers, it is anticipated that considerably more layers may be formed without compromising islet viability given the lack of toxicity exerted by PPB[2.5].

51
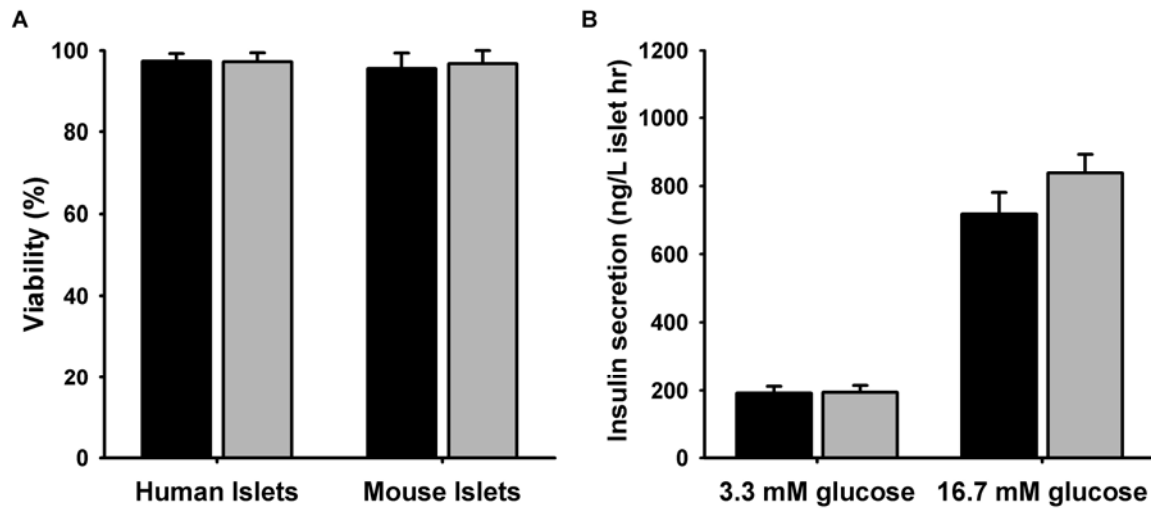
Figure 2.8. Islet viability and function are preserved after formation of a $(PPB[2.5]/SA)_8$ multilayer film. (A) Viability (mean ± SD) was assessed after film formation via calcein AM and ethidium homodimer staining. Image analysis of confocal micrographs revealed no statistical difference (p>0.05) in islet viability between untreated (black bar) and coated islets (grey bar) for both mouse and human islets. (B) Untreated (black bar) and coated islets (grey bar) secrete statistically similar (p>0.05) amounts of insulin at both 3.3 and 16.7 mM glucose, indicating that islet function is not influenced by film formation. Data points represent mean ± SE, for a minimum of seven independent measurements.

Intraportal transplantation of conformally coated islets. Islets coated with a (PPB[2.5]/SA)$_8$/PPB[2.5] multilayer film were transplanted into the portal vein of mice in a B10 to B6 allograft model; a final PPB layer was used to generate a terminal PEG layer to help prevent non-specific binding of serum proteins to the film [275, 284]. In this model of islet transplantation, a suboptimal number of islets (250) are infused into the portal vein of the liver, resulting in transient reversal of diabetes (euglycemic for >2 consecutive days) in only a fraction of recipients during the initial 2 weeks post-transplant [37, 45]. Therefore, differences in rates of conversion to euglycemia reflect changes in islet survival and function in the immediate post-transplant period. Of the 16 mice transplanted with untreated islets, 6 converted to euglycemia (37.5%), whereas 7 of 15 mice (46.7%) converted when receiving islets coated with a multilayer film (Figure 2.9). This difference was not statistically significant (χ^2 = 0.11), indicating that islets coated with a (PPB/SA)$_8$/PPB multilayer thin film maintain islet viability and function in vivo, and suggesting that the film itself does not invoke a deleterious non-specific inflammatory response. This is significant as intraportal transplantation of islets encapsulated in 350 μm microcapsules has been found to *impair* islet engraftment relative to non-encapsulated controls due, in part, to inflammatory responses elicited against the implant [131]. Moreover, the observed trend towards increased conversion to euglycemia suggests a potential beneficial impact of the film, an effect which may be rendered more pronounced by increasing film thickness, optimizing barrier permeability, or by incorporating bioactive film constituents, efforts which are currently ongoing. Significantly, this is the first study to report in vivo survival and function of nanoencapsulated cells or cell aggregates.

53
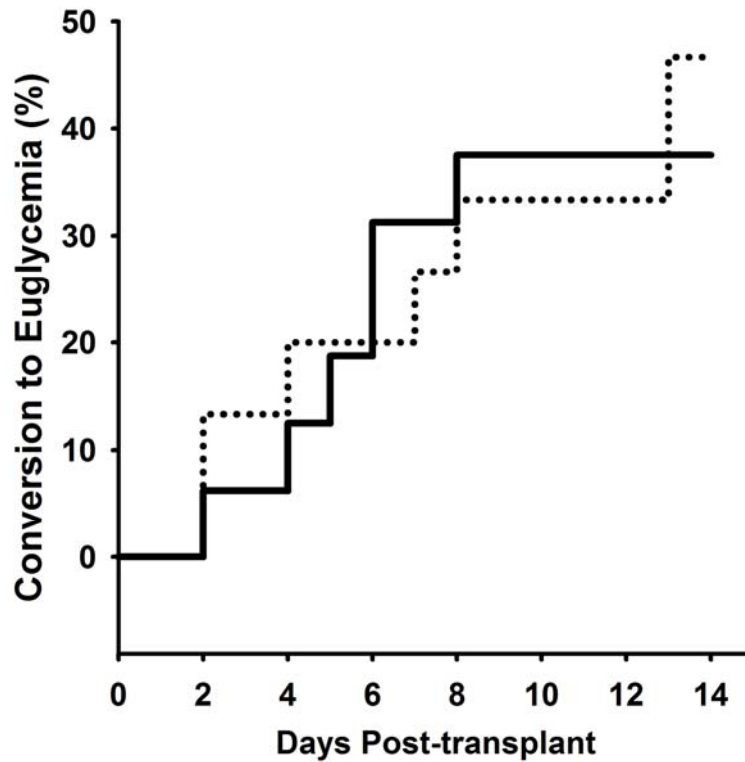
Figure 2.9. (PPB/SA)$_8$/PPB coated islets perform comparably to untreated islets after intraportal islet transplantation. Two hundred and fifty (250) untreated (solid line) or (PPB/SA)$_8$/PPB coated (dashed line) B10 mouse islets from were transplanted into the portal vein of diabetic B6 mice. Blood glucose levels were monitored daily for two weeks and conversion to euglycemia was defined as glucose levels < 200 mg/dl for > 2 consecutive days. Islets coated with a (PPB/SA)$_8$/PPB film resulted in an increased conversion to euglycemia (46.7%; 7/15) relative to untreated controls (37.5%; 6/16), however, this difference was not statistically significant (χ^2 = 0.11).

54

Covalent conjugation of PEG to islet surface proteins and carbohydrates has recently been explored as a strategy for attenuating host responses to transplanted allo- and xenografts [162, 168]. However, the efficacy of PEGylation may be limited, in part, by the lack of a defined pore structure, with primary dependence on barrier function through a steric exclusion effect. In principle, such limitations may be addressed through use of PPB/SA multilayer films, which are anticipated to generate PEG-rich networks rather than a monolayer of grafted PEG on the cell surface. Reports demonstrating in vivo efficacy of islet surface PEGylation have utilized different, in some cases less rigorous, animal models and/or adjunctive immunosuppressive therapy [13, 165, 168]. Therefore, PPB/SA multilayer films may demonstrate increased efficacy in other animal models of islet transplantation or may act in synergy with systemic administration of immunomodulatory agents.

PPB/SA films may also provide important advantages over covalent biotinylation strategies employed to immobilize bioactive molecules to the islet surface [236, 285]. As a multilayered structure, PPB/SA films may allow biotinylated or streptavidin-linked molecules to be embedded within the film, thereby facilitating greater loading than might be accomplished using a single layer of immobilized biotin moieties. Moreover, multilayer films assembled via (strept)avidin/biotin interactions may be disintegrated using excess biotin [281, 282], thereby allowing triggered release of embedded agents.

2.4. CONCLUSIONS

PPB/SA multilayer films provide a novel approach to generating nanothin, PEG-rich conformal islet coatings through a self-assembly process. While further characterization and optimization of properties is necessary to generate films capable of significantly improving in vivo islet engraftment, this work helps establishes a new paradigm for encapsulating and/or modifying islets prior to portal vein transplantation.

55

Additionally, this work provides mechanistic insight regarding the relationships between polycation charge density, cell surface localization, and cytotoxicity, with important implications for the design of cell and tissue-surface supported nanostructures. All told, PPB/SA multilayer films offer a unique approach to resurfacing the biochemical landscape of living cell and tissue interfaces with broad applications in tissue-targeted chemistry, biosensing, *in situ* tissue engineering, and targeted cell delivery.

CHAPTER 3

Cell Surface-Supported Polyelectrolyte Multilayer Thin Films as Conformal Islet Coatings

3.1   INTRODUCTION

Cell encapsulation provides a promising approach for attenuating deleterious inflammatory and immune responses that underlie the destruction of transplanted pancreatic islets [85, 87, 114, 222, 286]. However, despite considerable progress over the past several decades [109, 113] the efficacy of islet encapsulation remains limited, in part, by consequential mass transport limitations and large transplant volumes associated with use of conventional microencapsulation strategies [88, 89, 129-131, 222]. In response to these challenges, recent effort has been given towards reducing the size and void volumes of capsules through use of polymeric coatings that conform to the surface of individual islets. As such, coatings ranging in thickness from 5-50 μm have been created using emulsification [145], discontinuous gradient density centrifugation [141], selective withdrawal [146], and interfacial polymerization [148]. While promising, incomplete encapsulation, islet loss, and limited process scalability remain significant obstacles in the clinical realization of such approaches. On the other end of the spectrum, several investigators have sought to generate conformal barriers on the molecular scale through conjugation of poly(ethylene glycol) directly to the surface of islet surface proteins [13, 152-157]. As a hydrated, flexible polymer chain, PEG has been shown to present a steric barrier to a number of biochemical and cellular processes implicated in the destruction of islet grafts [158, 162-164]. However, as a consequence of the natural turnover of cell surface macromolecules, the stability of islet grafted PEG chains has recently come into question [287]. Moreover, as the success of

conventional encapsulation strategies is largely predicated upon preventing diffusion of antibodies and other macromolecules to their respective targets on the cell surface, the efficacy of cell surface-grafted PEG may be limited by lack of a defined pore structure and dependence on a steric exclusion effect.

Layer-by-layer (LbL) polymer assembly has recently emerged as a facile and versatile bottom-up approach to the design of thin films of tailored biophysiochemical properties [249-251, 288]. Though covalent bonding [289-291], biorecognition [278-280, 292], and hydrogen bonding [250, 293, 294] have recently been explored as driving forces for LbL assembly, polyelectrolyte multilayer (PEM) films assembled through alternating deposition of oppositely charged polyelectrolytes [249] represent the most commonly utilized and versatile LbL film architecture. Through appropriate control of film constituents, layer number, and solvent conditions, PEM films ranging in thickness from several nanometers to several microns [295] may be assembled on geometrically and chemically diverse substrates [253, 254, 288, 296, 297]. Significantly, PEM films have been used to generate barriers to molecular recognition between complementary molecules [252] and inhibit interactions between immobilized ligands and cell surface receptors [253, 254]. Of particular relevance to the design of conformal coatings, PEM films, most notably those comprised of poly(L-lysine) and alginate, have been commonly used to confer appropriate permselectivity to conventional microcapsulation devices [109, 186, 192]. Hence, LbL assembly of polyelectrolyte multilayer films directly on the negatively charged islet surface offers a rational approach for generating conformal coatings of tailored thickness and permeability.

Unlike conventional substrates, which are largely passive bystanders of film growth, the cell surface presents a complex and dynamic interface capable of chemically and physically restructuring in response to film constituents. As such, the well documented toxicity elicited by most synthetic and natural polycations in direct contact

58

with the cell surface [267-269, 298-303] poses a significant molecular hurdle in the development of cell surface-supported PEM films. Notwithstanding such accounts, Germain et al. have recently reported ~75% survival of adherent MELN cells upon fabrication of nine bilayers using poly(diallyldimethyl ammonium chloride) (PDDA) and poly(styrene sulfonate) [304] while Veerabadran et al. have reported encapsulation of mesenchymal stem cells with three bilayers comprised of poly(L-lysine) (PLL) and hyaluronic acid [305]. However, we have recently demonstrated significant decreases in islet viability upon short-term exposure to several commonly employed polycations, including PDDA and PLL [303]. While conformal islet coatings generated using LbL films assembled through covalent bonding [306] or receptor-ligand interactions [303, 307] may provide alternative, polycation-free architectures, they lack the unparalleled versatility and flexibility afforded by PEM films.

We have recently reported that conjugation of biotin-derivatized poly(ethylene glycol) (3.4kD) to ~40% of backbone lysine residues abrogates the cytotoxicity of poly(L-lysine) towards pancreatic islets, and that the resultant polycationic poly(L-lysine)-*graft*-PEG copolymer adsorbed to accessible extracellular surfaces within pancreatic islets [303] (Chapter 2). Based on such findings, we have postulated that structurally similar PLL-*g*-PEG copolymers comprised of shorter PEG grafts might be used to initiate and propagate the assembly of PEM films on pancreatic islets, while simultaneously preserving islet viability. We describe herein cell surface-supported polyelectrolyte multilayer films with tunable properties assembled on individual pancreatic islets through layer-by-layer deposition of alginate and PLL-*g*-PEG copolymers rendered cytocompatible through appropriate control of PEG length and grafting ratio. Additionally, these investigations begin to establish a conceptual framework for the rational design of cell surface-supported thin films, with the objective of translating the diverse biomedical and biotechnological applications of PEM films to cellular interfaces.

3.2. MATERIALS AND METHODS

Poly(L-lysine)$_M$-*g*[x]-poly(ethylene glycol)$_n$ copolymer synthesis and characterization. Poly(L-lysine)$_M$-*g*[x]-poly(ethylene glycol)$_n$ copolymers (M=PLL-HBr molecular weight, x=grafting ratio, n=number of PEG repeat units) were synthesized via active ester coupling between N-hydroxysuccinimidyl (NHS)-ester-functionalized methyl-PEG$_n$ (mPEG$_n$) and primary amines of the PLL backbone. mPEG$_4$-NHS was purchased from Pierce Biotechnology (Rockford, IL) and used as received. mPEG$_{12}$ and mPEG$_{24}$ were purchased from Quanta Biodesign (Powell, Ohio) and vacuum dried overnight before use to remove trace amounts of residual organic solvent. Poly(L-lysine)hydrobromide (Sigma Aldrich, St. Louis, MO; M_w=12, 45, or 98 kD by MALLS) was dissolved at 5 mg/ml in dilute phosphate buffered saline (7.7 mM NaCl, 0.28 mM Na$_2$HPO$_4$, pH=7.4) for 30 minutes at room temperature. mPEG$_n$-NHS (n=4, 12, or 24) was dissolved at 250 mM in dry DMSO (Pierce Biotechnology) and slowly added to PLL under vigorous stirring. After 120 minutes, 10x Dubelco's phosphate buffered saline (DPBS, Mediatech, Inc., Manassas, VA) was added to the reaction mixture 1:10 by volume; this was repeated at 150 and 180 minutes, after which the reaction was allowed to proceed for an additional 21 hours. This coupling protocol was empirically determined to yield more efficient grafting of mPEG$_n$ to PLL than simple mixing of constituents in PBS as generally performed. The product was transferred to dialysis cassettes (Slide-A-Lyzer Dialysis Cassette, 3.5 kD MWCO, Pierce Biotechnology) and dialyzed first against DPBS (pH 7.0, 3 x 24 hours, Mediatech, Inc.) and subsequently against distilled deionized water (3 x 24 hours). The product was then lyophilized until completely dry and stored at -20°C prior to use.

mPEG$_n$-NHS was added to PLL at various stoichiometric ratios to generate a library of PLL$_M$-*g*[x]-PEG$_n$ copolymers with a range of grafting ratios, x, where x is average number of modified and unmodified lysine residues per grafted side chain.

60

Grafting ratio of PLL_M-g[x]-PEG_n polymers was determined using ^{1}H NMR (INOVA 600) by taking the ratio of chemical shifts assigned to mPEG linked to lysine (3.15 ppm, m, -C$\underline{H}_2$NHC(O)OCH$_2$-) and ungrafted lysine chains (2.95 ppm, m, -C$\underline{H}_2$NH$_3^+$). Table 3.1 summarizes the structural properties of PLL_M-g[x]-PEG_n copolymers used in these investigations, including copolymer molecular weight which can be estimated based on the grafting ratio and the molecular weight of PLL and grafted PEG chains [308] and was used as the basis for determining the molar concentration of polymers.

Acetylated poly(L-lysine) synthesis and characterization. Random copolymers consisting of lysine and acetylated lysine monomers (PLL-Acetate, P12Ac), were synthesized in analogous manner to PLL_M-g[x]-PEG_n compounds using sulfosuccinimidyl acetate (sNHS-acetate, Pierce Biotechnology, Rockford, IL). sNHS-acetate was added to PLL-HBr (12 kD) at various stoichiometric ratios to generate copolymers with different degrees of lysine acetylation. The product was transferred to dialysis cassettes (Slide-A-Lyzer Dialysis Cassette, 3.5 kD MWCO, Pierce Biotechnology, Rockford, IL) and dialyzed first against DPBS (pH 7.0, 3 x 24 hours, Mediatech, Inc., Manassas, VA), and subsequently against distilled deionized water (3 x 24 hours). The product was then lyophilized until completely dry and stored at -20°C prior to use. The degree of acetylation was determined by ^{1}H NMR (INOVA 600) by taking the ratio of chemical shifts assigned to acetylated lysine (3.05 ppm, m, -C$\underline{H}_2$NHCOCH$_3$) and unmodified lysine chains (2.95 ppm, m, -C$\underline{H}_2$NH$_3^+$). Relevant structural properties of PLL-Acetate are summarized in Table 3.1.

61

Table 3.1. Structure of copolymers employed in this work

Polymer ID	PLL MW[a] (kD)	PEG$_n$ (n)	Grafting Ratio[e] (x)	% Lysine Modified[f]	Estimated MW[g] (Da)
P12P4[6.7]	12[b]	4	6.7	15	9,320
P12P4[4]	12[b]	4	4	25	10,700
P12P4[2.9]	12[b]	4	2.9	35	11,960
P12P4[2.5]	12[b]	4	2.5	40	12,850
P12P12[5]	12[b]	12	5	20	14,020
P12P12[4]	12[b]	12	4	25	15,660
P12P12[3.3]	12[b]	12	3.3	30	17,310
P12P12[2.9]	12[b]	12	2.9	35	18,960
P12P12[2.5]	12[b]	12	2.5	40	20,600
P12P24[10]	12[b]	24	10	10	15,040
P12P24[5]	12[b]	24	5	20	18,840
P12P24[2.5]	12[b]	24	4	25	23,280
P12P24[3.3]	12[b]	24	3.3	30	26,450
P12Ac[2.5]	12[b]	0	2.5	40	8,420
P45P4[2.5]	45[c]	4	2.5	40	48,810
P45P4[2.0]	45[c]	4	2	50	51,160
P45P4[1.7]	45[c]	4	1.7	60	55,850
P100P4[2.5]	100[d]	4	2.5	40	106,130

a: Molecular weight of PLL-HBr starting material, includes contribution of Br$^-$ counterion. **b:** 12 kD MW by MALLS, 1.2 M_w/M_m. **c:** 45 kD MW by MALLS. **d:** 98.8 kD MW by MALLS. **e:** Rounded to nearest tenth. **f:** Rounded to nearest multiple of 5. **g:** $MW_{copolymer} = MW_{PLL} + (MW_{PLL}/MW_{Lys})(x^{-1})(MW_{PEG})$, excludes contribution from Br$^-$, no approximations in grafting ratio were used for calculation.

Fluorescent labeling of polymers. To facilitate identification of PLL$_M$-g[x]-PEG$_n$ copolymers and PLL-acetate on islets with confocal microscopy, and to allow layer-by-layer film growth on planar substrates to be monitored with UV-vis spectroscopy, a portion of selected copolymers was labeled with Alexa Fluor ® 488 carboxylic acid, 2,3,5,6-tetrafluorophenyl ester (AF488-TFP ester; Molecular Probes, Eugene, OR) according to manufacturer's instructions. AF488-TFP was added at appropriate stoichiometric ratios to ensure labeling of less than 1% of backbone lysine monomers. Non-reacted dye was removed via dialysis (Slide-A-Lyzer Dialysis Cassette, 3.5 kD MWCO, Pierce Biotechnology, Rockford, IL), and the labeled product was lyophilized until completely dry. The degree of labeling was quantified using UV-vis spectroscopy (Cary 50; Varian Inc., Palo Alto, CA) and determined to be between 0.64% and 0.89%. To facilitate identification of PLL, FITC-labeled poly(L-lysine) (Sigma Aldrich, St. Louis, MO) was used.

To facilitate identification of alginate on islets with confocal microscopy, alginate (UP LVM, MW 75 kD, NovaMatrix, Sandvika, Norway) was labeled with fluorescein through sequential oxidation of uronate residues and reaction with fluorescein-5-thiosemicarbazide. Alginate oxidation was performed as previously described [309]. Alginate was dissolved at 10 mg/ml in molecular grade water and 0.25 M sodium metaperiodate (NaIO$_4$, Sigma Aldrich) in water was added at 0.01 equivalents with respect to uronate repeat units. After 24 hours, the reaction was quenched with 10 equivalents excess ethylene glycol (Sigma Aldrich), and the product dialyzed (Slide-A-Lyzer Dialysis Cassette, 3.5 kD MWCO, Pierce Biotechnology) 3 x 24 hours against distilled deionized water and lyophilized until completely dry. The extent of alginate oxidation was quantified as previously described [309]. Ten-fold excess of *tert*-butyl carbazate (Sigma Aldrich) was reacted with oxidized alginate for 24 hours. The amount of unreacted *tert*-butyl carbazate was determined by the addition of

trinitrobenzenesulfonic acid (TNBS) solution (Sigma Aldrich) and measuring the absorbance of the colored complex formed at 334 nm. The degree of oxidation was determined to be ~0.5%. Fluorescent labeling was achieved through thiosemicarbazone bond formation between fluorescein-5-thiosemicarbazide (Sigma Aldrich) and aldehyde groups of oxidized alginate. Three equivalents excess of fluorescein-5-thiosemicarbazide was added to oxidized alginate dissolved in phosphate buffered saline (Mediatech, Inc., Manassas, VA) at 5 mg/ml. After reaction for 24 hours, non-reacted dye was removed via gel filtration (PD-10, GE Healthcare, Piscataway, NJ). The fluorescent conjugate was lyophilized and stored protected from light at -20°C. Degree of fluorescent labeling was quantified by UV-vis spectroscopy, and confirmed to be less than 1%.

Islet isolation. Pancreatic islet isolations were performed as previously described [264]. B10.BR-H2k H2-T18a/SgSnJ (B10) mice (8 weeks old, Jackson Laboratory Bar Harbor, ME) pancreata were removed after distension with collagenase P (1 mg/ml, Roche, Indianapolis, IN) through the common bile duct. Following digestion, islets were purified by a Ficoll-Histopaque discontinuous gradient (Ficoll: 1.108, 1.096, and 1.037; Mediatech Inc., Manassas, VA). Isolated islets were cultured for 48-72 hours at 37°C in RPMI 1640 supplemented with 10% heat inactivated fetal calf serum, L-glutamine (2mM), and penicillin (100U/ml), streptomycin (100 μg/ml) and amphotericin B (0.25 μg/ml) (Mediatech Inc.), and media was changed daily.

Islet coating. Islets (<1000) were placed into 12 mm cell culture inserts with 12 μm pores (Millicell-PCF; Millipore, Billercia, MA). Prior to introduction of polymer solution, islets were washed six times by adding 700 μl serum free RPMI 1640 to the insert, followed by gentle repeated tapping of the insert on a polystyrene surface to facilitate

drainage of the wash solution through pores while retaining islets. The insert was placed into a well of a 24 well plate (Corning Inc., Corning, NY) and 700 μl of coating solution was added to the cell culture insert. After incubation in coating solution, the insert was removed from the well, solution drained through the insert as described above, and islets washed four times as described above to ensure adequate removal of polymer solution. To fabricate layer-by-layer thin films, the process of polymer incubation and washing was repeated using appropriate polymer solutions and incubation times. For assembly of PLL$_M$-g[x]-PEG$_n$/alginate multilayer films, islets were incubated in PLL$_M$-g[x]-PEG$_n$ for 5 minutes, washed four times with RPMI 1640, incubated in alginate for 5 minutes, and washed again to form a single bilayer. This process was repeated to assemble the desired number of bilayers.

Confocal microscopy. Confocal microscopy (Zeiss LSM 510 META; Carl Zeiss, Inc., Thornwood, NY) was used to identify fluorescently labeled film components on islets. A representative population of islets selected at random was placed in silicon isolators (Grace Bio-Labs, Bend, OR) adhered to glass coverslips (Fisher Scientific) containing serum free RPMI 1640. Coverslips were then placed on the microscope stage and images were captured within 15-90 minutes of polymer incubation or film deposition. In some instances, islets were incubated with 8 μM Hoechst 33342 (Molecular Probes, Eugene, OR) for 60-90 minutes before or after film assembly to allow individual cell nuclei within islets to be clearly identified. All experiments performed using Hoechst staining were repeated and results confirmed in the absence of staining to ensure Hoechst did not confound findings.

Assessment of islet viability. Islet viability was assessed as previously described [148] with some modifications. Briefly, islets were incubated in DPBS (Mediatech Inc., Manassas, VA) containing 4 μM calcein AM and 8 μM ethidium

homodimer-1 (Molecular Probes, Eugene, OR) for one hour, and a representative number of individual islets (35-50) were imaged with two-channel confocal microscopy using a 20x objective as described above. Confocal micrographs were analyzed using MATLAB® (The MathWorks, Natick, MA) to quantify the number of pixels corresponding to fluorescent emission from live (green) and dead (red) cells. Viability is expressed as the percentage of fluorescent pixels associated with emission from live cells.

Film assembly and characterization on planar substrates. Quartz slides (0.5 x 1 in.; Chemglass, Vineland, NJ) and silicon wafers (N/As(111) 500 μm SSP Prime with 30 nm thermal oxide, University Wafer, South Boston, MA) were used as substrates for characterizing film growth and properties by solid-state UV-vis spectroscopy and ellipsometry, respectively. Silicon wafers were diced into ~0.5 x 1.25" substrates prior to cleaning. Substrates were cleaned by immersion in $H_2O/H_2O_2/NH_4OH$ (5:1:1) for 15 minutes at 80°C, thoroughly rinsed with WFI quality water, and subsequently incubated with $HCl/H_2O_2/H_2O$ (1:1:5) at 80°C for 15 minutes. After cleaning, substrates were rinsed with WFI quality water followed by ethanol, dried under a gentle stream of argon, and stored in a vacuum desiccator prior to use. To minimize risk of contamination, all substrates were used 24-48 hours after cleaning.

Substrates were coated using a custom-built automated slide coater assembled using two BiSlide® assemblies and stepper motors purchased from Velmex, Inc. (Bloomfield, NY). Briefly, the coater is composed of two linear, screw driven actuators combined to allow translation of substrates in both horizontal and vertical directions. Vertically mounted substrates are immersed in and removed from polymer and wash solutions at 1.3 cm/s using the vertical actuator, and moved between different polymer and wash solutions at 5.1 cm/s with the horizontal actuator. The device is computer controlled by COSMOS software (Velmex, Inc.).

66

Prior to PLL$_M$-g[x]-PEG$_n$/alginate multilayer film assembly, substrates were incubated with 1% (w/v in water) poly(diallyldimethylammonium chloride) (PDDA) (MW 100-200 kD, Sigma-Aldrich, St. Louis, MO) for 30 minutes, rinsed four times for 30 seconds each by immersion in 500 ml of WFI quality water, followed by incubation in 1.5 mg/ml sodium alginate (UP LVM; NovaMatrix, Sandvika, Norway) in phosphate buffered saline for 20 minutes, and another 4x 30 second rinse with water to generate a negatively charged, carbohydrate-rich surface from which to initiate film growth. PLL$_M$-g[x]-PEG$_n$ copolymers were dissolved at desired concentration in HEPES buffered (25 mM, pH 7.4) RPMI 1640 supplemented with L-glutamine (2 mM), penicillin (100 U/ml), and streptomycin (100 ug/ml) (HRPMI). Alginate (UP LVM; NovaMatrix, Sandvika, Norway, MW~75kD) was dissolved at 2 mg/ml in HRPMI. To assemble a PLL$_M$-g[x]-PEG$_n$/alginate bilayer, substrates were immersed in PLL$_M$-g[x]-PEG$_n$ copolymer for 5 minutes, rinsed 4 x 20 seconds by immersion in 500 ml HRPMI, incubated with alginate for 5 minutes, and again rinsed four times HRPMI. This process was repeated until the desired number of bilayers was assembled.

LbL growth on quartz substrates was followed using solid-state UV-vis spectroscopy to monitor the absorbance at 495 nm of AF488-labeled PLL$_M$-g[x]-PEG$_n$ copolymers as function of layer number. Absorption spectra (200-800 nm) were recorded in WFI quality water using a UV-vis spectrophotometer (Cary 50; Varian Inc., Palo Alto, CA) beginning with the second PLL$_M$-g[x]-PEG$_n$ deposition and every other deposition thereafter through twelve bilayers. To compare absorbance values between polymers with different degrees of AF-488 labeling, absorbance at 495 nm was normalized by the percentage of backbone monomers modified with fluorescent label.

Spectroscopic ellipsometry (Woollam M-2000, J.A. Woollam Co, Inc., Lincoln, NE) was used to measure thickness of films assembled on silicon substrates. After assembly of the desired number of bilayers, samples were rinsed by immersion in WFI

quality water and carefully dried under a gentle stream of filtered argon gas. Films were stored in a vacuum desiccator prior to measurement, and measurements were taken 24-72 hours after film assembly. Measurements were performed between 370 nm and 1000 nm at an angle of incidence of 70°. Thickness measurements were performed on a minimum of three samples per film type, and thickness was measured at 2-4 spots per sample to account for possible non-uniformities in film thickness.

For data interpretation, the ellipsometric angles, Ψ and Δ, were fit using a multilayer model composed of silicon, silicon oxide, the PDDA/alginate precursor layer, and the PEM film of interest to obtain the thickness of films. The thickness of SiO_2 layers was determined using well-established optical constants. A unique oxide layer thickness was determined for each wafer from an average of three samples, and was used for determining the thickness of films assembled on substrates diced from a particular wafer. The average oxide layer thickness for all wafers used in these investigations was determined to be 28.5 ± 1.2 nm. The thickness of the PDDA/alginate precursor layer was determined by fitting data with the Cauchy approximation with A_n=1.5, B_n= 0.01, and C_n=0.0, and determined to be 1.08 ± 0.72 nm. When films are sufficiently thick, their refractive index can be explicitly determined from Ψ and Δ trajectories. The Cauchy coefficients A_n and B_n were uniquely determined for PEM films generated with different polycations using data obtained from films consisting of eight bilayers, the thickest films generated for each polyion pair. For films assembled using P12P4[2.5] and P45P4[1.7] as polycations, A_n=1.535, B_n=0.00509, for films assembled using P12P12[3.3], A_n=1.527, B_n=0.00469, and for films assembled using P12P24[4], A_n=1.5124, B_n=0.00349. To measure the thickness of PEM films, the thickness of the oxide and precursor layers were defined, and data fitted with the Cauchy approximation with A_n and B_n fixed at values determined as described above. Reported thickness

68

measurements do not include contributions from SiO_2 or precursor layers, and, therefore, reflect only the thickness of the assembled film.

Statistics. Tests for statistical significance between the means of two groups were conducted with the Student's t-test (two-tailed, homoscedastic). Tests between three or more groups were conducted with the one-way ANOVA followed by the Tukey HSD test.

3.3.   RESULTS

Grafting of methyl-PEG$_4$ to poly(L-lysine) attenuates cytotoxicity in a grafting ratio-dependent manner. Methyl-tetra(ethylene glycol) (mPEG$_4$) was grafted to primary amino groups of poly(L-lysine)hydrobromide (12kD) via NHS ester coupling to generate graft copolymers (PLL$_{12kD}$-g[x]-PEG$_4$(CH$_3$); P12P4[x]) with grafting ratios, x, of 6.7, 4.0, 2.9, and 2.5 (P12P4[6.7], P12P4[4.0], P12P4[2.9], P12P4[2.5], respectively). To investigate the effect of PEG$_4$ grafting on polycation toxicity, islets were incubated in PLL and P12P4[x] copolymers at ~80 μM (~4.5 mM modified and unmodified lysine residues) for 40 minutes, and islet viability was assessed via calcein AM and ethidium homodimer staining (Figure 3.1A) and subsequent quantification with image analysis (Figure 3.1B). P12P4[x] copolymers were synthesized from a common PLL backbone and polymer concentration was maintained at ~80 μM, and, therefore, differences in islet viability can be attributed to the effect of grafted PEG chains. Each polycation tested had significantly different (p<0.01) effects on islet viability relative to all other polycations, with the exception that no statistical difference between P12P4[2.9] and P12P4[2.5] was observed (p>0.05). Hence, PLL cytotoxicity towards pancreatic islets is significantly attenuated through grafting of PEG$_4$ side chains, and P12P4[x] cytotoxicity decreases as grafting ratio is reduced. However, only the viability of islets incubated with P12P4[2.5]

69

was found to be statistically indistinguishable from untreated controls (p>0.05 vs. untreated control group). It should be noted that small, but statistically significant, decreases in islet viability associated with some polycations (e.g., 95.6±1.5% (P12P4[2.9]) vs. 99.2±0.9% (untreated control), p<0.01), are largely due to death of cells only on the islet periphery (Figure 3.1A). While peripheral cell death may not dramatically influence *overall* islet viability or function, it is associated with changes in islet morphology (Figure 3.1A), intercellular internalization of film constituents (Figure 3.3), and eventual shedding/release of dead cells from the islet, all of which are likely to compromise the assembly, properties, and efficacy of cell surface-supported thin films. For this reason, the critical grafting ratio, x_c, for a PLL_M-g[x]-PEG_n copolymer is defined as the grafting ratio whereby no statistical difference (p>0.05) in islet viability relative to untreated controls is achieved under a given set of conditions (e.g., solvent, concentration, incubation time). Hence, the critical grafting ratio for P12P4[x] was found to be 2.5.

Decreasing grafting ratio reduces polycation charge density, and, consequently, at equimolar polymer concentrations, the total concentration of amino groups in solution that may interact with the cell membrane as well. To determine if the observed relationship between cytotoxicity and grafting ratio was simply a consequence of reduced solution amino group concentration, the viability of islets incubated with P12P4[2.5] and P12P4[4] at equimolar concentration of free amino groups (2.6 mM) was compared. The viability of islets incubated with P12P4[4] was found to be significantly less than those incubated with P12P4[2.5] (72.2±19.7% vs. 97.0±2.4%, p<0.01) indicating that the observed reduction in toxicity with increasing PEG_4 grafting is not merely a result of reduced primary amine concentration in solution, but rather a consequence of polymer structure.
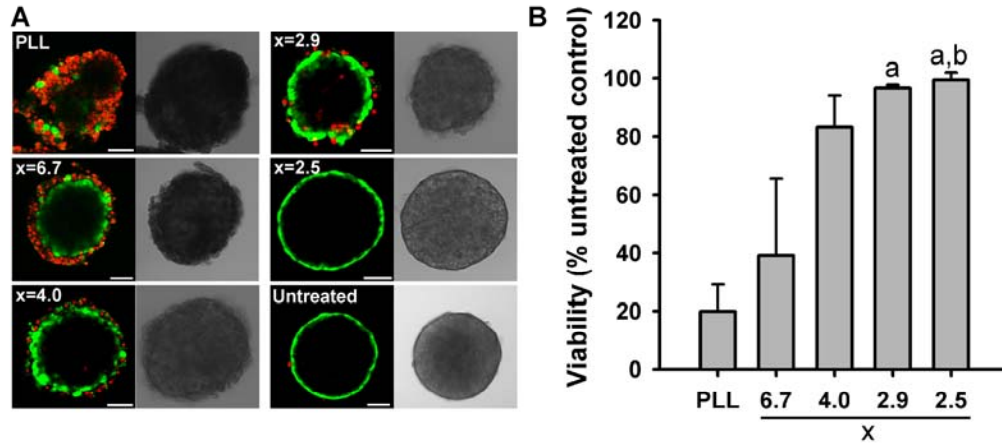
Figure 3.1. Grafting of mPEG$_4$ to poly(L-lysine) reduces cytotoxicity in a grafting ratio-dependent manner. (A) Representative confocal and bright field micrographs of islets stained with calcein AM (green, viable) and ethidum homodimer (red, non-viable) after incubation with PLL and PLL$_{12kD}$-g[x]-PEG$_4$ copolymers of different grafting ratio. Note that polycation-mediated peripheral cell death is associated with changes in islet morphology (scale bar = 50 μm). (B) Quantification of islet viability (relative to untreated control groups) by image analysis (mean ± SD) after incubation (40 m, 80 μM) with PLL and PLL$_{12kD}$-g[x]-PEG$_4$ copolymers of different grafting ratio. Unless otherwise indicated, groups are significantly different (p<0.01) from all other groups. Bars with the same letter label are not statistically different from each other (p>0.05). Bars labeled with the letter b are not statistically different from untreated controls (>0.05).

Effect of PLL molecular weight on PLL$_M$-g[x]-PEG$_4$ copolymer toxicity.

Polycation molecular weight plays an important role in the growth characteristics and properties of polyelectrolyte multilayer thin films [310]. However, the cytotoxicity of most polycations, including PLL, tends to increase with increasing molecular weight [269]. To explore the effect of PLL molecular weight, PLL$_M$-g[x]-PEG$_4$ copolymers with grafting ratios of ~2.5 and PLL backbone molecular weights, M, of 45 kD and 98.8 kD (P45P4[2.5] and P100P4[2.5], respectively) were synthesized. Viability was initially assessed at 1 mg/ml (40 min incubation), corresponding to ~20.5 μM and 9.5 μM, respectively. Even at such reduced molar concentrations, both P45P4[2.5] and P100P4[2.5] exerted significantly more toxicity ($p<0.01$) (Figure 3.2A) than their lower molecular weight counterpart, P12P4[2.5], indicating that PLL molecular weight plays an important role in the toxicity of PLL$_M$-g[x]-PEG$_4$ copolymers and, potentially, that x_c may be unique for a given PLL backbone. To address this possibility, P45P4[x] copolymers with x = 2 and 1.7 were synthesized and their effect on islet viability assessed at ~20.5 μM. Again, a grafting ratio dependence on islet viability was observed (Figure 3.2B), but the critical grafting ratio for PEG$_4$ decreased to 1.7. Comparison of P45P4[1.7] and P12P4[2.5] at equimolar concentration of free amino groups (2.6 mM NH$_2$) revealed no significant difference in islet viability between groups or between each group and corresponding untreated controls ($p>0.05$).
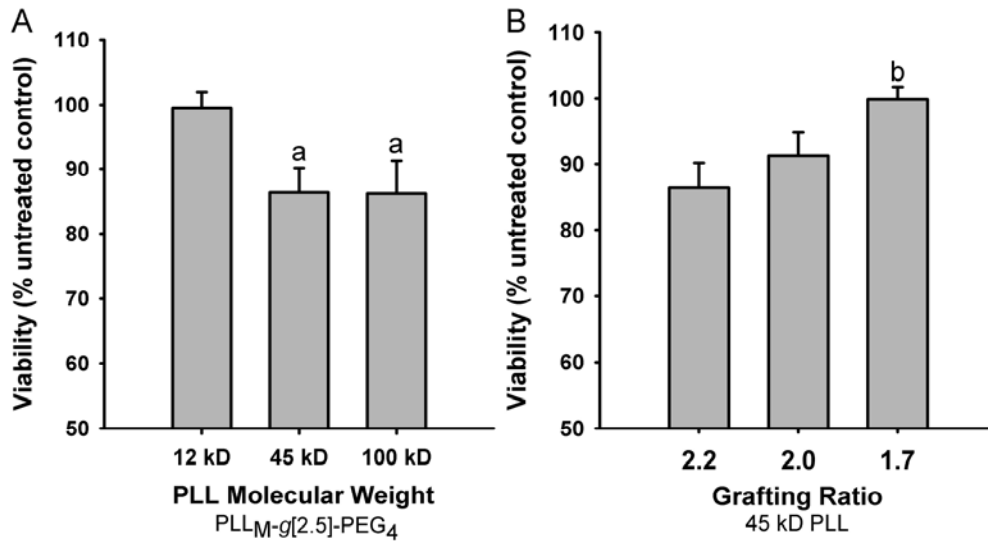
Figure 3.2. PLL molecular weight influences the toxicity of PLL$_M$-g[x]-PEG$_4$ copolymers. (A) At a grafting ratio of 2.5, increasing the molecular weight of the PLL backbone from 12 kD to 45 kD or 100 kD significantly reduces islet viability (mean ± SD, $p<0.01$). (B) Cytoxicity of PLL$_{45kD}$-g[x]-PEG$_4$ copolymers is reduced with decreasing grafting ratio, with a grafting ratio of 1.7 necessary to yield viability statistically indistinguishable from untreated controls. Unless otherwise indicated, groups on the same plot are significantly different ($p<0.1$) from all other groups. Bars with the same letter label are not statistically different from each other ($p>0.05$). Bars labeled with the letter b are not statistically different from untreated control groups ($p>0.05$).

Effect of PEG grafting and PEG chain length on PLL$_M$-*g*[x]-PEG$_n$ copolymer cytotoxicity. To investigate the relative contributions of grafting ratio (and, consequently, reduced polycation charge density) and grafted PEG chains, ~40% of PLL (12kD) backbone lysine monomers were acetylated using sulfosuccinimidyl acetate, yielding a random copolymer consisting of lysine and acetylated lysine (P12Ac[2.5]), an analogous compound to P12P4[2.5] without a PEG$_4$ spacer between the amide linkage and methyl head group. Islets were incubated in P12Ac[2.5] at ~80 μM for 40 minutes and islet viability assessed (Figure 3.3A). Attendant reduction of polycation charge density associated with 40% acetylation of lysine groups significantly (p<0.01) reduced polycation toxicity relative to non-modified poly(L-lysine), further supporting the importance of grafting ratio in polycation toxicity. However, unlike its PEGylated counterpart, P12P4[2.5], P12Ac[2.5] exerted significant toxicity towards islets (p<0.01), indicating that abrogation of toxicity associated with P12P4[2.5] is dependent not only on grafting ratio but also on the presence of grafted PEG chains.

The dependence of PLL$_{12}$-*g*[x]-PEG$_4$ toxicity on both grafting ratio and PEG suggests a possible synergism between the two whereby grafting ratio might be increased by grafting of longer PEG chains. To explore this possibility, methyl-PEG chains consisting of 12 and 24 repeat units (PEG$_{12}$, PEG$_{24}$) were grafted to PLL (12kD) at several different grafting ratios; a PLL backbone with identical properties to those used in the synthesis of P12P4[x] and P12Ac[2.5] copolymers was used to allow the effect of PEG chain length to be explicitly investigated. P12P12[x] copolymers with x=5, 4, 3.3, 2.9, and 2.5 were generated, and viability assessed under identical conditions to P12P4[x] copolymers (80 μM for 40 min). As shown in Figure 3.3B, grafting ratio dependence is still observed, with x=5.0 and x=4.0 statistically different from untreated controls, each other, and all other groups (p<0.01). No statistical difference was

74

observed between x=3.3 and untreated controls or x=2.9 or 2.5 (data not shown),

indicating that x_c for PEG_{12} grafted to PLL_{12kD} is reduced to 3.3. Accordingly, comparison

of islet viability at x=4 for PEG_4 and PEG_{12} (Figure 3.3D) reveals a significant difference

between groups (p<0.01), indicating that, at a given grafting ratio, increasing PEG chain

length reduces polycation toxicity. Grafting of PEG_{24} chains to PLL with grafting ratios of

10, 5, and 4 (P12P12[10], P12P12[5], P12P12[4]) yielded similar trends (Figure 3.3C).

Again, grafting ratio dependence is observed, as both x=10 and x=5 are statistically

different from both untreated control groups and each other (p<0.01), whereas islet

viability is maintained when x=4, indicating that the critical grafting ratio for PEG_{24}

grafted to PLL_{12} is ~4. Comparison of islet viability at x=5 for PEG_{12} and PEG_{24} (Figure

3.3D) reveals a significant increase in viability associated with PEG_{24} grafts, further

supporting the role of PEG chain length in attenuation of toxicity. Collectively, these

findings indicate that grafting ratio and PEG length act together to reduce PLL_{12}-g[x]-

PEG_n cytotoxicity, and that increasing the length of grafted PEG can, to some extent,

compensate for increased polycation charge density associated with an increased

grafting ratio.
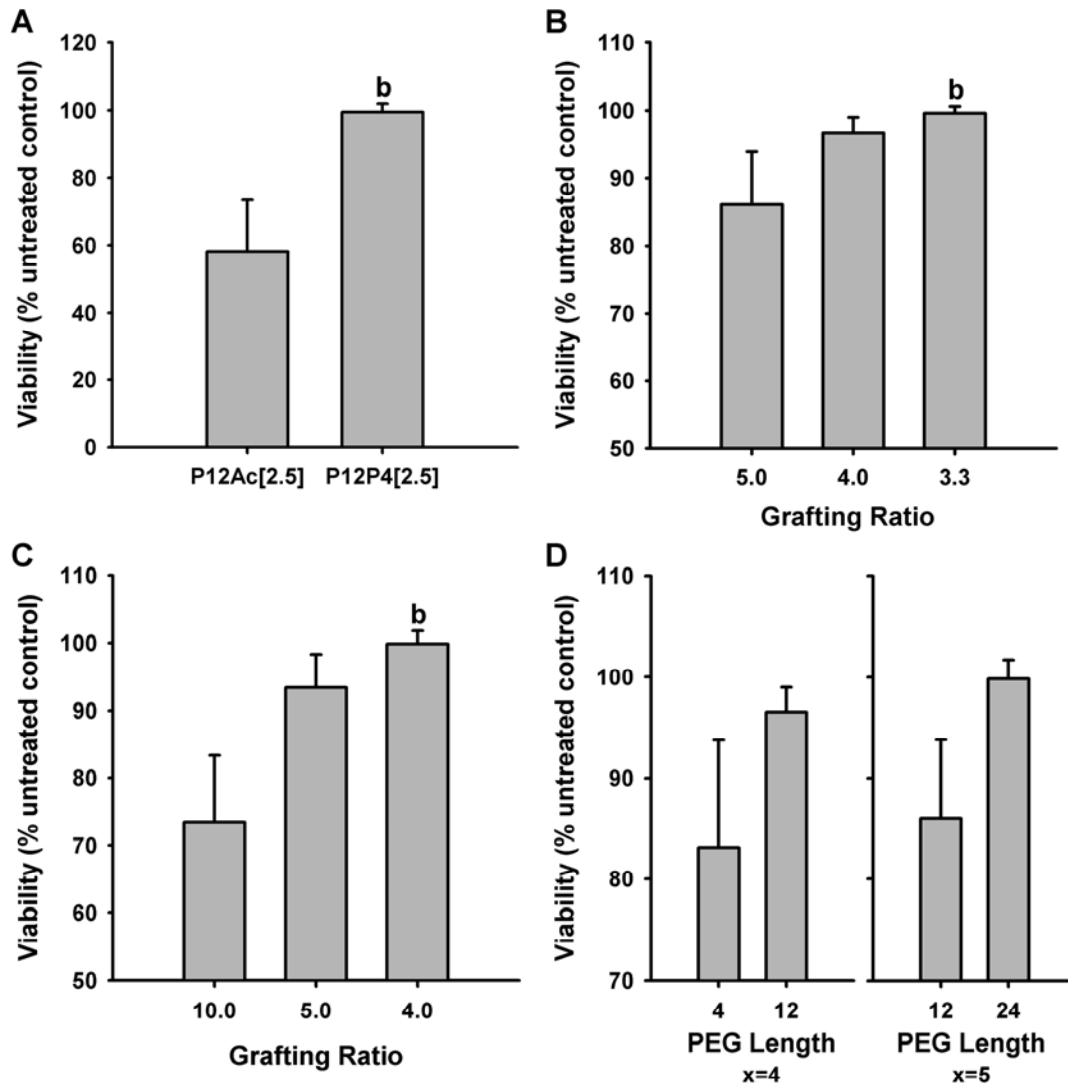
Figure 3.3. Increasing PEG chain length reduces PLL_{12kD}-g[x]-PEG_n copolymer toxicity. (A) Viability of islets (mean ± SD) incubated with copolymers in which 40% of lysine monomers were acetylated (P12Ac[2.5]) or conjugated to $mPEG_4$ (P12P4[2.5]). A significant decrease ($p<0.01$) in islet viability occurs upon incubation with P12Ac[2.5] relative to P12P4[2.5] and untreated controls, indicating a dependence on grafted PEG chains in PLL_{12kD}-g[x]-PEG_n cytotoxicity. Conjugation of PEG_{12} (B) and PEG_{24} (C) chains to PLL attenuates cytotoxicity in a grafting ratio-dependent manner, with grafting ratios of 3.3 and 2.5, respectively, yielding islet viabilities statistically indistinguishable from untreated controls ($p>0.05$). (D) For a given grafting ratio (x=4 and x=5), increasing PEG chain length decreases PLL_{12kD}-g[x]-PEG_n toxicity. Unless otherwise indicated groups on the same plot are significantly different ($p<0.01$) from all other groups. Bars labeled with the letter b are not statistically different from untreated control groups (>0.05).

76

PLL$_M$-*g*[x$_c$]-PEG$_n$ copolymers adsorb to extracellular surfaces of islets.

Many polycations, including PLL, have been shown to induce pore formation in the plasma membrane, a phenomenon which often mediates cell death and enables transport of molecules, including the polycation itself, across the cell membrane [267-269]. Indeed, incubation of islets with FITC-labeled PLL (~80 μM for 40 minutes) resulted in transport of PLL across the cell membrane and into the cytoplasm of individual cells, as indicated by colocalization with cell nuclei (Figure 3.4A,B). Similarly, P12Ac[2.5] labeled with AlexaFluor 488 (P12Ac[2.5]-AF, 80 μM, 40 min) was predominantly localized intercellularly (Figure 3.4C,D), despite a dramatic reduction in the polycation charge density. Conversely, confocal microscopy of islets during incubation (35-45 m) with AF488-labeled PLL$_M$-*g*[x]-PEG$_n$ copolymers at the critical grafting ratio (i.e., P12P4[2.5], P12P12[3.3], P12P24[2.5] (80 μM), P45P4[1.7] (30 μM)), indicates that fluorescent emission remains localized almost exclusively extracellularly, indicating that cell membrane integrity is maintained upon exposure to polymers and that cells did not actively endocytose polymers to an appreciable extent over the course of the incubation (Figure 3.5A-C). Upon rinsing away labeled PLL$_M$-*g*[x$_c$]-PEG$_n$, fluorescent emission was observed in a pattern consistent with the architecture of isolated pancreatic islets (Figure 3.5D-F), indicating that PLL$_M$-*g*[x$_c$]-PEG$_n$ adsorbed to accessible extracellular cell and/or matrix surfaces. The extracellular localization of PLL$_M$-*g*[x$_c$]-PEG$_n$ copolymers relative to PLL or P12Ac[2.5] suggests that conjugation of PEG chains to the PLL backbone inhibits or dramatically reduces the capacity PLL to cross the cell membrane, most likely through inhibition of membrane pore formation, consistent with the observed reduction in toxicity. Significantly, PLL$_M$-*g*[x$_c$]-PEG$_n$ copolymers adsorb to all accessible extracellular surfaces, reflecting the truly conformal nature of such

coatings, and demonstrating the potential to use such polymers to modify or coat

individual cells within a multicellular tissue such as islets.
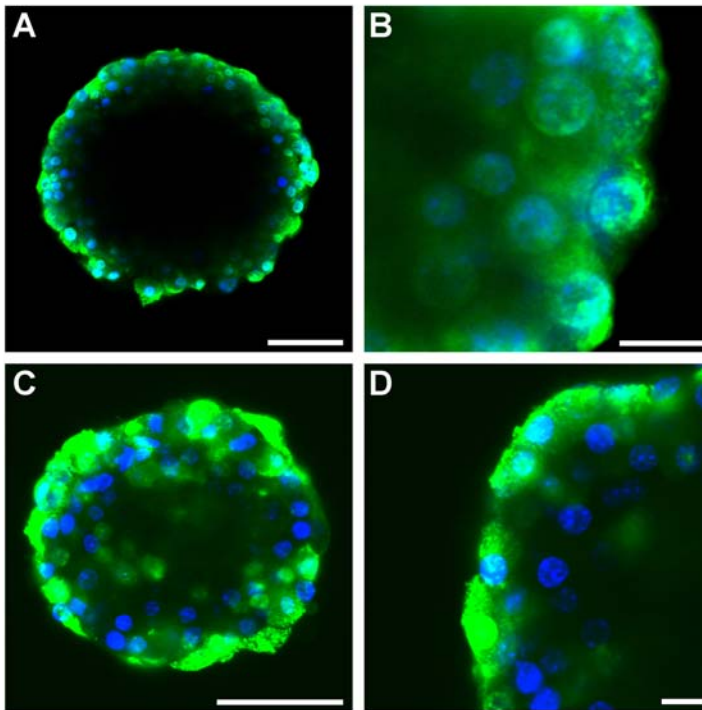
Figure 3.4. Poly(L-lysine) and P12Ac[2.5] localize intercellularly. Confocal micrographs of islets incubated with FITC-labeled PLL (A,B) and AF488-labeled P12Ac[2.5] (C,D) demonstrate fluorescence throughout the cytoplasm of individual cells within islets often colocalized with cell nuclei (blue) identified via Hoechst staining (scale bar: A,C = 50 μm; B,D = 10 μm).
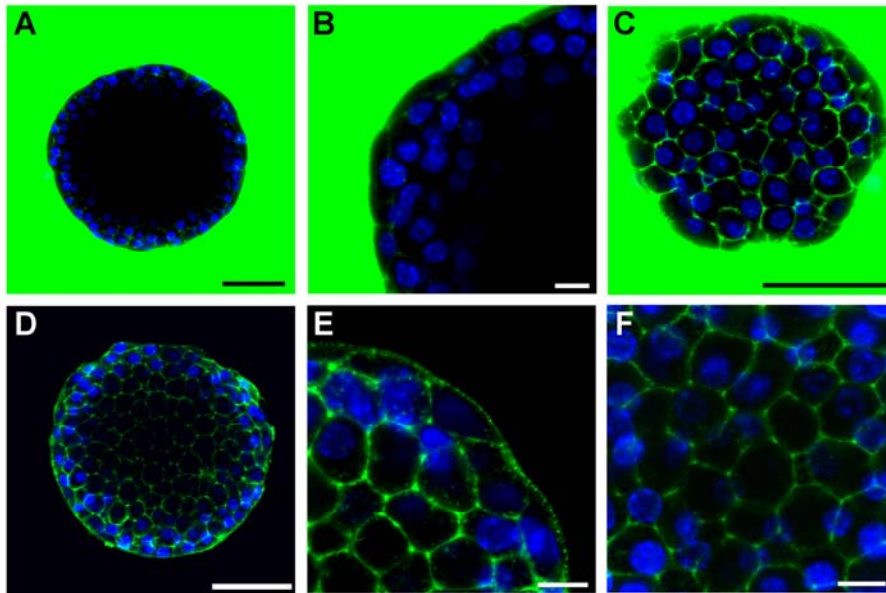
Figure 3.5. PLL$_M$-g[x]-PEG$_n$ copolymers at the critical grafting ratio, x$_c$, remain extracellular and adsorb to extracellular islet surfaces. (A-C) Confocal micrographs of islets during incubation with AF488-labeled PLL$_M$-g[x$_c$]-PEG$_n$ copolymers. After 40 minutes, polymer was observed almost exclusively extracellularly, indicating maintenance of cell membrane integrity and minimal polymer endocytosis. Polymers were able to diffuse into the core of islets through interstitial space and/or capillary networks (C). Upon rinsing, polymers were found to adsorb to the extracellular surface of cells and/or matrix (D-F). Copolymer adsorption was observed both on the islet periphery (D,E) as well as between individual cells within the core of the islet (E,F). Cell nuclei were identified via Hoechst staining (scale bar: A,C,D = 50 μm; B,E,F = 10 μm).

PLL$_M$-g[x$_c$]-PEG$_n$ copolymers facilitate growth of polyelectrolyte multilayer films on surface of viable pancreatic islets. As a consequence of their positive charge and cell surface localization, PLL$_M$-g[x]-PEG$_n$ copolymers at or below the critical grafting ratio provide an anchor for initiating growth of polyelectrolyte multilayer (PEM) thin films on the surface of pancreatic islets (Scheme 3.1). PEM film growth, however, is highly dependent on polycation charge density [311-318], and, therefore, the reduction of charge density associated with generation of PLL$_M$-g[x$_c$]-PEG$_n$ copolymers may preclude film growth. Moreover, surface immobilized PEG, particularly longer chains, may generate steric barriers to electrostatic interaction between positively charged lysine residues on the PLL backbone and alginate, the polyanion. To demonstrate PEM film growth on islets, films were assembled using PLL$_M$-g[x]-PEG$_n$ at x$_c$ (highest charge density) and fluorescein-labeled alginate (F-Alg). Confocal microscopy was used to detect F-Alg on the islet surface and qualitatively compare relative differences in fluorescent intensity between controls and islets coated with a single PLL$_M$-g[x$_c$]-PEG$_n$ bilayer or eight bilayers. To form a single bilayer, islets were incubated in PLL$_M$-g[x$_c$]-PEG$_n$ for 5 minutes, rinsed four times with serum free RPMI, incubated in F-Alg (2 mg/ml) for 5 minutes, and finally rinsed again four times. This process was repeated an additional seven times to generate an eight bilayer film. As a control, the polycation was replaced with RPMI (i.e., solvent only) and islets were treated in an otherwise similar manner. As shown in Figure 3.6A, in which P12P24[4] was used as the polycation in the assembly of an eight bilayer film, fluorescent emission from F-Alg was observed surrounding the islet periphery; qualitatively comparable results were obtained when using P12P12[3.3], P12P4[2.5], and P45P4[1.7] as the polycation. By contrast, controls treated only with alginate in a layer-by-layer manner (Figure 3.6C) demonstrated essentially no fluorescent emission from F-Alg, indicating that the polycationic component is necessary to facilitate immobilization of alginate on the islet surface.

80

Moreover, a dramatic difference in fluorescent intensity was observed between islets coated with eight bilayers (Figure 3.6A) and those coated with a single bilayer (Figure 3.6B). When P12P24[4] and P12P12[3.3] were used as film components, a discernable difference in fluorescent intensity could also be detected between controls and islets incubated with a single bilayer; this difference was not clearly evident when P12P4[2.5] or P45P4[1.7] were used, a potential indicator that less alginate becomes incorporated in the first bilayer when polycations with lower charge density are used. Collectively, these observations indicate that polyelectrolyte multilayer films can be assembled on the surface of islets via alternating deposition of PLL_M-g[x_c]-PEG_n and alginate.

In accord with its role as a component of a cell surface-supported thin film, alginate was concentrated predominately on the islet surface, as fluorescent emission did not colocalize with cell nuclei (Figure 3.6D). To a lesser extent, AlgF could also be identified in the interstitial space between individual cells, consistent with the observed adsorption of PLL_M-g[x_c]-PEG_n in these regions. By contrast, incubation of islets with non-modified PLL (80 μM, 5 minutes), followed by rinsing and incubation with F-Alg (2 mg/ml, 5 minutes) resulted in transport of alginate into the cytoplasm of individual cells on the islet periphery (Figure 3.6E,F), likely a result of membrane permeabilization by PLL and subsequent diffusion of alginate into the cytoplasm.

Importantly, the viability of islets coated with eight bilayer PLL_M-g[x_c]-PEG_n/alginate PEM films was found to be statistically indistinguishable (p>0.01) from untreated controls both immediately after film formation as well as 18-24 hours later, indicating that film formation does not induce late necrosis or apoptosis (Table 3.2). Additionally, islets could be incubated with PLL_M-g[x_c]-PEG_n copolymers (80 μM in DPBS supplemented with 11 mM glucose) for six hours with minimal or no significant decrease in islet viability (Table 3.3), a promising indication that considerably more layers may be

assembled if desired, and a further testament to the low cytotoxicity associated with these copolymers.
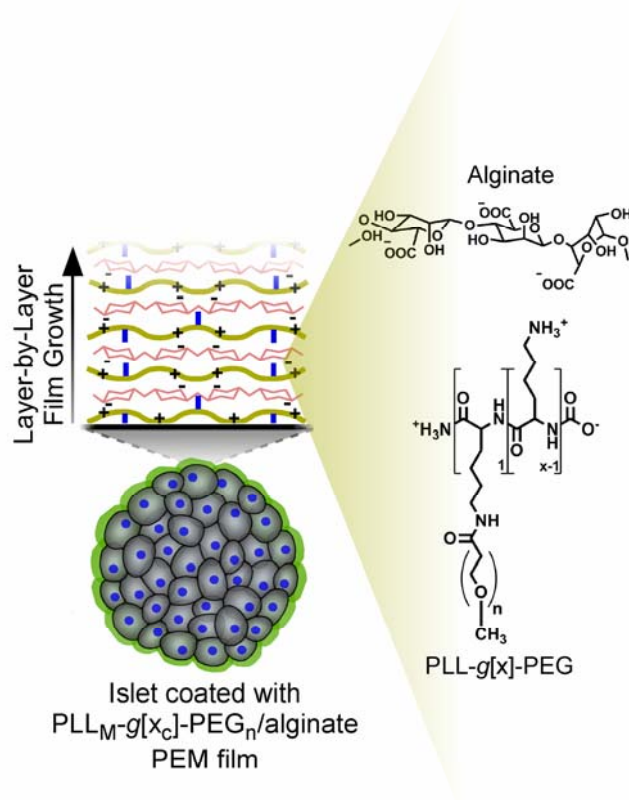
Scheme 3.1. Assembly of cell surface-supported polyelectrolyte multilayer thin films via layer-by-layer deposition of poly(L-lysine)-*g*[x]-poly(ethylene glycol)$_n$ at the critical grafting ratio, x_c, and alginate.
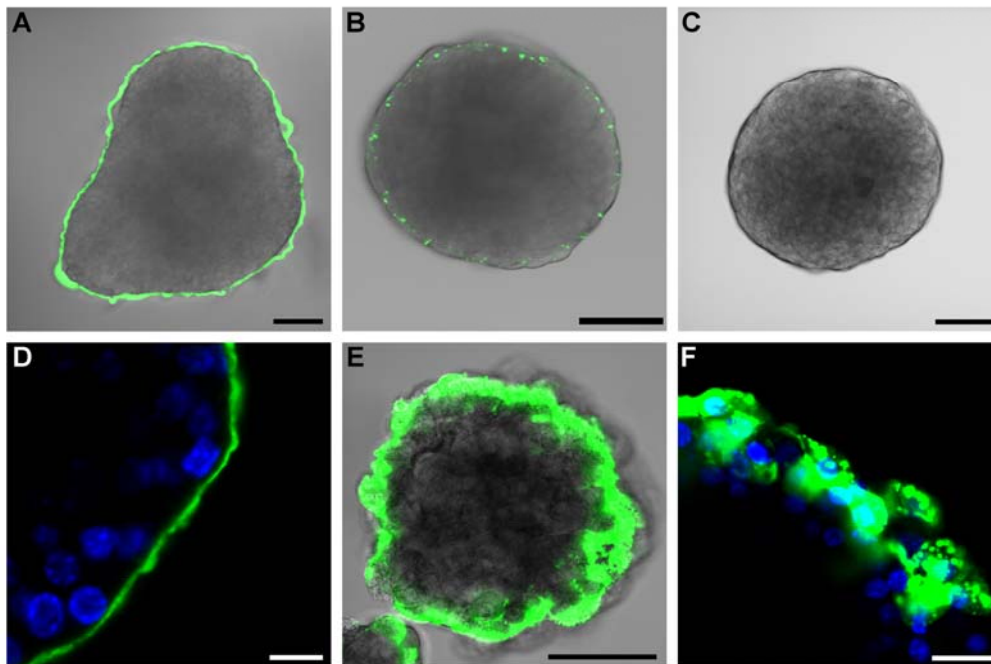
Figure 3.6. Polyelectrolyte multilayer (PEM) films can be assembled on individual pancreatic islets through layer-by-layer deposition of PLL_M-g[x_c]-PEG_n copolymers and alginate. Using P12P24[4] and fluorescein labeled alginate as polycation and polyanion, respectively, confocal micrographs of coated islets reveal dramatic differences in fluorescent intensity associated with films comprised of eight bilayers (A) and a single bilayer (B). Qualitatively comparable images were obtained using P12P12[3.3], P12P4[2.5], and P45P4[1.7] as polycations. Controls treated only with alginate eight times in an analogous layer-by-layer manner (C) demonstrate little or no fluorescence, indicating that alginate deposition is polycation-dependent. After assembly of eight bilayers, alginate incorporated into PEM films is localized predominantly on the extracellular surface of islets (D). By contrast, fabrication of a single PLL/alginate bilayer results in intercellular internalization of alginate by peripheral cells (E,F). Cell nuclei were identified via Hoechst staining (scale bar: A,B,C,E = 50 μm; D,E = 10 μm).

Table 3.2. Islet viability immediately and 18-24 hours after assembly of a $(PLL_M\text{-}g[x_c]\text{-}PEG_n/\text{alginate})_8$ PEM film

Polycation Used	Immediate[*]	18-24 h post-coating[*]
P12P24[4.0]	100.2 ± 1.3	99.3 ± 1.5
P12P12[3.3]	100.1 ± 1.9	100.7 ± 1.5
P12P4[2.5]	100.4 ± 0.8	99.3 ± 1.4
P45P4[1.7]	99.0 ± 1.4	100.9 ± 1.2

[*]No statistical difference vs. other groups (p>0.05) or vs. untreated controls (p>0.01)

Table 3.3. Islet viability after six hour polycation incubation

Polycation Used	Viability (% untreated control)[*]
P12P24[4.0]	99.4 ± 1.1
P12P12[3.3]	99.5 ± 1.7
P12P4[2.5]	99.5 ± 2.2
P45P4[1.7]	99.8 ± 2.0

[*]in DPBS supplemented with 11 mM glucose. No statistical difference between groups (p>0.05) or relative to untreated controls (p>0.01).

PLL$_M$-g[x$_c$]-PEG$_n$ copolymers generate PEM films with unique properties.

Employing PLL$_M$-g[x]-PEG$_n$ copolymers of variable charge density and PEG length and content offers the possibility of generating PEM films of unique or tailored properties. To gain insight into the properties of PEM films assembled using PLL$_M$-g[x]-PEG$_n$ at the critical grafting ratio, x$_c$, film growth characteristics and properties were investigated on planar substrates by solid-state UV-vis spectroscopy and ellipsometry. Solid-state spectroscopy (Figure 3.7) of films assembled using P12P4[2.5], P1212[3.3], and P12P24[4] as polycations demonstrate a non-linear, exponential-like growth pattern through 12 bilayers, with P12P24[4] displaying the steepest growth profile. Similar profiles have been reported for films assembled using non-modified PLL and alginate [270] or hyaluronic acid [319], and are generally distinguished from linear growth profiles by the ability of film constituents to diffuse within the film during assembly [320, 321]. Films assembled using P45P4[1.7] displayed evidence of film growth through six bilayers, but reached a plateau beyond this point, likely due to the low charge density (i.e., 40%) associated with this polymer. Incubation of all films in 5 M NaCl for 20 minutes resulted in complete film decomposition (Figure 3.7B), demonstrating that indeed PLL$_M$-g[x]-PEG$_n$/alginate films are assembled via electrostatic interactions [322].

Film thickness was measured using ellipsometry (Table 3.4) after formation of 4, 6, and 8 bilayers assembled using P12P4[2.5], P1212[3.3], and P12P24[4] as polycations; limited ellipsometric characterization of films assembled with P45P4[1.7] was performed due to stagnated growth observed in UV-vis spectroscopy experiments. Ellipsometric film thickness measurements provided further evidence of multilayer film growth, as thickness was found to increase with increasing layer number (Figure 3.8). Significantly, film thickness was also dependent on the PLL$_{12}$-g[x$_c$]-PEG$_n$ polycation employed for film formation. P12P24[4] yielded significantly thicker films at 4, 6, and 8 bilayers than both P12P12[3.3] and P12P4[2.5] (p<0.01). Films assembled with

P12P12[3.3] were significantly thicker than films assembled with P12P12[4] at both 6 and 8 bilayers ($p<0.01$), though thicknesses were statistically comparable ($p>0.05$) after assembly of four bilayers. Hence, film thickness may be tailored through control of layer number as well as PLL_{12}-g[x_c]-PEG_n properties.

After fabrication of eight bilayers, UV-vis spectroscopy revealed no significant difference ($p>0.05$) in absorbance at 495 nm between films assembled with P12P4[2.5] and P12P12[3.3]. Ellipsometric film thickness measurements, however, indicate that P12P12[3.3] films are significantly thicker than P12P4[2.5] films, suggesting an increased concentration of polycation in films assembled with P12P4[2.5]. Similarly, after fabrication of eight bilayers, films assembled using P12P24[4] are twice as thick as those assembled using P12P12[3.3], while absorbance at 495 nm is only 1.3 fold greater, again suggesting a difference in the interfilm concentration of the polycationic component. As the charge density of these polycations differs by only 5%, these observations suggest that the observed doubling of film thickness may be due to increased incorporation of PEG in films assembled using P12P24[4]. Hence, polyelectrolyte multilayer films of diverse thickness, structure, and composition may be generated using PLL_{12}-g[x]-PEG_n as film constituents, potentially allowing film properties to be tailored for a desired application.

Figure 3.7. Polyelectrolyte multilayer (PEM) films assembled using PLL_M-g[x_c]-PEG_n copolymers and alginate demonstrate unique growth profiles on planar substrates. Solid-state UV-vis spectroscopy was used to monitor film growth on quartz substrates. (A) Example of absorbance spectra recorded after the second PLL_M-g[x_c]-PEG_n (e.g., P12P24[4]) incubation and every other incubation thereafter through twelve depositions. (B) Absorbance values at 495 nm, corrected to account for differences in degree of labeling, as a function of layer number (mean ± SD). Use of P12P4[2.5] (●), P12P12[3.3] (○), and P12P24[4] (▼) as polycations resulted in layer-by-layer film growth with a non-linear, exponential-like growth pattern. By contrast, film growth using P45P4[1.7] (△) stagnated after six bilayers. After incubation of all films in 5 M NaCl for 20 minutes absorbance at 495 nm was essentially absent, indicating complete film decomposition and, hence, assembly through electrostatic interactions.

Figure 3.8. Film thickness increases with layer number and may be tailored through PLL_{12kD}-g[x_c]-PEG_n properties. Ellipsometric film thickness measurements (mean ± SD) after assembly of 4, 6, and 8 bilayers using P12P24[4] (●), P12P12[3.3] (○), and P12P4[2.5] (▼) as polycations and alginate as the polyanion. Measured thicknesses and statistical analysis are provided in Table 3.4.

Table 3.4. Ellipsometric film thickness measurements

Polycation Used	Layer Number		
	4	**6**	**8**
P12P24[4.0]	12.6 ± 1.3	28.1 ± 1.2	72.4 ± 1.9
P12P12[3.3]	8.5 ± 1.1[a]	16.9 ± 0.8	36.1 ± 2.6
P12P4[2.5]	6.6 ± 1.5[a]	13.8 ± 1.1	26.0 ± 1.3
P45P4[1.7]	6.8 ± 1.0[a]	NP	NP

[a]Not statistically different from each other (p>0.5). All other entries are statistically significant from each other (p<0.05). NP: not performed

3.4. DISCUSSION

Layer-by-layer (LbL) polymer self assembly represents a facile approach for coating diverse materials of heterogeneous morphology and composition with nanothin films of tailored surface chemistry, permeability, and bioactivity [249, 251, 288]. Consequently, several groups have begun to explore the possibility of constructing LbL films directly on the surface of mammalian cells and tissues [265, 303-307, 323]. While covalent [306] and receptor-ligand interactions [303, 307] have recently been explored as driving forces for assembling films on pancreatic islets, the well documented toxicity of most synthetic and natural polycations [267-269, 298-302] poses a significant challenge in the design of cell surface-supported polyelectrolyte multilayer (PEM) films, the most commonly employed and versatile LbL film architecture [250]. Regardless, several groups have sought to generate PEM films on adherent cell monolayers [304] or single cells in suspension [305] using polycations classically employed in PEM film fabrication. Germain et al. [304] attempted to coat adherent MELN and HeLa cells using a number of polycations and polyanionic poly(styrene sulfonate) (PSS) [304]. Most polycations explored, including PLL, were extremely cytotoxic, though films of composed of nine poly(diallyldimethylammonium chloride)/PSS bilayers could be assembled with a modest ~25% decrease in cell viability. Similarly, Veerabadran et al. have recently reported the assembly of PLL/hyaluronic acid multilayer films on mouse mesenchymal stem cells [305]. While different cell types are more susceptible to polycation-mediated damage than others [300, 301], these findings are surprising given the reported toxicity of PLL to a number of cell types at the concentrations (1 mg/ml) and deposition times (15 m) used in this investigation [269, 276, 298-302, 324, 325]. Regardless, as demonstrated herein, PLL exerts considerable toxicity to islets, and is an unsuitable film constituent for islet nanoencapsulation. Krol et al. have attempted coat human pancreatic islets with a poly(allylamine hydrochloride) (PAH)/PSS/PAH PEM film [265];

89

assembly of this film on islets, however, has recently been shown to reduce islet viability by approximately 70% [303], consistent with the known toxicity of PAH towards islets [302]. To help prevent direct contact between PLL and the islet surface, Miura et al. have attempted to assemble a very thin alginate/PLL/alginate film on islets by first inserting a cationic lipid conjugate into islet cell membranes, thereby generating a positively charged islet surface to facilitate electrostatic binding of negatively charged alginate [323]. While conceptually appealing, careful inspection of confocal micrographs of coated islets suggests intercellular localization of FITC-labeled PLL within the outer few cell layers, a likely indicator of peripheral cell death. In light of both the enormous potential and versatility of PEM films and the challenges adherent to their assembly on viable mammalian cell and tissue surfaces, a need exists to develop cytocompatible polycations and/or PEM film architectures.

We have previously demonstrated that conjugation of poly(ethylene glycol)$_{3.4kD}$(biotin) to ~40% of backbone lysine residues abrogates the cytotoxicity of PLL towards pancreatic islets, and that resultant the PLL-g-PEG$_{3.4kD}$(biotin) copolymer (PPB) provided a foundation for film assembly via receptor-ligand interactions [303] (Chapter 2). Given the non-toxic nature of this polymer, it was hypothesized that through proper control of grafting ratio and PEG chain length, PLL-g-PEG copolymers could be synthesized with sufficient charge density to initiate and propagate PEM film growth, while simultaneously preserving islet viability. However, most PLL-g-PEG copolymers synthesized to date, including PPB, have utilized ~2-5 kD PEG grafts which adopt a brush-like conformation upon interfacial adsorption of the copolymer, generating a steric barrier to protein adsorption and molecular recognition [262, 270-272, 284, 308]. While such brush-borders are useful for generating non-fouling interfaces, the steric barrier presented by grafted PEG chains might similarly hinder electrostatic interations with polyanions necessary to drive film growth. Therefore, in an effort to generate

cytocompatible polycations while minimizing steric barriers to electrostatic interactions, PLL_M-g[x]-PEG_n copolymers were synthesized with relatively short PEG chains consisting of 4, 12, or 24 repeat units.

Polycation charge density influences both cytotoxicity [267, 269] and PEM film growth [312-318]; while decreasing polycation charge density generally attenuates cytotoxicity, PEM film growth and properties may be compromised. In this regard, polycation charge density represents a critical variable for the design of cell surface-supported PEM films. As maintenance of cell viability is of utmost importance to islet encapsulation and surface engineering, the critical grafting ratio, x_c, whereby islet viability was preserved for a given set of conditions (e.g., solvent, concentration, incubation time) was determined by assessing the toxicity of copolymers synthesized with various grafting ratios. Through determining x_c the maximum permissible charge density for a given copolymer structure was achieved.

Though perhaps a simplification, it has been suggested that polycation cytotoxicity, beyond a critical number [276], is related to the number of attachments between cationic monomers and the cell surface, and, consequently, increasing the space between charged groups has been shown to decrease polycation toxicity [269, 276, 301]. Accordingly, for all copolymers synthesized with a common PLL backbone and PEG chain length, a decrease in cytotoxicity was observed with decreasing grafting ratio, i.e. increased average distance between non-modified lysine residues. Interestingly, increasing the molecular weight of the PLL backbone significantly increased toxicity of PLL_M-g[2.5]-PEG_4, mandating increased PEG incorporation to abrogate cytotoxicity. A similar phenomenon has been reported by Mao et al. upon grafting of PEG chains to chitosan [326]. Polycation toxicity has been shown to increase with increasing molecular weight, as more attachment sites per chain are available to interact with the cell membrane [269, 299, 300]. Moreover, as a random graft

91

copolymer, the probability of achieving a given number of consecutive lysine residues increases with molecular weight, and it is conceivable that such highly charged segments may be capable of eliciting cytotoxicity [276]. Hence, higher charge densities may be achieved by reducing the molecular weight of PLL.

In an effort to increase charge density or eliminate mPEG$_4$ grafts, copolymers bearing longer PEG chains (i.e., P12P12[x] and P12P24[x]) or no PEG chains at all (P12Ac[x]) were generated and cytotoxicity assessed. Interestingly, at a charge density of ~55-60%, substitution of mPEG$_4$ grafts with acetate groups resulted in a significant increase in polymer toxicity, suggesting a role for grafted mPEG$_4$ that is independent of net charge. Accordingly, increasing the length of PEG chains resulted in a significant decrease in polycation toxicity for a given grafting ratio. Similar findings have recently been reported for chitosan-*g*-PEG copolymers, as increasing the molecular weight of PEG from 550 Da (~PEG$_{12}$) to 5000 Da (~PEG$_{114}$) was associated with dramatic reductions in toxicity at a common charge density [326]. While a roughly linear relationship between grafted PEG$_n$ length and critical grafting ratio was observed between n=4 and n=12, previous results indicate that conjugation of biotin-PEG$_{70}$ chains to a similar PLL backbone does not abrogate toxicity at a grafting ratio of ~5.0 [303], and, therefore, it is anticipated that the PEG chain length dependence approaches an asymptotic limit.

Collectively, these findings suggest a cooperative relationship between grafted PEG chains and charge density in the attenuation of PLL cytotoxicity, a phenomenon that may be explained by the physiochemical properties of polymers in solution and at the cell interface. In addition to charge density, polycation architecture and conformational flexibility influence the specific arrangement of cationic monomers at the cell interface [269, 276, 298, 301]. Highly flexible polymers, such as PLL, more readily contort to access anionic groups, whereas charged residues within globular or

92

dendrimeric polycations are constrained. In this regard, steric repulsion between grafted PEG chains may restrict the conformational flexibility of the PLL backbone, an effect anticipated to be pronounced with longer PEG grafts. Indeed, such molecular "bottle brush" conformations have recently been described for comparable PLL-*g*-PEG copolymers, with an attendant increase in persistence length at decreased grafting ratios and longer PEG chains [327]. Decreased chain conformational freedom might also explain the common observation that poly(L-lysine) adsorbed to a flat surface, for example, glass coverslips, promotes cell adhesion, while not eliciting toxicity. Additionally, PLL has been shown to transition from a random coil in solution to an alpha helical conformation at the cell surface in order to maximize interfacial contact [328], a phenomenon that may be sterically interrupted by grafted PEG in a chain length-dependent manner. The interplay between electrostatic attraction of the PLL backbone to a negatively charged surface and steric repulsion caused by grafted PEG chains dictates the adsorption behavior of PLL-*g*-PEG copolymers [329], and, potentially, the density and distribution of cationic monomers in contact with the cell surface. Adsorbed polyelectrolytes can be considered to consist of loops and trains, where two trains which make intimate contact with the surface are connected by loops that extend into the bulk [330]. Through steric considerations, PEG grafts would reasonably be expected to increase the length of loops between trains: cationic monomers a sufficient distance from a grafted PEG chain would be free to interact with anionic groups on the cell membrane (trains), whereas those in closer proximity to PEG chains may be sterically hindered from such interactions, and, therefore, extend towards the bulk (loops). Increasing PEG chain length would be expected to further interfere with electrostatic interactions [327], forcing more cationic monomers into loops away from the cell surface. Hence, in such a model, increasing PEG length would have a similar effect to decreasing charge density in that the effective distance between charged groups

interacting with the cell surface is increased, thereby allowing higher main chain charge densities without increasing cytotoxicity.

To a lesser but notable extent, non-electrostatic interactions between polycations and cell surfaces also play a role in mediating cytotoxicity [331-333]. As such, otherwise identical polycations with respect to size, charge, and flexibility may invoke dramatically different cytotoxic effects depending on their specific molecular make up. Most notably, polymer hydrophobicity acts cooperatively with electrostatic interactions in disrupting cell membranes, at least in part, through increasing the favorability of interactions between the polymer and lipid tails within the plasma membrane [332-335]. Structurally identical poly(L-lysine)-based peptides bearing a high density of serine were found to be significantly less toxic than those bearing leucine residues, presumably due to incorporation of hydroxyl groups in the former [333]. As a hydrophilic macromolecule, PEG chains may act through similar mechanisms to reduce toxicity. Alternatively, administration of soluble PEG and PEG-based amphiphilic copolymers, most notably Poloxamers, to cells damaged through mechanical, thermal, or electrical insult has been shown to promote repair of damaged cell membranes [336-339]. Though mechanisms of repair remain poorly understood, PEG is thought to transiently seal the compromised portion of the membrane while lipids rearrange and re-establishment membrane integrity [337, 338]. As polycations exert toxicity in large part by generation of nanoscale holes in the cell membrane [267, 268], it is conceivable that grafted PEG chains may inhibit pore formation or promote sealing of pores generated by adjacent lysine residues. Given the importance of cell viability in the assembly of cell surface-supported PEM films and the complexity of biochemical and biophysical processes that dictate polycation toxicity, mechanisms through which grafting of PEG chains to PLL attenuate toxicity should be further investigated.

As the cell surface serves as the substrate for PEM film assembly, polycation-mediated membrane pore formation may also have adverse effects on the formation and/or properties of PEM films. The formation of nanoscale pores allows unregulated efflux of molecules across the plasma membrane, not only contributing to cell death, but also facilitating the passage of the polycation itself into the cytoplasm [267-269]. Indeed, PLL and P12Ac[2.5], both of which were found to exert significant toxicity, were localized predominantly intracellularly, evenly distributed throughout the cytoplasm of peripheral cells. Accordingly, attempts to assemble a PLL-alginate bilayer resulted in diffusion of alginate across the cell membrane and concentration within the cytoplasm. Cytotoxicity notwithstanding, membrane pore formation appears to lead to the formation of intracellular polyelectrolyte complexes rather than cell surface-supported films per se, an important distinction in light of the properties and potential applications of each. Previous reports utilizing conventional polycations to assemble films on islets [265, 323] have inadequately investigated the localization of film components and it is unclear if these approaches truly yield thin films.

Conversely, PLL_M-g[x]-PEG_n copolymers at the critical grafting ratio remain localized extracellularly, suggesting that grafting of PEG chains to PLL inhibits formation of membrane pores, a likely cause or consequence of reduced cytotoxicity. More importantly, however, PLL_M-g[x_c]-PEG_n copolymers adsorb to all accessible surfaces of pancreatic islets, presumably through electrostatic interactions, providing a foundation upon which film growth may be initiated. Among other variables, the capacity of adsorbed PLL_M-g[x_c]-PEG_n copolymers to initiate, and subsequently propagate, PEM film growth is thought to be dictated by an interplay between main chain charge density (electrostatic attraction) [312-314] and the length of grafted PEG chains (steric repulsion) [329, 340]. Hence, upon tailoring grafting ratio and PEG chain length to accommodate high islet viability, it was unclear whether the structure of resultant copolymers would

facilitate PEM film formation. In light of these constraints, it is perhaps not coincidental that, to the author's knowledge, only a single report exists to date describing fabrication of a PEM film using a polyelectrolyte with grafted PEG chains [340]. In this report, Boulmedais and co-workers assembled several bilayers atop an existing PEM structure using PLL and poly(L-glutamic acid) grafted with 2 kD PEG chains at a grafting ratio of ~5.0.

Using confocal microscopy and fluorescently-labeled alginate, which alone does not adsorb to islets in an appreciable manner, PEM film assembly on the surface of islets was clearly demonstrated, as evidenced by obvious differences in the fluorescent intensity between islets coated with none, one, or eight bilayers. The capacity of copolymers to initiate film growth suggests a sufficient number of lysine residues remain free from association with negatively charged groups on the cell membrane, an effect which, as discussed previously, may also contribute to reduced cytotoxicity. Of critical importance, islet viability and morphology were maintained after fabrication of eight bilayers, and, not coincidently, film growth was observed almost exclusively on the extracellular surface of individual cells within pancreatic islets. Interestingly, PEGylated polycations have also been used routinely to mediate intracellular delivery of nucleic acids [341-345], an objective that appears to contrast starkly with the development of polycations as components of cell surface-supported PEM films. As the polymer properties and/or biochemical mechanisms that mediate intracellular delivery may be different than those which promote polymer adsorption to the cell surface, further elucidation of such mechanisms will be critical to the rational design of LbL films as conformal cell coatings.

Though the properties of films assembled on the chemically and geometrically hetereogenous interfaces presented by cells may be different than those assembled on idealized planar supports, investigation of films by UV-vis spectroscopy and ellipsometry

96

was performed to provide insight into relationships between copolymer structure and film properties. Solid-state absorption spectra of films assembled using P12P4[2.5], P1212[3.3], and P12P24[4] as polycations demonstrated a non-linear, exponential-like growth pattern. Exponential-like growth is anticipated to yield thicker films for a given number of polymer depositions [320, 346], minimizing polycation exposure and coating time. By contrast, LbL films assembled as conformal islet coatings through covalent [306] or receptor-ligand [303] interactions demonstrate linear growth profiles. While perhaps less commonly observed than linear PEM film growth [249, 347-349], exponential film growth has been reported to occur for a number of polyelectrolyte pairs and/or solvent conditions [253, 319-321, 346, 350]. Interestingly, PLL appears commonly in the assembly of such films, including those assembled using alginate as the polyanion [253]. Exponential film growth is generally considered to occur as a consequence of polyelectrolyte diffusion into and out of the film during deposition and washing steps, leading to increased polyelectrolyte complexation at the outer surface of the film [319-321]. By contrast, linear growth is characterized by each layer penetrating only with neighboring ones [249, 351, 352]. However, while clearly non-linear, the growth profiles observed with UV-vis spectroscopy may also not be properly described as truly exponential. Indeed, Porcel et al. have recently described an exponential-to-linear transition that occurs during the growth of PLL/hyaluronic acid films, which demonstrate similar growth profiles to those observed in Figure 3.7 [353]. Importantly, these authors speculate that exponential-to-linear transitions occur due to a progressive restructuring or densification that prevents the aforementioned intrafilm diffusion of polyelectrolytes to deeper regions of the film [353]. In light of such a mechanism, the extent of deviation from exponential growth may reflect different degrees of film densification, a possible indication that film permeability may be controlled through both copolymer structure and layer number. Prior to this transition, however, intrafilm diffusion of the polycation [320,

97

354] might permit its interaction with the cell membrane even after deposition of a number of layers, further reinforcing the importance of cytocompatible polycations.

While increasing polycation molecular weight has been reported to yield thicker films [310, 355], film growth stagnated when P45P4[1.7] was used in film formation, likely as a result of the 60% decrease in charge density necessary to accommodate polycation cytocompatibility. Charge density plays a critical role in dictating the growth and properties of PEM films, and several investigators have defined a critical charge density beyond which film growth is no longer possible [311-318]. A considerable range of critical charge densities have been reported, from 10% [317] to 75% [312], with dependence on the polyelectrolyte pair used, solvent conditions, the charge density and size of the polyanion, and the prevalence of secondary, non-electrostatic interactions (e.g., hydrogen bonding). While not explicitly determined, a charge density above 40% appears to be necessary to promote assembly of films using P45P4 copolymers; such polymers, however, were found to exert cytoxicity towards islets. While such effects might be remedied through increasing the length of PEG grafts, these investigations suggest that PLL-g-PEG copolymers synthesized with lower molecular weight PLL backbones are structurally more suitable for assembling PEM films on islets.

Ellipsometric characterization revealed significant differences in film thickness depending on the PLL$_{12kD}$-g[x_c]-PEG$_n$ copolymer employed, providing a potential opportunity to tailor film thickness through both layer number and polymer structure. Depending on the polycation used, film thicknesses ranged from 25-70 nm in the *dry state* after fabrication of eight bilayers. PEM films, however, have been shown to swell considerably upon hydration [356-359]; for example, films assembled using PLL and poly(L-glutamic acid) were found to swell by ~150% [358], whereas chitosan/hyaluronic acid films may swell by as much 400% [356]. Moreover, given the high PEG content of these films, even greater degrees of swelling would be reasonably expected [360, 361].

Relative to those with linear growth profiles, films presenting exponential-like behavior are considered to be much less structured, adopting characteristics similar to viscoelastic hydrogels [362]. Indeed, upon assembly of twelve bilayers, films appeared highly hydrated and presented a gel-like appearance, particularly when P12P24[4] was used, a finding consistent with previous reports [253, 349]. Hence, while explicitly determining the hydrated thickness of films is an area of future investigation, in light of these considerations, it is reasonable to assume that eight bilayer films in the hydrated state, such as those on assembled on islets, may be on the order of hundreds of nanometers thick. By contrast, conformal islet coating strategies utilizing interfacial polymerization [147, 148], selective withdrawal [146], or emulsification [144] yield 5-50 *micron* thick coatings. Hence, assembly of polyelectrolyte multilayer films on the surface of islets allows conformal coatings many orders of magnitude thinner to be created.

It is unclear whether or not a critical or optimal thickness for conformal islet coatings exists. Previous reports describing the assembly of PEM films comprised of one or two bilayers [265, 323] are likely on the order of 10 nm thick [253, 346], comparable to the size of the cell surface targets they intend to cover. Elbert et al. demonstrated that 50 nm thick (measured in the dry state) PLL/alginate films prevented adhesion of fibroblasts to extracellular matrix, whereas 10 nm films proved less effective. Interestingly, films assembled using P12P4[2.5] are of comparable thickness (~25-30 nm) to films assembled using unmodified PLL [253], a potential indicator of comparable structure. Similarly, Thierry et al. [254] demonstrated that assembly of five chitosan/hyaluronic acid bilayers, estimated to be on the order of 20 nm in the dry state [356], inhibited platelet deposition to a damaged artery, a finding with potential implications for attenuating platelet-islet interactions during intraportal islet transplantation [286]. While clearly dependent on a number of other film properties as

well, most notably permeability and uniformity, coatings of nanoscale thickness may be successfully used as barriers to molecular recognition.

3.5. CONCLUSIONS

Cell surface-supported polyelectrolyte multilayer films assembled through layer-by-layer deposition of cytocompatible PLL-*g*-PEG copolymers and alginate provide a novel and versatile approach to conformal islet coating and surface modification. Through appropriate control of structural variables, PLL-*g*-PEG copolymers could be rendered effectively non-toxic while simultaneously facilitating the assembly of a unique class of PEM films with tunable properties. Additionally, through elucidating relationships between PLL-*g*-PEG copolymer structure, cytotoxicity, and PEM film properties, this work begins to establish a conceptual framework for the rational design of cell and tissue-surface supported nanoassemblies. While further characterization and optimization of film properties may be necessary to generate effective conformal barriers for islet transplantation, layer-by-layer assembly of PEM films offers an opportunity to decrease coating thickness by many orders of magnitude in a scalable manner without loss of islet number or viability. Finally, in light of the numerous and diverse biomedical and biotechnological applications of PEM films, the potential to translate such functionality to the surface of viable mammalian cells and tissue offers rich opportunities for re-engineering the biophysiochemical properties of cell and tissue interfaces.

CHAPTER 4

A Modular Approach to Cell and Tissue Surface Engineering Using Cytocompatible Poly(L-Lysine)-*graft*-poly(ethylene glycol) Copolymers and Polyelectrolyte Multilayer Films

4.1   INTRODUCTION

Cell surface engineering bestows control of the molecular and biochemical composition of the extracellular surface of mammalian cells. Cell surface engineering has introduced enzymes [363], receptors [364, 365], carbohydrates [366], fatty acids [367], fluorophores and photoaffinity labels [368], organic and inorganic nanostructures [303, 369], synthetic polymers [165, 270], reactive handles [370, 371], and peptide sequences [368, 372, 373] to the complex biochemical milieu of the cell surface through genetic, metabolic, enzymatic, chemical, and physical processes. Accordingly, cell surface engineering has provided an invaluable tool for investigating processes governed by cell-surface molecules, including signal transduction, endocytosis, membrane transport, and cell-cell and cell-matrix interactions [374-380]. More recently, strategies used for resurfacing cell and tissue interfaces have expanded beyond basic research and into biotechnological and biomedical applications, including drug delivery, cell-based therapeutics, biosensing, and tissue engineering, whereby cell surfaces may be engineered to locally control specific biochemical or cellular responses, [13, 227, 236, 363, 364, 377, 381, 382]. While genetic engineering has afforded unique opportunities for the regulated, 'de novo' synthesis of cell surface proteins, the utility of this approach to present lipids, carbohydrates, or synthetic molecules is clearly limited [382]. Moreover, genetic modification of primary cells and complex multicellular tissues has proven a more difficult challenge, particularly in vivo.

Accordingly, investigators have sought to develop strategies through which to incorporate exogenously derived molecules along side native constituents of the cell surface. Covalent coupling of molecules directly to cell surface proteins and carbohydrates is one such approach. Critical to the realization of this strategy, however, has been the development of organic chemical reactions that selectively target specific moieties on the cell surface without adversely effecting cell viability [157, 370, 374, 383, 384]. While the cell surface naturally presents a number of potentially reactive groups, only the amino group has found widespread use as a reactive handle, generally through reaction with N-hydroxysuccinimide ester derivatives [157]. Hence, a number of strategies have recently been developed to introduce noncanonical reactive groups to the cell surface that may undergo chemoselective ligation with a reactive partner in the bulk. A simple approach has been through selective chemical oxidation of terminal sialic-acid resides, facilitating coupling between the resultant aldehyde and hydrazide-, aminooxy-, β-amino thiol-, or thiosemicarbazide-functionalized molecules [384]. More recently, the metabolic machinery of cells has been harnessed to facilitate integration of unnatural biosynthetic precursors bearing ketones and azides into cell surface proteins and carbohydrates [370, 371, 376, 383]. Importantly, concomitant with cell-surface presentation of azido groups has been the development of novel compounds that react specifically and efficiently with azides under physiologic conditions [370, 385-387], some of which have recently been employed for in vivo cell surface engineering [378, 386]. While clearly promising, the dependence on cellular metabolism of synthetic precursors may limit the utility of this approach in cell types that are recalcitrant to tampering with metabolic pathways or in applications where rapid surface modification is desired. Exogenous enzymes have also been used to generate functional groups or otherwise modify cell and tissue surfaces; cell surface aldehyde groups may be generated using galactose oxidase [384], while fucosyltransferase and sialytransferases

have been utilized to transfer unnatural sugar residues to cell surface carbohydrates [157, 382]. More recently, generation of membrane fusion proteins bearing appropriate peptide recognition sequences has emerged as a strategy for enzymatically ligating molecules to the cell surface [368, 369, 372, 373, 379, 388]. While constrained by the limitations of genetic engineering, such approaches allow exogenous molecules to be coupled to the cell surface in a highly selective, site-specific manner. Noncovalent approaches to cell-surface engineering have also been explored, most commonly through passive insertion of exogenous molecules bearing lipophilic domains into the plasma membrane. Glycosylphosphatidylinositol-(GPI) anchored proteins removed from one cell membrane efficiently insert into a host cell membrane, providing a non-genetic approach to manipulating the cell surface proteome [157, 377]. Likewise, synthetic mimics of receptors [364] and glyolipids [366] have been presented on the cell surface using hydrophobic anchors including fatty acids, steroids, lipophilic peptides, and cholesterol. More recently, amphiphilic copolymers have been introduced to the cell surface through similar mechanisms [287, 389].

We have recently demonstrated that poly(L-lysine)-*graft*-poly(ethylene gycol) (PLL-*g*-PEG) copolymers could be rendered non-toxic to pancreatic islets through appropriate control of structural variables, namely grafting ratio and PEG chain length (Chapter 2 and 3). As a cause or consequence of this phenomenon, PLL-*g*-PEG copolymers adsorb to accessible extracellular interfaces, effectively re-engineering the islet surface with lysine groups and short PEG chains. Based on these findings, we have postulated that PLL-*g*-PEG copolymers may be used as 'cell surface active' molecular carriers for reactive handles, ligands, oligosaccharides, peptides, and other moieties. Towards this end, PLL-*g*-PEG copolymers bearing PEG grafts terminated with functional groups were synthesized and used, alone or in combination, to display biotin, hydrazide,

103

and azide moieties on the cell surface, which selectively captured probes through biorecognition or chemoselective ligation.

Appropriately structured PLL-*g*-PEG copolymers may also be used to initiate and propagate the assembly of cell surface-supported polyelectrolyte multilayer (PEM) films through a process of layer-by-layer (LbL) polymer self assembly (Chapter 3). PEM film assembly has recently emerged as a facile and versatile strategy for noncovalently engineering the surface chemistry and molecular landscape of biomedical devices and materials [288, 296, 390]. Through proper choice of film architecture and constituents, enzymes and other proteins [255, 256, 391-393], DNA [257, 394, 395], lipid vesicles [258], drug-containing nanoparticles [259], bioactive motifs [260, 261, 396], and reactive handles [291, 397] may be integrated into PEM films. However, until recently, the cytotoxicity associated with conventional polycations and film architectures has precluded the translation of such opportunities to the surface of viable cells and tissues. Herein, we present an example of cell surface engineering using cytocompatible PEM films assembled using an appropriately designed PLL-*g*-PEG copolymer and a naturally occurring polysaccharide, alginate, chemically modified to contain aldehyde groups (alginate-CHO). Using LbL self assembly, alginate-CHO could be introduced to the cell surface and aldehyde groups used to capture hydrazide-functionalized molecules. Hence, as a consequence of their low cytotoxicity, cell surface localization, and capacity to mediate immobilization of negatively charged macromolecules through PEM film assembly, PLL-*g*-PEG copolymers provide a modular, noncovalent approach to cell and tissue surface engineering.

4.2. MATERIALS AND METHODS

Synthesis and characterization of functionalized poly(L-lysine)-*g*[x]-poly(ethylene glycol)$_n$ copolymers. Poly(L-lysine)$_{12kD}$-*g*[x]-poly(ethylene glycol)$_n$(R) copolymers (x=grafting ratio, n=number of PEG repeat units, R=PEG head group) were synthesized via active ester coupling between primary amines of the PLL backbone and heterobifunctional poly(ethylene glycol)$_n$ derivatized with an N-hydroxysuccinimidyl (NHS)-ester on one end and a methyl, biotin, *t*-BOC protected hydrazide, or azide group on the other. NHS-PEG$_4$(CH$_3$) and NHS-PEG$_4$(biotin) were purchased from Pierce Biotechnology (Rockford, IL) and used as received. NHS-PEG$_4$(*t*-BOC-hydrazide), NHS-PEG$_4$(N$_3$), and NHS-PEG$_{12}$(N$_3$) were purchased from Quanta Biodesign (Powell, Ohio) and vacuum dried overnight before use to remove trace amounts of residual organic solvent. Poly(L-lysine)hydrobromide (Sigma Aldrich, St. Louis, M$_w$=12 kD by MALLS) was dissolved at 5 mg/ml in dilute phosphate buffered saline (7.7 mM NaCl, 0.28 mM Na$_2$HPO$_4$, pH=7.4) for 30 minutes at room temperature. PEGylation reagents were dissolved at 250 mM in dry DMSO (Pierce Biotechnology) and slowly added to PLL under vigorous stirring. After 120 minutes, 10x Dubelcco's phosphate buffered saline (Mediatech, Inc., Manassas, VA) was added to the reaction mixture 1:10 by volume; this was repeated at 150 and 180 minutes, after which the reaction was allowed to proceed for an additional 21 hours. This coupling protocol was empirically determined to yield more efficient grafting of PEG chains to PLL than simple mixing of constituents in PBS as generally performed. The product was transferred to dialysis cassettes (Slide-A-Lyzer Dialysis Cassette, 3.5 kD MWCO, Pierce Biotechnology) and dialyzed first against DPBS (pH 7.0, 3 x 24 hours, Mediatech, Inc.) and, subsequently against distilled deionized water (3 x 24 hours). The product was then lyophilized until completely dry and stored at -20°C prior to use.

To deprotect hydrazide-functionalized copolymers, t-BOC was removed by dissolving PLL$_{12kD}$-g[x]-PEG$_4$(t-BOC-NHNH$_2$) copolymers in 75% (v/v in water) trifluoroacetic acid (TFA; Sigma Aldrich, St. Louis, MO) for 18 hours. TFA was then neutralized by addition of saturated sodium bicarbonate solution, and the product again dialyzed against distilled deionized water (4 x 24 hours) and lyophilized until completely dry.

PEGylation reagents were added to PLL at various stoichiometric ratios to generate copolymers with a range of grafting ratios, x, where x is the average number of modified and unmodified lysine residues per grafted side chain. The grafting ratio of PLL$_{12kD}$-g[x]-PEG$_n$ polymers was determined using ^{1}H NMR (INOVA 600) by taking the ratio of chemical shifts assigned to mPEG linked to lysine (3.15 ppm, m, -C$\underline{H}_2$NHC(O)OCH$_2$-) and ungrafted lysine chains (2.95 ppm, m, -C$\underline{H}_2$NH$_3^+$). In the case of hydrazide functionalized copolymers, successful deprotection of the t-BOC group was verified by the absence of the $tert$-butyl peak at 1.45 ppm. In these investigations, only polymers with grafting ratios between 2.0 and 2.5 were used; Table 4.1 summarizes the properties of these copolymers, including copolymer molecular weight which can be estimated based on the grafting ratio and the molecular weight of PLL and grafted PEG chains [308].

Table 4.1. Structure of copolymers employed in this work

Polymer ID	PLL MW[a] (kD)	PEG$_n$ (n)	Grafting Ratio[b] (x)	% Lysine Modified	Estimated MW[c] (Da)
P12P4(CH$_3$)	12	4	2.3	43	12,850
P12P4(biotin)	12	4	2.2	45	19,720
P12P4(NHNH$_2$)	12	4	2.1	47	17,610
P12P4(N$_3$)	12	4	2.3	43	14,200
P12P12(N$_3$)	12	12	2.6	39	21,500

a: Molecular weight of PLL-HBr starting material (includes contribution of Br$^-$ counterion) = 12 kD MW by MALLS, 1.2 M$_w$/M$_m$. **b:** Rounded to nearest tenth. **c:** MW$_{copolymer}$=MW$_{PLL}$+(MW$_{PLL}$/MW$_{Lys}$)(x^{-1})(MW$_{PEG(R)}$), excludes contribution from Br$^-$, non-approximated grafting ratio used for calculation.

Alginate-aldehyde synthesis and characterization. Alginate oxidation was performed as previously described [309]. Sodium alginate (UP LVM, MW 75 kD, NovaMatrix, Sandvika, Norway) was dissolved at 10 mg/ml in molecular grade water and 0.25 M sodium metaperiodate (NaIO$_4$, Sigma Aldrich, St. Louis, MO) in water was added at 0.10 equivalents with respect to uronate repeat units. After 24 hours, the reaction was quenched with 10 equivalents excess ethylene glycol (Sigma Aldrich), and the product dialyzed (Slide-A-Lyzer Dialysis Cassette, 3.5 kD MWCO, Pierce Biotechnology, Rockford, IL) 3 x 24 hours against distilled deionized water and lyophilized until completely dry. The extent of alginate oxidation was quantified as previously described [309]. Ten-fold excess of *tert*-butyl carbazate (Sigma Aldrich) was reacted with oxidized alginate for 24 hours. The amount of unreacted *tert*-butyl carbazate was determined by the addition of trinitrobenzenesulfonic acid (TNBS) solution (Sigma Aldrich), and measuring the absorbance of the colored complex formed at 334 nm. The degree of oxidation was determined to be ~10.2%, corresponding to ~20 aldehyde groups per 100 monomer repeat units. To facilitate identification of oxidized alginate on islets with confocal microscopy, fluorescent labeling was achieved through thiosemicarbazone bond formation between aldehyde groups and fluorescein-5-thiosemicarbazide (Sigma Aldrich). Oxidized alginate (10% oxidation) was dissolved at 5 mg/ml in phosphate buffered saline (Mediatech, Inc., Manassas, VA) and fluorescein-5-thiosemicarbazide was added at an appropriate stoichiometric ratio to ensure labeling of no more than 5% of aldehyde groups. After reaction for 24 hours, non-reacted dye was removed via gel filtration (PD-10, GE Healthcare, Piscataway, NJ). The fluorescent conjugate, F-Alginate-CHO$_{10}$, was lyophilized and stored protected from light at -20°C. Degree of fluorescent labeling was quantified by UV-vis spectroscopy (Cary 50; Varian Inc., Palo Alto, CA) and determined to be less than 1%.

Islet isolation. Pancreatic islet isolations were performed, as previously described [264]. B10.BR-H2k H2-T18a/SgSnJ (B10) mice (8 weeks old, Jackson Laboratory Bar Harbor, ME) pancreata were removed after distension with collagenase P (1 mg/ml, Roche, Indianapolis, IN) through the common bile duct. Following digestion, islets were purified by a Ficoll-Histopaque discontinuous gradient (Ficoll: 1.108, 1.096, and 1.037; Mediatech Inc. Manassas, VA). Isolated islets were cultured for 48-72 hours at 37°C in RPMI 1640 supplemented with 10% heat inactivated fetal calf serum, L-glutamine (2 mM), and penicillin (100 U/ml), streptomycin (100 μg/ml) and amphotericin B (0.25 μg/ml) (Mediatech Inc, Manassas, VA), and media was changed daily.

Islet coating. Islets (<1000) were placed into 12 mm cell culture inserts with 12 μm pores (Millicell-PCF; Millipore, Billercia, MA). Prior to introduction of polymer solution, islets were washed six times by adding 700 μl serum free RPMI 1640 to the insert, followed by gentle repeated tapping of the insert on a polystyrene surface to facilitate drainage of the wash solution through pores while retaining islets. The insert was placed into a well of a 24 well plate (Corning Inc., Corning, NY) and 700 μl of polymer solution was added to the cell culture insert. After incubation, the insert was removed from the well, solution drained through the insert as described above, and islets washed four times as described above to ensure adequate removal of non-adsorbed polymer. To fabricate layer-by-layer thin films, the process of polymer incubation and washing was repeated using appropriate polymer solutions and incubation times.

For assembly of aldehyde-containing multilayer films, islets were incubated in PLL$_{12kD}$-g[2.5]-PEG$_4$(CH$_3$) at 1 mg/ml in RPMI for 5 minutes, washed four times with RPMI 1640, incubated in F-Alginate-CHO$_{10}$ at 2 mg/ml in RPMI for 5 minutes, and washed again to form a single bilayer. This process was repeated to assemble the desired number of bilayers.

Confocal microscopy. Confocal microscopy (Zeiss LSM 510 META; Carl Zeiss, Inc., Thornwood, NY) was used to identify fluorescently labeled film components and/or probes on islets. A representative population of islets selected at random was placed in silicon isolators (Grace Bio-Labs, Bend, OR) adhered to glass coverslips (Fisher Scientific) containing serum free RPMI 1640 or Dubelco's phosphate buffered saline with calcium and magnesium. Coverslips were then placed on the microscope stage and images captured at 20x or 40x magnification.

Assessment of islet viability. Islet viability was assessed as previously described [148] with some modifications. Briefly, islets were incubated in DPBS (Mediatech Inc., Manassas, VA) containing 4 μM calcein AM and 8 μM ethidium homodimer-1 (Molecular Probes, Eugene, OR) for one hour, and a representative number of individual islets (35-50) were imaged with two-channel confocal microscopy using a 20x objective as described above. Confocal micrographs were analyzed using MATLAB® (The MathWorks, Natick, MA) to quantify the number of pixels corresponding to fluorescent emission from live (green) and dead (red) cells. Viability is expressed as the percentage of fluorescent pixels associated with emission from live cells.

Probes for detection of functional groups. Biotinylated or fluorescently-labeled probes were purchased or synthesized to detect islet surface hydrazide, biotin, azide, and aldehyde groups via confocal microscopy. Biotin groups were detected by incubating islets in Cy3-labeled streptavidin (Cy3-SA; Sigma Aldrich, St. Louis, MO) at 0.1 mg/ml in DPBS for 30 minutes. To detect cell surface hydrazides, islets were incubated in fluorescently-labeled alginate-aldehyde (F-Alginate-CHO$_{10}$), synthesized as described above, at 2 mg/ml in DPBS for 60 minutes at room temperature. For detection of aldehyde groups, islets were reacted with biotinamidohexanoic acid hydrazide

109

(hydrazide-LC-biotin; Pierce Biotechnology, Rockland, IL) at 5 mM for 1 hour at room temperature, followed by detection of biotin groups as described above.

To detect cell surface azide groups, islets were incubated with triarylphosphine-poly(ethylene glycol)-biotin at 2mM in DPBS for 60 minutes at room temperature, followed by detection of biotin groups using Cy3-SA as described above. The triarylphosphine-poly(ethylene glycol)-biotin conjugate was synthesized by reaction of a heterobifunctional biotin-PEG$_{3.4kD}$-amine linker (CreativePEGWorks, Winston Salem, NC) with a pentafluorophenyl (PFP) active ester of triarylphosphine, synthesized as described previously [398, 399]. To a stirred solution of biotin-PEG$_{3.4kD}$-amine (100 mg, 0.029 mmol) in DCM (2 ml) was added the PFP-ester of triarylphosphine (31.17 mg, 0.058 mmol, 2 equiv) and Et$_3$N (8.08 μl, 2 equiv.), and the resultant mixture stirred at room temperature for 12-16 h, upon which time volatiles were evaporated under vacuum. The residue was dissolved in the minimum amount of cold DCM and the product was precipitated by cold ether. The pure compound was collected by filtration and dried in vacuum. ^{1}H NMR (400 MHz, CDCl$_3$) δ: 1.45 (m, 2H), 1.6-1.8 (m, 4H), 2.2 (t, J = 7.6 Hz, 2H), 2.8 (d, J = 12.8 Hz, 1H), 2.9 (dd, J = 4.8, 12.8 Hz, 1H), 3.2 (m, 1H), 3.3-3.9 (m, PEG), 3.7 (s, 1H), 4.3 (m, 1H), 4.5 (m, 1H), 6.7 (m, 2H), 7.2-7.4 (m, 11H), 7.8 (dd, J = 1.6, 8.4 Hz, 1H), 8.1 (dd, J = 4, 8.4 Hz, 1H).

Quantification of immobilized streptavidin. Following biotinylation, islets were incubated in a 1:50 mixture (by mass) of horseradish perioxidase (HRP)-labeled streptavidin (HRP-SA; Zymed Laboratories, Inc., San Francisco, CA) and streptavidin (Pierce Biotechnology, Rockland, IL) at 0.1 mg/ml in DPBS for 30 minutes. After rinsing as described above, groups of 30-50 islets were placed into wells of a 96 well plate. The microplate was briefly centrifuged to settle islets, supernatant was removed, and 100 μL of 3,3´,5,5´-tetramethylbenzidine (TMB) solution (1-Step^{TM} Ultra TMB-ELISA, Pierce

Biotechnology, Rockland, IL) was added to islets. Microwell plates containing islets and TMB were placed on a plate shaker (800 m^{-1}, MS1 Minishaker, IKA, Wilmington, NC) at room temperature for 20 minutes, upon which time 50μL 2M H_2SO_4 was added to quench the reaction. Microwell plates were briefly centrifuged to settle islets, 100 μL of solution was transferred to a fresh well, and absorbance was recorded at 450 nm using a microplate reader. The amount of streptavidin immobilized on islets was quantified using a standard curve relating absorbance at 450 nm to known concentrations of soluble SA-HRP.

Statistics. Tests for statistical significance between the means of two groups were conducted with the Student's t-test (two-tailed, homoscedastic). Tests between three or more groups were conducted with the one-way ANOVA followed by the Tukey HSD test.

4.3. RESULTS AND DISCUSSION

Design of cytocompatible PLL$_{12kD}$-g[x]-PEG$_n$ copolymers derivatized with ligands and reactive groups. As demonstrated in Chapter 3, the cytotoxicity of poly(L-lysine)-g[x]-poly(ethylene glycol)methyl copolymers towards pancreatic islets can be attenuated through control of grafted PEG chain length and grafting ratio, x. In an analogous manner, PLL$_{12kD}$-g[x]-PEG$_4$(R) copolymers were synthesized, substituting the head group, R, of grafted PEG$_4$ chains with a biotin, hydrazide, or azide functional group. Copolymers were synthesized with a grafting ratio, x, between 2.0 and 2.5, as required to abrogate the toxicity of copolymers synthesized using methyl-PEG$_4$, yielding PLL$_{12kD}$-g[2.0-2.5]-PEG$_4$(biotin) (P12P4(biotin)), PLL$_{12kD}$-g[2.0-2.5]-PEG$_4$(NHNH$_2$), (P12P4(NHNH$_2$)), and PLL$_{12kD}$-g[2.0-2.5]-PEG$_4$(N$_3$) (P12P4(N$_3$)) copolymers (Table 4.1).

111

To investigate the effect of PEG head group on PLL_{12kD}-g[2.0-2.5]-PEG_4(R) copolymer toxicity, islets were incubated in copolymers at 1 mg/ml for 40 minutes in serum free RPMI 1640, and islet viability was assessed and via calcein AM and ethidium homodimer staining and subsequent quantification with image analysis (Figure 4.1); untreated islets served as controls. Copolymers bearing PEG chains functionalized with biotin moieties (P12P4(biotin)) and hydrazide groups (P12P4($NHNH_2$)) were found to exert no discernable toxicity relative to non-treated controls or copolymers bearing methyl groups ($p > 0.05$). By contrast, despite a similar grafting ratio, P12P4(N_3) resulted in a significant decrease ($p > 0.05$) in islet viability relative to both controls and other copolymers. It should be noted that while the azide anion (e.g., NaN_3) is highly cytotoxic, organic azides have no intrinsic toxicity [374]. At a given grafting ratio, increasing the length of grafted PEG chains has been shown to reduce copolymer toxicity (Chapter 3), and, therefore, an azide-functionalized variant was synthesized using PEG_{12} grafts at a grafting ratio of 2.5 (P12P12(N_3)). At the same molar concentration, P12P12(N_3) was significantly less toxic than P12P4(N_3) ($p < 0.01$; Figure 4.1B-D), yielding islet viabilities statistically comparable to untreated controls ($p > 0.05$), and further demonstrating the importance of PEG chain length in the toxicity of PLL-g-PEG copolymers. Hence, cytocompatible PLL_{12kD}-g[x]-PEG_n(R) copolymers bearing biotin, hydrazide, and azide functional groups may be generated through proper control of PEG chain length and grafting ratio.

The increased toxicity associated with P12P4(N_3) relative to comparable polymers bearing methyl, biotin, or hydrazide suggests a potential dependence of copolymer toxicity on the chemical nature of the PEG head group, R. The dependence of copolymer toxicity on both the presence of grafted PEG chains as well as chain length (Chapter 3) suggests a role for PEG in dictating interactions between the polymer and the cell membrane, an effect which may be further influenced by the identity of PEG

112

head group. Indeed, the cytotoxicity and plasma membrane translocation potential of poly(L-lysine)-based branched polypeptides has been shown to be dependent not only the charge of the peptide, but also on branch length and amino acid composition [333, 334, 400]. For example, substitution of serine for leucine in an otherwise similar polypeptide is associated with a significant decrease in cytotoxicity [333]. Similarly, increasing the hydrophobicity of random copolymers of lysine and phenylalanine [335], as well as other cell-penetrating peptides, increases interactions between the polymer and lipid tails within the plasma membrane, promoting penetration into the cell membrane [332] and attendant decreases in cell viability [267]. While not necessarily linked to differences in hydrophobicity per se, termination of grafted PEG_4 chains with azido groups may influence copolymer-membrane interactions, partially overriding mechanisms through which grafted PEG attenuates toxicity. Increasing PEG chain length, and hence the relative mole fraction of PEG, appears to at least partially supersede adverse effects of the azido group. Further investigations comparing the cytotoxicity of copolymers comprised of various functional groups, grafting ratios, and PEG chain lengths are necessary to confirm these suppositions.

Figure 4.1. Cytocompatible PLL_{12kD}-g[x]-PEG_n(R) copolymers bearing biotin, hydrazide, and azido functional groups may be generated through proper control of grafting ratio and PEG chain length. (A) Islet viability after 40 m incubation with functionalized copolymers synthesized with PEG_4 and a grafting ratio, x, between 2.0 and 2.5. Copolymers containing hydrazide and biotin PEG head groups, R, had no discernable effect on islet viability relative to untreated controls or copolymers bearing methyl R groups ($p > 0.05$). An azido-functionalized variant, however, induced a significant reduction ($p < 0.01$) in islet viability (A,C). Increasing the length of PEG spacer from 4 to 12 repeat units significantly ($p < 0.05$) increased islet viability to levels statistically similar to controls as well as other functionalized polymers (B, D). Bars labeled with the letter a are statistically different ($p < 0.01$) from all other bars as well as untreated controls. Scale bars in C,D are 50 μm.

Generation of functional groups on the islet surface through adsorption of PLL-*g*[x]-PEG copolymers. Non-toxic PLL_M-*g*[x]-$PEG_n(CH_3)$ copolymers adsorb to the extracellular surface of pancreatic islets (Chapter 3), and, therefore, variants functionalized with ligands or reactive groups may offer a facile approach to re-engineering the surface of living cells and tissues in a non-covalent manner (Scheme 4.1). To explore this possibility, islets were incubated with hydrazide, azido, and biotin functionalized copolymers rendered non-toxic through control of appropriate structural variables as described above. After 40 minute incubation at 1 mg/ml, islets were washed to remove non-adsorbed copolymer and incubated with appropriate fluorescent probe(s) to detect functional groups on the islet surface via confocal microscopy (Figure 4.2). As a control, islets were incubated in copolymers synthesized using methyl-PEG_4 (R=CH_3) with a grafting ratio of 2.5 ($P12P4(CH_3)$) prior to incubation with various probe(s).

Aldehydes undergo chemoselective ligation with hydrazides to form stable N-acyl hydrazones [384]. Fluorescein-labeled alginate oxidized to generate to aldehyde groups on approximately 10% of monomer repeat units (F-Alginate-CHO_{10}) was used as probe for detecting islet surface hydrazide groups introduced upon incubation with $P12P4(NHNH_2)$. Confocal microscopy revealed a substantial increase in fluorescence intensity associated with islets incubated with $P12P4(NHNH_2)$ relative to those incubated with $P12P4(CH_3)$, indicating specific immobilization of F-Alginate-CHO_{10} through covalent reaction with islet-surface hydrazide groups (Figure 4.2). Additionally, the observed difference in fluorescent intensity suggests that covalent interaction between hydrazides and aldehydes yields considerably more alginate-CHO_{10} deposition than electrostatic interactions between positively charged lysine residues of the copolymer and carboxylic acid groups of alginate-CHO_{10}. Similarly, these results indicate that Schiff base formation between aldehyde groups on alginate and lysine residues on the polycation or naturally occurring on the cell surface does not favor formation of the imine

product [374]. Hence, PLL$_{12kD}$-g[x]-PEG$_4$(NHNH$_2$) copolymers can be used to introduce hydrazide groups to the surface of living cells and tissues, providing a facile approach for immobilizing aldehyde-bearing molecules.

Though chemoselective coupling using hydrazides is a commonly employed strategy for modifying cell and tissue surfaces, aldehydes and ketones, generated chemically, metabolically, or enzymatically, serve as the reactive anchor on the cell surface [365, 371, 381, 401-405]. By contrast, to the author's knowledge, there are no reports describing the generation of reactive cell surface hydrazide groups. This may be due, in part, to difficulty associated with covalently linking hydrazide-functionalized molecules to reactive groups naturally presented by cells. As a notable example, N-hydroxysuccinimide (NHS) esters, commonly used for linking molecules to cell surface amines [13, 157, 227, 236], react with hydrazides as well, preventing hydrazide immobilization in this manner. Use of a polymeric carrier for hydrazide groups, in this instance PLL-g-PEG, circumvents such limitations. Significantly, as aldehydes and ketones can be readily introduced into oligosaccharides and glycoconjugates [374, 376, 384], hydrazides may offer a unique and versatile handle for engineering cell surface glycosylation.

Perhaps more well known for their role as participants in "click" reactions [406], organic azides also undergo chemoselective ligation with triarylphosphine under physiological conditions via Staudinger ligation [370, 398]. Therefore, to probe for cell surface azido groups generated upon adsorption of P12P12(N$_3$), islets were incubated with triarylphosphine-derivatized poly(ethylene glycol)biotin (phos-PEG-biotin; 2 mM, 1 h), followed by subsequent biotin detection using Cy3-labeled streptavidin (Cy3-SA; 0.1 mg/ml, 30 m). As demonstrated in Figure 4.2, an increase in fluorescence intensity was observed for islets incubated with P12P12(N$_3$) relative to controls, though differences were more difficult to detect in this instance due to non-specific interaction of the

phosphine probe with controls. Fluorescent emission from controls, however, was sporadic and concentrated in discrete domains, whereas islets incubated with P12P12(N_3) demonstrated a pattern of fluorescence consistent with both the extracellular architecture of isolated islets as well as the previously observed pattern of PLL-*g*-PEG copolymer deposition (Chapter 3). Collectively, these observations indicate that cell surface azides may be generated through adsorption of P12P12(N_3) and used to immobilize macromolecules via Staudinger ligation.

With the advent of the modified Staudinger reaction [398] and more recent developments in copper-free cycloadditions [385, 386], organic azides have emerged as arguably the most versatile and chemoselective reactive handles for cell surface engineering. Cell surface azide groups have been most commonly generated through metabolic oligosaccharide engineering [370, 407]. Azide groups on cell-surface glycans in both cultured cells [370, 408] as well as in whole [375, 386] or developing [378] organisms have proven to be valuable tools for investigating a number of fundamental questions in glycobiology. While also an attractive method for cell surface engineering [370, 375], biosynthetic incorporation of azides within glycoconjugates requires metabolism of a synthetic azidosugar, a process which may require several days [370]. By contrast, azide-functionalized PLL-*g*-PEG copolymers facilitate presentation of cell surface azido groups within minutes, providing a facile and rapid alternative for chemically targeting cell surfaces via Staudinger ligation.

Biotinylation has long been employed as a facile strategy for linking molecules to cell surfaces via (strept)avidin-biotin interactions [227, 236] and, towards this end, a biotin functionalized PLL$_{12kD}$-*g*[x]-PEG$_4$(biotin) copolymer (P12P4(biotin)) was synthesized. In accord with previous studies using a similar bioconjugate (PPB, Chapter 2) [303], incubation of islets with P12P4(biotin) facilitated the specific immobilization of Cy3-labeled streptavidin to the islet surface (Figure 4.2).

117

Cell surface biotinylation has most commonly been achieved using amine-reactive NHS-esters [227, 236, 409]. To compare islet biotinylation achieved through covalent modification of amine groups and adsorption of biotin-derivatized PLL-*g*-PEG copolymers, islets were incubated with either NHS-PEG$_4$(biotin) or P12P4(biotin) at equimolar concentration of biotin (1.4 mM in DPBS) for one hour, and the amount of immobilized streptavidin measured. Both strategies yielded comparable densities of streptavidin on the islet surface (Figure 4.3A). However, islets treated with the NHS-ester reagent presented an altered morphology, characterized by more frequent cellular protusions, resulting in a more irregular periphery (Figure 4.3B). By contrast, islets incubated with P12P4(biotin) maintained the smooth border characteristic of isolated and cultured murine islets (Figure 4.3C). While such morphological changes are not well understood, it is reasonable to suspect that cell-cell and cell-matrix adhesive interactions essential for maintenance of islet integrity [410-412] may be compromised by covalent modification of proteins [157]. Moreover, as a tetrameric protein capable of binding four biotin molecules, streptavidin may act to effectively crosslink biotinylated cell surface molecules [413, 414], potentially triggering undesired signaling pathways. Cell and tissue biotinylation using PLL-*g*-PEG copolymers may circumvent such undesired consequences.

For obvious reasons, cell surface modification using NHS-esters must be performed in amine-free solvents, limiting the potential applicability of this approach to situations in which cells and tissues can be isolated from amine-containing environments (e.g., culture or in vivo). While levels of streptavidin incorporation were not quantified, confocal microscopy demonstrated that islets incubated with P12P4(biotin) in a complex, amine-containing media, RPMI 1640, were capable of specifically binding Cy3-labeled streptavidin. Moreover, given the short half-life of NHS-esters in aqueous solvents at physiological pH [415], PLL-*g*-PEG copolymers functionalized with reactive groups offer

118

increased flexibility, as polymers may be dissolved well in advance of application, used repeatedly or repurified, or used in situations where prolonged exposure to the polymer may be necessary.
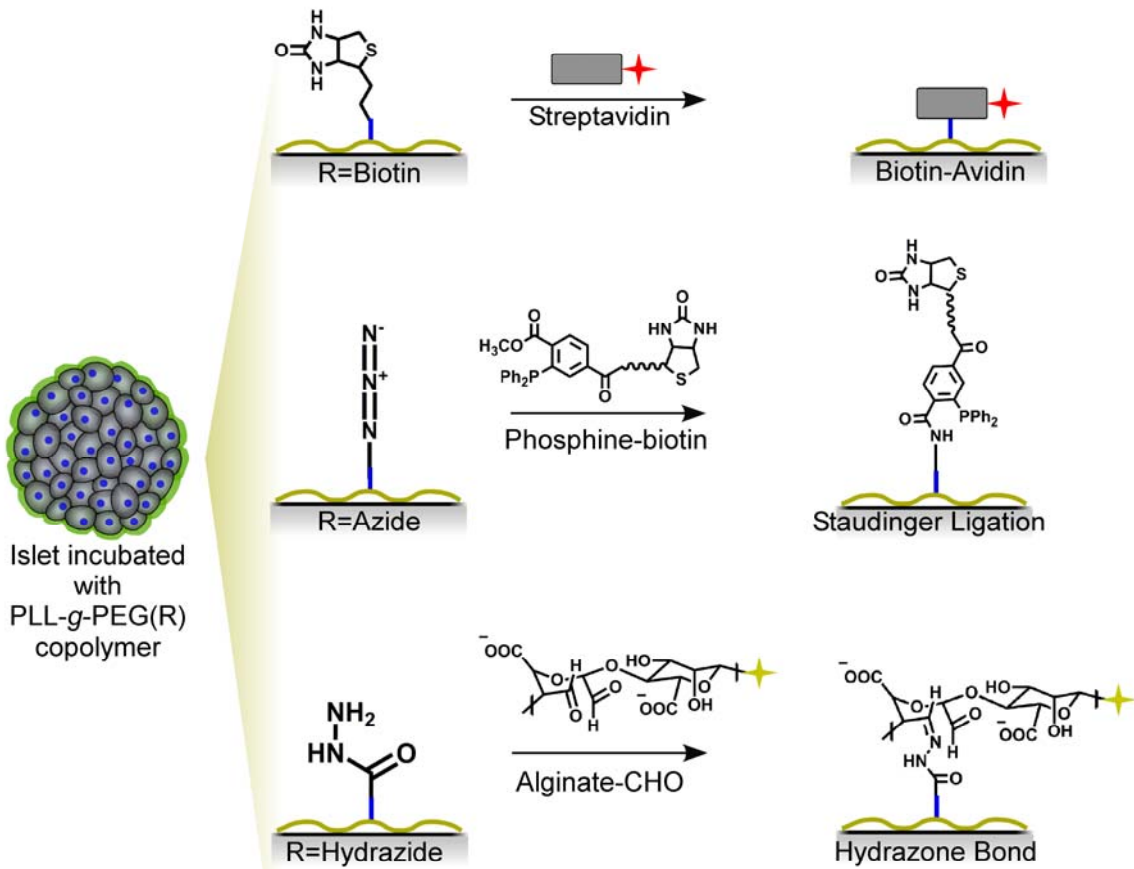
Scheme 4.1. Cell surface engineering using functionalized PLL-*g*-PEG copolymers. Adsorption of PLL-*g*-PEG copolymers functionalized with biotin, azide, and hydrazide moieties facilitates selective capture of streptavidin-, triphenylphosphine-, and aldehyde(CHO)-labeled probes, respectively, on the islet surface.
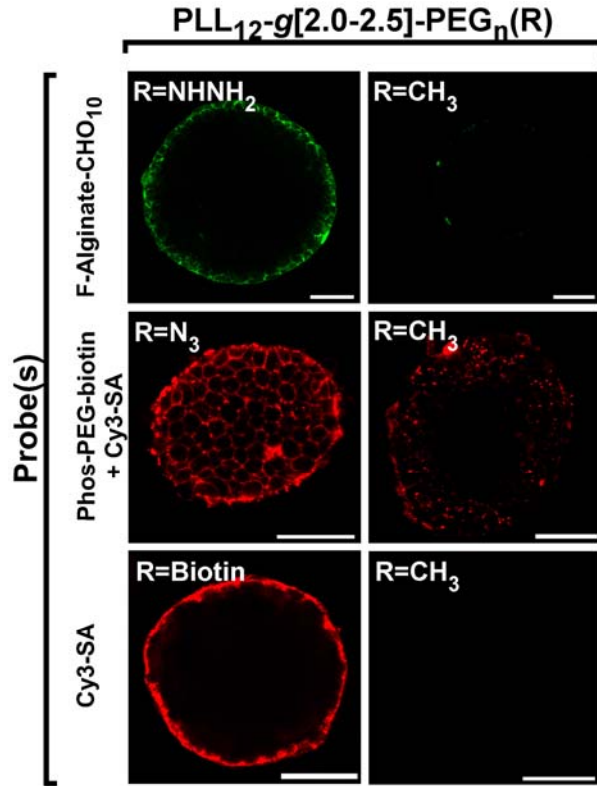
Figure 4.2. PLL_{12kD}-g[x]-PEG_n(R) copolymers can be used to generate functional groups on the islet surface. Islets were incubated with hydrazide ($NHNH_2$), azide (N_3), or biotin functionalized copolymers, and appropriate biotinylated or fluorescently-labeled probes were used to detect functional groups via confocal microscopy. Hydrazide groups were detected using fluorescein-labeled alginate oxidized to contain aldehyde groups on approximately 10% of monomer repeat units (F-Alginate-CHO_{10}). Cell surface azides were detected using a triphenylphosphine-$PEG_{3.4kD}$-biotin conjugate (Phos-PEG-biotin). Biotin groups were detected with Cy3-labeled streptavidin (Cy3-SA). Copolymers synthesized using methyl-PEG_4 (R=CH_3) with a grafting ratio of 2.5 (P12P4(CH_3)) were used as controls. Representative confocal micrographs are shown; scale bar = 50 μm.
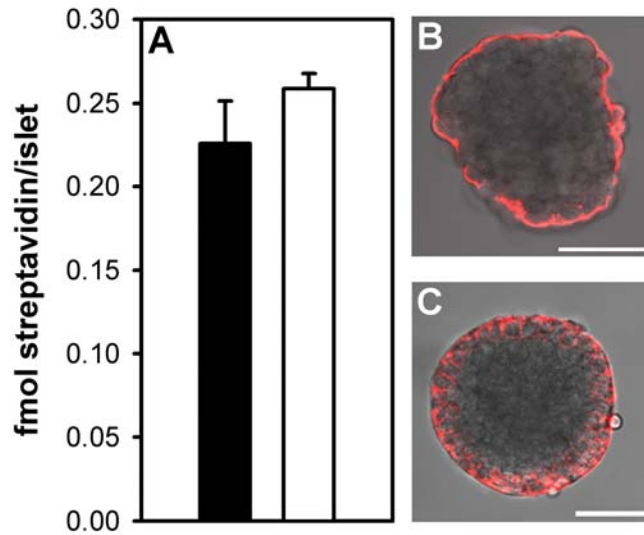
Figure 4.3. PLL_{12kD}-g[2.0-2.5]-PEG_4(biotin) copolymers provide an alternative to NHS-ester functionalized biotinylation reagents. At equimolar biotin concentration NHS-PEG_4(biotin) (black bar) and P12P4(biotin) (white bar) immobilized comparable ($p>0.05$) amounts of streptavidin (A). However, Islets treated with NHS-PEG_4(biotin) presented an irregular morphology (B), whereas islets incubated with P12P4(biotin) (C) maintained the smooth border characteristic of isolated and cultured murine islets. Scale bar = 50 μm.

Co-presentation of functional groups using PLL-*g*[x]-PEG copolymers.

Through sequential or co-adsorption of functionalized PLL_{12kD}-g[x]-PEG_n(R) copolymers on cell surfaces, multiple reactive groups may be displayed simultaneously. To demonstrate this possibility, islets were incubated in a solution of P12P4(biotin) and P12P4(hydrazide), each at 0.5 mg/ml in RPMI 1640, for 40 minutes. Upon rinsing away non-adsorbed copolymer, islets were incubated with either Cy3-SA, F-Alginate-CHO_{10}, or a mixture of the two probes. As demonstrated in Figure 4.4, islets incubated with a mixture of biotin- and hydrazide-functionalized copolymers were capable of capturing individual probes as well as both probes in combination, clearly demonstrating simultaneous display of both biotin and hydrazide moieties on the islet surface. In principle, a library of copolymers bearing a diverse array of functional groups, potentially including peptides, oligosaccharides, nucleic acids, and other bioorthogonally reactive groups, could be synthesized and used combinatorially to obtain exquisite control over the molecular landscape of living cells and tissues. Further exploration of this concept is an area of ongoing investigation.
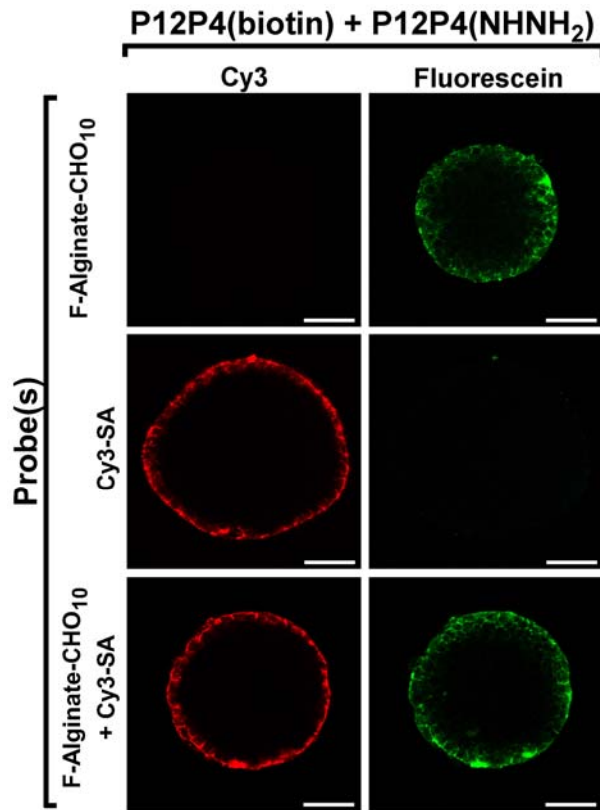
Figure 4.4. Biotin and hydrazide groups may be simultaneously displayed through co-adsorption of functionalized PLL-*g*-PEG copolymers. Islets were incubated in a mixture of P12P4(biotin) and P12P4(hydrazide), and subsequently incubated with F-Alginate-CHO$_{10}$ (top panel), Cy3-SA (middle panel), or a mixture of the two (bottom panel). Two-channel confocal microscopy was used to detect Cy3 (left panel) and flourescein (right panel). Representative confocal micrographs demonstrate simultaneous display of both biotin and hydrazide moieties on the islets surface. Scale bar = 50 μm.

Islet surface engineering using cytocompatible polyelectrolyte multilayer thin films. Polyelectrolyte multilayer (PEM) films can be assembled on the surface of viable pancreatic islets through layer-by-layer deposition of PLL_{12}-g[2.5]-$PEG_4(CH_3)$ and alginate (Chapter 3), offering an additional opportunity for cell surface engineering through incorporation of functionalized film constituents. As a demonstration of this concept, a modified polyanion, alginate-CHO_{10}, was used in film formation. To demonstrate growth of this PEM film on islets, films were assembled using P12P4[2.5](CH_3) as the polycation and fluorescein-labeled alginate-CHO_{10} (F-Alginate-CHO_{10}). Confocal microscopy was used to detect F-Alginate-CHO_{10} on the islet surface and qualitatively compare relative differences in fluorescent intensities between islets coated with a single bilayer, eight bilayers, or incubated with F-Alginate-CHO_{10} for an equivalent amount of time. As shown in Figure 4.5A, after fabrication of eight bilayers fluorescent emission from F-Alginate-CHO_{10} was observed surrounding the islet periphery. By contrast, islets treated with a single bilayer (Figure 4.5B) or only with F-Alginate-CHO_{10} (Figure 4.5C) demonstrated essentially no fluorescent emission, indicating assembly of PEM films containing oxidized alginate on the islet surface. To demonstrate the presence and reactivity of newly introduced aldehyde groups, islets coated with an eight bilayer P12P4[2.5]/F-Alginate-CHO_{10} film were subsequently incubated with biotinamidohexanoic acid hydrazide ($NHNH_2$-biotin) at 5 mM in DPBS for 1 hour, and biotin groups detected using Cy3-SA and confocal microscopy. As shown in Figure 4.6A, fluorescent emission associated with Cy3-SA (right panel) is observed on the islet surface and largely colocalized with F-Alginate-CHO_{10} (left panel). Incubation of coated islets with Cy3-SA demonstrated no or only sporadic fluorescent emission (Figure 4.6B), indicating that amines within streptavidin do not form stable imines via Schiff base formation with aldehyde groups within PEM films. Additionally, islets incubated only with F-Alginate-CHO_{10} and subsequently with biotin-$NHNH_2$ and Cy3-SA

(Figure 4.6C) demonstrated no or sporadic fluorescent emission (Figure 12D), indicating that biotin is immobilized in an aldehyde-specific manner. Interestingly, aldehyde groups remained reactive despite assembly of films in amine-containing solvent (RPMI 1640), again indicating that Schiff base formation between soluble amines and aldehyde groups on alginate-CHO_{10} is highly reversible under these conditions [374].

In addition to serving as a polymeric carrier for reactive groups, incorporation of negatively charged polysaccharides into thin films may provide an opportunity to introduce glycosylation patterns that generate desired biochemical or cellular responses. For example, synthetic oligosaccharides designed to mimic L-selectin ligands have been shown to downregulate L-selectin expression on inflammatory cells through multivalent interactions with the receptor [416-418], and, as an anionic polymer, may be included into films to attenuate inflammatory responses to islet grafts [52, 286]. Likewise, heparin could be employed as the polyanion [419, 420], potentially attenuating thrombogenic responses initiated by transplanted islets in contact with whole blood [54, 286]. Additionally, as they are generally non-toxic, other natural or synthetic polyanions may be utilized to confer bioactivity to the cell surface. Notably, use of DNA and other nucleic acid polymers as film components [421], may provide unique opportunities for cell surface-mediated gene delivery to islets or surrounding host cells post-transplantation.

Though not explicitly explored, PEM films may also be generated using functionalized, cytocompatible polycations, such as those discussed above, further expanding the repertoire of functional groups that may be incorporated and the versatility of the approach. Spatial distribution of functional groups might be controlled through incorporation of constituents at different points during the film formation process [422-424], providing an opportunity to tailor the phyioschemical and biochemical properties of cell surface-supported films. For example, through alternating deposition of constituents bearing orthogonally reactive groups, such as P12P4($NHNH_2$) and alginate-CHO_{10}, films

125

capable of crosslinking in situ might be generated [397, 425, 426] potentially enhancing

stability or facilitating control of film permeability. Previous reports indicate that the

density of molecules covalently linked to cell surface amines [287] and aldehydes [401]

is dramatically reduced within days, due, in part, to turnover and shedding or membrane

proteins and carbohydrates [158]. Though the stability of adsorbed copolymers and

assembled PEM films was not explored herein, electrostatically and/or covalently

crosslinked nanostructures non-specifically anchored to the cell surface may be more

resistant to such mechanisms of instability. Additionally, through proper choice of film

constituents or crosslinking strategies, functionalized polymers or embedded agents may

be released from films in a controlled manner [427-430], providing further opportunities

for controlling the local biochemical environment and directing cellular responses.
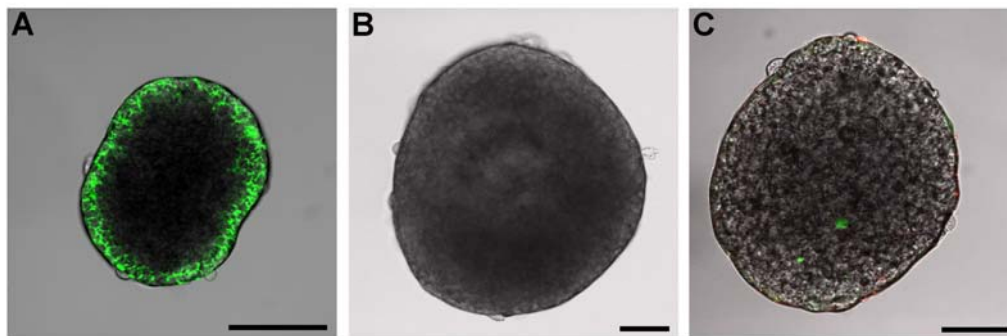
Figure 4.5. Polyelectrolyte multilayer (PEM) films can be assembled on individual pancreatic islets through layer-by-layer deposition of PLL_{12kD}-g[2.5]-$PEG_4(CH_3)$ and oxidized alginate. Using fluorescein-labeled alginate oxidized to contain aldehyde groups on approximately 10% of monomer repeat units (F-Alginate-CHO_{10}) as the polyanion, confocal micrographs of coated islets reveal dramatic differences in fluorescent intensity associated with films comprised of eight bilayers (A) and a single bilayer (B). Controls treated only with F-Alginate-CHO_{10} (C) demonstrate little or no fluorescence, indicating that alginate-CHO_{10} deposition is polycation-dependent.
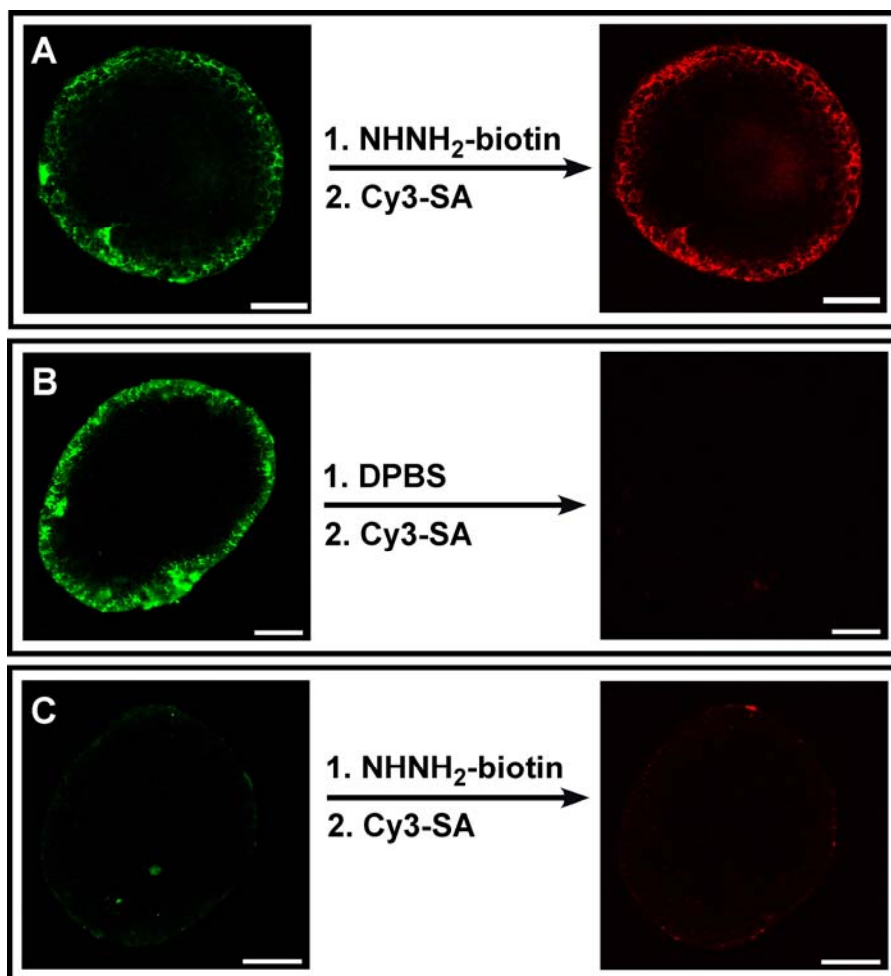
Figure 4.6. Cell surface-supported PEM films assembled using oxidized alginate facilitate presention of reactive aldehydes. (A) Islets coated with an eight bilayer P12P4[2.5]/F-Alg-CHO$_{10}$ film (left panel) were reacted with hydrazide-LC-biotin (NHNH$_2$-biotin) and biotin groups detected using Cy3-SA and confocal microscopy (right panel). (B) Incubation of coated islets (left panel) with only Cy3-SA (right panel) demonstrated no or only sporadic fluorescent emission, indicating that streptavidin is not incorporated via Schiff base formation with aldehyde groups. (C) Islets incubated only with F-Alg-CHO$_{10}$ (left panel) and subsequently with biotin-NHNH$_2$ and Cy3-SA (right panel) demonstrated no or sporadic fluorescent emission indicating that biotin is introduced in an aldehyde-specific manner.

4.4. CONCLUSIONS

Cell surface engineering has emerged as a powerful tool for landscaping the molecular interface of viable cells and tissue with potential applications in biosensing, tissue engineering, drug delivery, and cell-based therapeutics. Using cytocompatible PLL-*g*-PEG copolymers, and polyelectrolyte multilayer films assembled thereof, biotin, azide, hydrazide, and aldehyde groups could be displayed on extracellular surface of islets, either alone or in combination, and used to capture bio- or chemically orthogonal probes. In this regard, functionalized PLL-*g*-PEG copolymers may be used as modular design elements for remodeling the surface of pancreatic islets in a noncovalent manner. While specific biomedical and biotechnological applications of this work have yet to be fully identified, cell surface-supported PLL-*g*-PEG monolayers and PEM films offer a platform technology for cell and tissue surface engineering.

128

CHAPTER 5

Surface Re-engineering of Pancreatic Islets with Thrombomodulin

5.1. INTRODUCTION

With the inception of the Edmonton Protocol, intraportal islet transplantation has re-emerged as a promising cell-based therapy for type 1 diabetes [17-19]. However, despite the promise of islet transplantation, primary nonfunction and early nonimmune islet destruction, which have been observed both in animal models and in clinical trials, remain major hurdles in islet transplantation [431]. Notably, islets from two to four donor organs are typically required to reverse diabetes in a single patient, placing a significant burden on an already limited donor organ supply [12, 18, 20-23, 432]. Moreover, a requirement for successive islet infusions within the portal bed necessitates re-interventions with increased costs, the attendant risk of periprocedural morbidity, and has been associated with increasing portal vein pressures that may indicate the development of a presinusoidal form of portal hypertension [433, 434]. Early islet destruction in the immediate post-transplant period may be the consequence of poor functional quality of the grafted tissue, delayed and insufficient revascularization of the graft [41], glucose and lipotoxicity [43, 44], or ischemia-reperfusion injury [42]. However, substantial evidence now suggests that exposure to an early, nonimmune inflammatory injury is largely responsible for the observed functional stunning or destruction of islets and may well amplify subsequent immune reactions [37, 45-50, 435-437].

Although activation of the graft microenvironment by proinflammatory mediators released from islet grafts contribute to induction of a local inflammatory response [1, 36, 52, 70-81], recent evidence indicates that an acute blood mediated inflammatory reaction is initiated upon intraportal infusion of islets [3, 54-56]. Korsgren and

129

colleagues have demonstrated that tissue factor (TF), the primary physiological initiator of the coagulation system [57], is expressed by and released from β and α cells of isolated islets [55]. Indeed, in animal models and in recent clinical reports, marked activation of coagulation has been noted shortly after islet infusion, despite the presence of heparin in the infusate, as indicated by increases in thrombin–antithrombin (TAT) complexes, prothrombin activation fragments, and fibrinopeptide A   [56, 60]. Notably, thrombin is a direct mediator of inflammation [61], acting as a chemoattractant for neutrophils and monocytes and stimulating endothelial cells to express monocyte chemoattractant protein-1 (MCP-1) and other chemokines [64]. Thrombin also induces endothelial cell expression of ICAM-1, VCAM-1, E- and P-selectin, as well as platelet activating factor, all of which leads to further recruitment of platelets and leukocytes to the graft site [61, 63, 438]. Likewise, by-products of the thrombin response, including fibrinogen degradation products and fibrin, also act as chemoattractants and serve to localize this inflammatory response by adhesion-dependent processes. Furthermore, thrombin activated leukocytes express oxygen free radicals, IL-1β, TNF-α, IFN-γ, and iNOS [62], which can damage islets, inducing either functional impairment or death   [49, 51, 52]. Consistent with these observations, immunohistochemical analysis of grafts with primary nonfunction has demonstrated robust infiltration of macrophages and neutrophils [37, 46, 52].

Under normal physiological conditions, endothelial cells lining the extensive microvasculature of pancreatic islets actively regulate coagulation [1]. During islet isolation and culture, however, this barrier is disrupted [1, 2], exposing procoagulant and inflammatory mediators while simultaneously stripping away EC-derived regulators of thrombosis including heparin, CD39, and thrombomodulin (TM). TM, a 60 kD type I transmembrane protein, is the most important physiological regulator of coagulation in

130

the microcirculation, and acts as an important link between coagulation and inflammation [439]. TM forms a 1:1 molar complex with thrombin and exerts pronounced inhibitory effect on thrombotic, inflammatory, and redox related responses initiated in response to thrombin generation [440-444]. TM binds thrombin and switches off all of its known procoagulant/proinflammatory functions, channeling the catalytic power of the enzyme into complex anticoagulant/anti-inflammatory activities. Specifically, thrombin bound to TM is no longer capable of cleaving fibrinogen, nor is it able to activate factor V or platelets [445]. It is particularly noteworthy, however, that TM significantly enhances the rate of thrombin inactivation by ATIII (~8-fold) and dramatically accelerates (~20,000-fold) the ability of thrombin to activate protein C (APC). APC directly inhibits generation of factors VIIIa and Va, thereby further abrogating thrombin generation [439, 446]. Significantly, APC has also been shown to possess potent, coagulation-independent anti-inflammatory activity [439, 447], inhibiting macrophage production of proinflammatory cytokines (TNF-α, IL-1β, IL-6, IL-8) [448-452], endothelial cell expression of E-selectin and ICAM-1 [453, 454], and neutrophil binding to selectins [455].

Given these observations, we have postulated that administration of TM represents a rational strategy for inhibiting pernicious thrombotic and inflammatory processes that underlie early islet destruction. Specifically, through immobilization of exogenous TM to the islet surface, high local concentrations of APC may be continuously generated, so long as thrombin is present. Towards this objective, we have developed a strategy for biotinylating recombinant human TM (rTM) in a site-specific manner, facilitating its immobilization to the islet surface through well-established biotin-avidin interactions. Moreover, in an effort to maximize surface presentation of rTM, unique covalent islet surface modification techniques were employed with broad implications for chemical remodeling of islets. Finally, through optimization of islet

131

surface biotinylation and subsequent immobilization of rTM, rates of APC generation were significantly increased.

5.2.   MATERIALS AND METHODS

Animals. Male C57BL/6J (B6), and B10.BR-H2k H2-T18a/SgSnJ (B10) mice (8 weeks old, Jackson Laboratory Bar Harbor, ME) were used as islet donors. All animal studies followed local Institutional Animal Care and Use Committee guidelines at Emory University.

Islet isolation. *Murine islets.* Pancreatic islet isolations were performed, as previously described [264]. B10 or B6 mice (8 weeks old, Jackson Laboratory Bar Harbor, ME) pancreata were removed after distension with collagenase P (1 mg/ml, Roche, Indianapolis, IN) through the common bile duct. Following digestion, islets were purified by a Ficoll-Histopaque discontinuous gradient (Ficoll: 1.108, 1.096, and 1.037; Mediatech Inc., Manassas, VA). Isolated islets were cultured for 48-72 hours at 37°C in RPMI 1640 supplemented with 10% heat inactivated fetal calf serum, L-glutamine (2 mM), penicillin (100 U/ml), streptomycin (100 μg/ml) and amphotericin B (0.25 μg/ml) (Mediatech Inc.), and media was changed daily. *Human islets.* Human islets were provided by the Cell and Tissue Processing Laboratory in the Emory University Transplantation Center or obtained from an Islet Cell Resource Center, and cultured 24-72 hours in Miami Medium #1A (Mediatech Inc.) prior to use.

Detection of murine tissue factor. Two-hundred murine (B10) islets were resuspended in homogenization buffer (50 mM Tris-HCl, pH 7.5, 200 mM NaCl, 0.02% Brij-35, 0.5% Triton X-100, 0.1 mM PMSF). Islet tissue was disrupted using a motorized pellet pestle, and samples were clarified with centrifugation. Murine lung tissue was

132

harvested as a positive control. Lung tissue was resuspended in homogenization buffer and processed with a PowerGen homogenizer; samples were clarified with centrifugation. Total protein was quantified with the BCA protein assay kit (Pierce Biotechnology, Rockford, IL), and SDS-PAGE was performed according to Laemmli [456]. Western blot analysis was performed using rabbit anti-mouse tissue factor IgG (American Diagnostica Inc., Stamford, CT) and donkey anti-rabbit HRP (horseradish peroxidase) (GE Healthcare, Piscataway, NJ). Bands were visualized [457] using the ECL plus Western blotting detection kit (GE Healthcare).

Measurement of thrombomodulin activity. The cofactor activity of thrombomodulin (TM) on islets was determined by measuring the production of activated protein C (APC) in the presence of protein C, thrombin, and calcium. Groups of 40-50 human or B6 murine islets were handpicked under a dissecting microscope, placed into wells of a 96 well plate containing 75 μl of 20mM Tris-HCl (pH 7.4) containing 1 μM human protein C (Calbiochem, San Diego, CA), 1 nM thrombin (Haematologic Technologies, Essex Junction, VT), 5 mM $CaCl_2$, 100 mM $NaCl_2$, and 0.1% (wt) BSA. After 1 h incubation at 37°C, production of APC was quenched for 5 minutes by the addition of 2 IU/ml antithrombin III (American Diagnostica, Stamford, CT). Thirty microliter samples were collected and APC was detected by the addition of 0.5 mM Spectrozyme PCa (American Diagnostica). Absorbance measurements at 405 nm were recorded every 30 seconds for 40 minutes to determine the rate of chromogenic substrate conversion by APC. APC concentration was determined using a standard curve relating rates of chromogenic substrate conversion to known concentrations of APC (American Diagnostica) and normalized by islet number.

Preparation of a liposomal formulation of thrombomodulin. Large unilamellar vesicles (LUV) were prepared from a lipid solution of 12 mM 1-palmitoyl-2-

133

oleoyl-sn-glycero-3-phosphocholine (POPC) (Avanti Polar Lipids, Inc., Alabaster, AL) in PBS (80 mM Na_2HPO_4, 20 mM NaH_2PO_4, 100 mM NaCl, pH 7.4) by four successive freeze/thaw/vortex cycles using liquid nitrogen and a 45°C water bath. A total of 20 µg of rabbit thrombomodulin (TM; American Diagnostica, Stamford, CT) was added to 100 µl of the lipid solution and mixed gently for 1 hour at room temperature before it was extruded 21 times, each through two back-to-back 600 nm and then 100 nm polycarbonate membranes (Whatman, UK) [457].

Tubing loop model of blood-islet interactions. A tubing loop model of human blood- islet interactions was used to examine the effects of TM vesicle formulations [54, 55]. Human islets (5000 IEQ) were suspended in 100 µl of either TM-containing vesicles or empty vesicles suspended in PBS. Islets were transferred to loops comprised of heparin-bonded PVC tubing (6.3 mm ID, 40 mm length, Corline Systems, Uppsala, Sweden). Fresh human blood was obtained from healthy volunteers via venipuncture, and collected into heparin-bonded 60 ml syringes (Corline Systems). A total of 7 ml of blood was transferred to each loop containing human islets at 5000 IEQ and TM at 700 µg/ml, resulting in a final TM concentration of 10 µg/ml in each loop. A loop containing human islets in 100 ml of PBS was run as a negative control. To simulate portal blood flow, loops were rocked at 37°C to generate a flow rate of approximately 45 ml/min. After 1 hour, sodium citrate was added to quench reactions and blood samples collected for analysis. Platelet, white blood cell, and lymphocyte counts were determined using a Beckman Coulter ACT (Beckman Coulter Inc., Fullerton, CA). Commercially available ELISA kits were used to analyze plasma for levels of thrombin-antithrombin III (Enzygnost TAT, Dade Behring, Germany), β-thromboglobulin (Asserachrom, Diagnostica Stago, France), and prothrombin fragment 1+2 (Enzygnost F1+2, Dade Behring).

Expression and purification of recombinant human azido-thrombomodulin.
A DNA fragment encoding for EGF (4-6) domains of human TM was obtained by
polymerase chain reaction (PCR) using the primers 5'-
GTGGAACCGGTTGACCCGTGCT-3' and 5'-TTATTACATGCCACCGTCCACCTTGCC-
3'. Site-directed mutagenesis was used to mutate the single internal methionine residue
to leucine at position 388. PCR was used to create a C-terminus GlyGlyMet coding
region. The final construct was inserted into the pFLAG ATS expression system (Sigma,
St. Louis, MO) at HindIII. TM was expressed in the *E. coli* methionine auxotroph B834 in
minimal media supplemented with azido-functionalized methionine [458]. Recombinant
TM was purified with immunoaffinity chromatography using anti-FLAG affinity gel (Sigma
Aldrich).

Synthesis of biotin-PEG-triarylphosphine. A triarylphosphine-poly(ethylene
glycol)-biotin conjugate was synthesized by reaction of a heterobifunctional biotin-
$PEG_{3.4kD}$-amine linker (CreativePEGWorks, Winston Salem, NC) with a
pentafluorophenyl (PFP) active ester of triarylphosphine, synthesized as described
previously [398, 399]. To a stirred solution of biotin-$PEG_{3.4kD}$-amine (100 mg, 0.029
mmol) in DCM (2 ml) was added the PFP-ester of triarylphosphine (31.17 mg, 0.058
mmol, 2 equiv) and Et_3N (8.08 μl, 2 equiv.), and the resultant mixture stirred at room
temperature for 12-16 h, upon which time volatiles were evaporated by vacuum. The
residue was dissolved in the minimum amount of cold DCM and the product was
precipitated by cold ether. The pure compound was collected by filtration and dried in
vacuum. ^{1}H NMR (400 MHz, $CDCl_3$) δ: 1.45 (m, 2H), 1.6-1.8 (m, 4H), 2.2 (t, *J* = 7.6 Hz,
2H), 2.8 (d, *J* = 12.8 Hz, 1H), 2.9 (dd, *J* = 4.8, 12.8 Hz, 1H), 3.2 (m, 1H), 3.3-3.9 (m,
PEG), 3.7 (s, 1H), 4.3 (m, 1H), 4.5 (m, 1H), 6.7 (m, 2H), 7.2-7.4 (m, 11H), 7.8 (dd, *J* =
1.6, 8.4 Hz, 1H), 8.1 (dd, *J* = 4, 8.4 Hz, 1H).

135

Site-specific biotinylation of recombinant TM. Purified azido-functionalized TM was mixed with biotin-PEG-triarylphosphine (1:500 molar ratio) in PBS, and the reaction mixture incubated at 37°C for 48 hr (Scheme 5.1). Conjugation was monitored using SDS-PAGE/Commassie total protein stain. An approximate 4000 MW shift was observed upon reaction of TM with the biotin-PEG-triarylphosphine linker. Excess linker was removed with Amicon ultrafiltration using a 10,000 MWCO filter (Millipore, Billerica, MA), with additional purification achieved through anti-FLAG chromatography to capture the TM. The final desired TM-biotin product was obtained after monomeric avidin chromatography (Pierce Biotechnology, Rockland, IL). Total protein was quantified with the Bradford protein assay (Bio-Rad, Hercules, CA). Biotinylation was confirmed using the FluoReporter Biotin Quantitation Assay Kit (Molecular Probes, Eugene, OR).

Biotinylation of pancreatic islets. N-hydroxysuccinimide (NHS) esters and hydrazide-functionalized reagents were used to biotinylate cell surface amines and aldehydes, respectively (Scheme 5.2). Prior to biotinylation, islets (<1000) were placed into 12 mm cell culture inserts with 12 μm pores (Millicell-PCF; Millipore, Billercia, MA), and washed six times by adding 700 μl of Dubelco's phosphate buffered saline containing calcium and magnesium (DPBS) to the insert, followed by gentle repeated tapping of the insert on a polystyrene surface to facilitate drainage of the wash solution through pores while retaining islets. NHS-PEG$_{3.4kD}$-biotin (Nektar Therapeutics, Huntsville, AL) or sulfosuccinimidyl-6-(biotinamido) hexanoate (sNHS-LC-biotin; Pierce Biotechnology, Rockland, IL) were used to biotinylate islet surface amine groups. Compounds were dissolved at the desired concentration in DPBS supplemented with 11 mM glucose (DPBSG) and added to islets within 10 seconds of dissolution to minimize ester hydrolysis. Reactions were performed for one hour at room temperature, and islets were rinsed six times as described above to remove unreacted biotin. Islet surface

aldehyde groups were generated through periodate oxidation of *cis*-glycol groups. Islets were incubated in 1 mM sodium metaperiodate (NaIO$_4$; Pierce Biotechnology) in DPBS protected from light for 15 minutes. Islets were then rinsed six times with DPBS, and subsequently incubated in biotinamidohexanoic acid hydrazide (hydrazide-LC-biotin; Pierce Biotechnology) at the desired concentration and reaction time. Islets were then rinsed six times to remove unreacted reagent.

Assessment of islet viability. Islet viability was assessed as previously described [148] with some modifications. Briefly, a representative number (35-50) of islets were incubated in DPBS (Mediatech Inc., Manassas, VA) containing 4 μM calcein AM and 8 μM ethidium homodimer-1 (Molecular Probes, Eugene, OR) for one hour, and individual islets were imaged with two-channel confocal microscopy (Zeiss LSM 510 META; Carl Zeiss, Inc., Thornwood, NY) using a 20x objective as described above. Confocal micrographs were analyzed using MATLAB® (The MathWorks, Natick, MA) to quantify the number of pixels corresponding to fluorescent emission from live (green) and dead (red) cells. Viability is expressed as the percentage of fluorescent pixels associated with emission from live cells.

Quantification of immobilized streptavidin. Following biotinylation, islets were incubated in a 1:50 mixture (by mass) of HRP-labeled streptavidin (HRP-SA; Zymed Laboratories, Inc., San Francisco, CA) and streptavidin (Pierce Biotechnology, Rockland, IL) at 0.1 mg/ml in DPBSG for 30 minutes. After rinsing as described above, groups of 30-50 islets were placed into wells of a 96 well plate. The microplate was briefly centrifuged to settle islets, supernatant was removed, and 100 μL of 3,3´,5,5´-tetramethylbenzidine (TMB) solution (1-Step™ Ultra TMB-ELISA, Pierce Biotechnology) was added to islets. Microwell plates containing islets and TMB were placed on a plate

137

shaker (800 m^{-1}, MS1 Minishaker, IKA, Wilmington, NC) at room temperature for 20 minutes, upon which time 50 μL 2M H$_2$SO$_4$ was added to quench the reaction. Microwell plates were briefly centrifuged to settle islets, 100 μL of solution was transferred to a fresh well, and absorbance was recorded at 450 nm using a microplate reader. The amount of streptavidin immobilized on islets was quantified using a standard curve relating absorbance at 450 nm to known concentrations of soluble SA-HRP.

Immobilization of thrombomodulin on mouse islets. Following biotinylation, islets were incubated with 0.1 mg/ml streptavidin (Pierce Biotechnology, Rockland, IL) in DPBSG for 30 minutes. Islets were washed with DPBSG six times as described above to remove free streptavidin. Islets were then incubated with the rTM-PEG$_{3.4kD}$-biotin (rTM-biotin) conjugate (3.5 μM in DPBSG) for one hour at room temperature. Islets were then washed eight times to remove free rTM-biotin prior to measuring TM activity.

Statistics. Tests for statistical significance between the means of two groups were conducted with the Student's t-test (two-tailed, homoscedastic). Tests between three or more groups were conducted with the one-way ANOVA followed by the Tukey HSD test.

5.3. RESULTS

Co-expression of tissue factor and thrombomodulin by isolated pancreatic islets. Tissue factor (TF), the primary physiological initiator of the coagulation system [57], initiates the extrinsic arm of the coagulation pathway. Korsgren and colleagues have recently demonstrated that TF is expressed on the surface of α and β cells in both the intact human pancreas as well as isolated islets [55], and, consequently, is a key initiator of thrombosis and inflammation in intraportal islet transplantation. Accordingly,

138

tissue factor could also be detected on murine islets by immunoblotting (Figure 5.1A) as indicated by a clear band at 47 kD, corresponding to the molecular weight of tissue factor [55]. While expression patterns were not investigated, this finding corroborates previous findings demonstrating localized thrombosis in murine models of intraportal islet transplantation and lends credence to the use of such models [45].

Iino et al. [459] have recently provided histological evidence supporting endogenous expression of thrombomodulin (TM) on islet endocrine cells within the intact pancreas, suggesting regulatory cross-talk between TF and TM under normal physiologic conditions. To determine if endogenous TM expression and activity persisted upon isolation of islets, the capacity of human islets to activate protein C in the presence of thrombin was investigated. As shown in Figure 5.1B, islets activated protein C (APC) at a rate of 0.24 ± 0.02 fmol/minute per islet; repeating the experiment in the absence of thrombin abrogated APC generation, indicating that the observed response was dependent on formation of the TM-thrombin complex. As demonstrated later (Figure 5.5), murine islets generated APC to a comparable extent. Hence, isolated and cultured human and murine islets simultaneously express tissue factor and thrombomodulin.
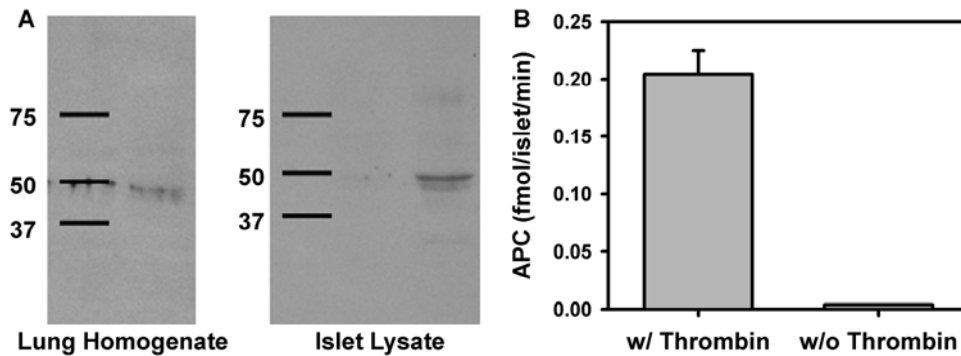
Figure 5.1. Co-expression of tissue factor and thrombomodulin by isolated and cultured pancreatic islets. (A) Western blot of murine islet lysate using rabbit anti-mouse tissue factor IgG demonstrates a distinct band at approximately 47 kD, corresponding to the expected molecular weight of tissue factor. Murine lung homogenate served as a positive control. (B) Thrombin-dependent production of activated protein C (APC) by human islets indicates endogenous thrombomodulin activity.

Liposomal formulations of TM inhibit islet-mediated coagulation. A tubing loop model was used to investigate thrombotic reactions mediated by human islets in contact with fresh, non-anticoagulated whole human blood. In accord with previous findings [54, 55], islets initiated a significant thrombotic response, characterized by thrombin generation and platelet activation (Table 5.1). The presence of islets resulted in a ~500 fold increase in thrombin-antithrombin III (TAT) production relative to control loops without islets. Similarly, levels of prothrombin fragment 1+2 were elevated nearly 200 fold in the presence of islets. Additionally, islet-blood contact induced significant platelet activation, as evidenced by a significant increase ($p < 0.01$) in the release of β-thromboglobulin (β-TG) and platelet consumption. Moreover, lymphocyte and white cell counts were also reduced due to entrainment of cells in large thrombi that formed in loops containing islets. Hence, islets initiate a significant thrombotic response despite expression of endogenous TM and an attendant ability to generate APC suggesting an imbalance in the expression levels of TM and TF.

In light of these findings, the potential efficacy of TM as an inhibitor of islet-mediated thrombosis was investigated. Incorporation of TM within a lipid bilayer significantly increases the catalytic efficiency of protein C activation [460]; as the objective of this experiment was to demonstrate the potential efficacy of TM a liposomal formulation of TM (lipo-TM) was used. Addition of lipo-TM reduced TAT levels by 98%, though TAT levels remained statistically higher than control loops ($p < 0.01$). Lipo-TM reduced levels of prothrombin fragment 1+2 by 95% to levels statistically similar to control loops ($p > 0.01$), decreased β-TG levels approximately three-fold, and significantly increased platelet count ($p < 0.01$). Finally, addition of lipo-TM inhibited thrombus formation, thereby, limiting changes in lymphocyte and white blood cell counts. These studies demonstrate the therapeutic potential of thrombomodulin as an inhibitor of islet-initiated thrombosis, and provide motivation for increasing the surface density of TM on the surface of pancreatic islets.

Table 5.1. Thrombotic activity of human islets in the presence or absence of TM liposomes

	0 min	60 min		
			Islets	
		Control	TM Vesicles	Empty Vesicles
Platelets (x10^3/μl)	270 ± 84	230 ± 52	160 ± 45[†]	3.3 ± 0.91[‡]
White blood cells (10^3/μl)	8.5 ± 2.7	8.1 ± 2.5	7.8 ± 2.3	3.6 ± 1.4
Lymphocytes (10^3/μl)	2.2 ± 0.10	2.5 ± 0.05	2.5 ± 0.06	1.6 ± 0.54
Thrombin-antithrombin III (μg/l)	29 ± 10	67 ± 12	650 ± 140[†]	33,000 ± 6,800[‡]
β-thromboglobulin (IU/ml)	390 ± 350	1,000 ± 100	3,200 ± 1,300	9,300 ± 780[‡]
Prothrombin F1+2 (pmol/l)	270 ± 95	320 ± 39	3,000 ± 1,700	59,000 ± 17,000[‡]

Data are n, mean ± standard deviation.
Control loops contained blood and PBS loading solution, but no islets.
[†]Significant difference ($p<0.01$) when compared with the control loop.
[‡]Significant difference ($p<0.01$) when compared with loops containing islets and TM-vesicles

Site-specific biotinylation of recombinant human thrombomodulin.

Immobilization of exogenous TM on the islet surface provides a rational approach to increasing local concentrations of APC at the site of transplantation. Towards this objective, a biotinylated TM was generated to facilitate immobilization on the islet surface via well-established biotin-(strept)avidin interactions. Though TM activity is maximized when inserted into a phospholipid bilayer [460], it is well established that the extracellular EGF-like domains 4-6 of human TM exhibit full cofactor activity [461]. Hence, a biosynthetic approach was used to generate recombinant human TM (rTM) containing these domains, as well as a non canonical, C-terminal azido-methionine analog (rTM-N_3) [462, 463]. Site-specific biotinylation was achieved through chemoselective Staudinger ligation between triphenylphosphine-derivatized poly(ethylene glycol)-biotin and the C-terminal azide of rTM-N_3 (Scheme 5.1). Upon reaction, SDS-PAGE of the crude mixture demonstrated the presence of two species separated by approximately 4 kD, corresponding to the desired conjugate (TM-PEG-biotin) and unreacted rTM-N_3 (Figure 5.2A). By contrast, only a single band was observed when rTM bearing a C-terminal methionine was used, demonstrating the specificity of the conjugation reaction. Densitometry indicated that roughly 50% of rTM-N_3 had been conjugated to the biotin-PEG linker. Upon subsequent purification with centrifugal dialysis and monomeric avidin chromatography, immunoblotting demonstrated the presence of a single species of molecular weight corresponding to the desired rTM-PEG-biotin conjugate (Figure 5.2B). Biotinylation was confirmed with Western blotting using HRP-labeled streptavidin (Figure 5.2C). Previous studies have demonstrated that TM activity is not lost upon site-specific conjugation of poly(ethylene glycol) [463]. Significantly, C-terminal biotinylation is anticipated to facilitate immobilization TM in a manner that closely mimics its structure as it appears on the cell surface, and, consequently preserve activity upon immobilization.

142
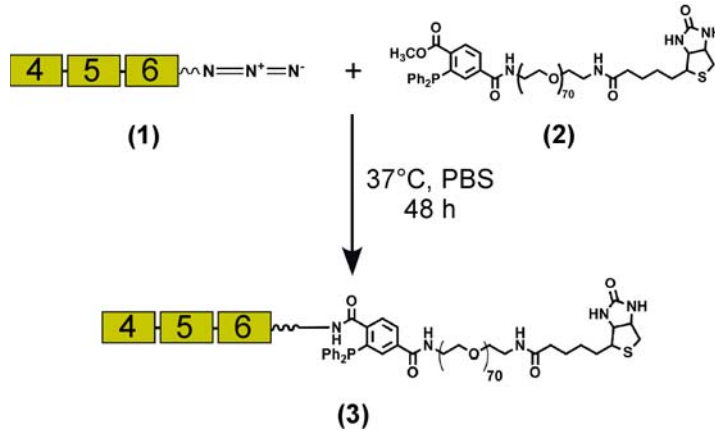
Scheme 5.1. Site-specific biotinylation of recombinant human thrombomodulin (rTM) through Staudinger ligation between rTM engineered with a C-terminal azido group **(1)** and triarylphosphine-PEG$_{3.4kD}$-biotin **(2)** linker.

143
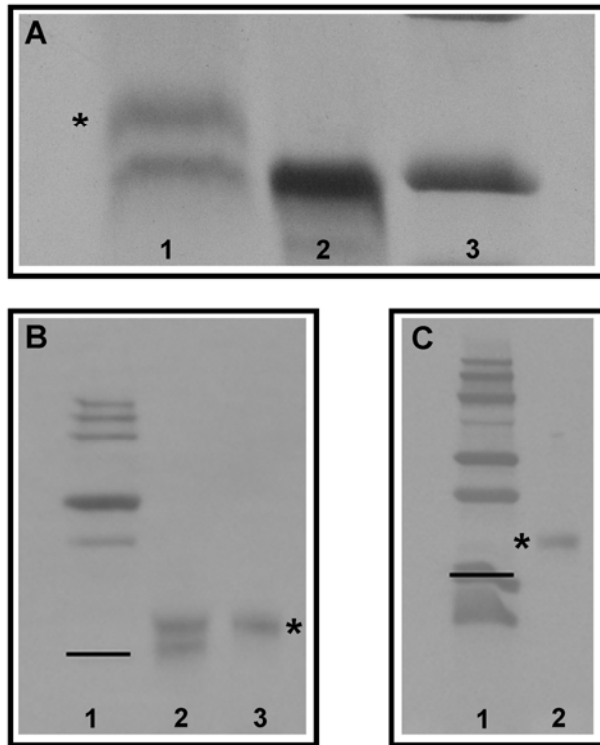
Figure 5.2. Site-specific biotinylation of recombinant human thrombomodulin. (A) Upon reaction between rTM-N$_3$ and triarylphosphine-PEG$_{3.4kD}$-biotin SDS PAGE reveals the presence of two species separated by approximately 4 kD (Lane 1), corresponding to the desired biotinylated conjugate (∗) and unreacted rTM-N$_3$. A molecular weight shift was not observed in a parallel control reaction using rTM engineered without an azido group (Lane 2), demonstrating the specificity of the Staudinger ligation. Lane 3 corresponds to a 20 kD marker. (B) Western blot against human TM after initial conjugation (Lane 2) and subsequent purification (Lane 3). After purification via centrifugal dialysis and monomeric avidin chromatography, a single species corresponding to the expected molecular weight of the desired biotin-PEG-TM conjugate is observed (∗). Lane 1: molecular weight ladder; 20 kD marker indicated. (C) Western blot against biotin using HRP-labeled streptavidin confirms biotinylation of the construct (∗; Lane 2). Lane 1: molecular weight ladder; 20 kD marker indicated.

Streptavidin binding may be maximized through optimization of cell surface biotinylation strategies. Biotinylation of pancreatic islets has commonly been employed as a facile strategy for immobilizing macromolecules on the islet surface [227, 236]. However, little work has been done to quantitatively optimize reaction schemes or conditions to maximize the surface density of biotin moieties, or subsequently immobilized (strept)avidin, while maintaining high islet viability. To date, covalent modification of islet surfaces has been accomplished nearly exclusively through amine-reactive chemistries, most commonly NHS-esters [13, 155, 165, 227, 236], though the dependence of conjugation efficiency on important reaction conditions, most notably concentration, are rarely investigated or reported. Cell-surface carbohydrates, in particular sialic acid residues, may be covalently modified through mild periodate oxidation of *cis*-glycol groups and subsequent hydrazone linkage between resultant aldehydes and hydrazine-activated molecules [384, 401, 403, 404]. While this approach has been used to label or modify a variety of cell types, its utility for chemically re-engineering the surface of pancreatic islets has not been explored. Therefore, in an effort to maximize the amount of rTM that may be immobilized on islets, the capacity of both NHS ester and aldehyde-hydrazide biotinylation strategies to facilitate immobilization of streptavidin was investigated (Scheme 5.2).

To determine the effect of a poly(ethylene gycol) (PEG) spacer arm between the covalent linkage and biotin moiety, islets were reacted with either NHS-PEG$_{3.4kD}$-biotin or sulfosuccinimidyl-6-(biotinamido) hexanoate (sNHS-LC-biotin) at 4 mM for 1 hour, and the amount of immobilized streptavidin (SA) compared. Use of NHS-PEG$_{3.4kD}$-biotin yielded significantly less SA than sNHS-LC-biotin ($p < 0.05$, Figure 5.3A), potentially due to generation of a steric barrier with increasing density of PEG chains on the islet surface [464]. Based on these findings, sNHS-LC-biotin was used to investigate the effect of concentration on conjugation efficiency. Increasing sNHS-LC-biotin

www.manaraa.com

concentration to 20 mM did not have a significant effect on the amount of surface-bound SA (Figure 5.3A), suggesting saturation of SA surface density through this approach. Increasing reaction time beyond 1 hour was not explored, as hydrolysis of NHS-esters occurs rapidly and is reported to be nearly complete within an hour [415].

Though less commonly employed, coupling between cell surface aldehydes and hydrazide-derivatized molecules offers an alternative to amine-reactive chemistries, and, therefore, was investigated as a means to biotinylate islets. Islets were treated with 1 mM $NaIO_4$ for 15 minutes to generate cell surface aldehyde groups [403], and subsequently reacted with 4 mM hydrazide-LC-biotin for 1 and 3 hours. No statistical difference ($p>0.05$) in immobilized SA was detected between 1 and 3 hour incubation times (Figure 5.3B), suggesting that hydrazone bond formation between hydrazide-LC-biotin and cell surface aldehydes approaches equilibrium after an hour. Increasing the concentration of hydrazide-LC-biotin to 20 mM resulted in a significant increase in SA binding ($p<0.05$), yielding levels statistically comparable ($p>0.05$) to optimized NHS-LC-biotin coupling. Exploration of higher concentrations was not possible due to the solubility limit of hydrazide-LC-biotin.

It was next postulated that biotin surface density might be further increased through combination of amine- and aldehyde-reactive coupling strategies. To investigate this possibility, islets were serially biotinylated using conditions optimized for each strategy. Islets were first treated with 1 mM $NaIO_4$ for 15 minutes, reacted with 20 mM hydrazide-LC-biotin for 1 hour, and finally reacted with 4 mM NHS-LC-biotin for 1 hour. This combination approach yielded a significant increase ($p<0.05$) in SA density of approximately 50 percent relative to either treatment alone (Figure 5.3C). Interestingly, a doubling in SA density was not observed, suggesting that the relative contributions from each conjugation strategy were not additive, a potential indicator of molecular crowding or surface saturation. Regardless, these results demonstrate that the surface density of

146

streptavidin, and, consequently, the surface density of biotinylated macromolecules, may be increased through chemically targeting multiple reactive groups on the cell surface.

Given the role of cell surface proteins and carbohydrates in diverse biochemical processes critical to cell survival, covalent modification of the islet surface may have detrimental impacts on islet viability. While previous reports demonstrate that islet viability and function are maintained upon biotinylation and subsequent immobilization of (strept)avidin [227, 236], suboptimal reaction conditions were used and aldehyde-hydrazide coupling was not explored. Therefore, the viability of islets biotinylated through the previously described combination approach and subsequently incubated with streptavidin was assessed via calcein AM and ethidium homodimer staining and subsequent quantification with image analysis (Figure 5.4). Combination treatment had no discernable impact on islet viability relative to non-treated controls, both immediately after treatment (97.2 ± 2.0% vs. 98.4 ± 2.0%, $p > 0.01$) as well as 24 hours later (98.3 ± 2.0% vs. 98.3 ± 1.6%, $p > 0.05$), indicating that combination biotinylation does not induce late necrosis or apoptosis. A slight change in islet morphology was noted immediately after combination treatment, but was found to return to normal after 18-24 hours in culture. Qualitative comparison of islets biotinylated using sNHS-LC-biotin or hydrazide-LC-biotin, indicate the observed changes in morphology may be attributed to use of sNHS-LC-biotin.

147
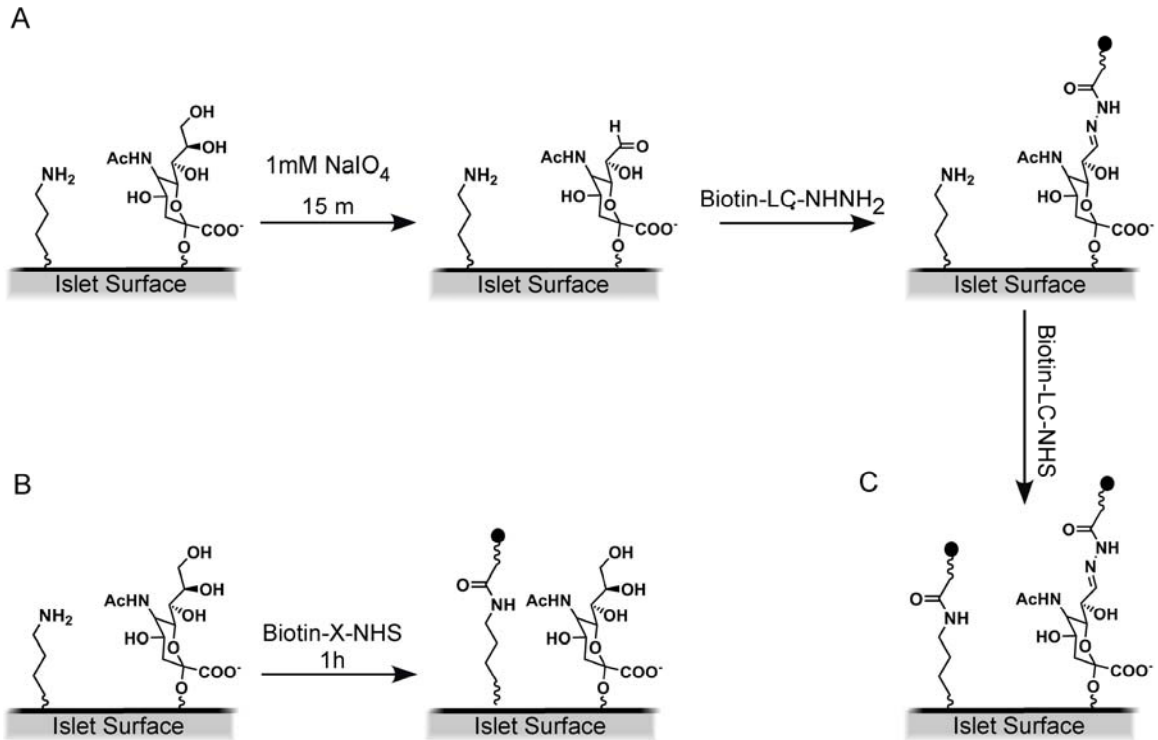
Scheme 5.2. Islet surface biotinylation through chemical targeting of amines and aldehydes. (A) Conjugation of biotin (●) via hydrazone bond formation between biotin-hydrazide and aldehydes generated through mild sodium metaperiodate (NaIO$_4$) oxidation of sialic acid residues. (B) Islet biotinylation using NHS-ester functionalized biotinylation reagents. (C) Strategies may be utilized in combination to increase density of biotin groups on the cell surface.

148

Table 5.2. Biotinylation Conditions

	Biotinylation Reagent	mM	t(h)
1	NHS-PEG*-B	4	1
2	sNHS-LC-B	4	1
3	sNHS-LC-B	20	1
4	NHNH$_2$-LC-B	4	1
5	NHNH$_2$-LC-B	4	3
6	NHNH$_2$-LC-B	20	1

*3.4kD. NHNH$_2$ = hydrazide. B=biotin
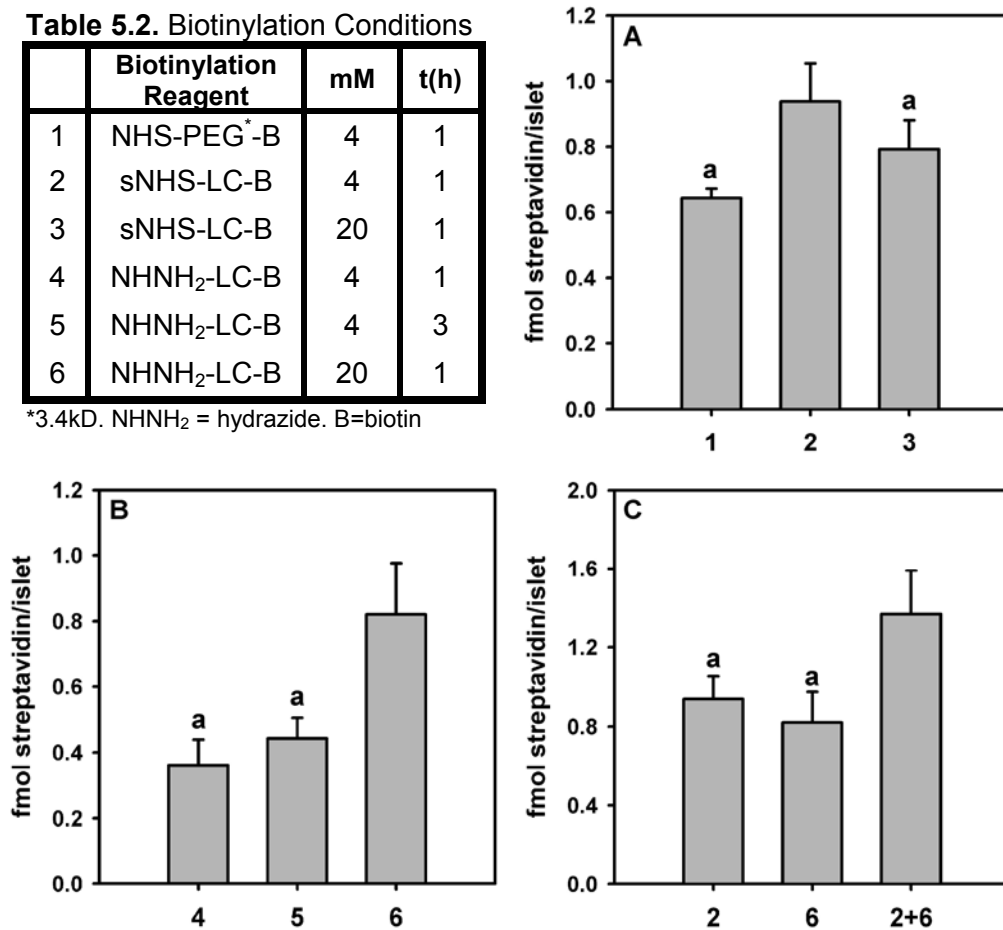
Figure 5.3. Islet surface density of streptavidin may be maximized through optimization of biotinylation reactions targeting cell surface amines and aldehydes. (A) Comparison of N-hydroxysuccinimide ester (NHS) functionalized biotinylation reagents and reaction conditions demonstrated maximum streptavidin incorporation using sulfosuccinimidyl-6-[biotinamido]hexanoate (sNHS-LC-B) at a concentration of 4 mM. (B) Comparison of reaction conditions used for coupling [biotinamido]hexanoate hydrazide (NHNH$_2$-LC-B) to cell surface aldehydes demonstrated a dependence on NHNH$_2$-LC-B concentration, but not on reaction time at 4 mM. (C) Optimized conditions for sNHS-LC-B and NHNH$_2$-LC-B (2+6) can be combined to increase streptavidin surface density by nearly 50% over either strategy alone. Bars labeled with the letter a are not statistically different from each other (p>0.05).

149
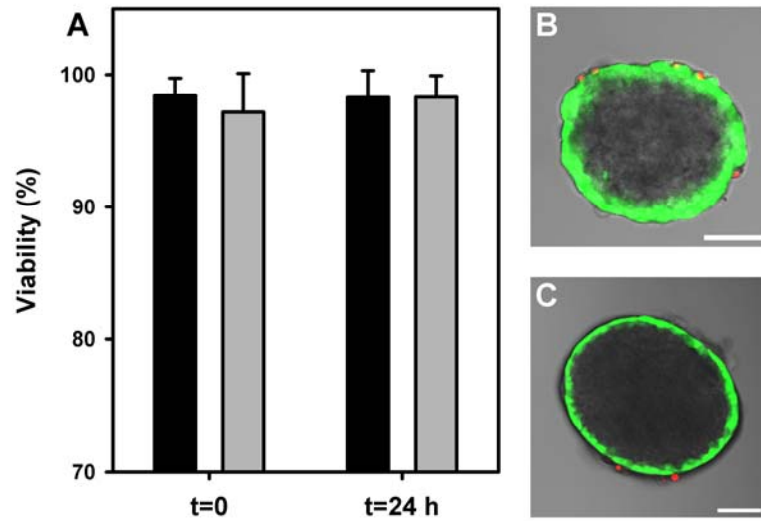
Figure 5.4. Sequential biotinylation of cell surface aldehydes and amines does not adversely influence islet viability. Islet viability upon combination biotinylation and subsequent immobilization of streptavidin (grey bars) was statistically similar (p>0.01) to untreated controls (black bars) immediately (t=0) and 24 hours (t= 24 h) after treatment (A). Representative bright field and confocal micrographs of islets stained with calcium AM (green, viable) and ethidium homodimer (red, non-viable) of islets immediately after treatment (B) and without treatment (C). Scale bar = 50 μm.

Immobilization of rTM on islets increases rates of protein C activation.

Maximizing the amount of streptavidin on the islet surface is anticipated to facilitate immobilization of a high density of rTM-biotin, with an attendant increase in the ability of islets to activate protein C. Islets were biotinylated via combination treatment, incubated with 0.1 mg/ml streptavidin for 30 minutes followed by incubation with rTM-biotin at 3.5 μM for one hour. Upon extensive rinsing of treated islets to remove unbound rTM-biotin, APC generation was measured and compared to untreated islets and islets treated only with biotinylation reagents and streptavidin as controls (Figure 5.5). Treatment of islets with rTM-biotin resulted in an approximately three-fold increase in APC production relative to untreated controls, which, as anticipated, activated protein C as a result of endogenous expression of TM. No significant difference in APC generation relative to untreated controls was observed after biotinylation and subsequent immobilization of streptavidin, indicating that the observed increase in APC production is not an artifact of increased endogenous TM expression, but rather a consequence of rTM-biotin incorporation. Hence, cell surface immobilization of thrombomodulin significantly increases the capacity of islets to activate protein C, with the potential to attenuate islet-mediated thrombotic responses initiated by islet-derived tissue factor.
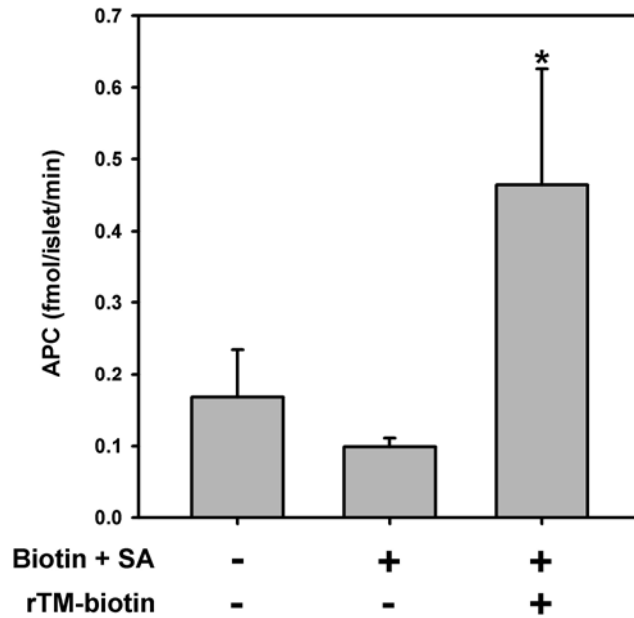
Figure 5.5. Immobilization of rTM on the islet surface via streptavidin-biotin interactions increases rates of activated protein C (APC) generation. Upon combination biotinylation and subsequent incubation with streptavidin (Biotin + SA) islets were incubated with rTM-biotin at 3.5 μM for 1 hour, resulting in an approximately three-fold increase in the rate of APC generation relative to untreated controls. Immobilization of streptavidin alone was found to have no effect on rates of APC generation (∗p<0.05).

5.4. DISCUSSION

Marked activation of coagulation has been noted minutes after islet infusion in patients undergoing clinical intraportal islet transplantation [56, 60], leading to significant levels of early islet destruction and primary non-function, as well as overt and subclinical episodes of portal vein thrombosis [433, 434]. While a number of factors have been implicated in the initiation of such responses, including release of islet-derived inflammatory mediators and local injury to endothelial cells [52], compelling evidence has recently emerged that tissue factor expression by islets acts as the primary initiator of inflammation in intraportal islet transplantation [3, 60, 465]. As a consequence of islet-initiated thrombin generation, activated platelets bind to the islet surface and further amplify thrombosis and inflammation, ultimately leading to fibrin clot formation [45], leukocyte infiltration [37, 45-47], and elevated levels of proinflammatory mediators that adversely effect islet viability and function [49, 51, 52].

In recognition of the prothrombotic effects of intraportal islet infusion, most centers performing allogeneic islet transplantation currently use systemic heparin at the time of transplantation [18, 25]. Despite administration as a bolus dose of ~75 U/kg body weight, corresponding to ~5,000 U for a 70-kg person (~1 U/ml blood), serum levels of TAT, fVIIa-AT, and D-dimer remain elevated. Korsgren and colleagues [54] have observed that heparin prevented islet-induced coagulation in an ex vivo model, but at a four-fold *higher* concentration than that used clinically (4 U/ml blood). Furthermore, extensive platelet and fibrin formation, as well infiltration of CD11b+ cells continued to be observed. Finally, even if one were to accept the risk of bleeding complications to be anticipated at a dosing level of 300 U heparin/kg, systemic heparin has a half-life of one hour and is therefore active for only a few hours. Thus, the potential therapeutic impact of intravenously administered heparin is limited both by its systemic anticoagulant activity that increases the risk of bleeding complications and short half-life.

153

As an alternative strategy, Contreras et al. have recently demonstrated that intravenous administration of APC dramatically inhibited interhepatic fibrin deposition, portal vein endothelial cell activation, cytokine production, and leukocyte infiltration, resulting in a reduced loss of functional mass in a murine model of intraportal islet transplantation [45]. While promising, APC was administered at a 10-fold higher dose than that recommended for clinical use. Moreover, the half-life of APC is approximately 10 to 20 minutes, which would necessitate repetitive dosing to achieve a sustained effect [219]. By contrast, thrombomodulin provides a means for prolonged generation of APC as long as exogenous TM remains active and elevated levels of thrombin are being produced. Indeed, studies have demonstrated that administration of TM reduces endotoxin induced lung injury [466], limits thrombosis in an arteriovenous shunt model [467], and attenuates thrombotic glomerulonephritis in rats [468].

While it is now generally accepted that islet-derived tissue factor is a key initiator of thrombosis and inflammation in islet transplantation, surprisingly little consideration has been given to mechanisms which regulate coagulation in the intact pancreas. We have demonstrated that both murine and human islets activate protein C in a thrombin-dependent manner, indicating TM expression by isolated and cultured islets. Though endothelial cells within islets are reportedly lost after several days of culture [1, 2], it is conceivable that islet-mediated APC generation is due to residual endothelial cells. However, TM expression has been previously noted in a β cell line [459], a likely indicator that endocrine cells contribute to the observed catalytic activity. These findings, together with previous reports demonstrating tissue factor expression by islets [55], suggest that islets possess the necessary machinery to regulate coagulation. However, despite an endogenous capacity to activate protein C, thrombin generation via the tissue factor pathway dominates the response, suggesting a polarization of isolated islets towards a pro-coagulant/pro-inflammatory phenotype. Indeed, as a result of

154

metabolic and mechanical stress associated with isolation and culture, a number of inflammatory signaling pathways are triggered [1, 36, 52, 70-81], potentially leading to increased tissue factor expression. Indeed, inhibition of inflammatory pathways through incubation of islets with corticosteriods resulted in a marked reduction in the expression of TF [469]. Moreover, pro-inflammatory cytokines, such as interleukin-1 and TNF-α, may also downregulate the expression of thrombomodulin by islets with a concomitant decrease in activated protein C production, as has been previously demonstrated to occur in endothelial cells [470, 471].

Accordingly, we postulated that by increasing levels of TM on the islet surface enhanced APC generation could be achieved, with an attendant attenuation of thrombotic responses initiated by tissue factor. Towards this objective, we used a biosynthetic approach to generate a recombinant human TM containing the extracellular EGF-like domains 4-6 as well as a C-terminal azido (N_3) group, to which biotin can be covalently coupled via Staudinger ligation [370] using a heterobifunctional biotin-PEG-tripheynlphosphine linker. While biotinylation of proteins is commonly performed, generally through targeting amino groups, the exquisite orthogonality of the Staudinger ligation [398] provides a strategy for biotinylation in a site-specific manner, thereby eliminating loss of protein activity associated with covalent modification of amino acids within the active site [463]. Moreover, through incorporating biotin at the C-terminus, separated from the active EGF-like domains by a PEG spacer arm, the construct may be linked to immobilized streptavidin in a manner that more closely mimics the presentation of native TM [439].

Despite the common use of biotin-(strept)avidin interactions for islet surface modification, little attention has been given to optimizing coupling chemistry or conditions. Moreover, covalent islet surface biotinylation strategies have almost exclusively targeted amino groups within cell surface proteins [13, 155, 165, 227, 236].

155

In an effort maximize the surface density of immobilized biotinylated TM, both amine-reactive N-hydroxysuccinimide (NHS) esters and aldehyde-hydrazide coupling were explored. Through sequential conjugation of hydrazide-LC-biotin to cell surface aldehydes and sulfoNHS-LC-biotin to amines, the amount of streptavidin that could be incorporated on the islet surface could be increased by ~50% relative to conventional cell surface biotinylation using NHS-esters. Significantly, to the author's knowledge, this is the first report describing chemical targeting of *both* amine and aldehyde groups on the surface of cells or tissue.

Immobilization of rTM-biotin on the islet surface resulted in an approximately three-fold increase in the rate of APC generation relative to untreated controls. Whether such rates of APC generation will be sufficient to improve the outcome of intraportal islet transplantation has yet to be determined and is an area of ongoing investigation. It should be reemphasized that the observed *fold* increase may be significantly higher upon islet transplantation as a consequence of decreased endogenous TM expression in response to inflammation. Moreover, several investigators have observed that inflammatory stimuli, similar to those generated upon intraportal islet transplantation, decreases thrombmodulin expression in hepatic sinusoidal endothelial cells [472-474], thereby further decreasing APC production in the liver. Hence, conjugation of TM to islets provides a strategy for targeting TM to the site of islet transplantation, potentially allowing high *local* concentrations of APC to be generated. Interestingly, it has recently been reported that surface heparinization of intraportal islet grafts reduced TAT production and early islet damage in an allogenic porcine model [227]. While a direct comparison with soluble heparin was not made, in light of the inefficacy of systemically administered heparin during clinical islet transplantation [18, 25, 55, 56, 60] these findings potentially illustrate the increased therapeutic benefit achieved through local

delivery of anticoagulants to the portal bed. Given the increased capacity of TM to inhibit thrombin generation, similar or more substantial effects might be reasonably anticipated.

Regulation of islet-initiated coagulation is governed by interplay between, among other factors, the relative amounts of TM and TF presented at the islet-blood interface. Hence, conjugation of TM to the islet surface may also act synergistically with strategies directed at inhibiting tissue factor expression or activity [202, 203, 469]. Notably, blockade of TF through pre-incubation of islets with site inactivated fVIIa or anti-TF antibody has been shown to inhibit thrombotic responses and improve islet survival both in vitro [55] and in vivo [221]. Interestingly, Wang et al. have demonstrated marked improvements in the therapeutic efficacy of a fusion protein consisting of a TF-neutralizing single-chain antibody and the active site of TM relative to administration of either component of the conjugate separately or in combination [475]. We have recently developed a family of multilayer polymer thin films of diverse architecture, properties, and composition that may be assembled directly on the islet surface, providing a potential strategy to mask islet-associated TF (Chapters 2 and 3). Moreover, film constituents have been designed to allow biotin, aldehyde, amino, and other reactive groups to be readily incorporated (Chapter 2 and 4), providing reactive handles through which rTM may be immobilized. Through simultaneous blockade of tissue factor and presentation of thrombomodulin, it may be possible to effectively restore the physical and biochemical barriers to thrombosis and inflammation afforded by endothelial cells within the intact pancreas.

5.5.   CONCLUSIONS

Though intrahepatic infusion of islets remains the clinical standard for islet transplantation, direct contact between islet-derived tissue factor and blood initiates thrombosis and inflammation in the immediate post-transplant period with deleterious

157

consequences to islet survival and function. We have presented a strategy for conferring anticoagulant potential to islets through immobilization of rTM on the islet surface. Through site-specific, C-terminal biotinylation of TM and optimization of cell surface biotinylation strategies targeting both amine and aldehyde groups, integration of rTM resulted in an approximately three-fold increase in the catalytic capacity of islets to activate protein C. Conjugation of TM to islets represents a facile strategy for increasing APC generation at the site of transplantation, and such localized delivery of anticoagulants offers the potential to increase rates of islet survival and function with attendant improvements in clinical outcomes.

158

CHAPTER 6

Conclusions and Future Directions

Protection of transplanted islets from deleterious host immune and inflammatory responses will be necessary to exploit the full clinical potential of islet transplantation, and islet encapsulation and cell surface modification stand to play pivotal roles towards this end. Despite considerably progress over the past decade, adherent challenges have spawned new paradigms in islet encapsulation including implantation of encapsulated islets into native tissue microvasculature, most notably the liver, minimization of capsule and transplant volume, and the design of biologically active barriers. The work presented in this dissertation describes the design of novel conformal coatings and cell surface modification strategies with broad implications for improving islet engraftment. Specifically, the process of layer-by-layer self assembly was employed to generate nanothin films of diverse architecture with tunable properties directly on the extracellular surface of individual islets. Importantly, these studies are the first to report in vivo survival and function of nanoencapsulated islets. Moreover, through proper design of film constituents, coatings displaying biotin groups and bioorthogonally reactive handles could be generated, providing a facile approach through which to integrate immunomodulatory or anti-inflammatory molecules into conformal coatings. Towards this end, a strategy was developed to tether thrombomodulin to the islet surface in a site-specific manner, thereby facilitating local generation of the powerful anti-inflammatory agent activated protein C. Collectively, the methodologies, polymers, and strategies described in this dissertation have helped established new paradigms for the design of anti-inflammatory conformal islet coatings. Furthermore, this work provides novel biomolecular strategies for resurfacing the biochemical landscape of living cell and

tissue interfaces with broad biomedical and biotechnological applications in cell-based therapy and beyond.

As these studies provide the foundation for the long-term goal of designing conformal barriers that improve islet engraftment, several recommendations for future investigations are proposed for each of the previous chapters.

Chapter 2. Layer-by-Layer Assembly of a Conformal Nanothin Poly(ethylene glycol) Coating for Intraportal Islet Transplantation. Using a combination of electrostatic interactions and biorecognition, PEG-rich thin films could be assembled on the surface of islets through layer-by-layer deposition of PPB and streptavidin. Prior to the initiation of these studies, not a singular report existed in the literature describing the assembly of layer-by-layer coatings on mammalian cells, and, in this regard, this work has helped launch a new paradigm in cell encapsulation. Perhaps most importantly, the observed relationships between PPB structure and islet viability served as the motivation for generating cytocompatible polyelectrolyte multilayer films described in Chapter 3.

Though it is significant that PPB/SA coated islets maintained function in vivo and did not impair engraftment, as has been reported upon intraportal transplantation of microencapsulated islets, the coating also did not significantly improve engraftment in this model. While a trend towards increased rates of euglycemia might suggest some protection afforded by the film, the barrier capacity of this coating appears to be insufficient, and, therefore, further characterization and subsequent optimization of film properties including thickness, permeability, and stability are an area of future investigation. Having used relatively long PEG chains in the synthesis of PPB and a relatively bulky molecule, streptavidin, to connect adjacent layers, it is conceivable, perhaps likely, that PPB/SA films yielded relatively large pores incapable of presenting a

barrier to diffusion of soluble mediators of inflammation and thrombosis to their respective targets on the islet surface. PPB with shorter PEG chains, for example P12P4(biotin) described in Chapter 4, might reasonably be expected to yield smaller pore sizes. Though inflammatory events that underlie early islet destruction are thought to resolve within ~24 hours, it is also possible that PPB/SA films were not sufficiently stable in vivo, particularly in an inflammatory environment. Stability might be increased through assembly of more layers or through integration of crosslinking strategies. For example, structurally similar terpolymers containing both PEG(biotin) as well as PEG(N$_3$) grafts might facilitate film growth via biorecognition while simultaneously providing a strategy for subsequent crosslinking with a bifunctionalized triphenylphosphine linker; such a film could be readily generated and investigated using the methods and bioconjugation strategies described in this dissertation. Furthermore, covalent crosslinking of films might also provide increased control of film permeability.

Chapter 3. Cell Surface-Supported Polyelectrolyte Multilayer Thin Films as Conformal Islet Coatings. The cytocompatibility of PPB described in Chapter 3 relative to conventional polycations prompted investigations aimed at developing polyelectrolyte multilayer (PEM) thin films that could be assembled directly on the islet surface without adversely influencing viability. Through control of grafting ratio, grafted PEG length, and PLL backbone molecular weight, several structural variants capable of initiating and propagating the growth of PLL-*g*-PEG/alginate PEM films on the extracellular surface of islets were identified. Planar characterization of this novel class of PEM films indicated that film thickness and composition may be tailored through appropriate control of layer number and copolymer properties. To date, only a handful of reports have described the assembly of PEM films directly on the surface of viable mammalian cells or tissue, and all have utilized polycations and/or conditions found to be highly cytotoxic to islets.

Hence, the polycations and PEM films described herein represent a unique opportunity to translate the diverse functionality afforded by PEM films to the surface of viable mammalian cells and tissue.

Critical to these investigations was the synthesis of a library of PLL-*g*-PEG copolymers that allowed partial elucidation of structure-cytotoxicity relationships and, importantly, critical grafting ratios to be defined. While these studies have revealed important trends and boundaries for polycation design, basic research exploring the biochemical and biophysical processes that dictate PLL-*g*-PEG cytotoxicity, interfacial conformation, and membrane translocation potential upon interaction with cell or model membranes is an important area of future study. Indeed, Lee and Larson have recently performed molecular dynamics simulations of PLL interacting with lipid bilayers and have observed a dependence on PLL charge density in the disruption of cell membranes [476]. Similar models of PLL-*g*-PEG variants may provide a valuable tool for the design and optimization of cytocompatible polycations as constituents in cell surface-supported PEM films.

From this work a minimum of three cytocompatible PEM films have emerged as candidates for conformal islet coating. Based on the available data, films assembled using P12P4[2.5] most closely mimic PLL/alginate with respect to thickness and appear to present the most compact and polyelectrolyte-dense film structure. However, further exploration into film thickness in the hydrated state, permeability, and resistance to protein adsorption will be necessary to select films with desired properties. Moreover, characterization of the stability of films assembled on islets will be necessary to more accurately predict the anticipated duration of efficacy. Inadequate film stability might be resolved through incorporation of film constituents bearing orthogonally reactive groups such as those described in Chapter 4. For example, layer-by-layer assembly of films using P12P4[2.5](hydrazide) and alginate-aldehyde may assemble through electrostatic

mechanisms while crosslinking *in situ* through hydrazone bond formation between film components. As film stability may also be linked to the capacity of cells to endocytose or otherwise internalize polymers neighboring the cell surface, increasing layer number, and hence thickness, may yield nanoassembled structures recalcitrant to such mechanisms of instability. Data presented herein demonstrates that prolonged exposure (6 hrs) to PLL-*g*-PEG copolymers at the critical grafting ratio does not adversely influence islet viability, suggesting considerably more layers may be deposited. Accordingly, current research efforts have been directed at the development of an automated system for assembly of islet-supported layer-by-layer thin films. Finally, the efficacy of optimized coating(s) must be assessed in a murine model of intraportal islet transplantation as described in Chapter 2.

Chapter 4. A Modular Approach to Cell and Tissue Surface Engineering Using Cytocompatible Poly(L-lysine)-*graft*-poly(ethylene glycol) Copolymers and Polyelectrolyte Multilayer Films. Critical to the development of effective conformal islet coatings is an inherent strategy through which to immobilize or otherwise incorporate bioactive molecules for directing desired biochemical or cellular responses. Towards this end, PLL-*g*-PEG copolymers functionalized with biotin, azide, and hydrazide moieties were synthesized and used, both alone or in combination, to capture streptavidin-, triphenylphosphine-, and aldehyde-labeled probes, respectively, on the islet surface. Alternatively, chemical and biological functionality may be conferred to films through integration of modified or bioactive polyanions. To exemplify this concept, PEM films assembled using alginate chemically modified to contain aldehyde groups could be used to integrate hydrazide-functionalized molecules with the film. Collectively, the strategies presented herein provide a modular approach to cell and tissue surface

engineering whereby diverse film constituents may be combined in unique manners to control the biochemical composition of the cellular interface.

In accord with the overall objective of this work, the approaches described in this chapter may be engaged to bestow anti-inflammatory capabilities to islets, and demonstration of this potential is clearly an area of future investigation. Functionalized copolymers may be employed to drive film assembly or used merely as an outer layer to display handles for simultaneous immobilization and presentation of appropriately functionalized anticoagulants or anti-inflammatories. For example, assembly of films via LbL deposition of P12P4(biotin) and alginate-aldehyde, followed by subsequent biotinylation of aldehydes with biotin-hydrazide, may present a dense array of biotin groups through which rTM-biotin, discussed in Chapter 5, may be immobilized. Alternatively, heparin could be employed as the polyanion, potentially attenuating thrombogenic responses initiated by transplanted islets in contact with whole blood. Finally, film constituents functionalized with biorthogonally reactive motifs provide opportunities for cytocompatible film crosslinking with potential implications for improving the barrier capacity of cell surface-supported PEMs.

More generally, future efforts may focus on identifying potential applications and limitations of the strategies presented herein as tools for cell and tissue surface engineering. This work has highlighted important advantages of adsorbed PLL-*g*-PEG monolayers relative to several other cell surface modification strategies. Notably, cell surface hydrazides were presented for the first time, azide groups could be generated quickly and without reliance on metabolic machinery, cell surfaces could be modified in complex biological media, and aldehyde groups could be generated without modifying native cell surface glycans. However, a need exists to quantitatively compare these strategies to existing covalent and noncovalent cell surface engineering approaches in terms of surface density, stability, and applicability towards other cell types.

Chapter 5. Surface Re-engineering of Pancreatic Islets with

Thrombomodulin Even a conformal barrier that protects islets from contact with host cells and macromolecules cannot prevent the diffusion of low molecular weight inflammatory mediators to and from the islet, and, therefore, the efficacy of conformal coatings may be improved through integrating anti-inflammatory capabilities. Through site-specific, C-terminal biotinylation of thrombomodulin (TM) and optimization of cell surface biotinylation, TM could be integrated with the islet surface, increasing the catalytic capacity of islets to activate protein C nearly three-fold.

Conjugation of TM to islets represents a facile strategy for increasing local concentrations of APC at the site of transplantation, and, accordingly, future efforts should assess the efficacy of this approach in a murine model of intraportal islet transplantation as described in Chapter 2 or in the tubing loop model of islet-blood contact described in Chapter 5. While immobilization of TM directly to the islet surface may prove effective, it is postulated that presentation of TM on a protective conformal coating will further enhance islet engraftment. In principle, the strategies used to immobilize TM to the islet surface may also be used to integrate TM with multilayer thin films so long as films present biotin or reactive handles for chemoselective biotinylation. However, verification of this supposition and measurement of resultant rates of APC generation remains necessary. Additionally, development of films bearing reactive handles (Chapter 4) may provide future opportunities for linking TM directly to the surface of films, eliminating the need for streptavidin. Through optimization of film properties and TM surface density, physical and biochemical barriers to thrombosis and inflammation may act synergistically in improving the outcome of islet transplantation.

APPENDIX A

In Vivo Biocompatibility and Stability of a Substrate-Supported

Polymerizable Membrane-Mimetic Film[§]

A.1. INTRODUCTION

The cell membrane offers a unique structural model for the molecular engineering of biocompatible and bioactive surfaces whereby physiochemical and biological properties may be modulated by a diverse set of self-assembled surface constituents. Supported lipid membranes, or membrane-mimetic thin films, can be produced by Langmuir-Blodgett deposition or exposure of surfaces to a dilute solution of emulsified lipids or unilamellar lipid vesicles [477]. Such films have emerged as powerful models of cell and tissue surfaces [478], and have garnered considerable interest as coatings for biosensing devices [479]. Significantly, supported phosphatidylcholine (PC) films have been shown to limit protein adsorption and subsequent cell adhesion in vitro [480-486], a phenomenon linked to the zwiterionic nature of the PC head group [481]. Despite these favorable characteristics, the use of membrane-mimetic thin films as coatings for *implantable biomaterials* remains limited, in part, by a lack of stability for most applications outside of a laboratory environment [487, 488]. In an effort to improve the stability of membrane-mimetic films several investigators have developed phospholipids functionalized with polymerizable moieties that can be polymerized *in situ*

---

after film formation [481, 489-492], while maintaining resistance to protein adsorption [492, 493]. However, the in vivo biostability and biocompatibility of substrate supported, polymerizable lipid membranes has not been evaluated. Moreover, these films have been fabricated on a limited number of substrates with relevance to implantable materials. PC-based polymers, however, have been used to modify a number of implantable biomaterials including Dacron® [494] and ePTFE vascular prostheses [495, 496], polyethylene joint prostheses [497], medical grade stainless steel [498], and coronary stents [499, 500], and have demonstrated excellent hemocompatibility and biocompatibility in vivo. However, the use of PC-based polymers does not create a uniform, closely packed array of PC groups at the host-material interface, and therefore, lacks the degree of structural control and versatility offered by self-assembled phosopholipid films.

We have previously reported the in situ polymerization of phospholipids on self-assembled monolayers of octadecyl mercaptan bound to gold [501], octadecyl trichlorosilane on glass [492, 502], and on an amphiphilic polymer cushion [503, 504]. Moreover, we have demonstrated the ability to functionalize these surfaces by creating glycocalyx-mimetic surfaces [505] and protein C activating surfaces by the functional reconstitution of thrombomodulin [506-508]. Significantly, we have recently extended this approach to form membrane-mimetic films on the surface of implantable biomaterials, such as cell encapsulation devices [504] and the lumenal surface of a small diameter ePTFE vascular prosthesis [509]. Notably, in an ex vivo baboon shunt model, platelet adhesion was dramatically reduced when ePTFE grafts were coated with a membrane-mimetic film compared to non-treated grafts. In this report, we evaluate the short term biostability and biocompatibility of a polymerizable membrane-mimetic film assembled on alginate microcapsules implanted into the peritoneal cavity of mice.

A.2.   MATERIALS AND METHODS

Reagents. All starting materials and synthetic reagents were purchased from commercial suppliers unless otherwise noted. HEPES buffered saline (HBS) was prepared by dissolving HEPES (Cellgro) at 25 mM in normal saline and adjusting pH to 7.4. Alginate (Alg; Pronova UP LVM) was obtained from NovaMatrix (Oslo, Norway) and used as received. Poly-L-lysine (PLL; MW > 300 kDa and MW 27 kDa), nicotinamide, $CaCl_2$, sodium citrate, and CHES were all purchased from Sigma. All solutions were filter sterilized using a bottle top filter (0.22 μm pore size, cellulose acetate, Corning, NY). A polyelectrolyte amphiphilic terpolymer with sulfonate anchoring groups, referred to as poly(HEA_6:DOD_3:SS_1), was synthesized, as detailed elsewhere [504]. Briefly, HEA (hydroxyethyl acrylate) is a hydrophilic monomer which forms a hydrophilic cushion, DOD (*N*,*N*-dioctadecylcarbamoyl-propionic acid) is a dialkyl bearing monomer which self-assembles to form an alkylated thin film, and SS (styrene sulfonate) facilitates electrostatic anchoring to positively charged surfaces. 1-Palmitoyl-2-(12-(acryloyloxy)dodecanoyl)-*sn*-glycero-3-phosphorylcholine (mono-AcrylPC) and 1-palmitoyl-2-(12-(acryloyloxy)dodecanoyl)-sn-glycero-3-phosphorylethanolamine-Texas red (mono-AcrylPE-TR) were synthesized, as previously described [510].

Formation of a membrane-mimetic film on alginate microcapsules. Alginate microcapsules were produced using an electrostatic bead generator (Nisco Engineering Inc, Switzerland) set at 4.7 kV. Alginate (2% w/v in HBS) was extruded at a flow rate of 6.0 ml/min through a flat-end needle with an internal diameter of 0.25 mm into a 1.1% w/v $CaCl_2$ solution in HBS. Microcapsules were then serially rinsed with 0.55 % and 0.28% w/v $CaCl_2$ in HBS, and finally washed in HBS.

A PEM film was assembled on the surface of alginate microcapsules through layer-by-layer deposition of PLL and alginate. Microcapsules were incubated with 0.1%

168

w/v PLL (MW > 300,000) in HBS for 2 minutes, rinsed twice with HBS, and then incubated for 2 minutes in 0.15% w/v alginate in HBS followed by two additional rinses in HBS. This process completed a cycle of forming a single PLL/Alg bilayer and was repeated a second time, to fabricate a $(PLL/Alg)_2$ film. Microcapsules were then incubated in sodium citrate (55 mM in HBS) for 20 minutes to liquefy the alginate core, and finally incubated with PLL to confer a positive surface charge and rinsed with normal saline.

To fabricate a membrane-mimetic film on the material surface, $(PLL/Alg)_2/PLL$ coated alginate microcapsules were incubated in a 0.1 mM solution of poly(HEA_6:DOD_3:SS_1) in 1% DMSO/HBS for 2 minutes and subsequently rinsed three times with HBS (Scheme A.1). The formation of a surface supported assembly of mono-acrylated lipids was achieved by incubating poly(HEA_6:DOD_3:SS_1) coated microcapsules (1 ml) in a lipid vesicle solution (4 ml) for 4h at 37 °C with gentle mixing as previously described [504]. The vesicle solution was doped with 0.1 mol % Texas Red labeled monoacryl lipid [510], which was utilized as a probe molecule to visualize the film and assess stability. In brief, large unilamellar vesicles (LUV) were prepared by three successive freeze/thaw/vortex cycles of 10 mM monoAcryl-PC in 20 mM sodium phosphate buffer (pH 7.4) using liquid nitrogen and a 60°C water bath. The LUVs were then extruded 21 times each through 2.0 μm and 600 nm polycarbonate filters and the lipid vesicle solution diluted to a final concentration of 1.2 mM with 20 mM sodium phosphate buffer (pH 7.4) and 150 mM NaCl. At the end of the incubation period, 10 μl of a photoinitiator mixture (10 mM Eosin Y, 225 mM triethanolamine, and 37 mM vinyl pyrollidone in water) was added. The solution was irradiated with visible light (50 mW/cm^2) for 30 min at room temperature, and, finally, capsules were rinsed with HBS. The structure of the membrane-mimetic film has been previously characterized using a

169

number of surface-sensitive techniques including XPS, FT-IR, ellipsometry, and neutron reflectivity [504, 511, 512].

In an effort to improve the biocompatibility of the membrane-mimetic film, an alternative alginate/PLL PEM cushion was utilized as a support for membrane-mimetic film formation. Alginate microbeads were incubated with 0.05% w/v PLL (MW 15,000 – 30,000) in normal saline for 6 minutes, rinsed once with 0.1% CHES buffer (pH 8.2) and subsequently with normal saline, and then incubated for 4 minutes in 0.2% alginate w/v in normal saline followed by two additional saline rinses. This process was repeated a second time, the alginate core was liquefied, and a terminal layer of PLL was adsorbed. A membrane-mimetic film, consisting of terpolymer and monoAcryl-PC, was assembled as described above. Membrane-mimetic films assembled alginate/PLL PEM films fabricated using this formulation will be referred to herein as modified membrane-mimetic capsules.
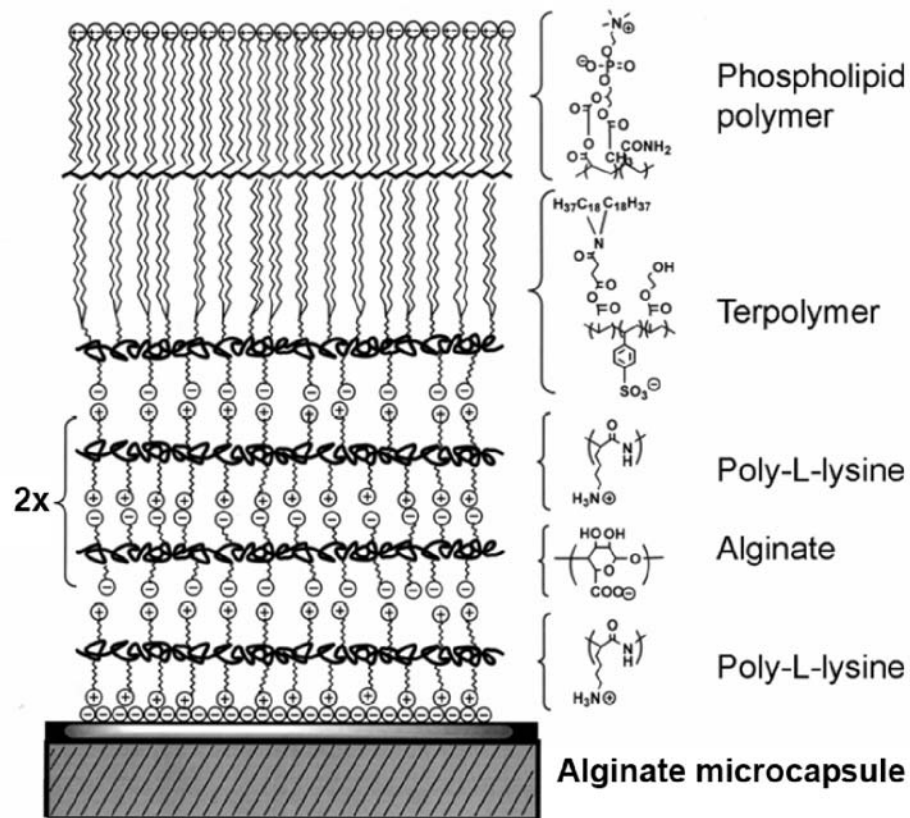
Scheme A.1. Construction of a polymerized, self-assembled, membrane-mimetic thin film on an alginate/poly(L-lysine) polyelectrolyte multilayer cushion. Alternating layers of poly(L-lysine) and alginate are first assembled on an alginate/Ca^{2+} hydrogel microsphere, followed by adsorption of an ampiphilic terpolymer with anionic anchoring groups. Following monolayer fusion of mono-acrylated phospholipids, photoinitiated polymerization was performed.

171

Animal model for biocompatibility testing. All animal studies followed local institutional guidelines at Emory University. Empty capsules were implanted into the peritoneal cavities of inbred male C57BL/6 mice weighing 25-30 g (Charles River Laboratories) for film stability and biocompatibility studies.

Assessment of capsule biostability and biocompatibility. Alginate microbeads coated with an (PLL/Alg)$_2$, or "double-wall" film assembled using PLL (MW 15,000 – 30,000) and the second of the two alginate/PLL PEM fabrication protocols described above, have been shown to resist fibrotic overgrowth within the peritoneal cavity of mice [513]. Therefore, these capsules were used as a comparative reference for film biocompatibility. Alginate beads coated with a double-wall or membrane-mimetic film were gently pipetted into a 3 ml syringe, and 1 ml of capsules was implanted into the peritoneal cavity of C57BL/6 mice.

Extent of cellular capsule overgrowth. Capsules were retrieved after one or four weeks and their biocompatibility was assessed using a semi-quantitative scoring system based on the extent and severity of cellular overgrowth. A minimum of 200 capsules were imaged under 10x magnification and individual capsules were assigned a score from 0 to 5 based on the approximate percentage of the capsule surface that was covered by adherent cells. Figure A.1 summarizes this scoring system; a score of 0 is assigned if no cellular attachment to the capsule surface is observed, a score of 1 indicates that ~1-25% of the capsule surface is covered with adherent cells, a score of 2, 26-50%, 3, 51-75%, 4, 76-99%, and 5 if the capsule is completely overgrown with host cells. Data is presented as the percentage of the total number of capsules observed that receive a given cellular overgrowth score. Additionally, the percent of freely floating capsules retrieved from the peritoneal cavity was determined by measuring the volume of capsules retrieved using a 3 ml syringe.

172
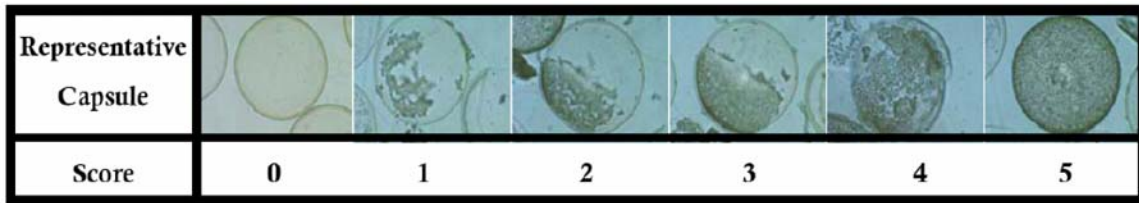
Figure A.1. Summary of fibrotic overgrowth scoring used to assess biocompatibility of microcapsules retrieved from the peritoneal cavity of mice. A minimum of 200 retrieved capsules were examined at 10x magnification and assigned a score from 0 (no cellular overgrowth) to 5 (completely overgrown) based on the approximate percentage of capsule area covered by adherent host cells and fibrosis.

Histological examination of adherent cells. Retrieved capsules were also processed for histological and immunohistochemical evaluation to facilitate identification of adherent cell types. A fraction of retrieved capsules were fixed in 10% neutral buffered formalin overnight and processed for paraffin embedding. Sections were prepared at 5 μm and stained with hematoxylin and eosin (H&E). Additionally, freshly retrieved capsules were mechanically fragmented to dislodge cells from the capsule surface and the lysate was filtered through a 100 μm cell strainer (Falcon) to retrieve dislodged cells. Cytospins of dislodged cells were prepared on glass slides using a cytocentrifuge (Cytospin 4, Thermo Shandon) at 600 rpm for 2 minutes. Slides were immediately fixed using cell fix (Thermo Shandon) and stained by Wright-Giemsa, according to standard protocols [514]. Different cell types were assessed by identifying cells with the morphological characteristics of monocytes/macrophages, lymphocytes, granulocytes, fibroblasts, and eosinophils. Cytospins were further analyzed through immunofluorescent staining. Cells were permeabilized with 0.5% Triton X-100 for 5 minutes, rinsed with DH_2O, and blocked with a serum free protein blocking solution (DakoCytomation) for 10 minutes. Cells were then incubated with appropriate primary antibody at 1:100 dilution for 60 minutes in a humid chamber. The primary antibodies used were as follows: anti-Mac-1 α_M chain against macrophages, monocytes, and

173

granulocytes, MB19-1 against CD19+ B lymphocytes, and 17A2 against CD3+ T cells (Pharmingen). Slides were then rinsed 3x with 1% BSA in PBS for 3 minutes each and incubated with FITC-conjugated secondary antibody (Pharmingen) at 1:200 dilution for 20 minutes. Slides were then rinsed with 1% BSA in PBS and imaged via fluorescent microscopy.

A.3. RESULTS

Membrane-mimetic and $(PLL/Alg)_2$ double-wall capsules implanted into the peritoneal cavity of C57BL/6 were retrieved after 1 week. Membrane-mimetic capsules elicited a severe foreign body response, with the majority of capsules found within large, cellularized aggregates of capsules that were often attached to intraperitoneal tissues. Capsules that remained freely floating in the peritoneal cavity were retrieved and a representative number (> 200 capsules) were subjected to cellular overgrowth scoring (Figure A.1). A majority of the capsules, 66 ± 5.9% (n=4), were completely overgrown with adherent cells, while less than 1% of capsules appeared free of cell adhesion (Figure 2A, 3). In contrast, 92.2 ± 3.2% (n=10) of double-wall capsules were found to be free of cell adhesion (Figure A.2B, A.3) and less than 1% of double-wall capsules were completely covered with adherent cells.

174
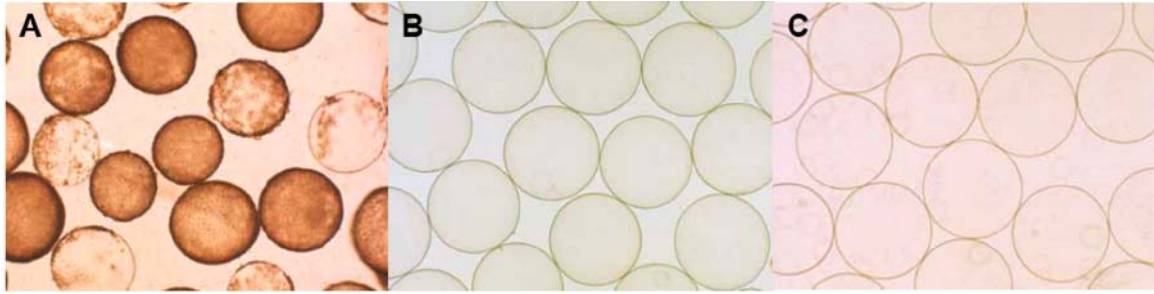
Figure A.2. Membrane-mimetic capsules (A), (PLL/Alg)$_2$ double-wall capsules (B), and *modified* membrane-mimetic capsules (C) retrieved from the peritoneal cavity of C57BL/6 mice 1 week post-implantation. As evidenced by a clear reduction in the extent of capsular fibrosis, modification of the underlying alginate/poly-L-lysine multilayer cushion significantly improved biocompatibility of microcapsules coated with a membrane-mimetic film.
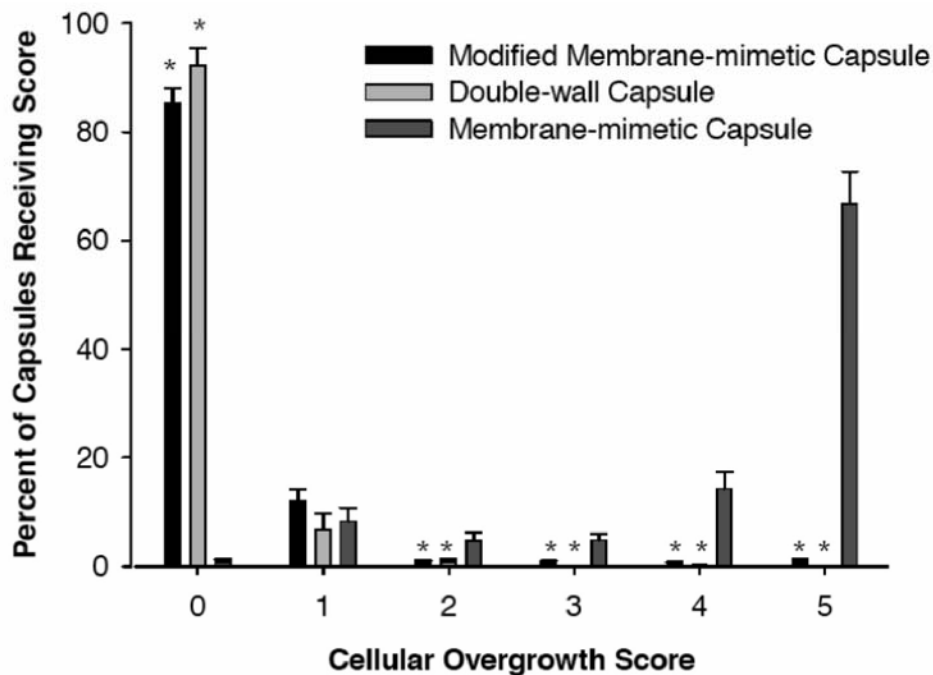
Figure A.3. Semi-quantitative cellular overgrowth scoring of empty membrane-mimetic and (PLL/alginate)$_2$ double-wall microcapsules retrieved from C57BL/6 mice at one week. *Modified* membrane-mimetic and double wall capsules vs. original membrane-mimetic capsules (ANOVA PLSD Fisher $p < 0.05$). Modified membrane-mimetic microcapsules and (PLL/alginate)$_2$ double-wall capsules have significantly less fibrotic overgrowth than original membrane-mimetic capsules and are not statistically different from each other.

175

Hematoxylin and Eosin, as well as Wright-Giemsa staining, clearly demonstrated the involvement of macrophages, granulocytes, and eosinophils in the host response to membrane-mimetic capsules (Figure A.4A, B). These findings are corroborated by immunofluorescent staining of cytospins (Figure A.4C), which demonstrate the involvement of Mac-1 positive cells in the foreign body response to implanted membrane-mimetic capsules. CD19 and CD3 staining were negative, indicating the absence of adherent T and B lymphocytes. These findings are consistent with a typical foreign body reaction characterized by the overgrowth of materials with inflammatory cells. Indeed, similar responses have been observed against empty microcapsules in the immediate postimplant period [180].
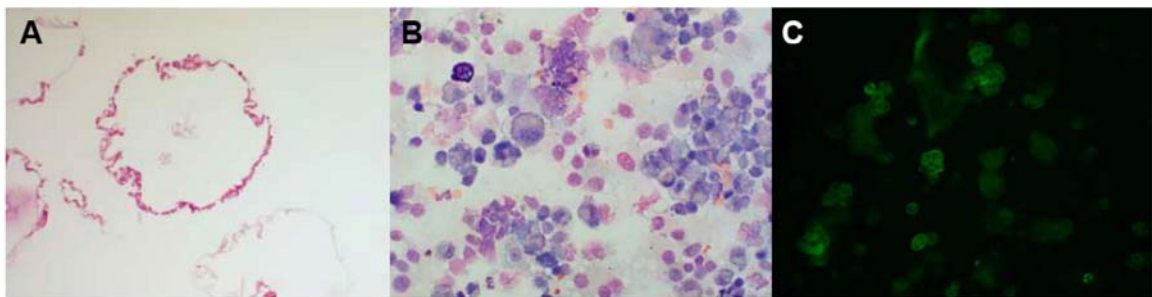
Figure A.4. Histological analysis of membrane-mimetic capsules retrieved 1 week post-implant. (A) H&E staining of formalin fixed, paraffin embedded capsules (10x) demonstrates the presence of adherent cells along the periphery of the capsule. (B) Wright-Giemsa staining (40x) of cells dislodged from membrane-mimetic capsules revealed the presence of macrophages, eosinophils, and granulocytes. (C) Immunofluorescent staining of cytospins prepared from dislodged adherent cells indicated the involvement of Mac-I positive cells in the host response to membrane-mimetic capsules (40x); staining for CD19+ B lymphocytes and CD3+ T lymphocytes was negative (data not shown).

As illustrated in Figure A.5, once labeled with Texas red, the surface of membrane-mimetic capsules were easily detected by confocal microscopy. Confocal microscopic evaluation of membrane-mimetic capsules retrieved after 1 week revealed a significant number of film defects and, in many cases, the film was completely absent (data not shown). This is in contrast to a control group stored at 37°C without light exposure, in which no gross film defects were observed.
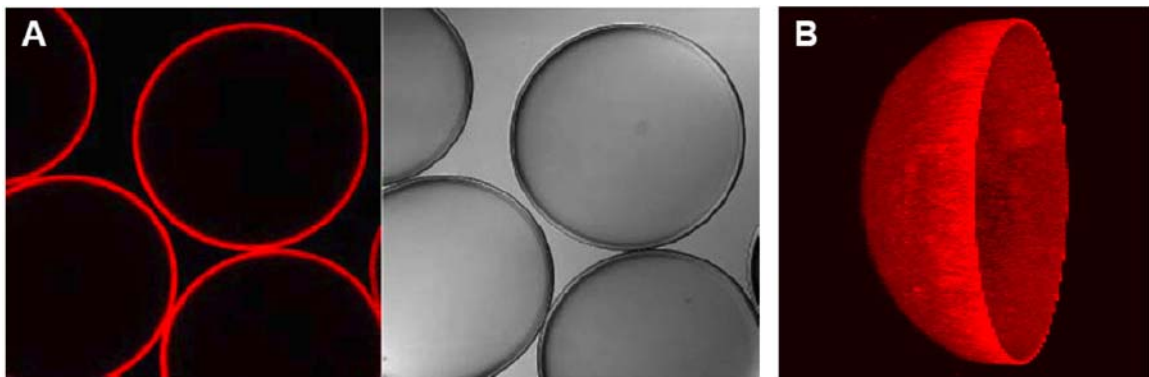
Figure A.5. By doping mono-acrylate PC films with 0.1 mol % Texas Red acrylate PE, membrane-mimetic films can be readily observed on the surface of microcapsules. (**A**) Confocal fluorescent and corresponding DIC micrograph (10x) of microcapsules coated with a membrane-mimetic thin film doped with 0.1 mol % Texas Red acrylate PE. (**B**) 3D reconstruction of 5 μm optical sections taken throughout half of a Texas Red-labeled membrane-mimetic capsule.

The inability of these empty membrane-mimetic capsules to limit cell adhesion prompted us to assemble the membrane-mimetic film on an alternative PLL/alginate PEM support. Membrane-mimetic films assembled on microcapsules fabricated using this PEM are film is referred to herein as *modified* membrane-mimetic capsules. Table A.1 summarizes the different conditions used to generate Alg/PLL PEMs as supports for membrane-mimetic film assembly. Double wall PLL/alginate microcapsules elicit little adverse cellular reaction and are comprised of a 27 kD PLL, while the PLL used in the initial PEM support had a molecular weight of >300 kD. Prior studies have suggested that a more compact PLL-alginate multilayer is produced using low molecular weight PLL due to a high degree of polymer interpenetration [180]. Thus, we speculated that the use of the high molecular weight polymer may have lead to exposed PLL chains that were not effectively covered by the membrane-mimetic film. With this in mind, membrane-mimetic films were re-fabricated on a modified PLL/Alg PEM film.

Modified membrane-mimetic capsules, along with standard double-wall capsules, were implanted into the peritoneal cavity of C57BL/6 mice and retrieved at 1 and 4 weeks. After one week, 70 ± 2.8% (n=4) of modified membrane-mimetic capsules were retrieved from the peritoneal cavity, 85.3± 2.8% (n=7) of which were free of cell adhesion (Figure A.2C, Figure A.3). These results were not statistically different (p>0.05) than those observed with double-wall capsules in which 73.8±5.5% of capsules were retrieved (n=4), wherein 92.2±3.2% capsules were free of cell adhesion (n=10) demonstrating equivalent biocompatibility between the two capsule types after one week. Similar results were obtained at one month, where 68±8.9% of modified membrane-mimetic capsules were retrieved, 81.3±7.8% (n=12) of which were free of cell adhesion. Double wall capsules had a 77±7.8% retrieval rate and 73.9±8.7% (n=8) of the capsules were free of cell adhesion, demonstrating equivalent resistance to fibrotic overgrowth between the two capsule types at 4 weeks (Figure A.6).

Confocal microscopy of modified membrane-mimetic capsules doped with a Texas Red labeled mono-AcrylPE demonstrated that at 4 weeks the vast majority of capsules were free of film defects and film fluorescent intensity was qualitatively similar to controls incubated at 37ºC, indicating a high degree of film stability in vivo (Figure A.7).

Table A.1. Comparision of PEM support fabrication protocols

Polyelectrolyte Condition	Membrane-mimetic	Modified Membrane-mimetic
Temperature	On ice	Room temperature
PLL MW	>300 kDa	27 kDa
PLL incubation time	2 minutes	6 minutes
PLL concentration	0.1 %	0.05%
PLL solvent	HBS, pH 7.4	Normal saline
Rinse after PLL layer	2x w/HBS, pH 7.4	1 x w/0.1% CHES, pH 8.2 1 x w/normal saline
Alginate incubation time	2 minutes	4 minutes
Alginate concentration	0.15 %	0.2%
Alginate solvent	HBS, pH 7.4	Normal saline
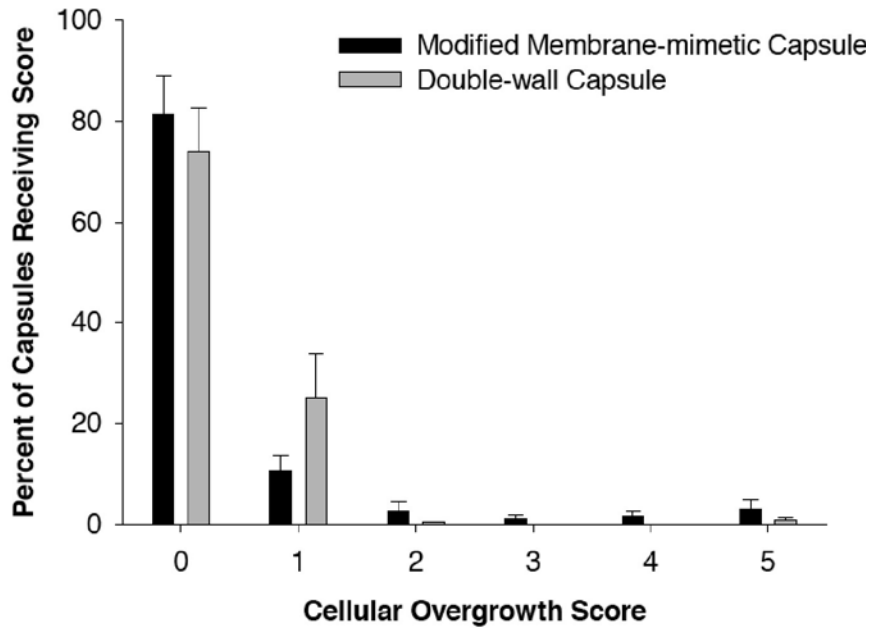
Figure A.6. Semi-quantitative fibrotic overgrowth scoring of empty *modified* membrane-mimetic and double-wall microcapsules retrieved from C57BL/6 mice at four weeks. The fibrotic response to *modified* membrane-mimetic microcapsules and double-wall capsules were not statistically different from each other (p>0.05).
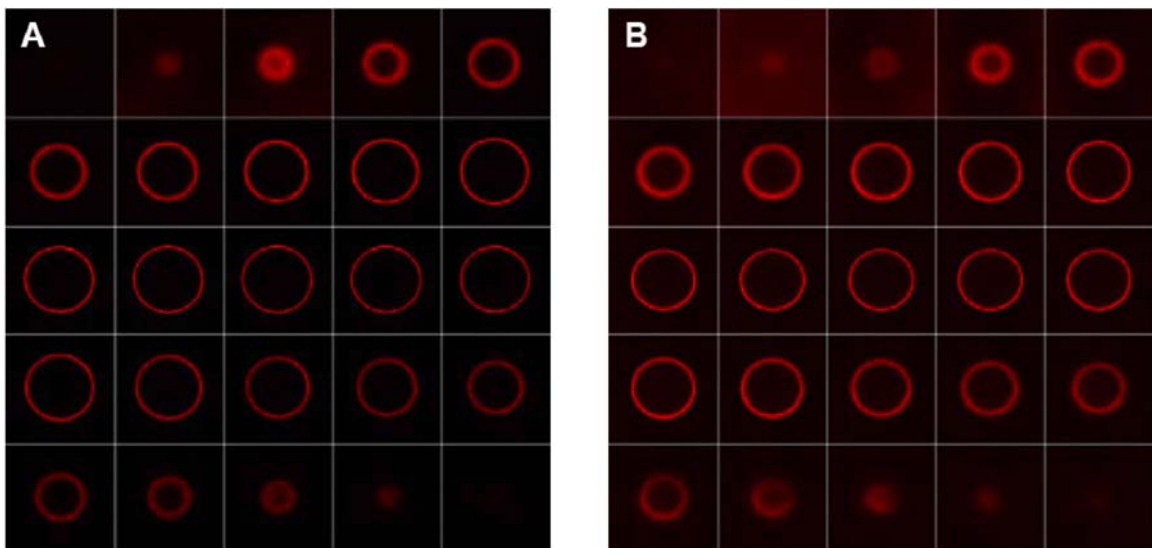
Figure A.7. Confocal fluorescence microscopy (10x) was used to obtain optical sections of a representative modified membrane-mimetic capsule stored at 37°C in PBS without light exposure (**A**) and harvested 4 weeks after implantation in a C57BL/6 mouse (**B**). To detect the film, capsules were coated with a Texas Red-labeled membrane-mimetic film.

A.4.   DISCUSSION

PC-based polymers have been widely utilized as biocompatible coatings for a number of implantable materials [494-500]. However, while such PC-based polymer coatings may offer high biocompatibility, they lack the unparalleled molecular control over surface order and chemistry offered by self-assembled supported lipid films, in particular the ability to generate bioactive materials through incorporation of membrane-based proteins and carbohydrates that may modulate the local biochemical milieu.

In order to coat materials with a robust, multicomponent membrane-mimetic film, our research efforts have been directed towards the development of a scheme for polymerization of surface-coupled planar lipid assemblies. We successfully synthesized monoacrylate functionalized lipid monomers and demonstrated that, as unilamellar vesicles, these lipid monomers can fuse onto a variety of alkylated substrates and form a two-dimensional thin film. Stabilization of the lipid assembly is then achieved using a rapid visible light-mediated photopolymerization scheme, which is effective at room temperature. Success in coating 2-D surfaces established a foundation for coating alginate microbeads [504] and ePTFE vascular grafts [509]. Detailed investigations of surface properties including contact angle goniometry, ESCA, ellipsometry, FT-IR spectroscopy, as well as neutron reflectivity and high resolution SEM have been reported for both 2-D and 3-D systems [504, 509, 511, 512]. Additionally, we have previously demonstrated the ability of membrane-mimetic films to serve as a versatile template for the assembly of membrane-bound macromolecules that may lead to improved hemocompatibility and biocompatibility [505-508, 515]. In this report, we evaluate, and subsequently improve, the in vivo stability and biocompatibility of polymerized, self-assembled membrane-mimetic thin films assembled on an alginate/PLL polyelectrolyte multilayer.

181

Stability and biocompatibility of the membrane-mimetic coating was demonstrated visually over a 4-week period after implantation of empty modified membrane-mimetic microcapsules in the peritoneal cavity of C57BL/6 mice. Prior studies have suggested that PC-based polymers should be associated with limited cell and protein reactivity, and studies from our group and others have demonstrated that membrane-mimetic surfaces exhibit little protein adsorption or cell adhesion [480-486, 492, 493]. However, the biocompatibility of membrane-mimetic films assembled on alginate microcapsules was dependent on the underlying polyelectrolyte multilayer on which the film was assembled, as modified membrane-mimetic capsules were significantly more biocompatible than those originally fabricated. Table A.1 summarizes the differences in the PLL-alginate polyelectrolyte multilayer between capsule types. The most notable differences in the multilayer are PLL molecular weight, concentration, and incubation time. Previous studies have demonstrated that these variables have important effects on microcapsule biocompatibility and mechanical properties. The molecular weight of PLL is considered a key parameter in determining microcapsule compressive strength. The relationship between capsule mechanical properties and polycation molecular weight is governed by the crosslink density and membrane thickness of the multilayer thin film. Very low molecular weight chains (<4 kD) do not provide a sufficient number of electrostatic interactions to stabilize capsules, while very high molecular weight polycations (>300 kD) form thin, frail membranes due to limited penetration into the alginate-calcium hydrogel. As a result, capsule compressive strength has been reported to be a maximum when a ~30 kD PLL is used [516]. Additionally, increased incubation time has been shown to result in increased membrane strength [517]. Therefore, it is possible that original membrane-mimetic capsules (PLL MW >300 kDa) were more susceptible to mechanical damage in the peritoneal cavity resulting in the exposure of reactive membrane components, such as PLL or terpolymer.

182

Indeed, transplantation of empty capsules in which the outer surface was either PLL or terpolymer generated a very rapid and robust cell adhesive response within one week of implantation (data not shown).

Previous studies have also implicated PLL in decreased microcapsule biocompatibility. Though microcapsule biocompatibility is greatly improved when an outer layer of alginate is used to cover reactive PLL, evidence suggests that this shielding is incomplete [518]. Additionally, PLL has been shown to be released from microcapsules over time [517], resulting in inflammatory cell necrosis and proinflammatory cytokine production [188]. Whether exposed PLL in the polyanion-polycation complex or free PLL leaking from capsules is responsible for capsule fibrosis is not clear. However, it is likely that PLL molecular weight plays an important role in both of these mechanisms due to the dependence of molecular weight on the ability of PLL to interpenetrate and complex with alginate layers.

Differences in biocompatibility might also be attributed to changes in membrane-mimetic film structure as the physiochemical properties of supported lipid films are dependent on the nature of the underlying substrate, in this instance an alkylated polyelectrolyte multilayer film. While elucidating such changes in lipid film structure is beyond the scope of this work, it is conceivable that differences in polyelectrolyte film structure, and therefore surface roughness, could influence the ability of lipid vesicles to fuse on the capsule surface [477, 519], possibly resulting in small defects in the outer surface and the exposure of underlying cell reactive components, such as PLL or terpolymer. Though the membrane-mimetic film has been previously characterized by a variety of surface-sensitive techniques including XPS, FT-IR, ellipsometry, and neutron reflectivity [504, 511, 512], the limited spatial resolution of these techniques within the plane of the film, combined with their capacity to probe restricted film regions, precludes the detection of small surface defects or inhomogeneities in the membrane-mimetic film.

183

A.5. CONCLUSIONS

The composition of the polyelectrolyte multilayer, which acts as a hydrophilic cushion for an overlying self-assembled membrane-mimetic thin film, significantly influences in vivo biocompatibility and film stability. Specifically, polymeric lipid films produced on a polyelectrolyte multilayer consisting of alginate and low molecular weight PLL resist cellular and fibrotic overgrowth and demonstrate a high degree of biostability after 4 weeks in C57BL/6 mice. Given the capacity of membrane-mimetic films to incorporate membrane-based proteins and carbohydrates, the present system offers a route through molecular self-assembly to robust and biocompatible coatings for implantable devices that may be both chemically and biologically heterogenous.

REFERENCES

1.   Linn T, Schmitz J, Hauck-Schmalenberger I, Lai Y, Bretzel RG, Brandhorst H, Brandhorst D. Ischaemia is linked to inflammation and induction of angiogenesis in pancreatic islets. Clin Exp Immunol 2006;144:179-187.

2.   Lukinius A, Jansson L, Korsgren O. Ultrastructural evidence for blood microvessels devoid of an endothelial cell lining in transplanted pancreatic islets. Am J Pathol 1995;146:429-435.

3.   Moberg L. The role of the innate immunity in islet transplantation. Ups J Med Sci 2005;110:17-55.

4.   Karvonen M, Tuomilehto J, Libman I, LaPorte R. A review of the recent epidemiological data on the worldwide incidence of type 1 (insulin-dependent) diabetes mellitus. World Health Organization DIAMOND Project Group. Diabetologia 1993;36:883-892.

5.   Tzakis AG, Ricordi C, Alejandro R, Zeng Y, Fung JJ, Todo S, Demetris AJ, Mintz DH, Starzl TE. Pancreatic islet transplantation after upper abdominal exenteration and liver replacement. Lancet 1990;336:402-405.

6.   Najarian JS, Sutherland DE, Matas AJ, Steffes MW, Simmons RL, Goetz FC. Human islet transplantation: a preliminary report. Transplant Proc 1977;9:233-236.

7.   Kemp CB, Knight MJ, Scharp DW, Ballinger WF, Lacy PE. Effect of transplantation site on the results of pancreatic islet isografts in diabetic rats. Diabetologia 1973;9:486-491.

8.   Ballinger WF, Lacy PE. Transplantation of intact pancreatic islets in rats. Surgery 1972;72:175-186.

9.   Williams P. Notes on diabetes treated with extract and by grafts of sheep's pancreas. British Medical Journal 1894;2:1303-1304.

10.   Robertson RP. Islet transplantation as a treatment for diabetes - a work in progress. N Engl J Med 2004;350:694-705.

11.   Markmann JF, Deng S, Desai NM, Huang X, Velidedeoglu E, Frank A, Liu C, Brayman KL, Lian MM, Wolf B, Bell E, Vitamaniuk M, Doliba N, Matschinsky F, Markmann E, Barker CF, Naji A. The use of non-heart-beating donors for isolated pancreatic islet transplantation. Transplantation 2003;75:1423-1429.

12.   Froud T, Ricordi C, Baidal DA, Hafiz MM, Ponte G, Cure P, Pileggi A, Poggioli R, Ichii H, Khan A, Ferreira JV, Pugliese A, Esquenazi VV, Kenyon NS, Alejandro R. Islet transplantation in type 1 diabetes mellitus using cultured islets and steroid-free immunosuppression: Miami experience. Am J Transplant 2005;5:2037-2046.

13.　Contreras JL, Xie D, Mays J, Smyth CA, Eckstein C, Rahemtulla FG, Young CJ, Anthony Thompson J, Bilbao G, Curiel DT, Eckhoff DE. A novel approach to xenotransplantation combining surface engineering and genetic modification of isolated adult porcine islets. Surgery 2004;136:537-547.

14.　de Vos P, Marchetti P. Encapsulation of pancreatic islets for transplantation in diabetes: the untouchable islets. Trends Mol Med 2002;8:363-366.

15.　Rajotte RV. Islet cryopreservation protocols. Ann N Y Acad Sci 1999;875:200-207.

16.　Frank A, Deng SP, Huang XL, Velidedeoglu E, Bae YS, Liu CY, Stephenson R, Mohiuddin M, Thambipillai T, Markmann E, Palanjian M, Sellers M, Barker CF, Markmann JF. Transplantation for type 1 diabetes - Comparison of vascularized whole-organ pancreas with isolated pancreatic islets. Ann Surg 2004;240:631-640.

17.　Gaglia JL, Shapiro AM, Weir GC. Islet transplantation: progress and challenge. Arch Med Res 2005;36:273-280.

18.　Shapiro AM, Lakey JR, Ryan EA, Korbutt GS, Toth E, Warnock GL, Kneteman NM, Rajotte RV. Islet transplantation in seven patients with type 1 diabetes mellitus using a glucocorticoid-free immunosuppressive regimen. N Engl J Med 2000;343:230-238.

19.　Shapiro AM, Ricordi C, Hering B. Edmonton's islet success has indeed been replicated elsewhere. Lancet 2003;362:1242.

20.　Hirshberg B, Rother KI, Digon BJ, 3rd, Lee J, Gaglia JL, Hines K, Read EJ, Chang R, Wood BJ, Harlan DM. Benefits and risks of solitary islet transplantation for type 1 diabetes using steroid-sparing immunosuppression: the National Institutes of Health experience. Diabetes Care 2003;26:3288-3295.

21.　Goss JA, Schock AP, Brunicardi FC, Goodpastor SE, Garber AJ, Soltes G, Barth M, Froud T, Alejandro R, Ricordi C. Achievement of insulin independence in three consecutive type-1 diabetic patients via pancreatic islet transplantation using islets isolated at a remote islet isolation center. Transplantation 2002;74:1761-1766.

22.　Ricordi C. Islet transplantation: a brave new world. Diabetes 2003;52:1595-1603.

23.　Korsgren O, Nilsson B, Berne C, Felldin M, Foss A, Kallen R, Lundgren T, Salmela K, Tibell A, Tufveson G. Current status of clinical islet transplantation. Transplantation 2005;79:1289-1293.

24.　Shapiro AMJ, Nanji SA, Lakey JRT. Clinical islet transplant: current and future directions towards tolerance. Immunol Rev 2003;196:219-236.

25.　Hering BJ, Kandaswamy R, Ansite JD, Eckman PM, Nakano M, Sawada T, Matsumoto I, Ihm SH, Zhang HJ, Parkey J, Hunter DW, Sutherland DE. Single-donor, marginal-dose islet transplantation in patients with type 1 diabetes. Jama 2005;293:830-835.

26.   Shapiro AM, Ricordi C, Hering BJ, Auchincloss H, Lindblad R, Robertson RP, Secchi A, Brendel MD, Berney T, Brennan DC, Cagliero E, Alejandro R, Ryan EA, DiMercurio B, Morel P, Polonsky KS, Reems JA, Bretzel RG, Bertuzzi F, Froud T, Kandaswamy R, Sutherland DE, Eisenbarth G, Segal M, Preiksaitis J, Korbutt GS, Barton FB, Viviano L, Seyfert-Margolis V, Bluestone J, Lakey JR. International trial of the Edmonton protocol for islet transplantation. N Engl J Med 2006;355:1318-1330.

27.   Emamaullee JA, Shapiro AM. Factors influencing the loss of beta-cell mass in islet transplantation. Cell Transplant 2007;16:1-8.

28.   Ryan EA, Lakey JR, Rajotte RV, Korbutt GS, Kin T, Imes S, Rabinovitch A, Elliott JF, Bigam D, Kneteman NM, Warnock GL, Larsen I, Shapiro AM. Clinical outcomes and insulin secretion after islet transplantation with the Edmonton protocol. Diabetes 2001;50:710-719.

29.   Davalli AM, Ogawa Y, Ricordi C, Scharp DW, Bonner-Weir S, Weir GC. A selective decrease in the beta cell mass of human islets transplanted into diabetic nude mice. Transplantation 1995;59:817-820.

30.   Davalli AM, Ogawa Y, Scaglia L, Wu YJ, Hollister J, Bonner-Weir S, Weir GC. Function, mass, and replication of porcine and rat islets transplanted into diabetic nude mice. Diabetes 1995;44:104-111.

31.   Biarnes M, Montolio M, Nacher V, Raurell M, Soler J, Montanya E. Beta-cell death and mass in syngeneically transplanted islets exposed to short- and long-term hyperglycemia. Diabetes 2002;51:66-72.

32.   Ryan EA, Paty BW, Senior PA, Bigam D, Alfadhli E, Kneteman NM, Lakey JR, Shapiro AM. Five-year follow-up after clinical islet transplantation. Diabetes 2005;54:2060-2069.

33.   Davalli AM, Scaglia L, Zangen DH, Hollister J, Bonner-Weir S, Weir GC. Vulnerability of islets in the immediate posttransplantation period. Dynamic changes in structure and function. Diabetes 1996;45:1161-1167.

34.   Mattsson G, Jansson L, Nordin A, Andersson A, Carlsson PO. Evidence of functional impairment of syngeneically transplanted mouse pancreatic islets retrieved from the liver. Diabetes 2004;53:948-954.

35.   Ahn YB, Xu G, Marselli L, Toschi E, Sharma A, Bonner-Weir S, Sgroi DC, Weir GC. Changes in gene expression in beta cells after islet isolation and transplantation using laser-capture microdissection. Diabetologia 2007;50:334-342.

36.   Lewis EC, Shapiro L, Bowers OJ, Dinarello CA. Alpha1-antitrypsin monotherapy prolongs islet allograft survival in mice. Proc Natl Acad Sci U S A 2005;102:12153-12158.

37.   Kaufman DB, Platt JL, Rabe FL, Dunn DL, Bach FH, Sutherland DE. Differential roles of Mac-1+ cells, and CD4+ and CD8+ T lymphocytes in primary nonfunction and classic rejection of islet allografts. J Exp Med 1990;172:291-302.

38.   Katz SM, Bennett F, Stecker K, Clark JH, Pham T, Wang ME, Kahan BD, Stepkowski SM. ICAM-1 antisense oligodeoxynucleotide improves islet allograft survival and function. Cell Transplant 2000;9:817-828.

39.   Toyofuku A, Yasunami Y, Nabeyama K, Nakano M, Satoh M, Matsuoka N, Ono J, Nakayama T, Taniguchi M, Tanaka M, Ikeda S. Natural killer T-cells participate in rejection of islet allografts in the liver of mice. Diabetes 2006;55:34-39.

40.   Gores PF, Sutherland DE, Platt JL, Bach FH. Depletion of donor Ia+ cells before transplantation does not prolong islet allograft survival. J Immunol 1986;137:1482-1485.

41.   Jansson L, Carlsson PO. Graft vascular function after transplantation of pancreatic islets. Diabetologia 2002;45:749-763.

42.   Emamaullee JA, Rajotte RV, Liston P, Korneluk RG, Lakey JR, Shapiro AM, Elliott JF. XIAP overexpression in human islets prevents early posttransplant apoptosis and reduces the islet mass needed to treat diabetes. Diabetes 2005;54:2541-2548.

43.   Lee Y, Ravazzola M, Park BH, Bashmakov YK, Orci L, Unger RH. Metabolic mechanisms of failure of intraportally transplanted pancreatic beta-cells in rats: role of lipotoxicity and prevention by leptin. Diabetes 2007;56:2295-2301.

44.   Robertson RP, Harmon JS. Diabetes, glucose toxicity, and oxidative stress: A case of double jeopardy for the pancreatic islet beta cell. Free Radic Biol Med 2006;41:177-184.

45.   Contreras JL, Eckstein C, Smyth CA, Bilbao G, Vilatoba M, Ringland SE, Young C, Thompson JA, Fernandez JA, Griffin JH, Eckhoff DE. Activated protein C preserves functional islet mass after intraportal transplantation: a novel link between endothelial cell activation, thrombosis, inflammation, and islet cell death. Diabetes 2004;53:2804-2814.

46.   Yasunami Y, Kojo S, Kitamura H, Toyofuku A, Satoh M, Nakano M, Nabeyama K, Nakamura Y, Matsuoka N, Ikeda S, Tanaka M, Ono J, Nagata N, Ohara O, Taniguchi M. Valpha14 NK T cell-triggered IFN-gamma production by Gr-1+CD11b+ cells mediates early graft loss of syngeneic transplanted islets. J Exp Med 2005;202:913-918.

47.   Montolio M, Tellez N, Soler J, Montanya E. Role of blood glucose in cytokine gene expression in early syngeneic islet transplantation. Cell Transplant 2007;16:517-525.

48.   Bottino R, Fernandez LA, Ricordi C, Lehmann R, Tsan MF, Oliver R, Inverardi L. Transplantation of allogeneic islets of Langerhans in the rat liver: effects of macrophage depletion on graft survival and microenvironment activation. Diabetes 1998;47:316-323.

49.   Montolio M, Biarnes M, Tellez N, Escoriza J, Soler J, Montanya E. Interleukin-1beta and inducible form of nitric oxide synthase expression in early syngeneic islet transplantation. J Endocrinol 2007;192:169-177.

50.   Satoh M, Yasunami Y, Matsuoka N, Nakano M, Itoh T, Nitta T, Anzai K, Ono J, Taniguchi M, Ikeda S. Successful islet transplantation to two recipients from a single

donor by targeting proinflammatory cytokines in mice. Transplantation 2007;83:1085-1092.

51.   Rabinovitch A, Suarez-Pinzon WL. Cytokines and their roles in pancreatic islet beta-cell destruction and insulin-dependent diabetes mellitus. Biochem Pharmacol 1998;55:1139-1149.

52.   Barshes NR, Wyllie S, Goss JA. Inflammation-mediated dysfunction and apoptosis in pancreatic islet transplantation: implications for intrahepatic grafts. J Leukocyte Biol 2005;77:587-597.

53.   Ziats NP, Miller KM, Anderson JM. In vitro and in vivo interactions of cells with biomaterials. Biomaterials 1988;9:5-13.

54.   Bennet W, Sundberg B, Groth CG, Brendel MD, Brandhorst D, Brandhorst H, Bretzel RG, Elgue G, Larsson R, Nilsson B, Korsgren O. Incompatibility between human blood and isolated islets of Langerhans: a finding with implications for clinical intraportal islet transplantation? Diabetes 1999;48:1907-1914.

55.   Moberg L, Johansson H, Lukinius A, Berne C, Foss A, Kallen R, Ostraat O, Salmela K, Tibell A, Tufveson G, Elgue G, Nilsson Ekdahl K, Korsgren O, Nilsson B. Production of tissue factor by pancreatic islet cells as a trigger of detrimental thrombotic reactions in clinical islet transplantation. Lancet 2002;360:2039-2045.

56.   Johansson H, Lukinius A, Moberg L, Lundgren T, Berne C, Foss A, Felldin M, Kallen R, Salmela K, Tibell A, Tufveson G, Ekdahl KN, Elgue G, Korsgren O, Nilsson B. Tissue factor produced by the endocrine cells of the islets of Langerhans is associated with a negative outcome of clinical islet transplantation. Diabetes 2005;54:1755-1762.

57.   Giesen PL, Nemerson Y. Tissue factor on the loose. Semin Thromb Hemost 2000;26:379-384.

58.   van Deijnen JH, Hulstaert CE, Wolters GH, van Schilfgaarde R. Significance of the peri-insular extracellular matrix for islet isolation from the pancreas of rat, dog, pig, and man. Cell Tissue Res 1992;267:139-146.

59.   Lamblin A, Tournoys A, Gmyr V, Jourdain M, Lefebvre J, Kerr-Conte J, Proye C, Pattou F. Blood mediated reaction following intraportal islet allograft in pigs. Ann Chir 2001;126:743-750.

60.   Bertuzzi F, Marzorati S, Maffi P, Piemonti L, Melzi R, de Taddeo F, Valtolina V, D'Angelo A, di Carlo V, Bonifacio E, Secchi A. Tissue factor and CCL2/monocyte chemoattractant protein-1 released by human islets affect islet engraftment in type 1 diabetic recipients. J Clin Endocrinol Metab 2004;89:5724-5728.

61.   Dugina TN, Kiseleva EV, Chistov IV, Umarova BA, Strukova SM. Receptors of the PAR family as a link between blood coagulation and inflammation. Biochemistry (Mosc) 2002;67:65-74.

62.   Coughlin SR. Thrombin signalling and protease-activated receptors. Nature 2000;407:258-264.

189

63.   Rabiet MJ, Plantier JL, Dejana E. Thrombin-induced endothelial cell dysfunction. Br Med Bull 1994;50:936-945.

64.   Esmon CT. Interactions between the innate immune and blood coagulation systems. Trends Immunol 2004;25:536-542.

65.   Zarbock A, Polanowska-Grabowska RK, Ley K. Platelet-neutrophil-interactions: linking hemostasis and inflammation. Blood Rev 2007;21:99-111.

66.   Gawaz M, Langer H, May AE. Platelets in inflammation and atherogenesis. J Clin Invest 2005;115:3378-3384.

67.   Yin D, Ding JW, Shen J, Ma L, Hara M, Chong AS. Liver ischemia contributes to early islet failure following intraportal transplantation: benefits of liver ischemic-preconditioning. Am J Transplant 2006;6:60-68.

68.   Moberg L, Korsgren O, Nilsson B. Neutrophilic granulocytes are the predominant cell type infiltrating pancreatic islets in contact with ABO-compatible blood. Clin Exp Immunol 2005;142:125-131.

69.   Ozmen L, Ekdahl KN, Elgue G, Larsson R, Korsgren O, Nilsson B. Inhibition of thrombin abrogates the instant blood-mediated inflammatory reaction triggered by isolated human islets: possible application of the thrombin inhibitor melagatran in clinical islet transplantation. Diabetes 2002;51:1779-1784.

70.   de Groot M, Schuurs TA, Keizer PP, Fekken S, Leuvenink HG, van Schilfgaarde R. Response of encapsulated rat pancreatic islets to hypoxia. Cell Transplant 2003;12:867-875.

71.   Gysemans CA, Waer M, Valckx D, Laureys JM, Mihkalsky D, Bouillon R, Mathieu C. Early graft failure of xenogeneic islets in NOD mice is accompanied by high levels of interleukin-1 and low levels of transforming growth factor-beta mRNA in the grafts. Diabetes 2000;49:1992-1997.

72.   Ozasa T, Newton MR, Dallman MJ, Shimizu S, Gray DW, Morris PJ. Cytokine gene expression in pancreatic islet grafts in the rat. Transplantation 1997;64:1152-1159.

73.   Johansson U, Olsson A, Gabrielsson S, Nilsson B, Korsgren O. Inflammatory mediators expressed in human islets of Langerhans: implications for islet transplantation. Biochem Biophys Res Commun 2003;308:474-479.

74.   Berney T, Molano RD, Cattan P, Pileggi A, Vizzardelli C, Oliver R, Ricordi C, Inverardi L. Endotoxin-mediated delayed islet graft function is associated with increased intra-islet cytokine production and islet cell apoptosis. Transplantation 2001;71:125-132.

75.   Matsuda T, Omori K, Vuong T, Pascual M, Valiente L, Ferreri K, Todorov I, Kuroda Y, Smith CV, Kandeel F, Mullen Y. Inhibition of p38 pathway suppresses human islet production of pro-inflammatory cytokines and improves islet graft function. Am J Transplant 2005;5:484-493.

76.   Ehrnfelt C, Kumagai-Braesch M, Uzunel M, Holgersson J. Adult porcine islets produce MCP-1 and recruit human monocytes in vitro. Xenotransplantation 2004;11:184-194.

77.   Bottino R, Balamurugan AN, Tse H, Thirunavukkarasu C, Ge X, Profozich J, Milton M, Ziegenfuss A, Trucco M, Piganelli JD. Response of human islets to isolation stress and the effect of antioxidant treatment. Diabetes 2004;53:2559-2568.

78.   Schroppel B, Zhang N, Chen P, Chen D, Bromberg JS, Murphy B. Role of donor-derived monocyte chemoattractant protein-1 in murine islet transplantation. J Am Soc Nephrol 2005;16:444-451.

79.   Piemonti L, Leone BE, Nano R, Saccani A, Monti P, Maffi P, Bianchi G, Sica A, Peri G, Melzi R, Aldrighetti L, Secchi A, Di Carlo V, Allavena P, Bertuzzi F. Human pancreatic islets produce and secrete MCP-1/CCL2: relevance in human islet transplantation. Diabetes 2002;51:55-65.

80.   Chen MC, Proost P, Gysemans C, Mathieu C, Eizirik DL. Monocyte chemoattractant protein-1 is expressed in pancreatic islets from prediabetic NOD mice and in interleukin-1 beta-exposed human and rat islet cells. Diabetologia 2001;44:325-332.

81.   Thomas HE, Darwiche R, Corbett JA, Kay TW. Interleukin-1 plus gamma-interferon-induced pancreatic beta-cell dysfunction is mediated by beta-cell nitric oxide production. Diabetes 2002;51:311-316.

82.   Fontaine MJ, Blanchard J, Rastellini C, Lazda V, Herold KC, Pollak R. Pancreatic islets activate portal vein endothelial cells in vitro. Ann Clin Lab Sci 2002;32:352-361.

83.   Clayton HA, Davies JE, Sutton CD, Bell PR, Dennison AR. A coculture model of intrahepatic islet transplantation: activation of Kupffer cells by islets and acinar tissue. Cell Transplant 2001;10:101-108.

84.   Chick WL, Like AA, Lauris V. Beta cell culture on synthetic capillaries: an artificial endocrine pancreas. Science 1975;187:847-849.

85.   Lim F, Sun AM. Microencapsulated islets as bioartificial endocrine pancreas. Science 1980;210:908-910.

86.   Li RH. Materials for immunoisolated cell transplantation. Adv Drug Deliv Rev 1998;33:87-109.

87.   Lanza RP, Hayes JL, Chick WL. Encapsulated cell technology. Nat Biotechnol 1996;14:1107-1111.

88.   Chaikof EL. Engineering and material considerations in islet cell transplantation. Annu Rev Biomed Eng 1999;1:103-127.

89.   Avgoustiniatos ES, Colton CK. Effect of external oxygen mass transfer resistances on viability of immunoisolated tissue. Ann N Y Acad Sci 1997;831:145-167.

90.	Dulong JL, Legallais C. A theoretical study of oxygen transfer including cell necrosis for the design of a bioartificial pancreas. Biotechnol Bioeng 2007;96:990-998.

91.	Gross JD, Constantinidis I, Sambanis A. Modeling of encapsulated cell systems. J Theor Biol 2007;244:500-510.

92.	Tziampazis E, Sambanis A. Tissue engineering of a bioartificial pancreas: modeling the cell environment and device function. Biotechnol Prog 1995;11:115-126.

93.	Dionne KE, Colton CK, Yarmush ML. Effect of hypoxia on insulin secretion by isolated rat and canine islets of Langerhans. Diabetes 1993;42:12-21.

94.	De Vos P, De Haan B, Pater J, Van Schilfgaarde R. Association between capsule diameter, adequacy of encapsulation, and survival of microencapsulated rat islet allografts. Transplantation 1996;62:893-899.

95.	Orive G, Hernandez RM, Rodriguez Gascon A, Calafiore R, Chang TM, de Vos P, Hortelano G, Hunkeler D, Lacik I, Pedraz JL. History, challenges and perspectives of cell microencapsulation. Trends Biotechnol 2004;22:87-92.

96.	Lee MK, Bae YH. Cell transplantation for endocrine disorders. Adv Drug Deliv Rev 2000;42:103-120.

97.	Welty JR, Wicks CE, Wilson RE, Rorrer GL. Fundamentals of momentum, heat and mass transfer. 4th ed. New York, NY: John Wiley; 2001.

98.	Dionne KE, Cain BM, Li RH, Bell WJ, Doherty EJ, Rein DH, Lysaght MJ, Gentile FT. Transport characterization of membranes for immunoisolation. Biomaterials 1996;17:257-266.

99.	Hiemstra H, Dijkhuizen L, Harder W. Diffusion of Oxygen in Alginate Gels Related to the Kinetics of Methanol Oxidation by Immobilized Hansenula-Polymorpha Cells. Eur J Appl Microbiol 1983;18:189-196.

100.	Li RH, Altreuter DH, Gentile FT. Transport characterization of hydrogel matrices for cell encapsulation. Biotechnol Bioeng 1996;50:365-373.

101.	Mehmetoglu U, Ates S, Berber R. Oxygen diffusivity in calcium alginate gel beads containing Gluconobacter suboxydans. Artif Cells Blood Substit Immobil Biotechnol 1996;24:91-106.

102.	de Haan BJ, Faas MM, de Vos P. Factors influencing insulin secretion from encapsulated islets. Cell Transplant 2003;12:617-625.

103.	Tatarkiewicz K, Garcia M, Omer A, Van Schilfgaarde R, Weir GC, De Vos P. C-peptide responses after meal challenge in mice transplanted with microencapsulated rat islets. Diabetologia 2001;44:646-653.

104.	Trivedi N, Keegan M, Steil GM, Hollister-Lock J, Hasenkamp WM, Colton CK, Bonner-Weir S, Weir GC. Islets in alginate macrobeads reverse diabetes despite minimal acute insulin secretory responses. Transplantation 2001;71:203-211.

105.   Wang T, Lacik I, Brissova M, Anilkumar AV, Prokop A, Hunkeler D, Green R, Shahrokhi K, Powers AC. An encapsulation system for the immunoisolation of pancreatic islets. Nat Biotechnol 1997;15:358-362.

106.   Canaple L, Rehor A, Hunkeler D. Improving cell encapsulation through size control. J Biomater Sci Polym Ed 2002;13:783-796.

107.   Chicheportiche D, Reach G. In vitro kinetics of insulin release by microencapsulated rat islets: effect of the size of the microcapsules. Diabetologia 1988;31:54-57.

108.   Lum ZP, Tai IT, Krestow M, Norton J, Vacek I, Sun AM. Prolonged reversal of diabetic state in NOD mice by xenografts of microencapsulated rat islets. Diabetes 1991;40:1511-1516.

109.   Calafiore R, Basta G, Luca G, Lemmi A, Montanucci MP, Calabrese G, Racanicchi L, Mancuso F, Brunetti P. Microencapsulated pancreatic islet allografts into nonimmunosuppressed patients with type 1 diabetes: first two cases. Diabetes Care 2006;29:137-138.

110.   Babensee JE, Sefton MV. Viability of HEMA-MMA microencapsulated model hepatoma cells in rats and the host response. Tissue Eng 2000;6:165-182.

111.   Kobayashi T, Aomatsu Y, Iwata H, Kin T, Kanehiro H, Hisanga M, Ko S, Nagao M, Harb G, Nakajima Y. Survival of microencapsulated islets at 400 days posttransplantation in the omental pouch of NOD mice. Cell Transplant 2006;15:359-365.

112.   Elliott RB, Escobar L, Tan PL, Garkavenko O, Calafiore R, Basta P, Vasconcellos AV, Emerich DF, Thanos C, Bambra C. Intraperitoneal alginate-encapsulated neonatal porcine islets in a placebo-controlled study with 16 diabetic cynomolgus primates. Transplant Proc 2005;37:3505-3508.

113.   Soon-Shiong P, Heintz RE, Merideth N, Yao QX, Yao Z, Zheng T, Murphy M, Moloney MK, Schmehl M, Harris M, et al. Insulin independence in a type 1 diabetic patient after encapsulated islet transplantation. Lancet 1994;343:950-951.

114.   Sun Y, Ma X, Zhou D, Vacek I, Sun AM. Normalization of diabetes in spontaneously diabetic cynomologus monkeys by xenografts of microencapsulated porcine islets without immunosuppression. J Clin Invest 1996;98:1417-1422.

115.   Polonsky K, Jaspan J, Emmanouel D, Holmes K, Moossa AR. Differences in the hepatic and renal extraction of insulin and glucagon in the dog: evidence for saturability of insulin metabolism. Acta Endocrinol (Copenh) 1983;102:420-427.

116.   Selam JL, Bergman RN, Raccah D, Jean-Didier N, Lozano J, Charles MA. Determination of portal insulin absorption from peritoneum via novel nonisotopic method. Diabetes 1990;39:1361-1365.

117.   De Vos P, Vegter D, De Haan BJ, Strubbe JH, Bruggink JE, Van Schilfgaarde R. Kinetics of intraperitoneally infused insulin in rats. Functional implications for the bioartificial pancreas. Diabetes 1996;45:1102-1107.

118.   de Vos P, Vegter D, Strubbe JH, de Haan BJ, van Schilfgaarde R. Impaired glucose tolerance in recipients of an intraperitoneally implanted microencapsulated islet allograft is caused by the slow diffusion of insulin through the peritoneal membrane. Transplant Proc 1997;29:756-757.

119.   Duvivier-Kali VF, Omer A, Parent RJ, O'Neil JJ, Weir GC. Complete protection of islets against allorejection and autoimmunity by a simple barium-alginate membrane. Diabetes 2001;50:1698-1705.

120.   The effect of intensive treatment of diabetes on the development and progression of long-term complications in insulin-dependent diabetes mellitus. The Diabetes Control and Complications Trial Research Group. N Engl J Med 1993;329:977-986.

121.   Intensive blood-glucose control with sulphonylureas or insulin compared with conventional treatment and risk of complications in patients with type 2 diabetes (UKPDS 33). UK Prospective Diabetes Study (UKPDS) Group. Lancet 1998;352:837-853.

122.   Sustained effect of intensive treatment of type 1 diabetes mellitus on development and progression of diabetic nephropathy: the Epidemiology of Diabetes Interventions and Complications (EDIC) study. Jama 2003;290:2159-2167.

123.   de Vos P, de Haan BJ, de Haan A, van Zanten J, Faas MM. Factors influencing functional survival of microencapsulated islet grafts. Cell Transplant 2004;13:515-524.

124.   Fritschy WM, van Straaten JF, de Vos P, Strubbe JH, Wolters GH, van Schilfgaarde R. The efficacy of intraperitoneal pancreatic islet isografts in the reversal of diabetes in rats. Transplantation 1991;52:777-783.

125.   Okugawa K, Fukuda Y, Sakimoto H, Nishihara M, Tashiro H, Urushihara T, Ikeda M, Iwata H, Dohi K. Intermittent intraperitoneal implantation of islets in rat islet transplantation. Cell Transplant 1996;5:S51-53.

126.   Siebers U, Horcher A, Bretzel RG, Klock G, Zimmermann U, Federlin K, Zekorn T. Transplantation of free and microencapsulated islets in rats: evidence for the requirement of an increased islet mass for transplantation into the peritoneal site. Int J Artif Organs 1993;16:96-99.

127.   Elliott RB, Escobar L, Calafiore R, Basta G, Garkavenko O, Vasconcellos A, Bambra C. Transplantation of micro- and macroencapsulated piglet islets into mice and monkeys. Transplant Proc 2005;37:466-469.

128.   Brendel MDH, B.J; Schultz, AO; Bretzel, RG. Insulin independence following islet transplantation: a comparison of different recipient categories. International Islet Transplant Registry 1999;8:5-18.

129.   Calafiore R, Basta G, Luca G, Boselli C, Bufalari A, Giustozzi GM, Moggi L, Brunetti P. Alginate/polyaminoacidic coherent microcapsules for pancreatic islet graft immunoisolation in diabetic recipients. Ann N Y Acad Sci 1997;831:313-322.

130.   Leblond FA, Simard G, Henley N, Rocheleau B, Huet PM, Halle JP. Studies on smaller (approximately 315 microM) microcapsules: IV. Feasibility and safety of intrahepatic implantations of small alginate poly-L-lysine microcapsules. Cell Transplant 1999;8:327-337.

131.   Schneider S, von Mach MA, Kraus O, Kann P, Feilen PJ. Intraportal transplantation of allogenic pancreatic islets encapsulated in barium alginate beads in diabetic rats. Artif Organs 2003;27:1053-1056.

132.   Robitaille R, Leblond FA, Bourgeois Y, Henley N, Loignon M, Halle JP. Studies on small (<350 microm) alginate-poly-L-lysine microcapsules. V. Determination of carbohydrate and protein permeation through microcapsules by reverse-size exclusion chromatography. J Biomed Mater Res 2000;50:420-427.

133.   Robitaille R, Pariseau JF, Leblond FA, Lamoureux M, Lepage Y, Halle JP. Studies on small (<350 microm) alginate-poly-L-lysine microcapsules. III. Biocompatibility Of smaller versus standard microcapsules. J Biomed Mater Res 1999;44:116-120.

134.   Toso C, Oberholzer J, Ceausoglu I, Ris F, Rochat B, Rehor A, Bucher P, Wandrey C, Schuldt U, Belenger J, Bosco D, Morel P, Hunkeler D. Intra-portal injection of 400- microm microcapsules in a large-animal model. Transpl Int 2003;16:405-410.

135.   Toso C, Mathe Z, Morel P, Oberholzer J, Bosco D, Sainz-Vidal D, Hunkeler D, Buhler LH, Wandrey C, Berney T. Effect of microcapsule composition and short-term immunosuppression on intraportal biocompatibility. Cell Transplantation 2005;14:159-167.

136.   De Vos P, De Haan B, Wolters GH, Van Schilfgaarde R. Factors influencing the adequacy of microencapsulation of rat pancreatic islets. Transplantation 1996;62:888-893.

137.   De Vos P, Van Straaten JF, Nieuwenhuizen AG, de Groot M, Ploeg RJ, De Haan BJ, Van Schilfgaarde R. Why do microencapsulated islet grafts fail in the absence of fibrotic overgrowth? Diabetes 1999;48:1381-1388.

138.   Zekorn T, Siebers U, Horcher A, Schnettler R, Zimmermann U, Bretzel RG, Federlin K. Alginate coating of islets of Langerhans: in vitro studies on a new method for microencapsulation for immuno-isolated transplantation. Acta Diabetol 1992;29:41-45.

139.   Park YG, Iwata H, Ikada Y. Microencapsulation of islets and model beads with a thin alginate-Ba2+ gel layer using centrifugation. Polym Advan Technol 1998;9:734-739.

140.   May MH, Sefton MV. Conformal coating of small particles and cell aggregates at a liquid-liquid interface. Ann N Y Acad Sci 1999;875:126-134.

141.   Sefton MV, May MH, Lahooti S, Babensee JE. Making microencapsulation work: conformal coating, immobilization gels and in vivo performance. J Control Release 2000;65:173-186.

142.   Khademhosseini A, May MH, Sefton MV. Conformal coating of mammalian cells immobilized onto magnetically driven beads. Tissue Eng 2005;11:1797-1806.

143.   Basta G, Osticioli L, Rossodivita ME, Sarchielli P, Tortoioli C, Brunetti P, Calafiore R. Method for Fabrication of Coherent Microcapsules - a New, Potential Immunoisolatory Barrier for Pancreatic-Islet Transplantation. Diabetes Nutr Metab 1995;8:105-112.

144.   Leung A, Ramaswamy Y, Munro P, Lawrie G, Nielsen L, Trau M. Emulsion strategies in the microencapsulation of cells: pathways to thin coherent membranes. Biotechnol Bioeng 2005;92:45-53.

145.   Calafiore R, Basta G, Luca G, Boselli C, Bufalari A, Bufalari A, Cassarani MP, Giustozzi GM, Brunetti P. Transplantation of pancreatic islets contained in minimal volume microcapsules in diabetic high mammalians. Ann N Y Acad Sci 1999;875:219-232.

146.   Wyman JL, Kizilel S, Skarbek R, Zhao X, Connors M, Dillmore WS, Murphy WL, Mrksich M, Nagel SR, Garfinkel MR. Immunoisolating pancreatic islets by encapsulation with selective withdrawal. Small 2007;3:683-690.

147.   Cruise GM, Hegre OD, Lamberti FV, Hager SR, Hill R, Scharp DS, Hubbell JA. In vitro and in vivo performance of porcine islets encapsulated in interfacially photopolymerized poly(ethylene glycol) diacrylate membranes. Cell Transplant 1999;8:293-306.

148.   Cruise GM, Hegre OD, Scharp DS, Hubbell JA. A sensitivity study of the key parameters in the interfacial photopolymerization of poly(ethylene glycol) diacrylate upon porcine islets. Biotechnol Bioeng 1998;57:655-665.

149.   Hill RS, Cruise GM, Hager SR, Lamberti FV, Yu X, Garufis CL, Yu Y, Mundwiler KE, Cole JF, Hubbell JA, Hegre OD, Scharp DW. Immunoisolation of adult porcine islets for the treatment of diabetes mellitus. The use of photopolymerizable polyethylene glycol in the conformal coating of mass-isolated porcine islets. Ann N Y Acad Sci 1997;831:332-343.

150.   www.novocell.com. Accessed June 2008.

151.   www.clinicaltrails.gov. Accessed June 2008.

152.   Chen AM, Scott MD. Immunocamouflage: prevention of transfusion-induced graft-versus-host disease via polymer grafting of donor cells. J Biomed Mater Res A 2003;67:626-636.

153.   Murad KL, Gosselin EJ, Eaton JW, Scott MD. Stealth cells: prevention of major histocompatibility complex class II-mediated T-cell activation by cell surface modification. Blood 1999;94:2135-2141.

154.   Scott MD, Murad KL, Koumpouras F, Talbot M, Eaton JW. Chemical camouflage of antigenic determinants: stealth erythrocytes. Proc Natl Acad Sci U S A 1997;94:7566-7571.

155.   Lee DY, Yang K, Lee S, Chae SY, Kim KW, Lee MK, Han DJ, Byun Y. Optimization of monomethoxy-polyethylene glycol grafting on the pancreatic islet capsules. J Biomed Mater Res 2002;62:372-377.

156.   Panza JL, Wagner WR, Role HLR, Rao RH, Beckman EJ, Russell AJ. Treatment of rat pancreatic islets with reactive PEG. Biomaterials 2000;21:1155-1164.

157.   Kellam B, De Bank PA, Shakesheff KM. Chemical modification of mammalian cell surfaces. Chem Soc Rev 2003;32:327-337.

158.   Chen AM, Scott MD. Current and future applications of immunological attenuation via pegylation of cells and tissue. BioDrugs 2001;15:833-847.

159.   Scott MD, Chen AM. Beyond the red cell: pegylation of other blood cells and tissues. Transfus Clin Biol 2004;11:40-46.

160.   Hashemi-Najafabadi S, Vasheghani-Farahani E, Shojaosadati SA, Rasaee MJ, Armstrong JK, Moin M, Pourpak Z. A method to optimize PEG-coating of red blood cells. Bioconjug Chem 2006;17:1288-1293.

161.   Nacharaju P, Boctor FN, Manjula BN, Acharya SA. Surface decoration of red blood cells with maleimidophenyl-polyethylene glycol facilitated by thiolation with iminothiolane: an approach to mask A, B, and D antigens to generate universal red blood cells. Transfusion 2005;45:374-383.

162.   Xie D, Smyth CA, Eckstein C, Bilbao G, Mays J, Eckhoff DE, Contreras JL. Cytoprotection of PEG-modified adult porcine pancreatic islets for improved xenotransplantation. Biomaterials 2005;26:403-412.

163.   Jang JY, Lee DY, Park SJ, Byun Y. Immune reactions of lymphocytes and macrophages against PEG-grafted pancreatic islets. Biomaterials 2004;25:3663-3669.

164.   Lee DY, Nam JH, Byun Y. Effect of polyethylene glycol grafted onto islet capsules on prevention of splenocyte and cytokine attacks. J Biomater Sci Polym Ed 2004;15:753-766.

165.   Lee DY, Park SJ, Lee S, Nam JH, Byun Y. Highly Poly(Ethylene) Glycolylated Islets Improve Long-Term Islet Allograft Survival Without Immunosuppressive Medication. Tissue Eng 2007.

166.   Lee DY, Park SJ, Nam JH, Byun Y. A combination therapy of PEGylation and immunosuppressive agent for successful islet transplantation. J Control Release 2006;110:290-295.

167.   Lee DY, Park SJ, Nam JH, Byun Y. A new strategy toward improving immunoprotection in cell therapy for diabetes mellitus: long-functioning PEGylated islets in vivo. Tissue Eng 2006;12:615-623.

168.   Yun Lee D, Hee Nam J, Byun Y. Functional and histological evaluation of transplanted pancreatic islets immunoprotected by PEGylation and cyclosporine for 1 year. Biomaterials 2007;28:1957-1966.

169.   Stuhlmeier KM, Lin Y. Camouflaging endothelial cells: does it prolong graft survival? Biochim Biophys Acta 1999;1428:177-190.

170.   Kessler L, Jesser C, Lombard Y, Karsten V, Belcourt A, Pinget M, Poindron P. Cytotoxicity of peritoneal murine macrophages against encapsulated pancreatic rat islets: in vivo and in vitro studies. J Leukoc Biol 1996;60:729-736.

171.   King A, Andersson A, Sandler S. Cytokine-induced functional suppression of microencapsulated rat pancreatic islets in vitro. Transplantation 2000;70:380-383.

172.   Kulseng B, Thu B, Espevik T, Skjak-Braek G. Alginate polylysine microcapsules as immune barrier: permeability of cytokines and immunoglobulins over the capsule membrane. Cell Transplant 1997;6:387-394.

173.   Cole DR, Waterfall M, McIntyre M, Baird JD. Microencapsulated islet grafts in the BB/E rat: a possible role for cytokines in graft failure. Diabetologia 1992;35:231-237.

174.   de Vos P, Smedema I, van Goor H, Moes H, van Zanten J, Netters S, de Leij LF, de Haan A, de Haan BJ. Association between macrophage activation and function of micro-encapsulated rat islets. Diabetologia 2003;46:666-673.

175.   Basta G, Sarchielli P, Luca G, Racanicchi L, Nastruzzi C, Guido L, Mancuso F, Macchiarulo G, Calabrese G, Brunetti P, Calafiore R. Optimized parameters for microencapsulation of pancreatic islet cells: an in vitro study clueing on islet graft immunoprotection in type 1 diabetes mellitus. Transpl Immunol 2004;13:289-296.

176.   Babensee JE, Anderson JM, McIntire LV, Mikos AG. Host response to tissue engineered devices. Adv Drug Deliv Rev 1998;33:111-139.

177.   Rihova B. Immunocompatibility and biocompatibility of cell delivery systems. Adv Drug Deliv Rev 2000;42:65-80.

178.   Tang L, Hu W. Molecular determinants of biocompatibility. Expert Rev Med Devices 2005;2:493-500.

179.   Anderson JM. Inflammatory response to implants. ASAIO Trans 1988;34:101-107.

180.   de Vos P, van Hoogmoed CG, de Haan BJ, Busscher HJ. Tissue responses against immunoisolating alginate-PLL capsules in the immediate posttransplant period. J Biomed Mater Res 2002;62:430-437.

181.   Robitaille R, Dusseault J, Henley N, Desbiens K, Labrecque N, Halle JP. Inflammatory response to peritoneal implantation of alginate-poly-L-lysine microcapsules. Biomaterials 2005;26:4119-4127.

182. de Vos P, Faas MM, Strand B, Calafiore R. Alginate-based microcapsules for immunoisolation of pancreatic islets. Biomaterials 2006;27:5603-5617.

183. Shoichet MS, Winn SR, Athavale S, Harris JM, Gentile FT. Poly(Ethylene Oxide) Grafted Thermoplastic Membranes for Use as Cellular Hybrid Bioartificial Organs in the Central-Nervous-System. Biotechnol Bioeng 1994;43:563-572.

184. La Flamme KE, Popat KC, Leoni L, Markiewicz E, La Tempa TJ, Roman BB, Grimes CA, Desai TA. Biocompatibility of nanoporous alumina membranes for immunoisolation. Biomaterials 2007;28:2638-2645.

185. Sawhney AS, Hubbell JA. Poly(ethylene oxide)-graft-poly(L-lysine) copolymers to enhance the biocompatibility of poly(L-lysine)-alginate microcapsule membranes. Biomaterials 1992;13:863-870.

186. Orive G, Tam SK, Pedraz JL, Halle JP. Biocompatibility of alginate-poly-L-lysine microcapsules for cell therapy. Biomaterials 2006;27:3691-3700.

187. King A, Sandler S, Andersson A. The effect of host factors and capsule composition on the cellular overgrowth on implanted alginate capsules. J Biomed Mater Res 2001;57:374-383.

188. Strand BL, Ryan TL, In't Veld P, Kulseng B, Rokstad AM, Skjak-Brek G, Espevik T. Poly-L-Lysine induces fibrosis on alginate microcapsules via the induction of cytokines. Cell Transplant 2001;10:263-275.

189. Lanza RP, Kuhtreiber WM, Ecker D, Staruk JE, Chick WL. Xenotransplantation of porcine and bovine islets without immunosuppression using uncoated alginate microspheres. Transplantation 1995;59:1377-1384.

190. Dufrane D, Goebbels RM, Saliez A, Guiot Y, Gianello P. Six-month survival of microencapsulated pig islets and alginate biocompatibility in primates: proof of concept. Transplantation 2006;81:1345-1353.

191. Schneider S, Feilen PJ, Brunnenmeier F, Minnemann T, Zimmermann H, Zimmermann U, Weber MM. Long-term graft function of adult rat and human islets encapsulated in novel alginate-based microcapsules after transplantation in immunocompetent diabetic mice. Diabetes 2005;54:687-693.

192. de Vos P, van Hoogmoed CG, van Zanten J, Netter S, Strubbe JH, Busscher HJ. Long-term biocompatibility, chemistry, and function of microencapsulated pancreatic islets. Biomaterials 2003;24:305-312.

193. Tatarkiewicz K. New membrane for cell encapsulation. Artif Organs 1988;12:446-448.

194. Wilson JT, Cui W, Sun XL, Tucker-Burden C, Weber CJ, Chaikof EL. In vivo biocompatibility and stability of a substrate-supported polymerizable membrane-mimetic film. Biomaterials 2007;28:609-617.

195. www.amcyte.com. Accessed June 2008.

196.   De Vos P, De Haan BJ, Wolters GH, Strubbe JH, Van Schilfgaarde R. Improved biocompatibility but limited graft survival after purification of alginate for microencapsulation of pancreatic islets. Diabetologia 1997;40:262-270.

197.   de Groot M, Schuurs TA, Leuvenink HG, van Schilfgaarde R. Macrophage overgrowth affects neighboring nonovergrown encapsulated islets. J Surg Res 2003;115:235-241.

198.   Chae SY, Lee M, Kim SW, Bae YH. Protection of insulin secreting cells from nitric oxide induced cellular damage by crosslinked hemoglobin. Biomaterials 2004;25:843-850.

199.   Wiegand F, Kroncke KD, Kolb-Bachofen V. Macrophage-generated nitric oxide as cytotoxic factor in destruction of alginate-encapsulated islets. Protection by arginine analogs and/or coencapsulated erythrocytes. Transplantation 1993;56:1206-1212.

200.   Kavdia M, Lewis RS. Free radical profiles in an encapsulated pancreatic cell matrix model. Ann Biomed Eng 2002;30:721-730.

201.   Omer A, Keegan M, Czismadia E, De Vos P, Van Rooijen N, Bonner-Weir S, Weir GC. Macrophage depletion improves survival of porcine neonatal pancreatic cell clusters contained in alginate macrocapsules transplanted into rats. Xenotransplantation 2003;10:240-251.

202.   Moberg L, Olsson A, Berne C, Felldin M, Foss A, Kallen R, Salmela K, Tibell A, Tufveson G, Nilsson B, Korsgren O. Nicotinamide inhibits tissue factor expression in isolated human pancreatic islets: implications for clinical islet transplantation. Transplantation 2003;76:1285-1288.

203.   Marzorati S, Antonioli B, Nano R, Maffi P, Piemonti L, Giliola C, Secchi A, Lakey JR, Bertuzzi F. Culture medium modulates proinflammatory conditions of human pancreatic islets before transplantation. Am J Transplant 2006;6:2791-2795.

204.   Marzorati S, Melzi R, Nano R, Antonioli B, Di Carlo V, Piemonti L, Bertuzzi F. In vitro modulation of monocyte chemoattractant protein-1 release in human pancreatic islets. Transplant Proc 2004;36:607-608.

205.   Amoli MM, Mousavizadeh R, Sorouri R, Rahmani M, Larijani B. Curcumin inhibits in vitro MCP-1 release from mouse pancreatic islets. Transplant Proc 2006;38:3035-3038.

206.   Eckhoff DE, Smyth CA, Eckstein C, Bilbao G, Young CJ, Thompson JA, Contreras JL. Suppression of the c-Jun N-terminal kinase pathway by 17beta-estradiol can preserve human islet functional mass from proinflammatory cytokine-induced destruction. Surgery 2003;134:169-179.

207.   Zeender E, Maedler K, Bosco D, Berney T, Donath MY, Halban PA. Pioglitazone and sodium salicylate protect human beta-cells against apoptosis and impaired function induced by glucose and interleukin-1beta. J Clin Endocrinol Metab 2004;89:5059-5066.

208. Yang ZD, Chen M, Ellett JD, Carter JD, Brayman KL, Nadler JL. Inflammatory blockade improves human pancreatic islet function and viability. Am J Transplant 2005;5:475-483.

209. Riachy R, Vandewalle B, Moerman E, Belaich S, Lukowiak B, Gmyr V, Muharram G, Kerr Conte J, Pattou F. 1,25-Dihydroxyvitamin D3 protects human pancreatic islets against cytokine-induced apoptosis via down-regulation of the Fas receptor. Apoptosis 2006;11:151-159.

210. Goss JA, Goodpastor SE, Brunicardi FC, Barth MH, Soltes GD, Garber AJ, Hamilton DJ, Alejandro R, Ricordi C. Development of a human pancreatic islet-transplant program through a collaborative relationship with a remote islet-isolation center. Transplantation 2004;77:462-466.

211. Nanji SA, Shapiro AM. Islet transplantation in patients with diabetes mellitus: choice of immunosuppression. BioDrugs 2004;18:315-328.

212. Arita S, Nagai T, Ochiai M, Sakamoto Y, Smith CV, Shevlin L, Mullen Y. Pravastatin prevents primary nonfunction of canine islet autografts. Transplant Proc 1998;30:411.

213. Arita S, Une S, Ohtsuka S, Atiya A, Kasraie A, Shevlin L, Mullen Y. Prevention of primary islet isograft nonfunction in mice with pravastatin. Transplantation 1998;65:1429-1433.

214. Kenmochi T, Miyamoto M, Mullen Y. Protection of mouse islet isografts from nonspecific inflammatory damage by recipient treatment with nicotinamide and 15-deoxyspergualin. Cell Transplant 1996;5:41-47.

215. Thomas JM, Contreras JL, Smyth CA, Lobashevsky A, Jenkins S, Hubbard WJ, Eckhoff DE, Stavrou S, Neville DM, Jr., Thomas FT. Successful reversal of streptozotocin-induced diabetes with stable allogeneic islet function in a preclinical model of type 1 diabetes. Diabetes 2001;50:1227-1236.

216. Beuneu C, Vosters O, Ling Z, Pipeleers D, Pradier O, Goldman M, Verhasselt V. N-Acetylcysteine derivative inhibits procoagulant activity of human islet cells. Diabetologia 2007;50:343-347.

217. Goto M, Johansson H, Maeda A, Elgue G, Korsgren O, Nilsson B. Low molecular weight dextran sulfate prevents the instant blood-mediated inflammatory reaction induced by adult porcine islets. Transplantation 2004;77:741-747.

218. Johansson H, Goto M, Dufrane D, Siegbahn A, Elgue G, Gianello P, Korsgren O, Nilsson B. Low molecular weight dextran sulfate: a strong candidate drug to block IBMIR in clinical islet transplantation. Am J Transplant 2006;6:305-312.

219. Berg DT, Gerlitz B, Shang J, Smith T, Santa P, Richardson MA, Kurz KD, Grinnell BW, Mace K, Jones BE. Engineering the proteolytic specificity of activated protein C improves its pharmacological properties. Proc Natl Acad Sci U S A 2003;100:4423-4428.

220.   Arita S, Nagai T, Ochiai M, Sakamoto Y, Shevlin LA, Smith CV, Mullen Y. Prevention of primary nonfunction of canine islet autografts by treatment with pravastatin. Transplantation 2002;73:7-12.

221.   Berman DM, Cabrera O, Kenyon NM, Miller J, Tam SH, Khandekar VS, Picha KM, Soderman AR, Jordan RE, Bugelski PJ, Horninger D, Lark M, Davis JE, Alejandro R, Berggren PO, Zimmerman M, O'Neil JJ, Ricordi C, Kenyon NS. Interference with tissue factor prolongs intrahepatic islet allograft survival in a nonhuman primate marginal mass model. Transplantation 2007;84:308-315.

222.   Wilson JT, Chaikof EL. Challenges and emerging technologies in the immunoisolation of cells and tissues. Adv Drug Deliv Rev 2008;60:124-145.

223.   Tibell LA, Sethson I, Buevich AV. Characterization of the heparin-binding domain of human extracellular superoxide dismutase. Biochim Biophys Acta 1997;1340:21-32.

224.   Edens RE, Linhardt RJ, Bell CS, Weiler JM. Heparin and derivatized heparin inhibit zymosan and cobra venom factor activation of complement in serum. Immunopharmacology 1994;27:145-153.

225.   Maillet F, Petitou M, Choay J, Kazatchkine MD. Structure-function relationships in the inhibitory effect of heparin on complement activation: independency of the anti-coagulant and anti-complementary sites on the heparin molecule. Mol Immunol 1988;25:917-923.

226.   Sahu A, Pangburn MK. Identification of multiple sites of interaction between heparin and the complement system. Mol Immunol 1993;30:679-684.

227.   Cabric S, Sanchez J, Lundgren T, Foss A, Felldin M, Kallen R, Salmela K, Tibell A, Tufveson G, Larsson R, Korsgren O, Nilsson B. Islet surface heparinization prevents the instant blood-mediated inflammatory reaction in islet transplantation. Diabetes 2007;56:2008-2015.

228.   Atkinson B, Dwyer K, Enjyoji K, Robson SC. Ecto-nucleotidases of the CD39/NTPDase family modulate platelet activation and thrombus formation: Potential as therapeutic targets. Blood Cells Mol Dis 2006;36:217-222.

229.   Robson SC, Wu Y, Sun X, Knosalla C, Dwyer K, Enjyoji K. Ectonucleotidases of CD39 family modulate vascular inflammation and thrombosis in transplantation. Semin Thromb Hemost 2005;31:217-233.

230.   Dwyer KM, Mysore TB, Crikis S, Robson SC, Nandurkar H, Cowan PJ, D'Apice AJ. The transgenic expression of human CD39 on murine islets inhibits clotting of human blood. Transplantation 2006;82:428-432.

231.   Cabric S, Elgue G, Nilsson B, Korsgren O, Schmidt P. Adenovirus-mediated expression of the anticoagulant hirudin in human islets: a tool to make the islets biocompatible to blood. Cell Transplant 2006;15:759-767.

232.   Giannoukakis N, Rudert WA, Ghivizzani SC, Gambotto A, Ricordi C, Trucco M, Robbins PD. Adenoviral gene transfer of the interleukin-1 receptor antagonist protein to

human islets prevents IL-1beta-induced beta-cell impairment and activation of islet cell apoptosis in vitro. Diabetes 1999;48:1730-1736.

233.   Tellez N, Montolio M, Biarnes M, Castano E, Soler J, Montanya E. Adenoviral overexpression of interleukin-1 receptor antagonist protein increases beta-cell replication in rat pancreatic islets. Gene Ther 2005;12:120-128.

234.   Gysemans C, Stoffels K, Giulietti A, Overbergh L, Waer M, Lannoo M, Feige U, Mathieu C. Prevention of primary non-function of islet xenografts in autoimmune diabetic NOD mice by anti-inflammatory agents. Diabetologia 2003;46:1115-1123.

235.   Lau HT, Yu M, Fontana A, Stoeckert CJ, Jr. Prevention of islet allograft rejection with engineered myoblasts expressing FasL in mice. Science 1996;273:109-112.

236.   Yolcu ES, Askenasy N, Singh NP, Cherradi SE, Shirwan H. Cell membrane modification for rapid display of proteins as a novel means of immunomodulation: FasL-decorated cells prevent islet graft rejection. Immunity 2002;17:795-808.

237.   Akgul C, Edwards SW. Regulation of neutrophil apoptosis via death receptors. Cell Mol Life Sci 2003;60:2402-2408.

238.   Grage-Griebenow E, Durrbaum-Landmann I, Pryjma J, Loppnow H, Flad HD, Ernst M. Apoptosis in monocytes. Eur Cytokine Netw 1998;9:699-700.

239.   Bunger CM, Tiefenbach B, Jahnke A, Gerlach C, Freier T, Schmitz KP, Hopt UT, Schareck W, Klar E, de Vos P. Deletion of the tissue response against alginate-pll capsules by temporary release of co-encapsulated steroids. Biomaterials 2005;26:2353-2360.

240.   Luca G, Basta G, Calafiore R, Rossi C, Giovagnoli S, Esposito E, Nastruzzi C. Multifunctional microcapsules for pancreatic islet cell entrapment: design, preparation and in vitro characterization. Biomaterials 2003;24:3101-3114.

241.   Ricci M, Blasi P, Giovagnoli S, Rossi C, Macchiarulo G, Luca G, Basta G, Calafiore R. Ketoprofen controlled release from composite microcapsules for cell encapsulation: effect on post-transplant acute inflammation. J Control Release 2005;107:395-407.

242.   Chae SY, Kim YY, Kim SW, Bae YH. Prolonged glucose normalization of streptozotocin-induced diabetic mice by transplantation of rat islets coencapsulated with crosslinked hemoglobin. Transplantation 2004;78:392-397.

243.   Chae SY, Kim SW, Bae YH. Effect of cross-linked hemoglobin on functionality and viability of microencapsulated pancreatic islets. Tissue Eng 2002;8:379-394.

244.   Brandhorst D, Brandhorst H, Zwolinski A, Nahidi F, Bretzel RG. Prevention of early islet graft failure by selective inducible nitric oxide synthase inhibitors after pig to nude rat intraportal islet transplantation. Transplantation 2001;71:179-184.

245.   Hsu BR, Chen ST, Fu SH. Enhancing engraftment of islets using perioperative sodium 4-phenylbutyrate. Int Immunopharmacol 2006;6:1952-1959.

246.   Ueki M, Yasunami Y, Motoyama K, Funakoshi A, Ikeda S, Tanaka M. The amelioration of hyperglycemia in streptozotocin-induced diabetic rats after the intraportal transplantation of an insufficient number of islets by nicotinamide treatment. Transplantation 1995;60:313-317.

247.   Ricordi C, Strom TB. Clinical islet transplantation: advances and immunological challenges. Nat Rev Immunol 2004;4:259-268.

248.   Barnett BP, Arepally A, Karmarkar PV, Qian D, Gilson WD, Walczak P, Howland V, Lawler L, Lauzon C, Stuber M, Kraitchman DL, Bulte JWM. Magnetic resonance-guided, real-time targeted delivery and imaging of magnetocapsules immunoprotecting pancreatic islet cells. Nature Medicine 2007;13:986-991.

249.   Decher G. Fuzzy nanoassemblies: Toward layered polymeric multicomposites. Science 1997;277:1232-1237.

250.   Quinn JF, Johnston APR, Such GK, Zelikin AN, Caruso F. Next generation, sequentially assembled ultrathin films: beyond electrostatics. Chemical Society Reviews 2007;36:707-718.

251.   Hammond PT. Form and function in multilayer assembly: New applications at the nanoscale. Advanced Materials 2004;16:1271-1293.

252.   Caruso F, Trau D, Mohwald H, Renneberg R. Enzyme encapsulation in layer-by-layer engineered polymer multilayer capsules. Langmuir 2000;16:1485-1488.

253.   Elbert DL, Herbert CB, Hubbell JA. Thin polymer layers formed by polyelectrolyte multilayer techniques on biological surfaces. Langmuir 1999;15:5355-5362.

254.   Thierry B, Winnik FM, Merhi Y, Tabrizian M. Nanocoatings onto arteries via layer-by-layer deposition: Toward the in vivo repair of damaged blood vessels. J Am Chem Soc 2003;125:7494-7495.

255.   Lvov Y, Ariga K, Ichinose I, Kunitake T. Assembly of Multicomponent Protein Films by Means of Electrostatic Layer-by-Layer Adsorption. J Am Chem Soc 1995;117:6117-6123.

256.   Jessel N, Atalar F, Lavalle P, Mutterer J, Decher G, Schaaf P, Voegel JC, Ogier J. Bioactive coatings based on a polyelectrolyte multilayer architecture functionalized by embedded proteins. Advanced Materials 2003;15:692-695.

257.   Jewell CM, Zhang JT, Fredin NJ, Lynn DM. Multilayered polyelectrolyte films promote the direct and localized delivery of DNA to cells. J Control Release 2005;106:214-223.

258.   Michel M, Vautier D, Voegel JC, Schaaf P, Ball V. Layer by layer self-assembled polyelectrolyte multilayers with embedded phospholipid vesicles. Langmuir 2004;20:4835-4839.

259.   Benkirane-Jessel N, Schwinte P, Falvey P, Darcy R, Haikel Y, Schaaf P, Voegel JC, Ogier J. Build-up of polypeptide multilayer coatings with anti-inflammatory properties

based on the embedding of piroxicam-cyclodextrin complexes. Adv Funct Mater 2004;14:174-182.

260. Picart C, Elkaim R, Richert L, Audoin T, Arntz Y, Cardoso MD, Schaaf P, Voegel JC, Frisch B. Primary cell adhesion on RGD-functionalized and covalently crosslinked thin polyelectrolyte multilayer films. Adv Funct Mater 2005;15:83-94.

261. Chluba J, Voegel JC, Decher G, Erbacher P, Schaaf P, Ogier J. Peptide hormone covalently bound to polyelectrolytes and embedded into multilayer architectures conserving full biological activity. Biomacromolecules 2001;2:800-805.

262. Huang NP, Voros J, De Paul SM, Textor M, Spencer ND. Biotin-derivatized poly(L-lysine)-g-poly(ethylene glycol): A novel polymeric interface for bioaffinity sensing. Langmuir 2002;18:220-230.

263. Cui W, Barr G, Faucher KM, Sun XL, Safley SA, Weber CJ, Chaikof EL. A membrane-mimetic barrier for islet encapsulation. Transplant Proc 2004;36:1206-1208.

264. Badet L, Titus TT, McShane P, Chang LW, Song ZS, Ferguson DJP, Gray DWR. Transplantation of mouse pancreatic islets into primates - In vivo and in vitro evaluation. Transplantation 2001;72:1867-1874.

265. Krol S, del Guerra S, Grupillo M, Diaspro A, Gliozzi A, Marchetti P. Multilayer nanoencapsulation. New approach for immune protection of human pancreatic islets. Nano Lett 2006;6:1933-1939.

266. Kemp CB, Knight MJ, Scharp DW, Lacy PE, Ballinger WF. Transplantation of isolated pancreatic islets into the portal vein of diabetic rats. Nature 1973;244:447.

267. Hong S, Leroueil PR, Janus EK, Peters JL, Kober MM, Islam MT, Orr BG, Baker JR, Jr., Banaszak Holl MM. Interaction of polycationic polymers with supported lipid bilayers and cells: nanoscale hole formation and enhanced membrane permeability. Bioconjug Chem 2006;17:728-734.

268. Chanana M, Gliozzi A, Diaspro A, Chodnevskaja I, Huewel S, Moskalenko V, Ulrichs K, Galla HJ, Krol S. Interaction of polyelectrolytes and their composites with living cells. Nano Lett 2005;5:2605-2612.

269. Fischer D, Li YX, Ahlemeyer B, Krieglstein J, Kissel T. In vitro cytotoxicity testing of polycations: influence of polymer structure on cell viability and hemolysis. Biomaterials 2003;24:1121-1131.

270. Elbert DL, Hubbell JA. Self-assembly and steric stabilization at heterogeneous, biological surfaces using adsorbing block copolymers. Chem Biol 1998;5:177-183.

271. Hansson KM, Tosatti S, Isaksson J, Wettero J, Textor M, Lindahl TL, Tengvall P. Whole blood coagulation on protein adsorption-resistant PEG and peptide functionalised PEG-coated titanium surfaces. Biomaterials 2005;26:861-872.

272.   Heuberger R, Sukhorukov G, Voros J, Textor M, Mohwald H. Biofunctional polyelectrolyte multilayers and microcapsules: Control of non-specific and bio-specific protein adsorption. Adv Funct Mater 2005;15:357-366.

273.   Kenausis GL, Voros J, Elbert DL, Huang NP, Hofer R, Ruiz-Taylor L, Textor M, Hubbell JA, Spencer ND. Poly(L-lysine)-g-poly(ethylene glycol) layers on metal oxide surfaces: Attachment mechanism and effects of polymer architecture on resistance to protein adsorption. J Phys Chem B 2000;104:3298-3309.

274.   Billinger M, Buddeberg F, Hubbell JA, Elbert DL, Schaffner T, Mettler D, Windecker S, Meier B, Hess OM. Polymer stent coating for prevention of neointimal hyperplasia. J Invasive Cardiol 2006;18:423-426; discussion 427.

275.   Ruiz-Taylor LA, Martin TL, Zaugg FG, Witte K, Indermuhle P, Nock S, Wagner P. Monolayers of derivatized poly(L-lysine)-grafted poly(ethylene glycol) on metal oxides as a class of biomolecular interfaces. Proc Natl Acad Sci U S A 2001;98:852-857.

276.   Ryser HJ. A membrane effect of basic polymers dependent on molecular size. Nature 1967;215:934-936.

277.   Hartmann W, Galla HJ. Binding of polylysine to charged bilayer membranes: molecular organization of a lipid.peptide complex. Biochim Biophys Acta 1978;509:474-490.

278.   Anzai J, Akase S. Preparation of an organized film composed of polymers, avidin, and concanavalin A and its binding properties. Macromol Biosci 2002;2:361-364.

279.   Cassier T, Lowack K, Decher G. Layer-by-layer assembled protein/polymer hybrid films: nanoconstruction via specific recognition. Supramol Sci 1998;5:309-315.

280.   Anzai J, Kobayashi Y, Nakamura N, Nishimura M, Hoshi T. Layer-by-layer construction of multilayer thin films composed of avidin and biotin-labeled poly(amine)s. Langmuir 1999;15:221-226.

281.   Inoue H, Anzai J. Stimuli-sensitive thin films prepared by a layer-by-layer deposition of 2-iminobiotin-labeled poly(ethyleneimine) and avidin. Langmuir 2005;21:8354-8359.

282.   Inoue H, Sato K, Anzai J. Disintegration of layer-by-layer assemblies composed of 2-iminobiotin-labeled poly(ethyleneimine) and avidin. Biomacromolecules 2005;6:27-29.

283.   Leroueil PR, Hong S, Mecke A, Baker JR, Jr., Orr BG, Banaszak Holl MM. Nanoparticle interaction with biological membranes: does nanotechnology present a Janus face? Acc Chem Res 2007;40:335-342.

284.   Huang NP, Michel R, Voros J, Textor M, Hofer R, Rossi A, Elbert DL, Hubbell JA, Spencer ND. Poly(L-lysine)-g-poly(ethylene glycol) layers on metal oxide surfaces: Surface-analytical characterization and resistance to serum and fibrinogen adsorption. Langmuir 2001;17:489-498.

206

285. Cabric S, Sanchez J, Lundgren T, Foss A, Felldin M, Kallen R, Salmela K, Tibell A, Tufveson G, Larsson R, Korsgren O, Nilsson B. Islet surface heparinization prevents the instant blood-mediated inflammatory reaction in islet transplantation. Diabetes 2007;56:2008-2015.

286. Wilson JT, Chaikof EL. Thrombosis and inflammation in intraportal islet transplantation: a review of pathophysiology and emerging therapeutics. Journal of Diabetes Science and Technology 2008;2:746-759.

287. Teramura Y, Kaneda Y, Totani T, Iwata H. Behavior of synthetic polymers immobilized on a cell membrane. Biomaterials 2008;29:1345-1355.

288. Tang ZY, Wang Y, Podsiadlo P, Kotov NA. Biomedical applications of layer-by-layer assembly: From biomimetics to tissue engineering. Advanced Materials 2006;18:3203-3224.

289. Kim J, Wacker BK, Elbert DL. Thin polymer layers formed using multiarm poly(ethylene glycol) vinylsulfone by a covalent layer-by-layer method. Biomacromolecules 2007;8:3682-3686.

290. Such GK, Quinn JF, Quinn A, Tjipto E, Caruso F. Assembly of ultrathin polymer multilayer films by click chemistry. J Am Chem Soc 2006;128:9318-9319.

291. Such GK, Tjipto E, Postma A, Johnston APR, Caruso F. Ultrathin, responsive polymer click capsules. Nano Lett 2007;7:1706-1710.

292. Dai Z, Wilson JT, Chaikof EL. Construction of pegylated multilayer architectures via (strept)avidin/biotin interactions. Mater Sci Eng C-Biomimetic Supramol Syst 2007;27:402-408.

293. Kim BS, Park SW, Hammond PT. Hydrogen-bonding layer-by-layer assembled biodegradable polymeric micelles as drug delivery vehicles from surfaces. ACS Nano 2008;2:386-392.

294. Lutkenhaus JL, Hrabak KD, McEnnis K, Hammond PT. Elastomeric flexible free-standing hydrogen-bonded nanoscale assemblies. J Am Chem Soc 2005;127:17228-17234.

295. Podsiadlo P, Kaushik AK, Arruda EM, Waas AM, Shim BS, Xu JD, Nandivada H, Pumplin BG, Lahann J, Ramamoorthy A, Kotov NA. Ultrastrong and stiff layered polymer nanocomposites. Science 2007;318:80-83.

296. Jewell CM, Zhang JT, Fredin NJ, Wolff MR, Hacker TA, Lynn DM. Release of plasmid DNA from intravascular stents coated with ultrathin multilayered polyelectrolyte films. Biomacromolecules 2006;7:2483-2491.

297. Fujimoto K, Toyoda T, Fukui Y. Preparation of bionanocapsules by the layer-by-layer deposition of polypeptides onto a liposome. Macromolecules 2007;40:5122-5128.

298. Singh AK, Kasinath BS, Lewis EJ. Interaction of Polycations with Cell-Surface Negative Charges of Epithelial-Cells. Biochim Biophys Acta 1992;1120:337-342.

299.   Arnold LJ, Jr., Dagan A, Gutheil J, Kaplan NO. Antineoplastic activity of poly(L-lysine) with some ascites tumor cells. Proc Natl Acad Sci U S A 1979;76:3246-3250.

300.   Morgan DML, Clover J, Pearson JD. Effects of Synthetic Polycations on Leucine Incorporation, Lactate-Dehydrogenase Release, and Morphology of Human Umbilical Vein Endothelial-Cells. J Cell Sci 1988;91:231-238.

301.   Morgan DML, Larvin VL, Pearson JD. Biochemical-Characterization of Polycation-Induced Cyto-Toxicity to Human Vascular Endothelial-Cells. J Cell Sci 1989;94:553-559.

302.   Prokop A, Hunkeler D, DiMari S, Haralson MA, Wang TG. Water soluble polymers for immunoisolation I: Complex coacervation and cytotoxicity. Microencapsulation - Microgels - Iniferters 1998;136:1-51.

303.   Wilson JT, Cui W, Chaikof EL. Layer-by-layer assembly of a conformal nanothin PEG coating for intraportal islet transplantation. Nano Lett 2008;8:1940-1948.

304.   Germain M, Balaguer P, Nicolas JC, Lopez F, Esteve JP, Sukhorukov GB, Winterhalter M, Richard-Foy H, Fournier D. Protection of mammalian cell used in biosensors by coating with a polyelectrolyte shell. Biosens Bioelectron 2005.

305.   Veerabadran NG, Goli PL, Stewart-Clark SS, Lvov YM, Mills DK. Nanoencapsulation of Stem Cells within Polyelectrolyte Multilayer Shells. Macromol Biosci 2007;7:877-882.

306.   Teramura Y, Kaneda Y, Iwata H. Islet-encapsulation in ultra-thin layer-by-layer membranes of poly(vinyl alcohol) anchored to poly(ethylene glycol)-lipids in the cell membrane. Biomaterials 2007;28:4818-4825.

307.   Teramura Y, Iwata H. Islets surface modification prevents blood-mediated inflammatory responses. Bioconjug Chem 2008;19:1389-1395.

308.   Tosatti S, De Paul SM, Askendal A, VandeVondele S, Hubbell JA, Tengvall P, Textor M. Peptide functionalized poly(L-lysine)-g-poly(ethylene glycol) on titanium: resistance to protein adsorption in full heparinized human blood plasma. Biomaterials 2003;24:4949-4958.

309.   Boontheekul T, Kong HJ, Mooney DJ. Controlling alginate gel degradation utilizing partial oxidation and bimodal molecular weight distribution. Biomaterials 2005;26:2455-2465.

310.   Sui ZJ, Salloum D, Schlenoff JB. Effect of molecular weight on the construction of polyelectrolyte multilayers: Stripping versus sticking. Langmuir 2003;19:2491-2495.

311.   Arys X, Jonas A, Laguitton B, Legras R, Laschewsky A, Wischerhoff E. Structural studies on thin organic coatings built by repeated adsorption of polyelectrolytes. Prog Org Coat 1998;34:108-118.

312.   Schoeler B, Kumaraswamy G, Caruso F. Investigation of the influence of polyelectrolyte charge density on the growth of multilayer thin films prepared by the layer-by-layer technique. Macromolecules 2002;35:889-897.

313.   Glinel K, Moussa A, Jonas AM, Laschewsky A. Influence of polyelectrolyte charge density on the formation of multilayers of strong polyelectrolytes at low ionic strength. Langmuir 2002;18:1408-1412.

314.   Sun QL, Tong Z, Wang CY, Ren BY, Liu XX, Zeng F. Charge density threshold for LbL self-assembly and small molecule diffusion in polyelectrolyte multilayer films. Polymer 2005;46:4958-4966.

315.   Schoeler B, Sharpe S, Hatton TA, Caruso F. Polyelectrolyte multilayer films of different charge density copolymers with synergistic nonelectrostatic interactions prepared by the layer-by-layer technique. Langmuir 2004;20:2730-2738.

316.   Voigt U, Jaeger W, Findenegg GH, Klitzing RV. Charge effects on the formation of multilayers containing strong polyelectrolytes. J Phys Chem B 2003;107:5273-5280.

317.   Schoeler B, Poptoschev E, Caruso F. Growth of multilayer films of fixed and variable charge density polyelectrolytes: Effect of mutual charge and secondary interactions. Macromolecules 2003;36:5258-5264.

318.   Voigt U, Khrenov V, Thuer K, Hahn M, Jaeger W, von Klitzing R. The effect of polymer charge density and charge distribution on the formation of multilayers. J Phys-Condens Mat 2003;15:S213-S218.

319.   Picart C, Lavalle P, Hubert P, Cuisinier FJG, Decher G, Schaaf P, Voegel JC. Buildup mechanism for poly(L-lysine)/hyaluronic acid films onto a solid surface. Langmuir 2001;17:7414-7424.

320.   Picart C, Mutterer J, Richert L, Luo Y, Prestwich GD, Schaaf P, Voegel JC, Lavalle P. Molecular basis for the explanation of the exponential growth of polyelectrolyte multilayers. P Natl Acad Sci USA 2002;99:12531-12535.

321.   Lavalle P, Picart C, Mutterer J, Gergely C, Reiss H, Voegel JC, Senger B, Schaaf P. Modeling the buildup of polyelectrolyte multilayer films having exponential growth. J Phys Chem B 2004;108:635-648.

322.   Schuler C, Caruso F. Decomposable hollow biopolymer-based capsules. Biomacromolecules 2001;2:921-926.

323.   Miura S, Teramura Y, Iwata H. Encapsulation of islets with ultra-thin polyion complex membrane through poly(ethylene glycol)-phospholipids anchored to cell membrane. Biomaterials 2006;27:5828-5835.

324.   Ferruti P, Knobloch S, Ranucci E, Duncan R, Gianasi E. A novel modification of poly(L-lysine) leading to a soluble cationic polymer with reduced toxicity and with potential as a transfection agent. Macromol Chem Physic 1998;199:2565-2575.

325.   Putnam D, Gentry CA, Pack DW, Langer R. Polymer-based gene delivery with low cytotoxicity by a unique balance of side-chain termini. Proc Natl Acad Sci U S A 2001;98:1200-1205.

326.   Mao S, Shuai X, Unger F, Wittmar M, Xie X, Kissel T. Synthesis, characterization and cytotoxicity of poly(ethylene glycol)-graft-trimethyl chitosan block copolymers. Biomaterials 2005;26:6343-6356.

327.   Feuz L, Strunz P, Geue T, Textor M, Borisov O. Conformation of poly(L-lysine)-graft-poly(ethylene glycol) molecular brushes in aqueous solution studied by small-angle neutron scattering. European Physical Journal E 2007;23:237-245.

328.   Hartmann W, Galla HJ. Binding of Polylysine to Charged Bilayer Membranes - Molecular-Organization of a Lipid - Peptide Complex. Biochim Biophys Acta 1978;509:474-490.

329.   Feuz L, Leermakers FAM, Textor M, Borisov O. Adsorption of molecular brushes with polyelectrolyte backbones onto oppositely charged surfaces: A self-consistent field theory. Langmuir 2008;24:7232-7244.

330.   Schonhoff M. Layered polyelectrolyte complexes: physics of formation and molecular properties. J Phys-Condens Mat 2003;15:R1781-R1808.

331.   Zugates GT, Tedford NC, Zumbuehl A, Jhunjhunwala S, Kang CS, Griffith LG, Lauffenburger DA, Langer R, Anderson DG. Gene delivery properties of end-modified polyo(beta-amino ester)s. Bioconjugate Chem 2007;18:1887-1896.

332.   Ziegler A. Thermodynamic studies and binding mechanisms of cell-penetrating peptides with lipids and glycosaminoglycans. Adv Drug Deliv Rev 2008;60:580-597.

333.   Hudecz F, Pimm MV, Rajnavolgyi E, Mezo G, Fabra A, Gaal D, Kovacs AL, Horvath A, Szekerke M. Carrier design: new generation of polycationic branched polypeptides containing OH groups with prolonged blood survival and diminished in vitro cytotoxicity. Bioconjug Chem 1999;10:781-790.

334.   Mezo G, Remenyi J, Kajtar J, Barna K, Gaal D, Hudecz F. Synthesis and conformational studies of poly(L-lysine) based branched polypeptides with Ser and Glu/Leu in the side chains. J Control Release 2000;63:81-95.

335.   Shibata A, Murata S, Ueno S, Liu S, Futaki S, Baba Y. Synthetic copoly(Lys/Phe) and poly(Lys) translocate through lipid bilayer membranes. Biochim Biophys Acta 2003;1616:147-155.

336.   Luo J, Borgens R, Shi R. Polyethylene glycol immediately repairs neuronal membranes and inhibits free radical production after acute spinal cord injury. J Neurochem 2002;83:471-480.

337.   Koob AO, Colby JM, Borgens RB. Behavioral recovery from traumatic brain injury after membrane reconstruction using polyethylene glycol. J Biol Eng 2008;2:9.

338.	Kilinc D, Gallo G, Barbee KA. Mechanically-induced membrane poration causes axonal beading and localized cytoskeletal damage. Exp Neurol 2008;212:422-430.

339.	Frim DM, Wright DA, Curry DJ, Cromie W, Lee R, Kang UJ. The surfactant poloxamer-188 protects against glutamate toxicity in the rat brain. Neuroreport 2004;15:171-174.

340.	Boulmedais F, Frisch B, Etienne O, Lavalle P, Picart C, Ogier J, Voegel JC, Schaaf P, Egles C. Polyelectrolyte multilayer films with pegylated polypeptides as a new type of anti-microbial protection for biomaterials. Biomaterials 2004;25:2003-2011.

341.	Mannisto M, Vanderkerken S, Toncheva V, Elomaa M, Ruponen M, Schacht E, Urtti A. Structure-activity relationships of poly(L-lysines): effects of pegylation and molecular shape on physicochemical and biological properties in gene delivery. J Control Release 2002;83:169-182.

342.	Luhmann T, Rimann M, Bitterman AG, Hall H. Cellular uptake and intracellular pathways of PLL-g-PEG-DNA nanoparticles. Bioconjugate Chem 2008;19:1907-1916.

343.	Choi YH, Liu F, Park JS, Kim SW. Lactose-poly(ethylene glycol)-grafted poly-L-lysine as hepatoma cell-targeted gene carrier. Bioconjugate Chem 1998;9:708-718.

344.	Choi YH, Liu F, Kim JS, Choi YK, Park JS, Kim SW. Polyethylene glycol-grafted poly-L-lysine as polymeric gene carrier. J Control Release 1998;54:39-48.

345.	Xiong MP, Bae Y, Fukushima S, Forrest ML, Nishiyama N, Kataoka K, Kwon GS. PH-Responsive multi-PEGylated dual cationic nanoparticles enable charge modulations for safe gene delivery. Chemmedchem 2007;2:1321-1327.

346.	Lavalle P, Gergely C, Cuisinier FJG, Decher G, Schaaf P, Voegel JC, Picart C. Comparison of the structure of polyelectrolyte multilayer films exhibiting a linear and an exponential growth regime: An in situ atomic force microscopy study. Macromolecules 2002;35:4458-4465.

347.	Caruso F, Lichtenfeld H, Donath E, Mohwald H. Investigation of electrostatic interactions in polyelectrolyte multilayer films: Binding of anionic fluorescent probes to layers assembled onto colloids. Macromolecules 1999;32:2317-2328.

348.	Ladam G, Schaad P, Voegel JC, Schaaf P, Decher G, Cuisinier F. In situ determination of the structural properties of initially deposited polyelectrolyte multilayers. Langmuir 2000;16:1249-1255.

349.	Podsiadlo P, Michel M, Lee J, Verploegen E, Kam NWS, Ball V, Lee J, Qi Y, Hart AJ, Hammond PT, Kotov NA. Exponential growth of LBL films with incorporated inorganic sheets. Nano Lett 2008;8:1762-1770.

350.	Pardo-Yissar V, Katz E, Lioubashevski O, Willner I. Layered polyelectrolyte films on Au electrodes: Characterization of electron-transfer features at the charged polymer interface and application for selective redox reactions. Langmuir 2001;17:1110-1118.

351.   Schmitt J, Grunewald T, Decher G, Pershan PS, Kjaer K, Losche M. Internal Structure of Layer-by-Layer Adsorbed Polyelectrolyte Films - a Neutron and X-Ray Reflectivity Study. Macromolecules 1993;26:7058-7063.

352.   Jomaa HW, Schlenoff JB. Salt-induced polyelectrolyte interdiffusion in multilayered films: A neutron reflectivity study. Macromolecules 2005;38:8473-8480.

353.   Porcel C, Lavalle P, Ball V, Decher G, Senger B, Voegel JC, Schaaf P. From exponential to linear growth in polyelectrolyte multilayers. Langmuir 2006;22:4376-4383.

354.   Lavalle P, Vivet V, Jessel N, Decher G, Voegel JC, Mesini PJ, Schaaf P. Direct evidence for vertical diffusion and exchange processes of polyanions and polycations in polyelectrolyte multilayer films. Macromolecules 2004;37:1159-1162.

355.   Porcel C, Lavalle P, Decher G, Senger B, Voegel JC, Schaaf P. Influence of the polyelectrolyte molecular weight on exponentially growing multilayer films in the linear regime. Langmuir 2007;23:1898-1904.

356.   Miller MD, Bruening ML. Correlation of the swelling and permeability of polyelectrolyte multilayer films. Chem Mater 2005;17:5375-5381.

357.   Burke SE, Barrett CJ. Swelling behavior of hyaluronic acid/polyallylamine hydrochloride multilayer films. Biomacromolecules 2005;6:1419-1428.

358.   Halthur TJ, Claesson PM, Elofsson UM. Stability of polypeptide multilayers as studied by in situ ellipsometry: Effects of drying and post-buildup changes in temperature and pH. J Am Chem Soc 2004;126:17009-17015.

359.   Nolte AJ, Treat ND, Cohen RE, Rubner MF. Effect of relative humidity on the Young's modulus of polyelectrolyte multilayer films and related nonionic polymers. Macromolecules 2008;41:5793-5798.

360.   Peppas NA, Hilt JZ, Khademhosseini A, Langer R. Hydrogels in biology and medicine: From molecular principles to bionanotechnology. Advanced Materials 2006;18:1345-1360.

361.   Ostroha J, Pong M, Lowman A, Dan N. Controlling the collapse/swelling transition in charged hydrogels. Biomaterials 2004;25:4345-4353.

362.   Collin D, Lavalle P, Garza JM, Voegel JC, Schaaf P, Martinoty P. Mechanical properties of cross-linked hyaluronic acid/poly-(L-lysine) multilayer films. Macromolecules 2004;37:10195-10198.

363.   Totani T, Teramura Y, Iwata H. Immobilization of urokinase on the islet surface by amphiphilic poly(vinyl alcohol) that carries alkyl side chains. Biomaterials 2008;29:2878-2883.

364.   Boonyarattanakalin S, Martin SE, Sun Q, Peterson BR. A synthetic mimic of human Fc receptors: defined chemical modification of cell surfaces enables efficient endocytic uptake of human immunoglobulin-G. J Am Chem Soc 2006;128:11463-11470.

212

365.   Lee JH, Baker TJ, Mahal LK, Zabner J, Bertozzi CR, Wiemer DF, Welsh MJ. Engineering novel cell surface receptors for virus-mediated gene transfer. J Biol Chem 1999;274:21878-21884.

366.   Rabuka D, Forstner MB, Groves JT, Bertozzi CR. Noncovalent cell surface engineering: incorporation of bioactive synthetic glycopolymers into cellular membranes. J Am Chem Soc 2008;130:5947-5953.

367.   Amatore C, Arbault S, Bouret Y, Guille M, Lemaitre F, Verchier Y. Regulation of exocytosis in chromaffin cells by trans-insertion of lysophosphatidylcholine and arachidonic acid into the outer leaflet of the cell membrane. Chembiochem 2006;7:1998-2003.

368.   Chen I, Howarth M, Lin W, Ting AY. Site-specific labeling of cell surface proteins with biophysical probes using biotin ligase. Nat Methods 2005;2:99-104.

369.   Bonasio R, Carman CV, Kim E, Sage PT, Love KR, Mempel TR, Springer TA, von Andrian UH. Specific and covalent labeling of a membrane protein with organic fluorochromes and quantum dots. Proc Natl Acad Sci U S A 2007;104:14753-14758.

370.   Saxon E, Bertozzi CR. Cell surface engineering by a modified Staudinger reaction. Science 2000;287:2007-2010.

371.   Mahal LK, Yarema KJ, Bertozzi CR. Engineering chemical reactivity on cell surfaces through oligosaccharide biosynthesis. Science 1997;276:1125-1128.

372.   Fernandez-Suarez M, Baruah H, Martinez-Hernandez L, Xie KT, Baskin JM, Bertozzi CR, Ting AY. Redirecting lipoic acid ligase for cell surface protein labeling with small-molecule probes. Nat Biotechnol 2007;25:1483-1487.

373.   Tanaka T, Yamamoto T, Tsukiji S, Nagamune T. Site-specific protein modification on living cells catalyzed by Sortase. Chembiochem 2008;9:802-807.

374.   Prescher JA, Bertozzi CR. Chemistry in living systems. Nat Chem Biol 2005;1:13-21.

375.   Prescher JA, Dube DH, Bertozzi CR. Chemical remodelling of cell surfaces in living animals. Nature 2004;430:873-877.

376.   Bertozzi CR, Kiessling LL. Chemical glycobiology. Science 2001;291:2357-2364.

377.   Medof ME, Nagarajan S, Tykocinski ML. Cell-surface engineering with GPI-anchored proteins. Faseb J 1996;10:574-586.

378.   Laughlin ST, Baskin JM, Amacher SL, Bertozzi CR. In vivo imaging of membrane-associated glycans in developing zebrafish. Science 2008;320:664-667.

379.   Johnsson N, George N, Johnsson K. Protein chemistry on the surface of living cells. Chembiochem 2005;6:47-52.

213

380.   Vivero-Pol L, George N, Krumm H, Johnsson K, Johnsson N. Multicolor imaging of cell surface proteins. J Am Chem Soc 2005;127:12770-12771.

381.   Ong SM, He L, Thuy Linh NT, Tee YH, Arooz T, Tang G, Tan CH, Yu H. Transient inter-cellular polymeric linker. Biomaterials 2007;28:3656-3667.

382.   Mahal LK, Bertozzi CR. Engineered cell surfaces: fertile ground for molecular landscaping. Chem Biol 1997;4:415-422.

383.   van Swieten PF, Leeuwenburgh MA, Kessler BM, Overkleeft HS. Bioorthogonal organic chemistry in living cells: novel strategies for labeling biomolecules. Org Biomol Chem 2005;3:20-27.

384.   Lemieux GA, Bertozzi CR. Chemoselective ligation reactions with proteins, oligosaccharides and cells. Trends Biotechnol 1998;16:506-513.

385.   Ning X, Guo J, Wolfert MA, Boons GJ. Visualizing metabolically labeled glycoconjugates of living cells by copper-free and fast huisgen cycloadditions. Angew Chem Int Ed Engl 2008;47:2253-2255.

386.   Baskin JM, Prescher JA, Laughlin ST, Agard NJ, Chang PV, Miller IA, Lo A, Codelli JA, Bertozzi CR. Copper-free click chemistry for dynamic in vivo imaging. Proc Natl Acad Sci U S A 2007;104:16793-16797.

387.   Codelli JA, Baskin JM, Agard NJ, Bertozzi CR. Second-generation difluorinated cyclooctynes for copper-free click chemistry. J Am Chem Soc 2008;130:11486-11493.

388.   Chidley C, Mosiewicz K, Johnsson K. A designed protein for the specific and covalent heteroconjugation of biomolecules. Bioconjug Chem 2008;19:1753-1756.

389.   Chung HA, Kato K, Itoh C, Ohhashi S, Nagamune T. Casual cell surface remodeling using biocompatible lipid-poly(ethylene glycol)(n): development of stealth cells and monitoring of cell membrane behavior in serum-supplemented conditions. J Biomed Mater Res A 2004;70:179-185.

390.   Ai H, Jones SA, Lvov YM. Biomedical applications of electrostatic layer-by-layer nano-assembly of polymers, enzymes, and nanoparticles. Cell Biochem Biophys 2003;39:23-43.

391.   Caruso F, Niikura K, Furlong DN, Okahata Y. Assembly of alternating polyelectrolyte and protein multilayer films for immunosensing .2. Langmuir 1997;13:3427-3433.

392.   Derbal L, Lesot H, Voegel JC, Ball V. Incorporation of alkaline phosphatase into layer-by-layer polyelectrolyte films on the surface of Affi-gel heparin beads: Physicochemical characterization and evaluation of the enzyme stability. Biomacromolecules 2003;4:1255-1263.

393.   Vodouhe C, Schmittbuhl M, Boulmedais F, Bagnard D, Vautier D, Schaaf P, Egles C, Voegel JC, Ogier J. Effect of functionalization of multilayered polyelectrolyte films on motoneuron growth. Biomaterials 2005;26:545-554.

394. Zhang JT, Chua LS, Lynn DM. Multilayered thin films that sustain the release of functional DNA under physiological conditions. Langmuir 2004;20:8015-8021.

395. Yamauchi F, Kato K, Iwata H. Layer-by-layer assembly of poly(ethyleneimine) and plasmid DNA onto transparent indium-tin oxide electrodes for temporally and spatially specific gene transfer. Langmuir 2005;21:8360-8367.

396. Schultz P, Vautier D, Richert L, Jessel N, Haikel Y, Schaaf P, Voegel JC, Ogier J, Debry C. Polyelectrolyte multilayers functionalized by a synthetic analogue of an anti-inflammatory peptide, alpha-MSH, for coating a tracheal prosthesis. Biomaterials 2005;26:2621-2630.

397. Zhong Y, Li BY, Haynie DT. Control of stability of polypeptide multilayer nanofilms by quantitative control of disulfide bond formation. Nanotechnology 2006;17:5726-5734.

398. Saxon E, Armstrong JI, Bertozzi CR. A "traceless" Staudinger ligation for the chemoselective synthesis of amide bonds. Org Lett 2000;2:2141-2143.

399. Hsiao SC, Crow AK, Lam WA, Bertozzi CR, Fletcher DA, Francis MB. DNA-Coated AFM Cantilevers for the Investigation of Cell Adhesion and the Patterning of Live Cells. Angew Chem-Int Edit 2008;47:8473-8477.

400. Szabo R, Mezo G, Pallinger E, Kovacs P, Kohidai L, Bosze S, Hudecz F. In vitro cytotoxicity, chemotactic effect, and cellular uptake of branched polypeptides with poly[L-lys] backbone by J774 murine macrophage cell line. Bioconjug Chem 2008;19:1078-1086.

401. De Bank PA, Kellam B, Kendall DA, Shakesheff KM. Surface engineering of living myoblasts via selective periodate oxidation. Biotechnol Bioeng 2003;81:800-808.

402. De Bank PA, Hou Q, Warner RM, Wood IV, Ali BE, Macneil S, Kendall DA, Kellam B, Shakesheff KM, Buttery LD. Accelerated formation of multicellular 3-D structures by cell-to-cell cross-linking. Biotechnol Bioeng 2007;97:1617-1625.

403. Sinclair J, Salem AK. Rapid localized cell trapping on biodegradable polymers using cell surface derivatization and microfluidic networking. Biomaterials 2006;27:2090-2094.

404. Iwasaki Y, Maie H, Akiyoshi K. Cell-specific delivery of polymeric nanoparticles to carbohydrate-tagging cells. Biomacromolecules 2007;8:3162-3168.

405. Zheng B, Brett SJ, Tite JP, Lifely MR, Brodie TA, Rhodes J. Galactose oxidation in the design of immunogenic vaccines. Science 1992;256:1560-1563.

406. Lutz JF, Zarafshani Z. Efficient construction of therapeutics, bioconjugates, biomaterials and bioactive surfaces using azide-alkyne "click" chemistry. Adv Drug Deliv Rev 2008;60:958-970.

407.   Laughlin ST, Bertozzi CR. Metabolic labeling of glycans with azido sugars and subsequent glycan-profiling and visualization via Staudinger ligation. Nat Protoc 2007;2:2930-2944.

408.   Vocadlo DJ, Hang HC, Kim EJ, Hanover JA, Bertozzi CR. A chemical approach for identifying O-GlcNAc-modified proteins in cells. Proc Natl Acad Sci U S A 2003;100:9116-9121.

409.   Elia G. Biotinylation reagents for the study of cell surface proteins. Proteomics 2008;8:4012-4024.

410.   Ilieva A, Yuan S, Wang R, Duguid WP, Rosenberg L. The structural integrity of the islet in vitro: the effect of incubation temperature. Pancreas 1999;19:297-303.

411.   Rosenberg L, Wang R, Paraskevas S, Maysinger D. Structural and functional changes resulting from islet isolation lead to islet cell death. Surgery 1999;126:393-398.

412.   Wang RN, Rosenberg L. Maintenance of beta-cell function and survival following islet isolation requires re-establishment of the islet-matrix relationship. J Endocrinol 1999;163:181-190.

413.   Muzykantov VR, Smirnov MD, Samokhin GP. Avidin attachment to biotinylated erythrocytes induces homologous lysis via the alternative pathway of complement. Blood 1991;78:2611-2618.

414.   Zhu W, Okollie B, Artemov D. Controlled internalization of Her-2/ neu receptors by cross-linking for targeted delivery. Cancer Biol Ther 2007;6:1960-1966.

415.   Hermanson GT. Bioconjugate Techniques. 2 ed. New York, NY: Elsevier; 2008.

416.   Gordon EJ, Sanders WJ, Kiessling LL. Synthetic ligands point to cell surface strategies. Nature 1998;392:30-31.

417.   Gordon EJ, Strong LE, Kiessling LL. Glycoprotein-inspired materials promote the proteolytic release of cell surface L-selectin. Bioorg Med Chem 1998;6:1293-1299.

418.   Sanders WJ, Gordon EJ, Dwir O, Beck PJ, Alon R, Kiessling LL. Inhibition of L-selectin-mediated leukocyte rolling by synthetic glycoprotein mimics. J Biol Chem 1999;274:5271-5278.

419.   Boddohi S, Killingsworth CE, Kipper MJ. Polyelectrolyte multilayer assembly as a function of pH and ionic strength using the polysaccharides chitosan and heparin. Biomacromolecules 2008;9:2021-2028.

420.   Tan QG, Ji J, Barbosa MA, Fonseca C, Shen JC. Constructing thromboresistant surface on biomedical stainless steel via layer-by-layer deposition anticoagulant. Biomaterials 2003;24:4699-4705.

421.   Jewell CM, Lynn DM. Multilayered polyelectrolyte assemblies as platforms for the delivery of DNA and other nucleic acid-based therapeutics. Adv Drug Deliv Rev 2008;60:979-999.

422.   Garza JM, Schaaf P, Muller S, Ball V, Stoltz JF, Voegel JC, Lavalle P. Multicompartment films made of alternate polyelectrolyte multilayers of exponential and linear growth. Langmuir 2004;20:7298-7302.

423.   Peralta S, Habib-Jiwan JL, Jonas AM. Ordered Polyelectrolyte Multilayers: Unidirectional FRET Cascade in Nanocompartmentalized Polyelectrolyte Multilayers. Chemphyschem 2008.

424.   Swiston AJ, Cheng C, Um SH, Irvine DJ, Cohen RE, Rubner MF. Surface Functionalization of Living Cells with Multilayer Patches. Nano Lett 2008.

425.   Welsh ER, Schauer CL, Santos JP, Price RR. In situ cross-linking of alternating polyelectrolyte multilayer films. Langmuir 2004;20:1807-1811.

426.   Kohli P, Blanchard GJ. Design and demonstration of hybrid multilayer structures: Layer-by-layer mixed covalent and ionic interlayer linking chemistry. Langmuir 2000;16:8518-8524.

427.   Lynn DM. Peeling back the layers: Controlled erosion and triggered disassembly of multilayered polyelectrolyte thin films. Advanced Materials 2007;19:4118-4130.

428.   Volodkin D, Arntz Y, Schaaf P, Moehwald H, Voegel JC, Ball V. Composite multilayered biocompatible polyelectrolyte films with intact liposomes: stability and temperature triggered dye release. Soft Matter 2008;4:122-130.

429.   Zhong Y, Whittington CF, Zhang L, Haynie DT. Controlled loading and release of a model drug from polypeptide multilayer nanofilms. Nanomedicine-Nanotechnology Biology and Medicine 2007;3:154-160.

430.   Chen J, Huang SW, Lin WH, Zhuo RX. Tunable film degradation and sustained release of plasmid DNA from cleavable polycation/plasmid DNA multilayers under reductive conditions. Small 2007;3:636-643.

431.   Bretzel RG, Brandhorst D, Brandhorst H, Eckhard M, Ernst W, Friemann S, Rau W, Weimar B, Rauber K, Hering BJ, Brendel MD. Improved survival of intraportal pancreatic islet cell allografts in patients with type-1 diabetes mellitus by refined peritransplant management. J Mol Med 1999;77:140-143.

432.   Hirshberg B, Rother KI, Harlan DM. Islet transplantation: where do we stand now? Diabetes Metab Res Rev 2003;19:175-178; discussion 175.

433.   Shapiro AM, Lakey JR, Rajotte RV, Warnock GL, Friedlich MS, Jewell LD, Kneteman NM. Portal vein thrombosis after transplantation of partially purified pancreatic islets in a combined human liver/islet allograft. Transplantation 1995;59:1060-1063.

434.   Froberg MK, Leone JP, Jessurun J, Sutherland DE. Fatal disseminated intravascular coagulation after autologous islet transplantation. Hum Pathol 1997;28:1295-1298.

435. Brandhorst D, Brandhorst H, Zwolinski A, Nahidi F, Jahr H, Bretzel RG. Primary nonfunction is not caused by accelerated rejection after pig-to-rat islet transplantation. Transplant Proc 1998;30:407-408.

436. Deng S, Ketchum RJ, Kucher T, Weber M, Naji A, Brayman KL. Primary nonfunction of islet xenografts in rat recipients results from non-T-cell-mediated immune responses. Transplant Proc 1997;29:1726-1727.

437. Liu X, Hering BJ, Mellert J, Brandhorst D, Brandhorst H, Federlin K, Bretzel RG, Hopt UT. Prevention of primary nonfunction after porcine islet allotransplantation. Transplant Proc 1997;29:2071-2072.

438. Kerr R, Stirling D, Ludlam CA. Interleukin 6 and haemostasis. Br J Haematol 2001;115:3-12.

439. Esmon CT. Crosstalk between inflammation and thrombosis. Maturitas 2004;47:305-314.

440. Owen WG, Esmon CT. Functional properties of an endothelial cell cofactor for thrombin-catalyzed activation of protein C. J Biol Chem 1981;256:5532-5535.

441. Esmon CT, Owen WG. Identification of an endothelial cell cofactor for thrombin-catalyzed activation of protein C. Proc Natl Acad Sci U S A 1981;78:2249-2252.

442. Esmon NL, Owen WG, Esmon CT. Isolation of a membrane-bound cofactor for thrombin-catalyzed activation of protein C. J Biol Chem 1982;257:859-864.

443. Esmon CT, Gu JM, Xu J, Qu D, Stearns-Kurosawa DJ, Kurosawa S. Regulation and functions of the protein C anticoagulant pathway. Haematologica 1999;84:363-368.

444. Esmon CT, Ding W, Yasuhiro K, Gu JM, Ferrell G, Regan LM, Stearns-Kurosawa DJ, Kurosawa S, Mather T, Laszik Z, Esmon NL. The protein C pathway: new insights. Thromb Haemost 1997;78:70-74.

445. Esmon NL, Carroll RC, Esmon CT. Thrombomodulin blocks the ability of thrombin to activate platelets. J Biol Chem 1983;258:12238-12242.

446. Van de Wouwer M, Collen D, Conway EM. Thrombomodulin-protein C-EPCR system - Integrated to regulate coagulation and inflammation. Arterioscl Throm Vas 2004;24:1374-1383.

447. Esmon CT. Coagulation inhibitors in inflammation. Biochem Soc T 2005;33:401-405.

448. Hancock WW, Grey ST, Hau L, Akalin E, Orthner C, Sayegh MH, Salem HH. Binding of activated protein C to a specific receptor on human mononuclear phagocytes inhibits intracellular calcium signaling and monocyte-dependent proliferative responses. Transplantation 1995;60:1525-1532.

449. Grey ST, Tsuchida A, Hau H, Orthner CL, Salem HH, Hancock WW. Selective Inhibitory Effects of the Anticoagulant Activated Protein-C on the Responses of Human

Mononuclear Phagocytes to Lps, Ifn-Gamma, or Phorbol Ester. J Immunol 1994;153:3664-3672.

450.   Murakami K, Okajima K, Uchiba M, Johno M, Nakagaki T, Okabe H, Takatsuki K. Activated protein C attenuates endotoxin-induced pulmonary vascular injury by inhibiting activated leukocytes in rats. Blood 1996;87:642-647.

451.   Murakami K, Okajima K, Uchiba M, Johno M, Nakagaki T, Okabe H, Takatsuki K. Activated protein C prevents LPS-induced pulmonary vascular injury by inhibiting cytokine production. Am J Physiol-Lung C 1997;16:L197-L202.

452.   Hancock WW, Bach FH. Immunobiology and therapeutic applications of protein C protein S thrombomodulin in human and experimental allotransplantation and xenotransplantation. Trends Cardiovas Med 1997;7:174-183.

453.   Grinnell BW, Hermann RB, Yan SB. Human Protein-C Inhibits Selectin-Mediated Cell-Adhesion - Role of Unique Fucosylated Oligosaccharide. Glycobiology 1994;4:221-225.

454.   Joyce DE, Gelbert L, Ciaccia A, DeHoff B, Grinnell BW. Gene expression profile of antithrombotic protein C defines new mechanisms modulating inflammation and apoptosis. Journal of Biological Chemistry 2001;276:11199-11203.

455.   Grinnell BW, Hermann RB, Yan SB. Human protein C inhibits selectin-mediated cell adhesion: role of unique fucosylated oligosaccharide. Glycobiology 1994;4:221-225.

456.   Gallagher SR. One-dimensional SDS gel electrophoresis of proteins. Curr Protoc Immunol 2006;Chapter 8:Unit 8 4.

457.   Haller CA, Cui W, Wen J, Robson SC, Chaikof EL. Reconstitution of CD39 in liposomes amplifies nucleoside triphosphate diphosphohydrolase activity and restores thromboregulatory properties. J Vasc Surg 2006;43:816-823.

458.   Cazalis CS, Haller CA, Chaikof EL. Site-specific pegylation of a thrombomodulin derivative. Abstr Pap Am Chem S 2004;227:U520-U520.

459.   Iino S, Abeyama K, Kawahara KI, Aikou T, Maruyama I. Thrombomodulin expression on Langerhans' islet: can endogenous 'anticoagulant on demand' overcome detrimental thrombotic complications in clinical islet transplantation? J Thromb Haemost 2004;2:833-834.

460.   Galvin JB, Kurosawa S, Moore K, Esmon CT, Esmon NL. Reconstitution of Rabbit Thrombomodulin into Phospholipid-Vesicles. Journal of Biological Chemistry 1987;262:2199-2205.

461.   Parkinson JF, Nagashima M, Kuhn I, Leonard J, Morser J. Structure-Function Studies of the Epidermal Growth-Factor Domains of Human Thrombomodulin. Biochemical and Biophysical Research Communications 1992;185:567-576.

462.   Kiick KL, Saxon E, Tirrell DA, Bertozzi CR. Incorporation of azides into recombinant proteins for chemoselective modification by the Staudinger ligation. P Natl Acad Sci USA 2002;99:19-24.

463.   Cazalis CS, Haller CA, Sease-Cargo L, Chaikof EL. C-terminal site-specific PEGylation of a truncated thrombomodulin mutant with retention of full bioactivity. Bioconjug Chem 2004;15:1005-1009.

464.   Nishizawa N, Nishimura J, Saitoh H, Fujiki K, Tsubokawa N. Grafting of branched polymers onto nano-sized silica surface: Postgrafting of polymers with pendant isocyanate groups of polymer chain grafted onto nano-sized silica surface. Prog Org Coat 2005;53:306-311.

465.   Bennet W, Groth CG, Larsson R, Nilsson B, Korsgren O. Isolated human islets trigger an instant blood mediated inflammatory reaction: implications for intraportal islet transplantation as a treatment for patients with type 1 diabetes. Ups J Med Sci 2000;105:125-133.

466.   Uchiba M, Okajima K, Murakami K, Johno M, Okabe H, Takatsuki K. Recombinant thrombomodulin prevents endotoxin-induced lung injury in rats by inhibiting leukocyte activation. Am J Physiol 1996;271:L470-475.

467.   Aoki Y, Takei R, Mohri M, Gonda Y, Gomi K, Sugihara T, Kiyota T, Yamamoto S, Ishida T, Maruyama I. Antithrombotic effects of recombinant human soluble thrombomodulin (rhs-TM) on arteriovenous shunt thrombosis in rats. Am J Hematol 1994;47:162-166.

468.   Ikeguchi H, Maruyama S, Morita Y, Fujita Y, Kato T, Natori Y, Akatsu H, Campbell W, Okada N, Okada H, Yuzawa Y, Matsuo S. Effects of human soluble thrombomodulin on experimental glomerulonephritis. Kidney Int 2002;61:490-501.

469.   Lund T, Fosby B, Korsgren O, Scholz H, Foss A. Glucocorticoids reduce pro-inflammatory cytokines and tissue factor in vitro and improve function of transplanted human islets in vivo. Transpl Int 2008;21:669-678.

470.   Nawroth PP, Handley DA, Esmon CT, Stern DM. Interleukin 1 induces endothelial cell procoagulant while suppressing cell-surface anticoagulant activity. Proc Natl Acad Sci U S A 1986;83:3460-3464.

471.   Nawroth PP, Stern DM. Modulation of endothelial cell hemostatic properties by tumor necrosis factor. J Exp Med 1986;163:740-745.

472.   Kume M, Hayashi T, Yuasa H, Tanaka H, Nishioka J, Ido M, Gabazza EC, Kawarada Y, Suzuki K. Bacterial lipopolysaccharide decreases thrombomodulin expression in the sinusoidal endothelial cells of rats -- a possible mechanism of intrasinusoidal microthrombus formation and liver dysfunction. J Hepatol 2003;38:9-17.

473.   Terada Y, Eguchi Y, Nosaka S, Toba T, Nakamura T, Shimizu Y. Capillary endothelial thrombomodulin expression and fibrin deposition in rats with continuous and bolus lipopolysaccharide administration. Lab Invest 2003;83:1165-1173.

474.   Arai M, Mochida S, Ohno A, Ogata I, Obama H, Maruyama I, Fujiwara K. Blood coagulation equilibrium in rat liver microcirculation as evaluated by endothelial cell thrombomodulin and macrophage tissue factor. Thromb Res 1995;80:113-123.

475.   Wang YX, Wu C, Vincelette J, Martin-McNulty B, Alexander S, Larsen B, Light DR, McLean K. Amplified anticoagulant activity of tissue factor-targeted thrombomodulin: in-vivo validation of a tissue factor-neutralizing antibody fused to soluble thrombomodulin. Thromb Haemost 2006;96:317-324.

476.   Lee H, Larson RG. Lipid bilayer curvature and pore formation induced by charged linear polymers and dendrimers: The effect of molecular shape. J Phys Chem B 2008;112:12279-12285.

477.   Sackmann E. Supported membranes: Scientific and practical applications. Science 1996;271:43-48.

478.   Tanaka M, Sackmann E. Polymer-supported membranes as models of the cell surface. Nature 2005;437:656-663.

479.   Sackmann E, Tanaka M. Supported membranes on soft polymer cushions: fabrication, characterization and applications. Trends Biotechnol 2000;18:58-64.

480.   Andersson AS, Glasmastar K, Sutherland D, Lidberg U, Kasemo B. Cell adhesion on supported lipid bilayers. J Biomed Mater Res A 2003;64A:622-629.

481.   Chapman D. Biomembranes and New Hemocompatible Materials. Langmuir 1993;9:39-45.

482.   Glasmastar K, Larsson C, Hook F, Kasemo B. Protein adsorption on supported phospholipid bilayers. J Colloid Interf Sci 2002;246:40-47.

483.   Lu JR, Murphy EF, Su TJ, Lewis AL, Stratford PW, Satija SK. Reduced protein adsorption on the surface of a chemically grafted phospholipid monolayer. Langmuir 2001;17:3382-3389.

484.   Murphy EF, Lu JR, Brewer J, Russell J, Penfold J. The reduced adsorption of proteins at the phosphoryl choline incorporated polymer-water interface. Langmuir 1999;15:1313-1322.

485.   Tegoulia VA, Rao WS, Kalambur AT, Rabolt JR, Cooper SL. Surface properties, fibrinogen adsorption, and cellular interactions of a novel phosphorylcholine-containing self-assembled monolayer on gold. Langmuir 2001;17:4396-4404.

486.   Vermette P, Gauvreau V, Pezolet M, Laroche G. Albumin and fibrinogen adsorption onto phosphatidylcholine monolayers investigated by Fourier transform infrared spectroscopy. Colloid Surface B 2003;29:285-295.

487.   Hui SW, Viswanathan R, Zasadzinski JA, Israelachvili JN. The Structure and Stability of Phospholipid-Bilayers by Atomic-Force Microscopy. Biophys J 1995;68:171-178.

488.   Winger TM, Ludovice PJ, Chaikof EL. Formation and stability of complex membrane-mimetic monolayers on solid supports. Langmuir 1999;15:3866-3874.

489.   Ross EE, Rozanski LJ, Spratt T, Liu SC, O'Brien DF, Saavedra SS. Planar supported lipid bilayer polymers formed by vesicle fusion. 1. Influence of diene monomer structure and polymerization method on film properties. Langmuir 2003;19:1752-1765.

490.   Hub HH, Hupfer B, Koch H, Ringsdorf H. Polyreactions in Ordered Systems .20. Polymerizable Phospholipid Analogs - New Stable Biomembrane and Cell Models. Angew Chem Int Edit 1980;19:938-940.

491.   Hayward JA, Chapman D. Biomembrane Surfaces as Models for Polymer Design - the Potential for Hemocompatibility. Biomaterials 1984;5:135-142.

492.   Marra KG, Winger TM, Hanson SR, Chaikof EL. Cytomimetic biomaterials .1. In-situ polymerization of phospholipids on an alkylated surface. Macromolecules 1997;30:6483-6488.

493.   Ross EE, Spratt T, Liu SC, Rozanski LJ, O'Brien DF, Saavedra SS. Planar supported lipid bilayer polymers formed by vesicle fusion. 2. Adsorption of bovine serum albumin. Langmuir 2003;19:1766-1774.

494.   Yoneyama T, Ishihara K, Nakabayashi N, Ito M, Mishima Y. Short-term in vivo evaluation of small-diameter vascular prosthesis composed of segmented poly(etherurethane) 2-methacryloyloxyethyl phosphorylcholine polymer blend. J Biomed Mater Res 1998;43:15-20.

495.   Chen CY, Ofenloch JC, Yianni YP, Hanson SR, Lumsden AB. Phosphorylcholine coating of ePTFE reduces platelet deposition and neointimal hyperplasia in arteriovenous grafts. J Surg Res 1998;77:119-125.

496.   Chen CY, Lumsden AB, Ofenloch JC, Noe B, Campbell EJ, Stratford PW, Yianni YP, Taylor AS, Hanson SR. Phosphorylcholine coating of ePTFE grafts reduces neointimal hyperplasia in canine model. Ann Vasc Surg 1997;11:74-79.

497.   Moro T, Takatori Y, Ishihara K, Konno T, Takigawa Y, Matsushita T, Chung UI, Nakamura K, Kawaguchi H. Surface grafting of artificial joints with a biocompatible polymer for preventing periprosthetic osteolysis. Nat Mater 2004;3:829-836.

498.   Goreish HH, Lewis AL, Rose S, Lloyd AW. The effect of phosphorylcholine-coated materials on the inflammatory response and fibrous capsule formation: In vitro and in vivo observations. J Biomed Mater Res A 2004;68A:1-9.

499.   Lewis AL, Tolhurst LA, Stratford PW. Analysis of a phosphorylcholine-based polymer coating on a coronary stent pre- and post-implantation. Biomaterials 2002;23:1697-1706.

500.   Lewis AL, Furze JD, Small S, Robertson JD, Higgins BJ, Taylor S, Ricci DR. Long-term stability of a coronary stent coating post implantation. J Biomed Mater Res 2002;63:699-705.

501.   Marra KG, Kidani DDA, Chaikof EL. Cytomimetic biomaterials .2. In-situ polymerization of phospholipids on a polymer surface. Langmuir 1997;13:5697-5701.

502.   Orban JM, Faucher KM, Dluhy RA, Chaikof EL. Cytomimetic biomaterials. 4. In-situ photopolymerization of phospholipids on an alkylated surface. Macromolecules 2000;33:4205-4212.

503.   Chon JH, Marra KG, Chaikof EL. Cytomimetic biomaterials. 3. Preparation and transport studies of an alginate amphiphilic copolymer polymerized phospholipid film. J Biomat Sci-Polym E 1999;10:95-107.

504.   Liu H, Faucher KM, Sun XL, Feng J, Johnson TL, Orban JM, Apkarian RP, Dluhy RA, Chaikof EL. A membrane-mimetic barrier for cell encapsulation. Langmuir 2002;18:1332-1339.

505.   Faucher KM, Sun XL, Chaikof EL. Fabrication and characterization of glycocalyx-mimetic surfaces. Langmuir 2003;19:1664-1670.

506.   Feng J, Tseng PY, Faucher KM, Orban JM, Sun XL, Chaikof EL. Functional reconstitution of thrombomodulin within a substrate-supported membrane-mimetic polymer film. Langmuir 2002;18:9907-9913.

507.   Tseng PY, Rele SS, Sun XL, Chaikof EL. Membrane-mimetic films containing thrombomodulin and heparin inhibit tissue factor-induced thrombin generation in a flow model. Biomaterials 2006;27:2637-2650.

508.   Tseng PY, Jordan SW, Sun XL, Chaikof EL. Catalytic efficiency of a thrombomodulin-functionalized membrane-mimetic film in a flow model. Biomaterials 2006;27:2768-2775.

509.   Jordan SW, Faucher KM, Caves JM, Apkarian RP, Rele SS, Sun XL, Hanson SR, Chaikof EL. Fabrication of a phospholipid membrane-mimetic film on the luminal surface of an ePTFE vascular graft. Biomaterials 2006;27:3473-3481.

510.   Sun XL, Liu HB, Orban JM, Sun LJ, Chaikof EL. Synthesis and terminal functionalization of a polymerizable phosphatidylethanolamine. Bioconjugate Chem 2001;12:673-677.

511.   Murphy MR, Faucher KM, Sun XL, Chaikof EL, Dluhy RA. Analysis of photoinitiated polymerization in a membrane mimetic film using infrared spectroscopy and near-IR Raman microscopy. Colloid Surface B 2005;46:226-232.

512.   Perez-Salas UA, Faucher KM, Majkrzak CF, Berk NF, Krueger S, Chaikof EL. Characterization of a biomimetic polymeric lipid bilayer by phase sensitive neutron reflectometry. Langmuir 2003;19:7688-7694.

513.   Weber CJ, Zabinski S, Koschitzky T, Wicker L, Rajotte R, Dagati V, Peterson L, Norton J, Reemtsma K. The Role of Cd4+ Helper T-Cells in the Destruction of Microencapsulated Islet Xenografts in Nod Mice. Transplantation 1990;49:396-404.

514. Woronzoff-Dashkoff KK. The Wright-Giemsa stain - Secrets revealed. Clin Lab Med 2002;22:15-+.

515. Tseng PY, Rele SM, Sun XL, Chaikof EL. Fabrication and characterization of heparin functionalized membrane-mimetic assemblies. Biomaterials 2006;27:2627-2636.

516. Gugerli R, Cantana E, Heinzen C, Von Stockar U, Marison IW. Quantitative study of the production and properties of alginate/poly-L-lysine microcapsules. J Microencapsul 2002;19:571-590.

517. Thu B, Bruheim P, Espevik T, Smidsrod O, SoonShiong P, SkjakBraek G. Alginate polycation microcapsules .1. Interaction between alginate and polycation. Biomaterials 1996;17:1031-1040.

518. Vandenbossche GMR, Bracke ME, Cuvelier CA, Bortier HE, Mareel MM, Remon JP. Host-Reaction against Empty Alginate-Polylysine Microcapsules - Influence of Preparation Procedure. J Pharm Pharmacol 1993;45:115-120.

519. Swain PS, Andelman D. The influence of substrate structure on membrane adhesion. Langmuir 1999;15:8902-8914.